ProQuest LLC.
789 East Eisenhower Parkway
P.O. Box 1346
Ann Arbor, MI 48106 – 1346

Structural and Preparative Studies of Doped Silica Glasses

A thesis submitted in partial fulfilment of the requirements of the Nottingham Trent University for the degree of Doctor of Philosophy

by
Séverine AUBONNET

August 1999

Department of Chemistry & Physics
The Nottingham Trent University

To Patrick

'Envers et contre tout'

ACKNOWLEDGEMENTS

First of all, I would like to thank my supervisor Dr C.C.Perry for her supervision and guidance throughout this research project. I would also like to thank Mr D.Irish and Mr J.Hammond from UNICAM for giving me helpful advice on the use of the Vision software and funding my PhD.

My thanks go to Mr M.Wood for all the ^{29}SiNMR analysis he has done for me, Mrs P.Fleming for her technical assistance and Dr A.Slawin from Loughborough University for the single crystal structure analysis and the X-ray powder analysis.

A lot of thanks to the unforgettable inorganic research group, Ana Maria Caballero, Martin Gardener, Chris McLean-Tooke and Dr Melanie Webb.

Finally I would like to take the opportunity to thank Patrick who was always there to support and encourage me through the many ups and downs of this project.

Abstract

The sol-gel process has been used for the preparation of high optical quality materials. Doped sol-gel glasses were made using the pre-doped method which consists of doping the sol-gel glass during its preparation, as soon as the precursors are mixed together. In this work, solid standards for the UV region were prepared using the sol-gel process.

Initially, Nd^{3+} and Ce^{3+} metal ions were used as dopants. The effect of the two different dopants on the silica matrix was studied. During the drying process of doped and undoped sol-gel glasses, the dopant affects the rate at which the glass dries. High concentration (9.48wt%) Nd^{3+} doped sol-gels showed a slower drying rate than normal sol-gels. At lower concentrations (0.948wt% to $9.48.10^{-4}$wt%), the drying rate was quicker than normal sol-gels. At $9.48.10^{-5}$wt%, the drying behaviour of the doped sol-gel was very similar to that of the normal sol-gel. However, the drying rate was slowed down in the presence of cerium regardless of its concentration in the glass (8.99% to 0.00128wt%). FTIR(mid and NIR) showed that the dopant, according to its concentration in the sol-gel glass, affects the structure of the silica matrix. The number of hydroxyl functionalities varied between doped and undoped sol-gels. Consequently the dopant interacts with the matrix. To understand the nature of this interaction, the first hour of hydrolysis and condensation reactions was studied. The gelation time was monitored according to the hydrolysis time for doped and undoped samples. In the presence of high concentrations of dopant, the gelation time increased in comparison with undoped sol-gels. At a high concentration of Ce^{3+} metal ion (0.0128M), the gelation time of the sol-gel solution was longer than in the presence of a high concentration of Nd^{3+} (0.0128M). At lower concentration ranges, the gelation time of the sol-gel solution was lower than in the presence of Nd^{3+}. A qualitative study of the silica species during hydrolysis and condensation reactions was performed by ^{29}SiNMR. Variation of the silica species according to the type of sol-gel shows that the dopant affects the rates of hydrolysis and condensation reactions. The dopant has a catalytic effect. pH studies demonstrated that the catalytic effect of the dopant was due to the metal ion itself and not to the ligands around it, more specifically to the acidity of the metal ion. Not only has the metal ion an effect on the silica matrix, but the metal ion is affected by its environment. Studies were carried out using Nd^{3+} which has hypersensitive electronic transitions. Nd^{3+} ions in crystals, in solution and in sol-gels were studied. For these studies, single crystal X-ray analysis, UV-VIS spectroscopy and EXAFS analysis were performed. As a crystal, the metal ion was sensitive to the type of ligand present. A coordination number of 10 was found with NO^-_3 ligands and a coordination number of 8 with Cl^- ligands. In solution, the metal ion was influenced by the ligands and the solvents. Only the solvent had an effect on the coordination number. A coordination number of 9 was found in aqueous solution and 7 coordination was present in ethanol solutions. In the glass, the coordination number was not dependent on the ligands and the solvents in which the metal ion had been prepared. The electronic transitions were sensitive to the structure of the glass. A coordination number of 7 was found in the glass suggesting that the metal ion surrounded by its ligands was electrostatically bonded to the matrix. The bond distance between Nd-O was 2.55Å. After dehydration, the metal ion loses one water ligand, now having a coordination number of 6. A bond distance between Nd-O of 2.549Å was found. Finally when the sample has been thermally treated, a coordination number of only 4 was observed. It was covalently bonded to the silica matrix via four oxygens of the siloxane groups. A bond distance between Nd-O of 2.495 Å was found.

Knowing that the metal ions (Nd^{3+} and Ce^{3+}) interact with the silica matrix, the preparation of standards was carried out. A series of UV solid standards was prepared using Ce^{3+} metal ion as the dopant. The concentration of the metal ion in the sol-gel glasses was varied in order to obtain a series of standards with bands having intensities between 0.5A to 2A for a pathlength of 1mm±0.1mm. The effect of the environment on the electronic transitions of Ce^{3+} was also studied by UV-VIS spectroscopy. After dehydration, a shift of the bands was observed. After heat treatment (800°C), the bands characteristic of the metal ion were no longer observable. A change in the oxidation state from Ce^{3+} to Ce^{4+} possibly occurred during heat treatment. The Ce^{4+} ion does not possess any bands in the UV region. Unsuccessful results were obtained when a combined standard for the UV and VIS regions was prepared by using Ce^{3+} and Nd^{3+}. The two metal ions interacted with each other and the bands of Ce^{3+} ion in the UV region were no longer observable.

As a standard, the sol-gel glass needed to be stable with time and no changes in the transmittance should be observed. Preliminary studies were carried out on the aging of the samples. A decrease of the transmittance with time was observed due to the moisture from the air which gets into the pores of the glass.

Finally, some doped sol-gels for use as visible standards were prepared. The transition elements of the first row were studied. The effect of the environment on their electronic transitions was monitored by UV-VIS spectroscopy. Chromium and vanadium were two potential candidates for the preparation of such standards as they exhibit broad bands in the visible region.

Contents

Chapter 1: Introduction

Chapter 2: Sample Preparation and Analysis

Chapter 3: Effect of Dopants on the Drying Process of Sol-Gel Glasses

Chapter 4: Effect of the Precursors and the Sol-Gel Matrix on the Coordination Chemistry of the Dopant Metal Ions

Chapter 5: Solid Absorbance Standards

Chapter 6: 1st Row transition metals as dopants in the visible region

Chapter 1: Introduction

1.1- Introduction

The sol-gel process can be used for the preparation of glass with high optical quality and high purity [1,2]. Koone et al. have used this technique as an alternative route to manufacture flat lenses [3].

In this program of research, the sol-gel process has been used to prepare solid standards suitable for use in the 200-350nm (UV) wavelength region.

After a brief explanation of the sol-gel process and of the standards in chapter I, a description of the methods and techniques used during this work is given in chapter II.

In chapters III & IV, the interaction between rare earth dopants and the matrix is studied.

A method for the formation and characterisation of solid standards containing rare earth ions in the UV region is proposed in chapter V.

Finally in chapter VI investigation into the possibility of preparing solid-standards in the visble region using transition metals are presented.

1.2-The sol-gel process

1.2.1-Introduction

Ceramic materials and glasses have always been produced at high temperature (1000-2000°C). For the glass a three dimensional network is formed during cooling from above the liquidus and is preserved without crystallisation by supercooling the melt [4]. The use of the sol-gel process enables the preparation of porous or dense glasses with superior homogeneity, purity, low optical loss (high transmittance) and near net shape characteristics at low temperature [1].

Since the 1950's the sol-gel process has been increasingly used for the preparation of glasses and other ceramic materials [5]. This process permits the preparation of compounds at room temperature (25°C) although higher temperature may later be used in processing for particular applications. The technology allows also the control of the surfaces of the material during the first stage of production.

Sol-gel glasses are potentially applicable to a range of optical products including lenses, mirrors, waveguides, optical fibres and host materials for filters and lasers.

A new class of materials has been created using the sol-gel process where the porous characteristics of inorganic materials are used to encapsulate organic molecules [6].

1.2.2- Definitions

Before explaining the sol-gel process it is necessary to give the following definitions. *Colloids* are solid particles with 1-100nm diameter. A *Sol* is a dispersion / colloidal suspension of solid particles or large molecules (1-500 nm diameter) in a liquid. An interconnected, rigid network with pores smaller than a micrometer and polymeric chains bigger than a micrometer is a *gel* [7] .

Sol-gel process is the transition of a system of colloidal particles in a solution into a disordered, branched, continuous network, which are interpenetrated by a liquid.

A classification of three types of gels according to the dispersion medium can be found: *hydrogel or aquagel* when the medium is water, *alcogel* when it is alcohol and *aerogel* when it is air.

1.2.3-Preparation

The sol-gel process consists of a series of different steps:

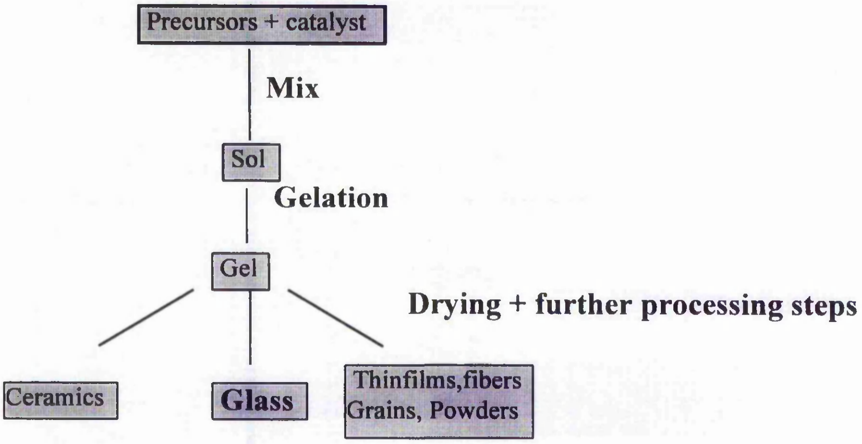

1.2.3.1- Sol-gel formation

The understanding of gel formation is important as the physical and chemical properties of monolithic gels depend upon their structure.

Two different methods can be used to prepare sol-gels:

1-The gelation of a solution of colloidal powder called *the particulate/colloidal route.*

2-The hydrolysis and polycondensation of alkoxide precursors known as *the alkoxide route.*

The most flexible route is the *alkoxide route*, which allows homogeneous mixing of reactants at the molecular level although problems associated with shrinkage and cracking during drying have been reported [8-10].

In this study, the alkoxide route has been used where the fundamental polymeric nature of a sol-gel is set up during the initial stages of the sol-gel process. The reactions which take place during the establishment of the sol-gel network are those of hydrolysis and condensation which in the system utilised in this study was carried out in the presence of an acid catalyst and a moderately low level of water.

In order to understand the following investigations of the hydrolysis and condensation reactions during the first hour of reaction it is necessary to understand the molecular mechanisms occurring.

The experimental protocol used during these experiments was a system with low water and an acid catalyst [1,4,6]. The simplest silica precursors are tetraethylorthosilicate (TEOS) and tetramethylorthosilicate (TMOS). For this study, TEOS has been used because it hydrolyses at a slower rate and is not known to cause damage to eye tissues unlike TMOS [11].

Hydrolysis reaction:

Due to the fact that the system used was a low water/acid catalyst, the hydrolysis reaction consists of the substitution of an alkoxide group for an hydroxyl group.

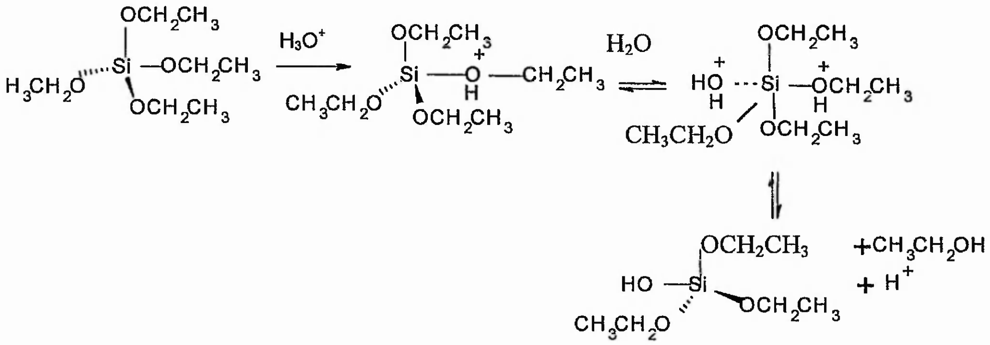

(1)

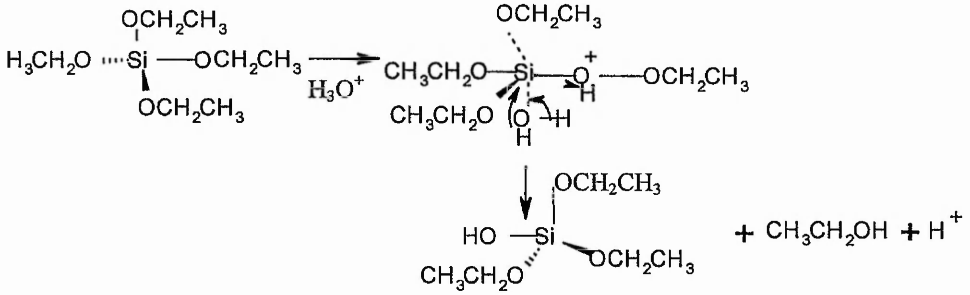

(2)

Routes (1)& (2) are the two valid possibilities for the hydrolysis reaction.

The intermediate silicon species is 5-coordinate which results from a bimolecular S_N2 nucleophilic substitution reaction. Protonation of alkoxide groups by acid increases the acidity of the group and allows the central silicon atom to be attacked by a water molecule. The water acquires a partial positive charge and partially reduces the charge on the alkoxide making it a better leaving group [6].

Condensation reaction:

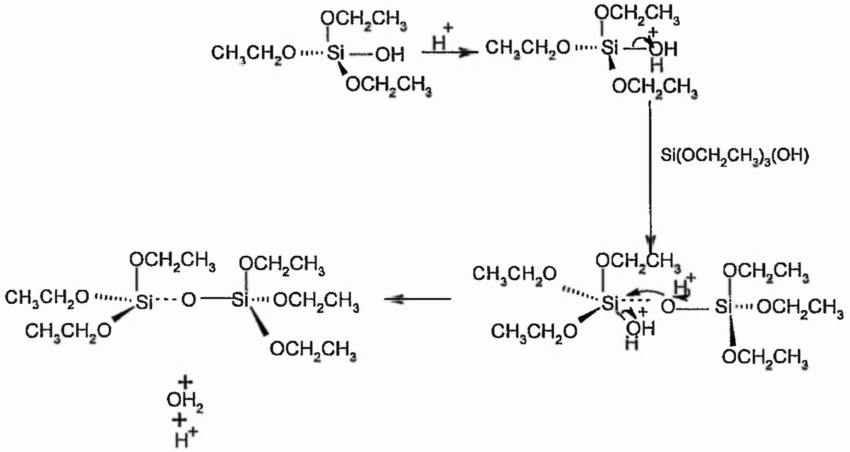

(3)

The reaction occurs via a nucleophilic condensation mechanism where water and alcohols may be released. Water release is favored unless water concentrations are very low when alcohol liberation becomes significant. At low pH the most basic silanols are protonated first. Protonation of the silanol groups increases the acidity of the group and renders silicon atoms more susceptible to attack by nucleophiles [6].

The nature of a particular sol-gel network is determined by a number of factors such as the pH of the solutions, the precursors used for the preparation of the sol-gel, the temperature of mixing, the length of mixing, the method/period of aging the sol-gel, the reagent concentrations, the H_2O/Si molar ratio, the catalyst identity.

All these factors affect the final structure of the gel and they also affect the mechanism and the rate of both hydrolysis and condensation reactions. By controlling these factors, it is possible to vary the structure and properties of the sol-gel derived inorganic network.

Catalytic effect:

The catalyst has an effect as it speeds up the hydrolysis and condensation reactions.

Two types of catalysts are used for the preparation of sol-gels [6].

Low water/acid catalysis:

Hydrolysis takes place via substitution of an alkoxy group with an hydroxyl group. Three and five co-ordinate silicon species are possible transition state intermediates, five coordinate being the most sensible. Under these conditions, water preferentially attacks the silicon alkoxide bonds rather than Si-O-Si bonds. The rate of hydrolysis is proportional to the concentration of the acid, the alkoxide and water.

With acid catalysts, polymeric products are formed (Figure 1.1) which are usually optically transparent.

Figure 1.1: Schematic figure of polymeric products from the acid catalysed alkoxide sol-gel route

High water/base catalysis

A pentacoordinate transition state is proposed with the hydroxyl anion attacking an electropositive silicon resulting in partial negative charge developing on the silicon atom. Hydrolysis is more likely to occur in species that have already been partially hydrolysed. The reactions of hydrolysis and condensation are distinct from one another. The rate of hydrolysis is proportional to the concentration of the base and the alkoxide.

Highly porous particulate products are formed, colloidal type (Figure 1.2). The transparency of the resulting materials is dependant on the silicate precursor used.

Figure 1.2: Schematic figure of highly porous particulate products from the base catalysed alkoxide sol-gel route

1.2.3.2- Gelation

After the *precursors* have been mixed together in a homogeneous solution for a certain period of time, they are poured into a mould without adhesion of the gel.

The sol changes into a gel by polycondensation during the gelation period.

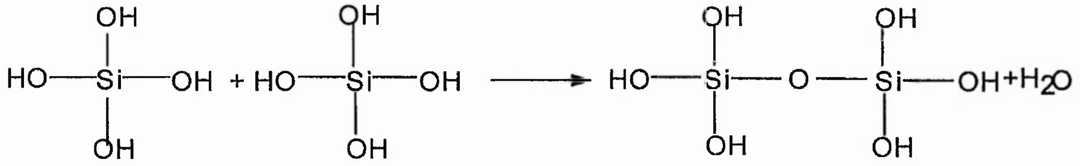

$$\mathrm{HO{-}Si(OH)_2{-}OH + HO{-}Si(OH)_2{-}OH \longrightarrow HO{-}Si(OH)_2{-}O{-}Si(OH)_2{-}OH + H_2O}$$

N.B: Further condensation of non-hydrolysed precursors is also possible.

From the polycondensation process, colloidal particles and condensed silicas link together to form a silica glass network (Figure 1.3).

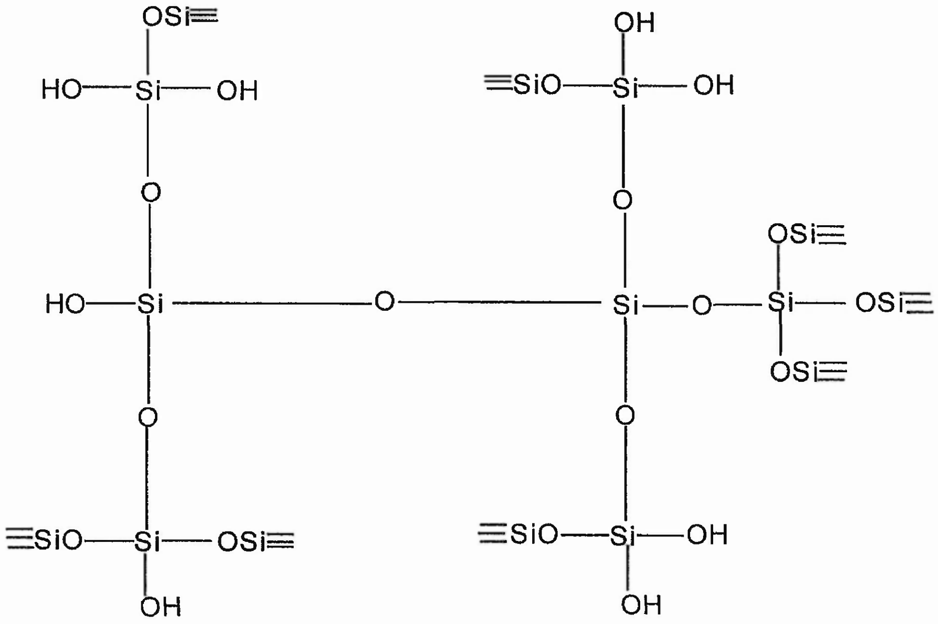

Figure 1.3: Formation of a silica glass network where OSi≡ refers to an individual silicon atom coordinated through oxygen to 4 other groups.

1.2.3.3- Aging

Once the gel has formed, chemical reactions continue in the aging period increasing the strength of the gel, which is necessary for drying and for thermal treatment.

Different forms of sol-gels can be made which include monoliths [7], thin films [12], fibres [13,14] and powders.

1.2.3.4- Drying

The gels are wet bodies. The removal of the solvent has to be done under controlled conditions (T°C, time). The liquid is removed from the interconnected pore network. Significant stress can occur resulting from inhomogeneous shrinkage.

1.2.3.5- Thermal treatment

The glass is thermally treated to obtain the desired material. The removal of surface silanols and pore water is necessary to obtain dense materials. The water can be found in two forms in the sol-gel:

1-*Physisorbed water*: Free water can be found within the gel structure. To remove it, dehydration of the gel at a temperature around 180°C is necessary. A dried gel still contains a very large concentration of chemically bound water.

2-*Chemisorbed water*: It corresponds to water bound to the hydroxyl groups (Si-OH) on the surface of the pores. Chemisorbed water is remove by thermally treating the glass at temperatures higher than 400°C (usually between 500-800°C).

The porous gel is heated at around 500-600°C to burn out residual organics [15], reinforce the strength of the glass and also to reduce the number of pores (densification). This densification process depends on the dimensions of the pore network and the surface area [16]. For a full densification, a temperature of 1100-1200°C is required.

Two types of monoliths can be prepared namely *aerogels* and *xerogels.*

Aerogels are prepared by removing the liquid within the gel above its critical temperature and pressure. Bockhorst et al. have used liquid CO_2 by static and dynamic purging in an autoclave [17].

Xerogels are produced by removing the liquid within the gel through simple evaporation.

During this project, xerogel monoliths were prepared and studied.

1.3- Pre-doped and Post-doped sol-gel materials

Porous sol-gel materials provide an excellent vehicle for the incorporation of secondary phases including metal ions and organic molecules.

The dopant can be introduced into the gel matrix either by adding the dopant during the mixing stage, incorporating it homogeneously into the gel as it forms which is called the *pre-doping method*, or by using the porous characteristics of the gel and impregnating the partially densified gel glass in an appropriate solution containing the dopant, known as the *post-doping method.*

In this project, the behaviour of the dopant in sol-gels produced by the pre-doping method was studied.

1.4- Absorbance Standards

In science, standards are necessary for calibration. Absorbance standards can be used at any absorbance level in the instrument's range.

Two types of absorbance standards exist: *liquid standards* and *solid standards*

1.4.1- Liquid standards

Liquid standards are used to check the entire working procedure (from the experimental solutions used to the apparatus). Providing that Beer's law is obeyed for the standard concerned, the use of solution standards can be used at any absorbance level in the instrument's range. This method utilises a reference blank.

The most commonly used standard for the UV region is potassium dichromate in sulphuric acid [18]. Inorganic compounds such as potassium nitrate can also be used as can organic compounds, including nicotine or acridine solutions [19].

The advantage of using a solution as an absorbance standard is that the procedure for its measurement resembles that of normal samples [20,21].

However the disadvantages of solution standards are that they do not have a high degree of coefficients than solid standards are required.

Moreover certain problems occur with these standards such as fluorescence, stray-light effects, absorption of water and bacterial growth which limit the suitability of these liquid standards.

1.4.2- Solid standards

Solid standards are used to check the absorbance accuracy of spectrophotometers without solutions. They are used to determine the intrinsic performance of the instrument. The standards currently used are glass standards [22] such as National British Standard glass filters [23,24]. Different type of solid standards can also be used such as metal screens which consist of woven wire screens [25]. Sector discs are also utilised. They use an optical chopper to attenuate the beam rather than an absorbing filter (for example a rotating disc with apertures of known size in it) [26]. Finally the last type of solid standards which can be used are metallic filters using a particular nichrom alloy without any cover glass [27]. These are however difficult to calibrate and are unstable with time, a decrease in transmittance with time being observed.

Solid standards are required which have a high transmittance and must be highly stable with time. The drawbacks of conventional glass neutral density filters are the fact that they cannot be used in the UV as absorbing glasses have a cut off edge just below the visible range. It was thought that the use of the sol-gel process could reduce this cut off to the ultraviolet region and hence enable the preparation of solid standards for use in this region of the electromagnetic spectrum.

1.5- Aims

The first aim of the project was concerned with the preparation and structural study of glassy sol-gel materials with potential application as absorbance standards in the UV region (230-350nm) of the electromagnetic spectrum. A method of drying the samples was developed in order to obtain materials with optimum transparency.

These materials were utilised to fine tune the absorbance behaviour of the dopant ions or molecules. Initial studies were carried out on the behaviour of the material produced with respect to long term stability.

The second aim of the project was to understand the extent and effect of molecular interactions on the spectroscopic behaviour of all components in the gel-glass composite. The structure of the components present (network, dynamic behaviour of surface versus bulk, defects and coordination chemistry) was investigated by UV/Vis, NIR, FTIR, NMR and EXAFS spectroscopy qualitatively and quantitatively .

An explanation of the interaction between the precursors and the dopant could then be proposed.

REFERENCES

[1] L.L.Hench, Ceramics International, **17**, 206, (1990)

[2] C.J.Brinker, K.D.Keefer, D.W.Schaefer, C.S.Ashley, J.Non-Cryst.Solids, **481**, 117, (1982)

[3] N.D.Koone, T.W.Zerda, J.Non-Cryst.Solids, **183**, 243, (1995)

[4] E.M.Rabinovich, *Processing Sol-Gel Optics,* (publisher Kluwer, London), 1, (1993)

[5] R.C.Mehrotra, *Spectroscopy and Applications of Sol-Gel Glasses,* (publishers Reisfeld & Jørgensen), **vol.1**, (1992)

[6] C.C.Perry, *Sol-Gel Technology-Sira Technology Center*, (1 day course, not published), (1998)

[7] L.L.Hench, J.K.West, Chemical Review, **90**, 33, (1990)

[8] C.J.Brinker, G.W.Scherer, *Sol-Gel Science*, (publishers Academic Press inc, London), (1990)

[9] R.Deshpande, D.M.Smith, D.J.Brinker, Mat.Res.Soc.Symp.Proc., **271**, 553, (1992)

[10] G.W.Scherer, Mat.Res.Soc.Symp.Proc., **271**, 527, (1992)

[11] Aldrich Material Safety Data Sheet, catalogue.number.681/845

[12] C.J.Brinker, C.J.Hurd, J.Non-Cryst.Solids, **121**, 294, (1990)

[13] S.J.Sakka, J.Non-Cryst.Solids, **121**, 417, (1990)

[14] A.R.Cooper, *Ceramic Processing Before Firing,* (publisher Wiley, London), 261, (1978)

[15] E.M.Rabinovich, D.W.Johnson, J.Am.Ceram.Soc., **66**, 688, (1983)

[16] W.Vasconcelos, R.T.Dehoff, *Processing of Ceramics, Glasses and Composites*, (publisher Tuscon), 2, (1989)

[17] M.Bockhorst, K.Heinloth, G.M.Pajonk, R.Begag, E.Elaloui, J.Non-Cryst.Solids, **186**, 388, (1995)

[18] D.Irish, *Standards in Absorption Spectrometry*, (publishers Chapman and Hall, London), **vol.1,** 48, (1981)

[19] G.Milazzo, S.C.M.Palumbo-Doretti, Anal.Chem., **49**, 711, (1977)

[20] C.Burgess, A.Knowles, *Standards in Absorption Spectrometry* (publishers Chapman and Hall, London), **vol.3**, (1981)

[21] O.Menis, J.I.Schultz, National British Standard Technical Notes, 544, (1970)

[22] J.A.Dobrowolski, G.E.Marsh, Appl.Opt., **11**, 594, (1990)

[23] K.S.Gibson, National British Standard Circular, 484,(1949)

[24] K.S.Gibson, M.M.Balcom, J.Res.Nat.Bur.Std., **38**, 601,(1947)

[25] P.A.Newman, R.Binder, Rev.Sci.Instr., **32**, 351, (1961)

[26] O.C.Jones, F.J.J.Clarke, Nature, **191**, 1290, (1951)

[27] F.J.J.Clarke, UV Spec.Gp.Bull., **5**, 104, (1977)

Chapter 2: Sample Preparation and Analysis

In this chapter, first the preparation of sol-gel samples is described, then information on the techniques used to analyse the samples are given.

2.1- Preparation of samples

2.1.1- The sol-gel preparation

Using the sol-gel process silica monoliths were prepared. Non-doped and doped silica gel glasses were made using tetraethylorthosilicate 98% (Aldrich) mixed with dry ethanol (distilled from 95% ethanol over magnesium) and stirred gently for a few seconds to obtain an homogeneous solution. Then, if required, the dopant was added. Finally, 0.5M HCl (prepared from 11.3M HCl (Fisher)) was added at the following molar ratio:

For normal sol-gels:

1 TEOS:4 EtOH:4 H_2O:0.045 HCl

For doped sol-gels:

The molar ratio was the same as above with the dopant either in the aqueous or ethanolic phase.

The solution was mixed at room temperature for one hour before being put (4ml) in polystyrene petri dishes (diameter 3.5cm, depth 1cm from Nunc) covered with Nesco film® in which 5 holes (0.6mm diameter) had been made before being placed in a fan assisted oven at 40°C to dry. The choice of this method is explained in section 2.1.2. For every type of sol-gel, a batch of 8 samples was simultaneously prepared.

Samples were weighed daily (%weight loss versus time was plotted). Statistical analysis using the student's t-test was performed in order to assess the significance of variations measured. When the weight had stabilised the matrix structure and silanol functionality were investigated using FTIR spectroscopy and the coordination chemistry of the dopant investigated using UV-VIS spectroscopy. Samples were investigated as dried pieces of glass immediately after dehydration by subjecting the samples to a vacuum pressure of 6mbar (measured by an Edwards Pirani 10 pressure sensor) for 18 hours, and after thermal treatment at 180, 500 and 800°C. A Carbolite programmable furnace was used, set to reach the desired temperature with ramped heating. More information about temperature profiles is given in section 3.2.

2.1.2- An investigation of drying methods

The usual method of drying the sol-gel samples is to leave them at room temperature which takes a long time (up to three months) in order to have monoliths with good strength and optical qualities which are able to resist thermal treatment.

For this project another method was necessary to reduce the time of drying and hopefully improve the optical quality (transmittance) of the material.

Three different methods were tested:

- The pinhole method
- The glass tube experiment
- The oven process [1,2]

2.1.2.1- Techniques for drying

2.1.2.1.1- Pinhole method

The pinhole method is mentioned in the literature [1] without any indication of the temperature control and the type of lid and number of holes in it. From this, the following method was created.

4 mls of normal sol-gel was introduced into petri dishes. Instead of using a lid, some Nesco film® was used. Different numbers (1 to 8) of holes were made (0.6mm in diameter using a needle). The samples were either left at room temperature or in a fan circulating oven at 40°C to dry.

2.1.2.1.2- Glass tube experiment

This method was created and developed in order to obtain a slow evaporation of the solvent.

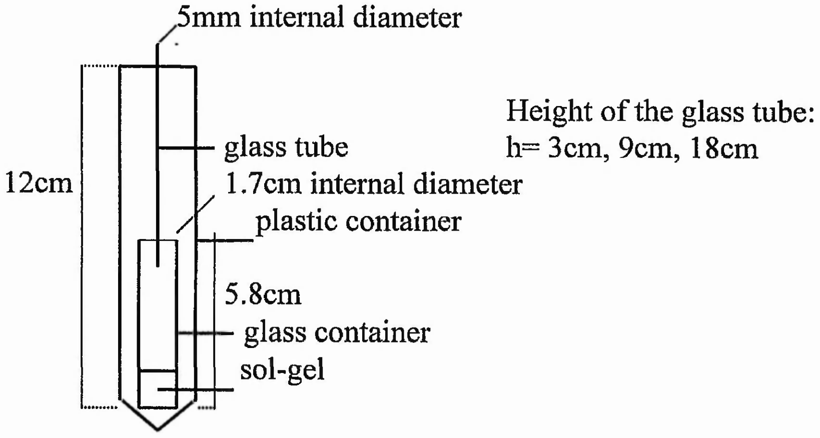

A normal solution of sol-gel was prepared.

The container above was used to store the samples and let them dry.

In the glass container 1.5ml of the sol-gel was placed.

A hole in the plastic lid was made in order that the glass tube went through.

The glass tubes had different lengths: 3cm, 9cm and 18cm, the tube having an internal diameter of 5mm.

This method allowed the study of the evolution of the sample according to the length of the tube and enabled us to monitor any change in the aspect of the sol-gel samples.

Also as the vapor pressure of ethanol varies with temperature, a series of tubes were placed in an oven at 40°C with others left at room temperature in the laboratory (24°C to 26°C).

2.1.2.1.3- Oven process

This method was derived from a method used in the literature [1, 2].

Normal sol-gels were prepared. 3ml and 4ml of the sol-gels were put in polystyrene petri dishes. Some samples were surrounded by Nesco film®, the others had just a normal lid without Nesco film®. The samples were put in the oven at 40°C and left to dry.

All the samples from the three different methods were weighed every day.

The blank sample used was a normal sol-gel (4ml) dried in a covered polystyrene petri dish at room temperature.

2.1.2.2-Results

	Average time of drying (days) to constant weight	**Sample cracking (8 samples measured)**	**Sample transparency**
Glass tube method at 40°C	3cm tube: 19 9cm tube: 22 18cm tube: 31	Cracked	Transparent
Glass tube method at RT	3cm tube: 27 9cm tube: 34 18cm tube: 49	Cracked	Transparent
Pinhole method	1 hole RT: 52 1 hole 40°C: 37 5 holes RT: 35 5 holes 40°C: 21	12.5 % cracked 25 % cracked 37 % cracked 50 % cracked	Transparent
Oven method	Nesco film®: 32 days No Nesco film®: 2 days	12.5% cracked 75% cracked	Transparent

Table 2.1: Drying behaviour of the sol-gel using different methods

Comparing the drying time required for the samples prepared with the three methods, it was observed that the samples in the oven were drying faster. The drying time at 40°C was 3-4 weeks compared with 7 weeks at RT. Above 40°C the samples dried too fast, a relatively slow process was necessary to obtain samples which were resistant to heat treatment. The sol-gels prepared need to have flat surfaces with no defects. The method which meets those requirements was the pinhole method with 5 holes with samples being placed in the oven at 40°C. With a lower number of holes the sample dried too slowly and with a higher number it dried too fast, having a curved shape with a lot of cracking (data not presented). To obtain a flat disc it was better to use 4ml (even 5ml) than 3ml of the starting solution for the preparation of the sol-gel.

Infrared analysis, although in principle should show differences in hydroxyl and associated H_2O in the sample, insufficient differences between the samples were observed in order to use this method.

UV-Vis analysis was done to compare the optical quality of the samples prepared by the three methods.

For all the spectra, the lamp change occured at 325nm.

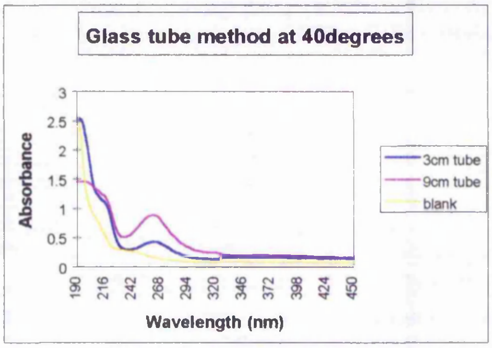

Figure 2.4: UV-VIS of normal sol-gels produced by the Glass tube method at 40°C.

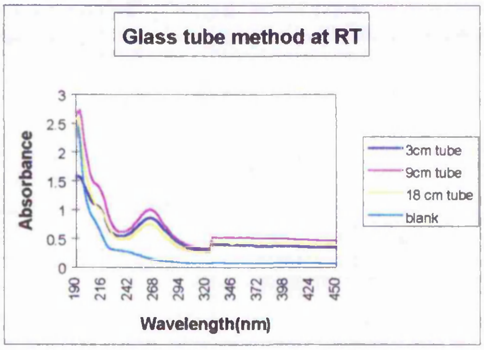

Figure 2.5: UV-VIS of normal sol-gels produced by the Glass tube method at RT.

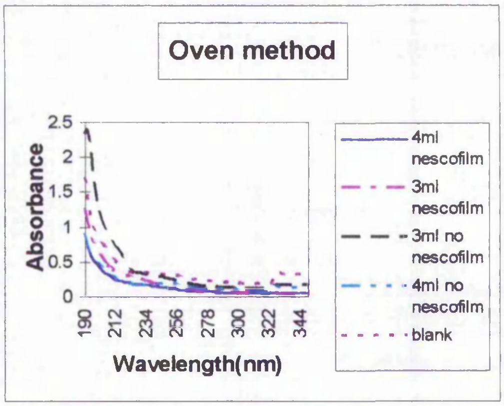

Figure 2.6: UV-VIS of normal sol-gels produced by the Oven method

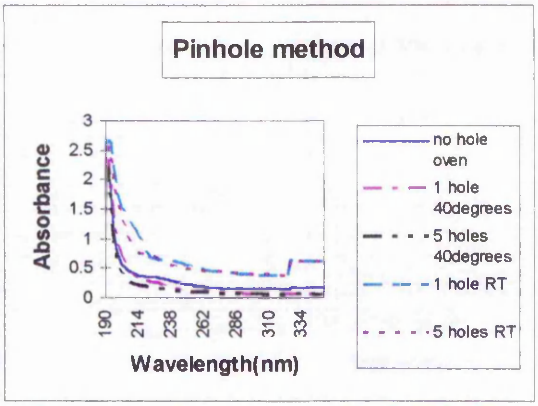

Figure 2.7: UV-VIS of normal sol-gels produced by the Pinhole method

The UV-Vis spectrum needs to have a high transmittance and its cut off has to be toward short wavelength (190nm-200nm). Using the glass tube method, a large peak around 260nm was observed (Figures 2.4, 2.5), most pronounced for sample prepared at RT.

It corresponds to ethanol present in the sample. So this method is not good as the solvent is not removed efficiently from the sample.

The oven method (Figure 2.6) gave the best results for 4ml of sample covered with Nesco film®.

The pinhole method (Figure 2.7) showed that the best results were obtained for samples with 5 holes dried at 40°C with an absorbance of 0.1 down to 190nm.

The transmittance cut off moved toward shorter wavelengths when the evaporation of the solvent was slowed down (longer tube for Glass tube experiment or presence of Nesco film® around the petri dishes for the Oven experiment) and when the sample was dried in the oven.

2.2.3-Conclusion

On comparison of the analyses performed on the samples, the best drying method was that created from the pinhole method with 5 holes at 40°C. These samples dried relatively quickly but not too fast, so there is time for the formation of a rigid network. The samples obtained were crack free and flat. The optical quality of the disc was good with a high transmittance and solvent was removed easily from the samples.

2.2-Techniques

In this section the different analytical techniques used are described including details of the instruments used and the methods of sample preparation for analysis.

2.2.1-UV-VIS

UV-VIS spectroscopy is used to study the transitions between atomic and molecular electronic energy levels. Both qualitative and quantitative analysis are possible.

2.2.1.1-Theory

There are three distinct wavelength regions.

Region	Wavelength range (nm)
Far UV-Vis	<200
Near UV	200-400
Visible	400-750

The Far UV-VIS region is also called the vacuum region. Gases are analysed below 185nm. The measurements can only be made using instruments in evacuated enclosures. When continuous radiation passes through a transparent material, a portion of the radiation may be absorbed. If that occurs, the residual radiation, when it is passed through a prism, yields a spectrum with gaps in it: the absorption spectrum [3].

When UV-VIS radiation encounters an atom or molecule, an increase in the energy of the electrons of the atom or molecule occurs [4,5].

If a molecule absorbs an appropriate amount of energy, an electron from an occupied orbital may be excited to an unoccupied or partially occupied orbital.

As the energies of the orbitals are quantized, it follows that each transition from the highest occupied molecular orbital (HOMO) to the lowest unoccupied molecular orbital (LUMO) often corresponds to the ultraviolet (UV) or visible region of the electromagnetic spectrum [6,7].

The molecular orbitals of a molecule may be bonding, non-bonding or anti-bonding. The bonding and anti-bonding orbitals may have σ or π (or other) symmetry.

For most molecules, the lowest energy occupied molecular orbitals are the σ orbitals, which correspond to the σ bonds. The π orbitals generally lie at higher energy.

The unoccupied or antibonding orbitals (π^* and σ^*) are the orbitals of highest energy.

Most organic compounds and inorganic ions absorb radiation in the UV-VIS region.

The spectrum of this absorption by a compound has a shape characteristic of the particular compound.

In the UV-VIS region data are normally presented in terms of wavelength.

E, the energy, is related to the frequency or the wavelength of the radiation.

Then $E=h\nu=hc/\lambda \cdot 10^9$

with ν= frequency (Hz), λ=wavelength (nm), c=velocity of light ($m.s^{-1}$),

h=Planck's constant (J.s)

The absorption spectrum obtained corresponds to all the different energy levels of a molecule with each electronic energy [8]. In a transition the electrons in an atom jump between a limited number of defined energy levels, subject to certain limitations called selection rules [9]. Transitions involving many electron excitations are usually forbidden [10].

When radiation travels through the solution of an absorbing compound it is reduced in intensity by each molecule that it encounters according to an exponential law: the Beer Lambert law. The amount of radiation absorbed by a solution is an exponential function of the concentration of the solution and the distance that the radiation passes through.

$$A=\varepsilon bC$$

A=absorbance (optical density)

b=optical path (cm)

C=concentration of the solution ($mol.l^{-1}$)

ε=molar absorptivity ($M^{-1}cm^{-1}$ also called the extinction coefficient)

2.2.1.2-Apparatus

For the analysis, the apparatus used was an ATS UNICAM UV2 series which has a double beam [11] (Figure 2.8).

The optical system is based around an Ebert monochromator using a 1200line/mm Holographic grating. The crucial optic components are the light source, the monochromator, the beam splitting system and the detector.

The UV series 2 spectrometer uses two sources to cover the wavelength range specified. The tungsten lamp is used in the visible region (350-1100nm) and the deuterium lamp in the UV region (190-350nm). Wavelength accuracy is achieved by software compensation. After leaving the monochromator the beam is directed into a beam splitter to produce the sample and the reference beams.

A detail explanation of the evolution of the instrumentation itself has been written by I.R.Altemose [12,13].

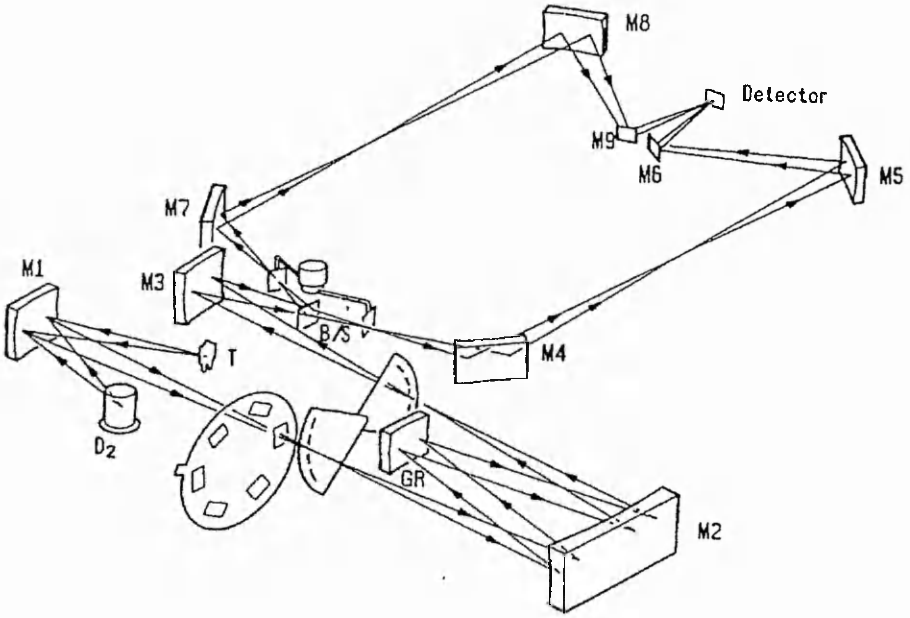

M1= motor driven mirror, Mn= mirror, T=Tungsten lamp, D_2= Deuterium lamp, GR=grating, BS=beamsplitter

Figure 2.8:Optical diagram of a UV Series spectrometer

The beam splitter sends most of the available energy down the sample beam. After passing through the sample compartment the beams are recombined and directed onto the detector. The detector is a photodiode detector which is a solid state detector made of doped crystalline silicon.

2.2.1.3-Sampling

The sample cell must be constructed of a material which is transparent to the electromagnetic radiation being used. For the visible region, cells of glass and plastics can be used but not in the UV as they absorb in this region. Quartz cuvettes are used for analysis below 350nm.

Liquid samples were analysed using quartz cuvettes (10 mm path length).

Solid samples (sol-gel glasses) were analysed in the bulk using a metallic holder supported with Blue Tack®. The thickness of the sol-gel glass was measured with a micrometer. An average thickness of 1mm±0.1mm was found which allow the comparison of the absorbance value between various sol-gel glass. Moreover as a double beam spectrometer was used, the reference sample was a normal sol-gel glass in order that the different effects observed on the spectrum were due to the dopant and not to the material itself.

2.2.2-Fourier Transform Infrared spectroscopy (FTIR)

FTIR techniques are used as a fingerprint technique to characterise a material. An IR spectrum records absorption of infrared radiation that is associated with the vibrational modes of molecules. Using this technique, quantitative and qualitative analysis can be carried out.

2.2.2.1-Theory

Infrared spectroscopy is a way of analysing substances using radiation in the infrared region (Table 2.1). FTIR is a simpler method than any dispersive method as there is only one moving part in the instrument used and the entire spectrum can be scanned in a few seconds or less [14] . Molecules are excited to a higher quantized energy state when they absorb infrared radiation. A molecule absorbs only selected frequencies of IR radiation which correspond to the range encompassing the stretching and bending vibrational frequencies of the bonds in most covalent molecules.

In the absorption process, the frequencies which match the natural vibrational frequencies of the molecule are absorbed and the energy absorbed serves to increase the amplitude of the vibrational motion of the bonds in the molecule.

Only bonds which have a dipole moment that changes as a function of time are capable of absorbing IR radiation. Most of the organic and inorganic compounds having covalent bonds will be found to absorb various frequencies of electromagnetic radiation in the infrared region of the spectrum [15].

Table 2.2: The different wavelength regions for FTIR analysis

	Wavenumber (cm^{-1})	Wavelength (nm)
FAR IR	700-10	14,286-100000
IR	4000-400	2500-25000
NIR	13,333-5000	750-2000

As for UV-VIS spectroscopy, molecules are excited to a higher state when they absorb infrared radiation.

Usually wavenumbers are used to describe any FTIR data.

There are different types of vibrational motion in a molecule which may be infrared active:

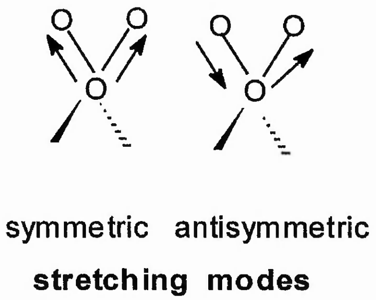

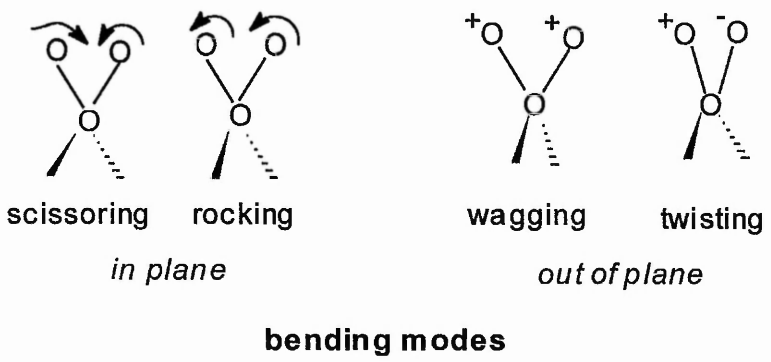

In general antisymmetric stretching vibrations occur at lower wavelengths than stretching vibrations and stretching vibrations occur at lower wavelengths than bending vibrations. Scissoring, rocking, wagging or twisting motions are commonly used to describe the origins of IR bands.

2.2.2.2-Apparatus

FTIR analysis has the advantages of unusually high sensitivity, resolution and speed of data acquisition as all wavelengths are detected and measured simultaneously. A higher signal to noise ratio can be obtained in comparison with other methods [16,17].

Various sampling methods can be used with FTIR such as diffuse reflectance, photoacoustic reflectance [18] as well as the transmission mode.

The key component for the FTIR spectrometer is the Michelson interferometer (Figure 2.9). The design of the optical pathway produces a pattern or interferogram. The Fourier Transform method then mathematically separates the individual absorption frequencies from the interferogram producing a spectrum virtually identical to that obtained using a dispersive spectrometer. Glasser gives a very detailed explanation of the FTIR technique [19,20,21]. The advantage of FT method over dispersive method is the acquisition of the interferogram in less than a second.

All the measurements were made with a Nicolet Magna IR^{TM} 750 spectrometer capable of up to 0.125 cm^{-1} resolution.

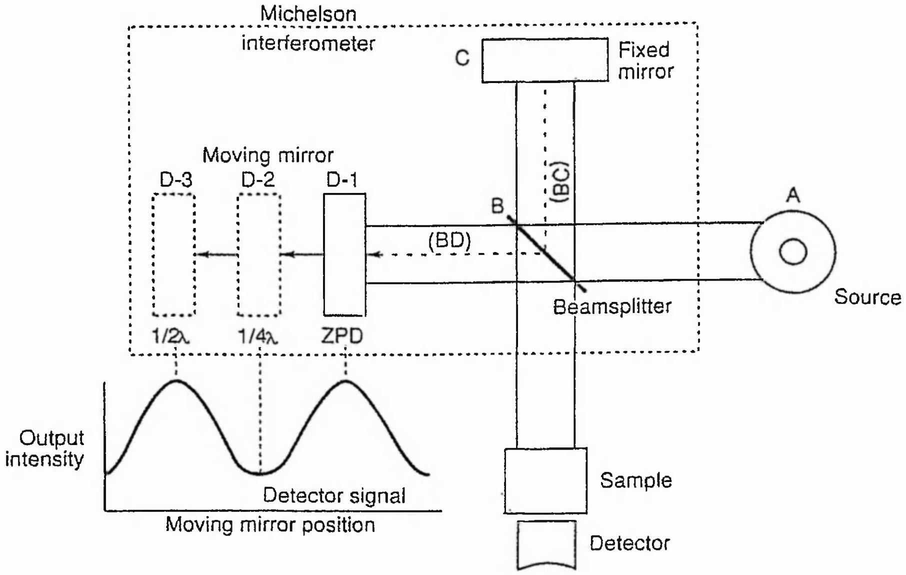

B=beamsplitter, C=fixed mirror, D=moving mirror, ZPD=Zero path difference.

Figure 2.9:Optical diagram of a FTIR spectrometer

2.2.2.3-Sampling

A KBr beamsplitter and DTGS detector were used in the mid IR region. Solid samples were prepared as discs mixed with KBr powder in known proportion and quantities to allow qualitative and quantitative analysis. Liquid samples and gels were analysed using NaCl plates.

For analysis in the NIR region a liquid nitrogen cooled InSb detector was used and the system purged to remove unwanted water. A KBr beamsplitter was used.

Bulk samples of glasses were analysed in the transmission mode.

Analysis in the FAR IR required the use of samples mixed with Nujol being placed on polyethylene discs. A solid substrate beamsplitter, a DTGS detector and the purge system were used to remove traces of moisture which interfere with spectral collection in this region.

Analysis was performed between 4000-400cm^{-1} for midIR, between 7000-4000cm^{-1} for NIR and between 700-50cm^{-1} for FAR IR spectroscopy.

2.2.3-Nuclear Magnetic Resonance Spectroscopy (NMR)

NMR gives information about the number of magnetically distinct atoms of the type being studied [22,23].

It allows us to determine molecular structure and to study the dynamic behaviour of species in solution and in the solid state.

2.2.3.1-Theory

Any atomic nucleus which possesses either odd mass number, odd atomic number or both has quantised spin angular momentum and a magnetic moment. For each nucleus with spin, the number of allowed spin states it may adopt is quantised and is determined by the nuclear spin quantum number I. In the absence of an applied magnetic field, all the spin states of a given nucleus are of equivalent energy and in a collection of atoms, all of the spin states should be almost equally populated with the same number of atoms having each of the allowed spin states. A nucleus with odd spin has 2I+1 possible orientations given by the value of the magnetic quantum number m (-I,-I+1,→+I).

However spin states are not of equivalent energy in an applied magnetic field as the nucleus is a charged particle and any moving charge generates a magnetic field of its own. The protons have their magnetic moments either aligned with the field or opposed to it. The nuclear magnetic resonance phenomenon occurs when nuclei aligned with an applied field absorb energy and change their spin orientation with respect to the applied field [24]. The nuclear magnetic moment (μ) is directly proportional to the spin.

$$\mu=(q/2m)\mathbf{I}$$

where q and m are the charge and mass of the particle.

The energy of interaction is proportional to the nuclear moment and the applied field.

$$E=-(\gamma h/2\pi)m_I B$$

where B is the applied field and γ the magnetogyric ratio (constant for each particular nucleus).

All spectral measurements and energy are in Hz and chemical shifts are given in ppm.

$$\nu=\gamma B/2\pi$$

where ν is the frequency of the applied radiation

For a nucleus of spin I=1/2 two possible orientations exist: $m_I=\pm 1/2$

$m_I=+1/2$ lower energy, more stable: α

m_I=-1/2 upper state, β

There are two allowed transitions: α→β absorption of energy

β→α induced emission

The NMR signal obtained is directly proportional to the number of nuclei producing it as long as the nuclei are allowed to relax back to their equilibrium distribution by spin-spin (T_2, sharing of excess spin energy directly between nuclei) and spin-lattice (T_1, excess spin energy equilibrates with the surroundings) relaxation pathways.

When a molecule containing the nucleus under observation is placed in the magnetic field, the electrons within the molecule shield the nuclei from the external applied field. The field at the nucleus is not equal to the applied field. The difference, which is the nuclear shielding, is proportional to the applied field.

The chemical shift is a function of the nucleus and its environment.

Nuclear magnetic resonance has a great utility because not all nuclei of one type in a molecule exhibit resonance at the same frequency owing to differences in chemical and magnetic environment.

Nucleus	**Spin**	**Resonance frequency (MHz) in field of 2.3487T**	**g value (Lange splitting factor)**
^{1}H	1/2	100	5.585
^{13}C	1/2	25.14	1.404
^{17}O	5/2	13.56	-0.7572
^{29}Si	1/2	19.87	-1.110

Table 2.2: Properties of some nuclei with non-zero spin [25]

2.2.3.2-Apparatus

^{29}SiNMR was used to monitor the presence of silicon containing species present in solution.

The apparatus used was a JEOL EX270MHZ NMR spectrometer operating at 53.54 MHz. 1000 scans were collected between 0 and -130ppm for every spectrum with an acquisition time of 1.488sec and a pulse delay of 6.5sec. The data were collected at -60.6°C in the NNE mode (Nuclear Overhauser enhancement (NOE)-eliminated ^{1}H complete decoupled measurement) with the negative nuclear overhauser effect suppressed by inverse-gated decoupling.

To analyse the data JEOL SpecNMR1.1 and GRAMS/32 software packages were used.

2.2.3.3- Sampling

^{29}SiNMR spectroscopy was performed on the reaction mixtures used to prepare doped and undoped sol-gels in order to identify the different silica species present in the system at certain times of hydrolysis and condensation. The samples were prepared at a molar ratio of 1TEOS: 4EtOH: 4H_2O: 0.045HCl with the dopant being either in the aqueous or ethanolic phase. Cerium doped sol-gels were prepared (from $CeCl_3.6H_2O$ Aldrich) at concentrations of 0.0897M-0.0128M-0.00128M for the metal ion in the sol-gel solution, as well as neodymium doped sol-gel (from $Nd(NO_3)_3.6H_2O$ Aldrich) with the concentrations between 0.128M and $1.28.10^{-7}$M for the metal ion in the sol-gel solution.

The samples were placed in liquid nitrogen at the required times to stop further reaction. Due to the long relaxation time of ^{29}Si a constant amount of chromium(III) $(acac)_3$ was added to the sample to shorten relaxation times. Spectra collected with/without the addition of $Cr(acac)_3$ were indistinguishable (data not presented).

The internal standard (in a 5mm diameter tube coaxially suspended in the sample to prevent any possible interaction with the sample) was a mixture of deuterated acetone with 25% TMS (tetramethylorthosilicate) as reference.

2.2.4- EXAFS

This technique allows the determination of the environment around a defined metal ion (coordination chemistry, type of ligands, bond distance) by comparison with a model system.

2.2.4.1-Theory

Extended X-ray Absorption Fine Structure (EXAFS) results from the oscillating variation of the X-ray absorption as a function of photon energy beyond an absorption edge [26,27]. The measurement of the attenuation of X-rays upon their passage through a material allows the determination of the absorption coefficient (μ). An abrupt increase in the absorption coefficient, the absorption edge, occurs when the X-rays photon energy (E) is tuned to the limiting energy of some core level of an atom type in the material.

The absorption coefficient decreases monotonically as a function of energy beyond the edge for isolated atoms whereas for atoms in a molecule, the variation of the absorption coefficient at energies above the absorption edge displays a complex fine structure (EXAFS) [28].

The absorption of an X-ray photon depends on both the initial and the final energy states of the electron. The initial state is the localized core level corresponding to the absorption edge. The final state is that of the ejected photoelectron which can be represented as an outgoing spherical wave originating from the X-ray absorbing atom. If the absorbing atom is surrounded by neighbouring atoms, the outgoing photoelectron wave will be backscattered by the neighbouring atoms consequently producing an incoming electron wave. The final state is the sum of the outgoing and all the coming waves, one for each neighbouring atom. It is the interference between the outgoing and the incoming waves that give rise to a sinusoidal variation of the absorption coefficient versus the X-ray photon energy.

As the photoelectron wave must travel from the absorber to the scatterer and back, the frequency of each EXAFS wave depends on the distance between the absorbing atom and the neighbouring atoms.

The photoelectron has a phase shift (Coulomb interaction) of the absorber twice (once going out and once coming back) and one phase shift of the scatterer (scattering). The interatomic distances in the vicinity of the absorber can be obtained from the phase shift. The amplitude of each EXAFS wave depends upon the number and the backscattering power of the neighbouring atoms as well as on its bonding to and distance from the absorber. EXAFS gives information about the environment. Each shell of equivalent neighbours gives rise to its own modulation. The overall magnitude of the wave is proportional to the number of the scatterers in the shell, while the shape of the envelope is characteristic of the atomic number of the scatterer and the relative motion of the absorber and the scatterer [29,30]. Following data analysis by absorption or fluorescence, the EXAFS function $\chi(K)$ was extracted and Fourier Transform method and Curve fitting were applied [31].

2.2.4.2-Experimental

EXAFS is most commonly used to determine the local structure around the excited atom type in amorphous solids, liquids and complex crystals.

The synchrotron radiation from the electron storage ring, represented not on the true scale by a broken ellipse at the upper corner of figure 2.10, is collected by a teroidal mirror and monochromatized by a double crystal monochromator (Figure 2.10).

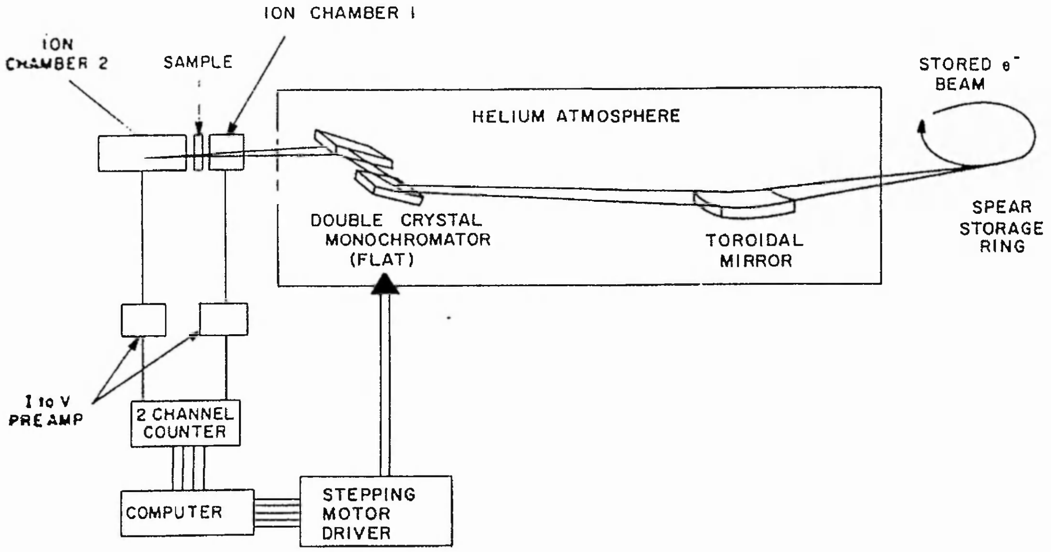

Figure 2.10: Synchrotron radiation apparatus in transmission mode.

The EXAFS measurements are made between 40-1000eV of the absorption edge. Near or below the edge, there generally appear absorption peaks due to excitation of the core electrons to some bound states.

The experiments were carried out using synchrotron radiation emitted by the storage ring at Daresbury running between 2-2.5GeV with an average current of 200mA on the 8.1 station. Si(III) crystal allows monochromotization of the incoming beam. The samples were mounted at 90° to the direct beam for transmittance mode and 45° for the fluorescence mode.

Spectra were obtained at room temperature for Nd L_{III}- edge energy.

The data were analysed using UNIX system connected on XSSERV1 with the software programs EXCALIB (calibration of the curve), EXBROOK (pre-edge background subtraction and normalisation of the EXAFS data) and EXCURV98 (analysis of the EXAFS data).

The data analysis resulted in a photoelectron scattering profile as a function of the radial distance from the absorber. The positions of the peaks are related to the distance between the absorber and the neighbouring atoms while the size of the peaks are related to the numbers and types of the neighbouring atoms.

2.2.4.3- Sampling

Nd^{3+} crystals were ground into a fine powder which was placed as a thin layer between two films of Sellotape® for analysis using the transmittance mode. 3 scans were recorded for every sample.

Nd^{3+} solutions were injected in a polycarbonate cell. The window was covered with Mylar film glued to the cell. For every sample, 4 spectra were recorded in the fluoresence mode.

Nd^{3+} sol-gels were analysed as monolith placed on a metallic holder. The spectra were collected in the fluorescence mode, 8 scans were necessary for every samples.

The evacuated sol-gel samples were covered with Sellotape® to prevent rehydration of the material.

For all the samples, the scans recorded were very noisy due to a lot of disorder around the metal ion.

2.2.5- X-rays analysis

2.2.5.1- Theory

The X-ray electromagnetic radiations are of the same nature as light but of shorter wavelength (0.5-2.5Å). Therefore the X-ray region is between gamma and ultraviolet rays in the electromagnetic spectrum. The electromagnetic radiation carries energy. The intensity (I) correspond to the rate of flow of the energy through unit area perpendicular to the direction of motion of the wave [32].

X-rays are produced when any electrically charged particle of sufficient kinetic energy is rapidly decelerated. The radiation is produced in an x-ray tube which contains a source of electrons and two metal electrodes. When the voltage on an X-ray tube is raised above a certain critical value, characteristic of the metal, sharp intensity maximum appear at certain wavelengths, superimposed on the continuous system. Since they are narrow and since their wavelengths are characteristic of the metal used. They are all characteristic lines form sets (K,L,M). X-ray diffraction can be considered in terms of reflection of X-rays by planes of atoms in a crystal. X-ray data of a material can give information about the unit cell and the atomic arrangement within the cell.

2.2.5.2- Experiment

Single crystal structure and powder XRD analysis were carried out on crystals. The single crystals were analysed on collaboration with Dr A.Slawin (Loughborough University). The instrument used was a Brucker Smart CCD system with MoKα (0.71073 Å) radiation and the data analysed were carried out using a commercial SHELXTL and powder X-ray diffraction using a Philips X50 diffractometer operating with CuKα (1.5418 Å).

References

[1] C.J.Brinker, K.D.Keefer, J.Non-Cryst.Solids, **48**, 47, (1987)

[2] A.Duran, C.Serna, V.Fornes, J.Non-Cryst.Solids, **82**, 69, (1986)

[3] D.L.Pava, G.M.Lampman, G.S.Kriz, *Introduction to Spectroscopy*, 2nd edition, (publisher Harcourt Brace College, London), (1996)

[4] D.Thorburn, *UV Spectroscopy*, (publisher B.J.Clark, London), 4, (1993)

[5] O.Howarth, *Theory of Spectroscopy*, (publisher Nelson, London), (1973)

[6] K.S.Gibson, National British Standard Circular, 484,(1949)

[7] K.S.Gibson, M.M.Balcon, J.Res.Nat.Bur.Std., **38**, 601, (1947)

[8] A.Knowles, *Practical Absorption Spectrometry*, (publisher Chapman and Hall, London), **4**, (1984)

[9] O.Howarth, *Theory of Spectroscopy*, (publisher Nelson), (1973)

[10] C.N.R.Rao, *Ultraviolet and Visible Spectroscopy*, 2nd edition, (publisher Butterworth, London), (1975)

[11] UNICAM, UV Series 1, issue 4, (1995)

[12] I.R.Altemose, J.Chem.Educ., **63**, 9, (1986)

[13] E.Lesley, L.E.Locke, I.R.Altemose, J.Chem.Educ., **63**, 11, (1986)

[14] K.Nakamoto, *IR and Raman Spectra of Inorganic and Coordination Compounds*, 3rd edition, (publisher Wiley, New York), (1978)

[15]H.Ishida, *FTIR Characterisation of Polymers*, (publisher Plenum press, New York), (1987)

[16] W.D.Perkins, J.Chem.Educ., **63**, 1, (1986)

[17] W.D.Perkins, J.Chem.Educ., **64**, 11, (1987)

[18] W.D.Perkins, J.Chem.Educ., **64**, 12, (1987)

[19] L.Glasser, J.Chem.Educ., **64**, 10, (1987)

[20] L.Glasser, J.Chem.Educ., **64**,11, (1987)

[21] L.Glasser, J.Chem.Educ., **64**, 12, (1987)

[22] E.Ehsworth, D.Rankin, S.Cradock, *Structural Methods of Inorganic Chemistry*, (publication Blackwell scientific, London), (1987)

[23] D.L.Pavia, G.M.Lampman, G.S.Kritz, *Introduction to Spectroscopy*, 2nd edition, (publisher Harcourt Brace college, London), (1996)

[24] R.J.Abraham, J.Fisher, P.Loftus, *Introduction to NMR Spectroscopy*, (publisher John Wiley, New York), (1988)

[25] C.N.Banwell, E.R.McCash, *Fundamentals of Molecular Spectroscopy*, 4th edition, (publisher McGraw-Hill, London), (1997)

[26] B.K.Teo, *EXAFS Spectroscopy Techniques & Applications*, (publisher Plenum Press, New York), (1981)

[27] E.A.Sterm, *EXAFS Spectroscopy Techniques & Applications*, (publisher Plenum Press, New York), (1981)

[28] S.P.Cramer, K.O.Hodgson, Prog.Inorg.Chem., **25**, 1, (1979)

[29] R.L.Kronig, Z.Phys., **70**, 317, (1931)

[30] R.L.Kronig, Z.Phys., **75**, 191, (1932)

[31] S.J.Gurman, J.Synchrotron Rad., **2**, 56, (1995)

[32] B.D.Cullity, *Elements of X-ray Diffraction*, 2nd edition, (publisher Addison-Wesley, London), (1978)

Chapter 3: Effect of Dopants on the Drying Process of Sol-Gel Glasses

3.1-Introduction

Glasses have been conventionally prepared by high temperature methods [1] but the use of the sol-gel process enables the preparation of porous or dense glasses with superior homogeneity, purity and good optical qualities (high transmittance) at significantly lower temperatures [2]. Moreover this method of glass preparation offers a large variety of high purity glasses as a great number of synthetic chemical precursors is available compared to more conventional sources for ceramic materials.

Wide applications using sol-gel materials can be found with optical, chemical and electrical functionalities.

Sol-gel materials provide an excellent vehicle for the incorporation of secondary phases including metal ions, organic molecules and macromolecules. These species may be doped into the gel-matrix as it is being formed (*pre-doping*) or incorporated after the glass has been prepared (*post-doping*). During this work the *pre-doping* method has been used with Nd^{3+} ions and Ce^{3+} as the dopant.

In order to form a sol two main chemical reactions are involved: *hydrolysis* and *condensation* reactions [3,4,5].

Several studies on the dynamics of the early stage of the hydrolysis and condensation reaction have been reported.

The condensation reaction of monosilicic acid prepared by hydrolysis of TMOS was studied by Engelhart [6]. Hanis [7] and Hench [4] reported investigations of aqueous solutions of silicates for sol-gel glass formation. No comparison was done between silica precursors and silica precursors doped with inorganic ions.

Brinker and Scherer [5] have shown that the drying process of the sol-gel and then the formation of the glass depend on the precursors used to form the sol-gel, on the catalyst and the solvents. James [8] explained that the chemistry prior to gelation greatly influences the character of the glass and consequently the drying process.

Bernards [9] has worked on the gelation point using a new characterisation method for silica sol-gel systems (hydrolysis versus gelation time) and studied how gelation is affected by different types of precursors, catalysts, solvents etc...

Extensive investigations have been reported [10] concerning the relation between the hydrolysis time in the acid step and gelation time in the basic step in the two step SiO_2 sol-gel process (effect of hydrolysis temperature, solvent, catalyst concentration).
The kinetics and mechanisms of hydrolysis and condensation reactions prior to the gel point have also been studied by Atlenburg et al. [11].
^{29}Si NMR has also been extensively used to understand hydrolysis and condensation reactions. Pouxviel [12] studied the different stages of hydrolysis reaction of precursors, Assink and Kay [13-15] also investigated the kinetics and mechanisms of hydrolysis and condensation reactions. Jonas [16] and Artaki [17-19] have also studied the effect of pressure, solvents and temperature on polymerisation kinetics. The work of Öye [20] has shown however, that the metal ions can affect gelation times as experiments performed with $Ni(NO_3)_2.6H_2O$ and $Ca(NO_3)_2.4H_2O$ as dopants showed that gel formed with Ni^{2+} as the dopants had the fastest hydrolysis rate (FTIR spectroscopy data). An investigation in this area was continued using the rare earth metal ions Nd^{3+} and Ce^{3+} ions as dopants. The effect of the metal ion was investigated on the bulk properties of the glasses (transmittance, drying times) and then the possibility of interaction was investigated between the dopant and the gel matrix at different stages during the formation of the sol-gel derived glasses.

3.2- Methods

3.2.1-Sol-gel preparation and drying experiments

Using the sol-gel process silica monoliths were prepared.
Non-doped and doped silica gel glasses were made using tetraethylorthosilicate 98% (Aldrich) mixed with dry ethanol (distilled from 95% ethanol over magnesium) and stirred gently for few seconds to obtain homogeneous solutions.
Then, if required, the dopant was added. Finally, 0.5M HCl (prepared from 11.3M HCl (Fisher)) was added in the following molar ratio:
For normal sol-gels:
$1TEOS:4EtOH:4H_2O:0.045HCl$
For doped sol-gels:
The molar ratio was the same as above with the dopant either in the aqueous or ethanolic phase at a range of concentrations from 10^{-6} M to 1M in the initial solutions (water or

ethanol) with $Nd(NO_3)_3.6H_2O$ (Aldrich) and 0.7M to 0.01M with $CeCl_3.6H_2O$ (Aldrich) used as the dopant.

The solution was mixed at room temperature for one hour before being put (4ml) in petri dishes (diameter 3.5cm, depth 1cm from Nunc) covered with Nesco film® in which 5 holes (0.6mm diameter) had been made before being placed in a fan assisted oven at 40°C to dry. For every different type of sol-gel, a batch of 8 samples was prepared at the same time. Samples were weighed daily (%weight loss versus time was plotted). Statistical analysis using the students t-test was performed on the data obtained in order to assess the significance of variations measured.

The concentration of the dopant when mixed with the precursors in the sol-gel solution was calculated.

The %weight of dopant in the glass was calculated using an average weight of the dry sol-gel and the number of moles of metal ions used to prepare the glass. No statistical variation was observed in the calculation of the concentration of Nd^{3+} in the glass as the weight of the glass only varied of ±0.003g.

Table 3.1: Nd^{3+} concentrations in solution, in the sol-gel solution, in the glass

Concentration of Nd^{3+} in solution (mol/l)	**Concentration of Nd^{3+} in the sol-gel solution (mol/l)**	**%weight of Nd^{3+} in the glass**
1	0.1282	9.48
0.6	0.0769	5.69
0.3	0.0385	2.844
0.1	0.01282	0.948
0.05	0.00641	0.474
10^{-2}	$1.283.10^{-3}$	0.0948
10^{-3}	$1.283.10^{-4}$	$9.48.10^{-3}$
10^{-4}	$1.283.10^{-5}$	$9.48.10^{-4}$
10^{-5}	$1.283.10^{-6}$	$9.48.10^{-5}$
10^{-6}	$1.283.10^{-7}$	$9.48.10^{-6}$

Table 3.2: Ce^{3+} concentrations in solution, in the sol-gel solution, in the glass

Concentration of Ce^{3+} in solution (mol/l)	**Concentration of Ce^{3+} in the sol-gel solution (mol/l)**	**%weight of Ce^{3+} in the glass**
0.7	0.0897	8.99
0.1	0.0128	1.283
10^{-2}	$1.28.10^{-3}$	0.1283
10^{-3}	$1.28.10^{-4}$	$1.283.10^{-2}$
10^{-4}	$1.28.10^{-5}$	$1.283.10^{-3}$

3.2.2-FTIR Analysis

FTIR analyses were carried out on the sol-gel samples in order to obtain two types of information. MidIR gave information about the structure of the sol-gel matrix and NIR about the presence of water and how it was bonded to the matrix.

The sol-gel matrix was analysed at different stages of formation, as a solution, during the various stages of the silica network formation, and as a piece of glass when the silica network had completely formed.

3.2.2.1-During the drying process

The matrix structure and silanol functionality were investigated at different times of the drying process using FTIR spectroscopy with a Nicolet Magna IR^{TM} 750 spectrometer capable of up to 0.125cm^{-1} resolution. In our case a 4cm^{-1} resolution was used in a range between 4000cm^{-1}-400cm^{-1} with a KBr beamsplitter and DTGS detector. 64 scans were collected for every spectrum.

For liquid or viscous sol-gels, NaCl plates were used on which a droplet of known volume of the sample was placed. For gels or dry materials KBr discs were prepared.

During the formation of the silica matrix and the removal of the excess solvent, 3 different samples showing the same %weight loss, were analysed.

NIR spectroscopy was performed between 7500-3500cm^{-1} (resolution 4cm^{-1}) using a liquid nitrogen cooled InSb detector and KBr beamsplitter. A purge of air was turned on one hour prior to the experiment and kept on during the analysis in order to avoid any contamination from water vapour in the air.

3.2.2.2-During the silica matrix formation

FTIR of the sol-gel solutions was recorded during the first hour of reaction at regular intervals for normal sol-gels and Nd sol-gels with the following concentrations of Nd^{3+} in the sol-gel solution: 0.00128M-0.0128M-0.128M.

%weight was not used to indicate concentration as the samples were not dry. A sol-gel solution was prepared (as explain in paragraph 3.2.1) then at a defined time after the start of the experiment, 5μl of the solution was pipetted and placed between NaCl plates which were introduced in a beaker to avoid contamination from the liquid nitrogen. The beaker was then immersed in liquid nitrogen for 30 seconds to stop further reaction. In order to have reproducible results the experiment was done several times (between 4-6 times) for each type of sol-gel and each time point of the reaction. The spectrum of the sample was recorded at a resolution of $4cm^{-1}$ in a range between $4000cm^{-1}$-$400cm^{-1}$ with 40 scans using a Nicolet Magna IR^{TR} 750 spectrometer.

In order to interpret the spectra, the spectra of the precursors (TEOS and dry ethanol) were recorded as well.

The intensity of the bands corresponding to the precursors, to the silica network formation and to the presence of water were measured (using the OMNIC software) and plotted (EXCEL).

3.2.3-Gelation experiment

To study the gelation point and the influence of Nd^{3+}/Ce^{3+} ion on the establishment of the structure in the sol-gel glass, the hydrolysis/gelation experiments were carried out by Bernards [9] were set up, although the molar ratio for the preparation of the sol-gel was not the same as used by these workers.

The aim of this experiment was to hydrolyse the precursors for a set time under acid conditions (t_H) and to introduce a base and then to record the time when the solution gelled t_G (time of gelation). To study the gelation point a solution of ammonia 35% (Fisher) was used mixed with dry ethanol with the following molar ratio: $3NH_3$: 2EtOH

Normal sol-gels and doped sol-gels were prepared with the molar ratios used for the preparation of sol-gel monoliths described in section 3.2.1.

In this experiment, the concentration of the metal ion referred to was the concentration corresponding to the metal ions in the sol-gel solution.

First the precursors were mixed together in 50ml sealed plastic falcon tubes at a time t=0. Then the ammonia solution was added to the precursors after a time of hydrolysis t_H at a molar ratio of 3TEOS:1NH_3.

When the solution was completely gelled, it was possible to invert the tube with no movement of the gel, the time of gelation t_G was recorded.

For every hydrolysis time (t_H), the experiment was repeated 10 times on the same day to avoid problems due to variation of temperature. Statistics were applied on the data using the Student t-test with an allowed error of ±5%.

Throughout all the experiments, a variation of temperature of 20±3°C was observed.

3.2.4-^{29}SiNMR measurements

^{29}SiNMR spectroscopy was performed on the reaction mixtures used to prepare doped and undoped sol-gels in order to identify the different silica species present in the system at defined times of hydrolysis and condensation. The samples were prepared at the molar ratio of 1TEOS: 4EtOH: 4H_2O: 0.045HCl with the dopant being either in the aqueous or ethanolic phase. Cerium doped sol-gels were prepared (from $CeCl_3.6H_2O$ Aldrich) at concentrations of 0.0897M-0.0128M-0.00128M for the metal ion in the sol-gel solution, as well as neodymium doped sol-gel (from $Nd(NO_3)_3.6H_2O$ Aldrich) with the concentrations between 0.128M and $1.28.10^{-7}$M for the metal ion in the sol-gel solution.

The samples were placed in liquid nitrogen at the required times to stop further reaction and analysed using a JEOL EX270MHZ NMR spectrometer operating at 11.013 KHZ. 1000 scans were collected between 0 and -130ppm for every spectrum with an acquisition time of 1.488sec and a pulse delay of 6.5sec. The data were collected at -60.6°C in the NNE mode (NOE-eliminated ^{1}H complete decoupled measurement) with the negative nuclear overhauser effect suppressed by inverse-gated decoupling. Due to the long relaxation time of ^{29}Si a constant amount of chromium(III) acetylacetone was added to the sample to shorter relaxation times. Spectra collected with/without the addition of $Cr(acac)_3$ were indistinguishable (data not presented).

The internal standard (in a 5mm diameter tube coaxially suspended in the sample to prevent any possible interaction with the sample) was a mixture of deuterated acetone with 25% TMS as reference. Chemical shifts are reported as ppm downfield from TMS.

3.2.5-pH measurement of gelling system

All measurements were made with a PHM93 pH meter (Radiometer Copenhagen) with a combined antimony electrode which was not affected by the sol-gel mixture. The discrepancy of the pH-meter was ± 0.02 units.

The pH of solution was measured for various solutions of TEOS, ethanol and Nd^{3+} ions (1M-10^{-2}M).

Normal and doped sol-gels were measured. The samples were prepared as described in section 3.2.1. After every series of measurements, the electrode was placed in a buffer at pH 7 to stabilise it.

For every system, three separate runs were performed to validate the measurements.

3.2.6-Measurement of the water present around the metal ion using the Karl Fisher technique.

A Karl Fisher experiment was carried out on $Nd(NO_3)_3.6H_2O$ and $CeCl_3.7H_2O$ (Aldrich) in solution in order to determine the exact number of water ligands in the inner sphere of the metal ion or more exactly to know if the water ligands around the metal ion stay covalently bonded or react with the environment when in solution (ethanol/ water).

The technique was used as described by Skoog et al. [21] and a Model 602 Karl Fisher apparatus from Analysis Automation Ltd, Oxford was used. The apparatus was thoroughly dried to avoid any contamination from moisture in the air. For the titration, a Karl Fisher reagent (from Fisher) was used. The solvent, dry ethanol, was titrated in case of the presence of water in the solvent which could have been caused by absorption of water vapour from the air. Then a calibration of water was done. Finally neodymium solutions in methanol and dry ethanol were titrated. The titrations were repeated until a minimum of three results were obtained with a discrepancy of ±2%. Measurements on Ce^{3+} containing solutions were not carried out.

3.3-Results and Discussion

3.3.1-Studies of sol-gel glasses during the drying process

3.3.1.1-Results

When salts of neodymium were used in the formulation to produce doped sol-gels they affected the rate at which the weight of the gel matrix stabilised (figure 3.1)

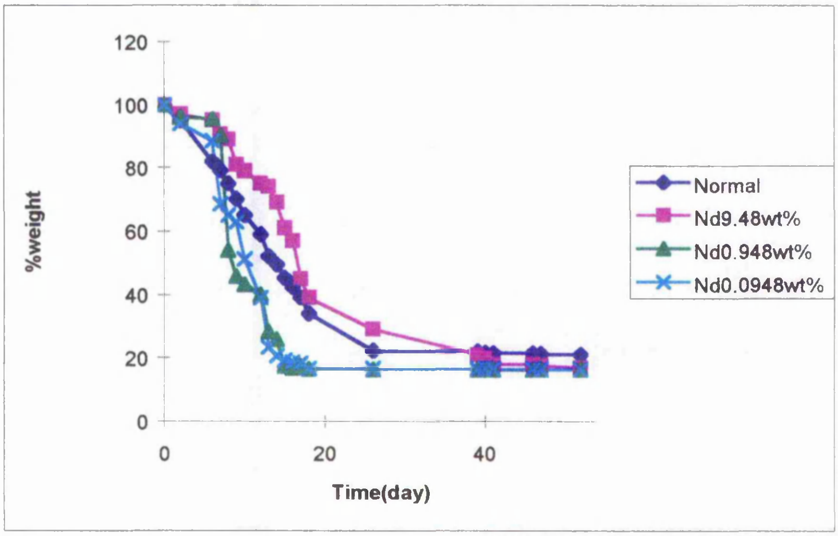

Figure 3.1.a

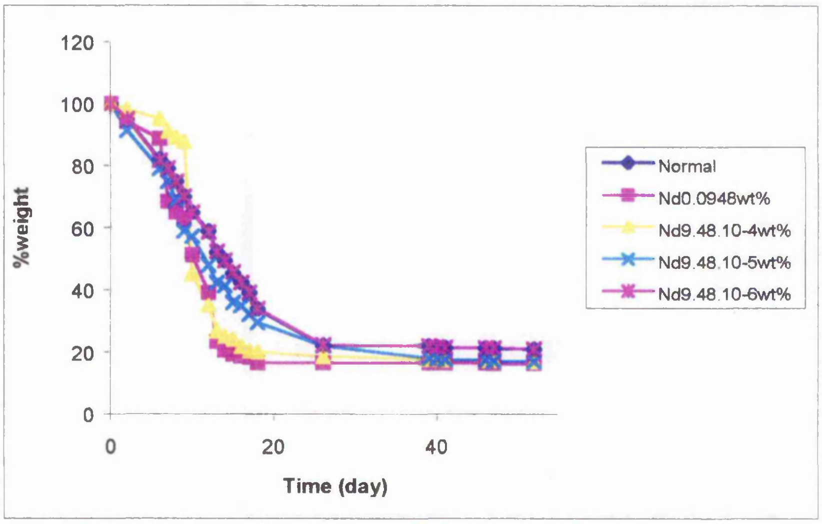

Figure 3.1b

Figure 3.1.a.b:The effect of neodymium on the time taken for weight stabilisation for undoped and doped sol-gel

An average of 8 samples was used for every type of sol-gels. Statistical analysis was carried out using the student t-test. The calculation can be found in Appendix 1.

The data point represented on the figures 3.1 correspond to the average mean value of the %weight of the sample at different drying times.

Similar behaviour was observed if the salt solutions were added to the alcoholic phase rather than the aqueous phase.

Normal sol-gels showed an essentially linear weight loss during the first period of drying (up to 19 days), the matrix was formed and the solvent removed, followed by a slower transition to a stable weight. During the slower transition, the excess solvent in the gel was removed to obtain samples with a stable weight.

For doped sol-gels regardless of the concentration of the dopant used (from $9.48.10^{-4}$ M to 9.48wt%) the weight loss showed three different stages. During the first period (up to 10 days for 9.48wt%). the weight loss was slower than for undoped sol-gels, the matrix started to be formed. Due to the dopants the solvent could be retained by the structure because of the solvation of the additional cations and anions in the system. After 8-10 days the weight loss was rapid, the elimination of the residual solvent quick.

At $9.48.10^{-5}$wt%, the drying behaviour of the doped sol-gel was very similar to that of the normal sol-gel An approximately linear weight loss was observed followed by a stabilisation of the weight.

The weight of the doped sol-gels stabilised quicker than for undoped sol-gels. Below a certain concentration ($9.48.10^{-5}$wt%) the dopant did not affect the sol-gel during the drying process and especially the removal of the solvent.

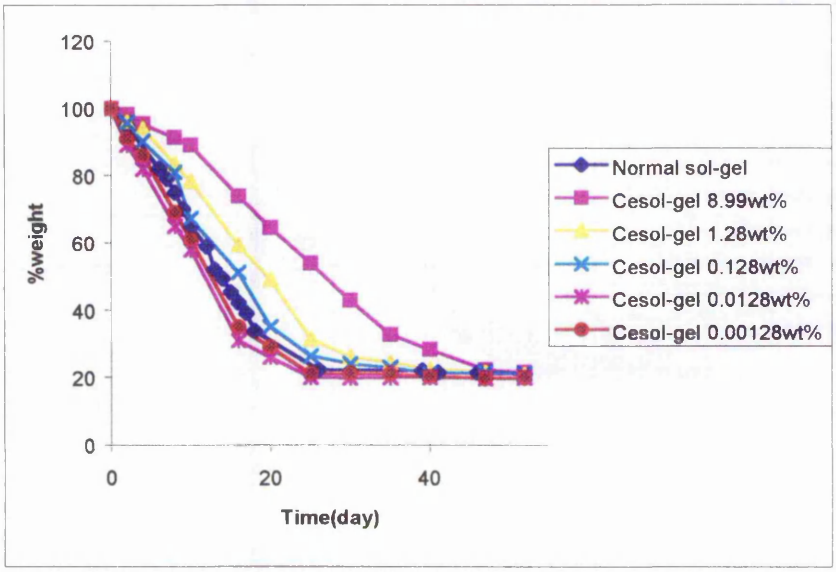

Figure 3.1.c: The effect of cerium on the time taken for weight stabilisation for undoped and doped sol-gels.

In the presence of cerium, the sol-gel glasses took longer to dry. Two stages were observed for the drying process of normal sol-gels. A linear decrease was observed for around 19 days followed by a period of time with a slower weight loss. After 25 days, the samples were dry. In the presence of Ce^{3+} as the dopant, the sol-gel showed a three stage drying process. A slow weight loss was observed for a few days at the beginning of the drying process, followed by a linear weight loss and finally a stabilisation of the weight after 38-40 days. The effect of the dopant decreased as the concentration of the dopant in the sol-gel was reduced. With a %weight of $1.28.10^{-3}$, the drying process of the doped sol-gel became similar to the drying behaviour of normal sol-gel.

3.3.1.2.Discussion

Both cerium and neodymium ions have an effect on the drying process. As observed, their effect is different from one another and according to their concentrations in the sol-gel. While with neodymium ion only highly doped sol-gels showed a slower drying rate than for normal sol-gels, the drying rate was slowed down in the presence of cerium regardless of its concentration in the glass, although this effect was very little at Ce^{3+} wt% concentration of ca.$1.28.10^{-3}$wt%.

The presence of the metal ions affected the rate of drying of the gel-silicas suggesting a direct interaction between the gel matrix and the metal ions themselves. Consequently the hydrolysis and condensation reactions which occur during the formation of the sol-gel matrix may have been affected by the dopant. The presence of the dopant also affected the stabilisation of the structure and the loss of solvent to the environment. In the drying process, gelation corresponds to the time when the colloidal particles and condensed species link together to become a three dimensional network [6]. The primary particles are formed by polycondensation which favours closed clusters of tetrahedra rather than linear chains. After gelation the sample dries which means that there is expulsion of liquid from the pores of the samples increasing the number of bridging bonds and causing contraction of the gel network [23]. The slow progressive loss of weight observed corresponds to the partial elimination of the remaining solvent in the pores of the gel.

To know if the presence of the dopants had affected the structure of the dry glass, FTIR analysis were carried out.

The UV-VIS spectra of the doped and undoped sol-gels presented in chapter 4 show that the dopant has an effect on the transmittance and the UV cut off. In essence, it was observed that the presence of metal ion tends to reduce the transmittance and moves the cut off toward longer wavelengths.

3.3.2-FTIR studies of the development the sol-gel matrix

Previous studies using FTIR [23-28] have been carried out during the sol-gel process for making silica. The sol-gel process was monitored during its early stages and during the formation of the silica glass network in order to detect any effect of the metal ion on the silica matrix.

3.3.2.1-Studies on the dry sol-gel glasses by midIR and NIR

3.3.2.1.1-Results

The changes in the gel network at the molecular level caused by the presence of the neodymium salt solutions present in the gelation medium are shown in the midIR spectra (Figure 3.3). For every midIR and NIR spectrum, 3 samples were analysed for every sol-gel which gave consistent results in intensity and shapes of the bands.

Table 3.3 gives the FTIR values of the different chemical groups present in the dry sol-gels [29,30].

Wavenumber(cm^{-1})	Group
3500-3450	-OH (H bonded)
2976	methyl asymmetric stretch
2940	-CH_3 stretching
2897	methyl symmetric stretch
1677	$\delta(H_2O)$
1465	-CH_2-(bend)
1381	-CH_3 (bend)
1335	-O-H (bend)
1275	C-O (stretching)
1160	C-OH (stretching)
1200	δ_{as}(Si-O-Si) LO
1100	δ_{as}(Si-O-Si) TO
970	$_{vs}$(Si-OH)
880	$_{vs}$(SiO) oxygen stretching, bending frequencies
809	$_{vs}$(Si-O-Si)
550	O-Si-O(LO) bending
450	O-Si-O(TO) bending

Table 3.3: FTIR values of the different chemical groups present in the dry sol-gels.

A good explanation of the transverse optic (TO) and longitudinal optic (LO) modes is given by Galeener and Lucorsky [31].

The optical modes represent motions of the ions relative to one another in the same cell or rotations of the group within the unit cell, in our case in the amorphous silica.

TO corresponds to a transverse mode in which the average electric vector k is perpendicular to the direction of periodicity of the wave in the reciprocal lattice. k is also called the crystal momentum. [32]. LO corresponds to the longitudinal mode and is a complementary set whose average electric field is completely parallel to the direction of periodicity. Longitudinal modes resonate at zero of ε (complex dielectric function of the medium) (Figure 3.2).

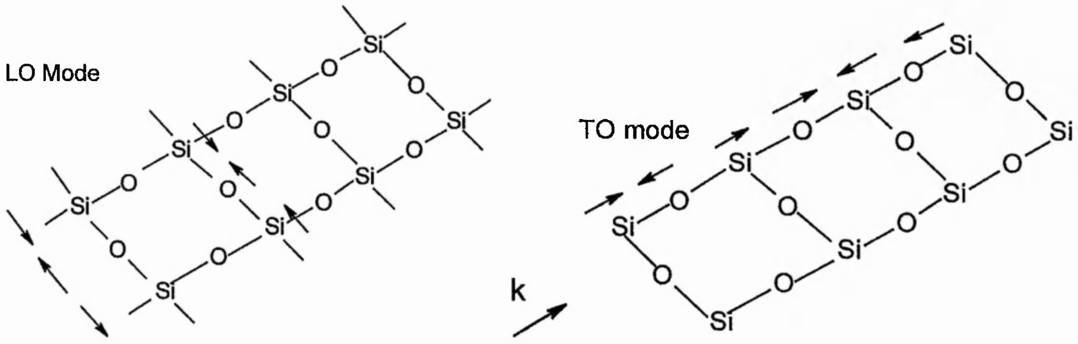

Figure 3.2: Longitudinal and transverse optic modes.

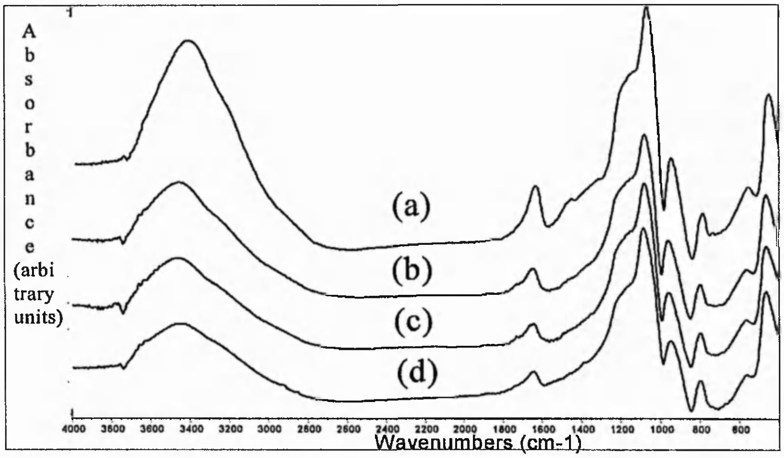

Figure 3.3: FTIR spectra of doped and undoped sol-gels prepared from $Nd(NO_3)_3.6H_2O$ dried at 40°C, a) 9.48wt% of metal salt in the sol-gel, b) 0.948wt% of metal salt in the sol-gel, c) $9.48.10^{-2}$wt% of metal salt in the sol-gel, d) Normal sol-gel

The silica network exhibited bands at ca. $1100cm^{-1}$ (antisymmetric Si-O-Si stretch, transverse optic mode, with the shoulder at ca. $1200cm^{-1}$ arising from the longitudinal optic mode), ca. $980cm^{-1}$ (SiOH), ca. $800cm^{-1}$ (symmetric Si-O-Si stretch) and ca. $470cm^{-1}$ (Si-O-Si bending). In addition, bands at ca. $3400cm^{-1}$ and ca.$1640cm^{-1}$ arise from hydroxyl groups associated with the silica.

Low %weight of the dopant phase (below $9.48.10^{-3}$ wt%) did not appear to show any gross effects on the molecular character of the gel phase. At %weight of $9.48.10^{-2}$ and above significant differences in the intensity and shapes of the bands were observed in comparison with the spectrum from a normal sol-gel.

First an increase in the band ($550cm^{-1}$) was noticed due to longitudinal O-Si-O bending. An increase in the hydroxyl functionalities associated with silica ($3400cm^{-1}$ and $1640cm^{-1}$) were also observed [33]. The band at $3400cm^{-1}$ was narrower for doped sol-gels whereas for normal sol-gels the band was much broader involving the presence of several types of hydroxyl functionalities (free or bonded to the matrix). Both will exhibit several types of OH groups with the normal sol-gel having more numerous varieties of them. When the relative intensity of the bands at $1100cm^{-1}$ and at $970cm^{-1}$ were compared between normal and doped sol-gels, an increase in intensity of the $1100cm^{-1}$ band was noticed and a decrease of the $970cm^{-1}$ band was noticed for doped sol-gels. This shows a larger presence of TO(SiOSi) rather than (SiOH). In the presence of the dopant fewer hydroxyl groups were present in the system. Moreover for doped sol-gels, the presence of LO(SiOSi) bonds was more characteristic and the shoulder at 1200cm^{-1} was broader.

To confirm the presence of neodymium ions in the matrix, FTIR measurements were performed on $Nd(NO_3)_3.6H_2O$ in ethanolic solution and in powder form supplied by Aldrich.

In solution, bands arising from ethanol overlap with the bands arising from nitrate ions but when the powdered form of $Nd(NO_3)_3.6H_2O$ was analysed it was possible to identify the bands characteristic of nitrate ions (Figure 3.4). The bands at 730cm^{-1} and at 530cm^{-1} correspond respectively to the νNd-OH$_2$ rocking mode and the νNd-OH$_2$ wagging mode [34,35].

The band at 832cm^{-1} is characteristic of the free nitrate ion and the band at 820cm^{-1} of coordinated nitrate ions [37]. We observed a band at 821cm^{-1} which corresponds to the nitrate ion in the outer coordination sphere of the metal ion. The bands at 1385cm^{-1} and at 1450cm^{-1} were characteristic of the NO_3^- symmetric stretching mode of $Nd(NO_3)_3$ [37]. The band at 1620cm^{-1} and the broad band at 3400cm^{-1} corresponded to the water ligands in the inner coordination sphere of the metal ion.

A series of small bands were present for highly doped sol-gels (9.48wt%) between 1400-1250cm^{-1} and at 715cm^{-1} which were characteristic of nitrate groups [38] probably associated with the neodymium ions.

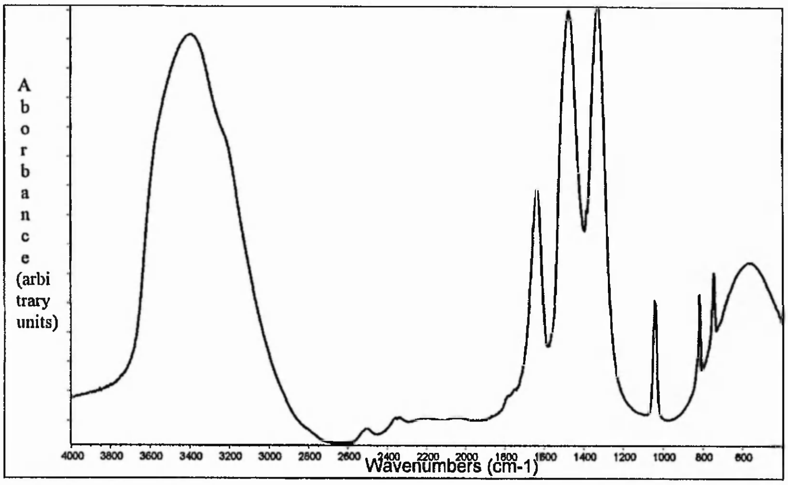

Figure 3.4: FTIR of $Nd(NO_3)_3.6H_2O$ from Aldrich

From these first experiments, we can definitely see that the dopant has an influence on the sol-gel matrix.

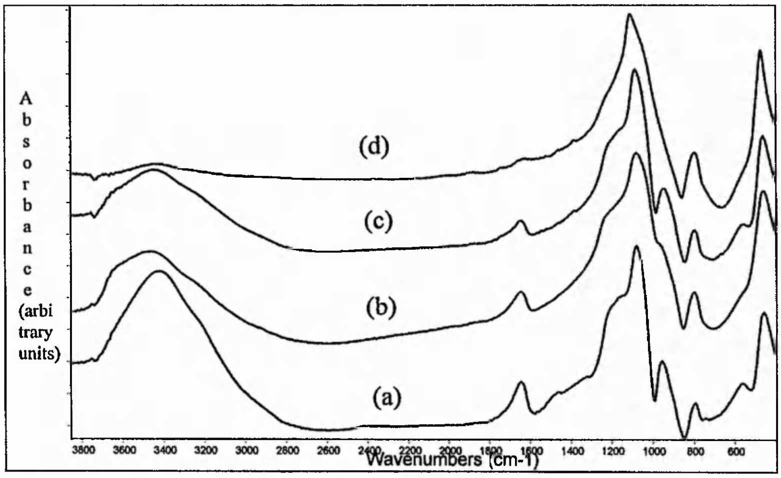

Figure 3.5: FTIR spectra of doped and undoped sol-gels ,
a) Nd(NO$_3$)$_3$ .6H$_2$0 9.48 wt% sol-gel dried at 40°C, b) heated to 800°C,
c) Normal sol-gel dried at 40°C, d) heated to 800°C

When the normal sol-gel sample was heated (Figure 3.5d) the bands due to Si-OH groups, -OH and H$_2$O disappeared (dehydration of the samples) as well as the band corresponding to the OSiO bending (550cm^{-1}) in favour of the SiOSi bending at 450cm^{-1}.
In the case of the doped sol-gel (Figure 3.5b), the dehydration was only partial with the presence of hydroxyl functionalities in the heated gel. A shoulder at 970cm^{-1} was observed corresponding to the $_{vs}$(Si-OH) bonds as well as the bands arising from -OH and H$_2$O functionalities. A small shift of the band at 3400cm^{-1} was observed confirming the partial dehydration (perhaps suggesting that predominately only one type of water species had been removed). Moreover when the normal sol-gel was heated, the (Si-O-Si) species with a LO mode increased as the band arising from the TO mode before treatment had slightly shifted toward a higher wavenumber and was broader.
In Nd sol-gel, after heat treatment, the bands characteristic of nitrate were no longer detectable. NO$_3^-$decomposed at these temperatures.

NIR spectroscopy was carried out in order to look at the water functionalities and consequently detect the presence of the metal ion within the matrix. Several similar studies have been done [29,30,39,40] in order to understand the structure of sol-gel matrices.

By this method we hoped to gain complementary information on the effect of the dopant on the matrix structure.

This method allows us to monitor the behaviour of surface structural OH groups and absorbed water molecules on the silica sol-gel in the presence or absence of the dopant [41].

The different bands (figure 3.7) were assigned according to the literature [22,29,30,41-43]:

Wavenumbers (cm^{-1})	Groups
7333	First overtones of the stretching modes of SiOH and H_2O. Combination with fundamental symmetric stretching mode of the silica network at 800cm^{-1} $_{2vOH}$(SiOH, free), (H_2O, monomer)
7143	Combination of symmetric and antisymmetric OH stretching vibration of water (isolated water molecules hydrogen bonded to silanol groups)
5285	Combination of stretching and deformation vibration for H_2O shoulder $_{vOH}$(H_2O,M) $+_{\delta}$(H_2O,M)
4405	Combination of stretching vibration for SiOH with a contribution from the bulk matrix $_{vOH}$(SiOH,H) $+_{vs}$(SiOSi)

The NIR spectrum of $Nd(NO_3)_3.6H_2O$ powder from Aldrich was run.

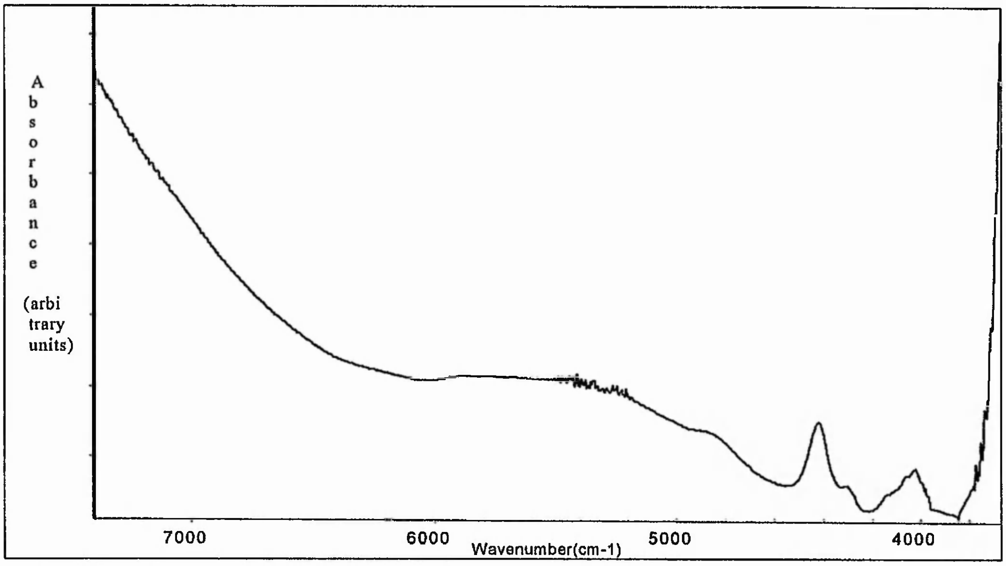

Figure 3.6: NIR spectrum of $Nd(NO_3)_3.6H_2O$ powder from Aldrich

From figure 3.6, the two sharp bands observed at 4000cm^{-1} and 4400cm^{-1}, and the broad band observed at 5400cm^{-1} corresponded to various combination and deformation vibrations of H_2O contained in the powder.

The band at 4000cm^{-1} corresponded to H-bonded water coordinately bonded to Nd^{3+} metal ion. The band at 4400cm^{-1} corresponded to a combination of stretching vibrations coming from the water group bonded to the metal ion. The water molecules in the powder were both bonded to the metal ion and in polymeric clusters. This explained the presence of a broad band at 5200cm^{-1}.

Spectra of doped and undoped samples were obtained (Figure 3.7).

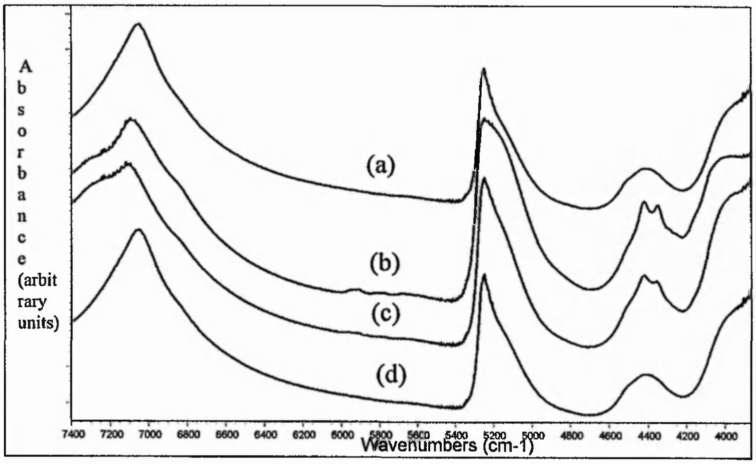

Figure 3.7: NIR spectra of doped and undoped sol-gels dried at 40°C
a) Normal sol-gel, b) Nd9.48wt% sol-gel, c) Nd0.948wt% sol-gel,
d) Nd9.48.10^{-6}wt% sol-gel

The spectrum of normal sol-gel (figure 3.7) showed three distinct sets of bands. The increasing slope below 4100cm^{-1} corresponded to an equilibrium in air which produced water

H-bonded to surface SiOH groups [42]. The first band which is broad, was observed at 4424cm^{-1} and corresponds to a combination of the stretching vibration for SiOH with a contribution from the bulk matrix.

A shoulder was noticed which is due to the presence of water molecules hydrogen bonded to one another [22]. Perry et al. [29, 30] proposed a slightly different assignment for this band and suggested a combination of fundamental OH stretching of free SiOH groups with the fundamental symmetric stretching mode of the silica network at 800cm^{-1}.

The band at 5285cm^{-1} is characteristic of a combination of stretching and deformation vibrations from water. The band is sharp for normal sol-gels indicating that the majority of water groups are free.

Finally a band was observed at 7143cm^{-1} which corresponded to a combination of symmetric and antisymmetric OH stretching vibrations of water.

When the spectrum of a normal sol-gel was compared to the spectrum of Nd doped sol-gel, the presence of the dopant had an effect on the OH groups present in the system.

At a high concentration of Nd^{3+} (9.48wt%), instead of the broad band at 4424cm^{-1} observed for the normal sol-gel, two bands at 4350cm^{-1} and 4445cm^{-1} were observed with a shoulder and a possible broad band hidden by the two sharper bands. These two last bands are characteristic of the stretching vibrations of SiOH. As the concentration of the dopant in the sol-gel decreased (down to 0.948wt%), the intensity of the bands decreased to become a broad band as observed for normal sol-gels.

Moreover the band at 4350cm^{-1} could be characteristic of $Nd(NO_3)_3.6H_2O$. The NIR spectrum of $Nd(NO_3)_3.6H_2O$ as powder (figure 3.6) showed a low intensity band at 4350cm^{-1}. In the sol-gel, the intensity of this band decreased as the concentration of the dopant in the sol-gel decreased.

In the presence of the dopant, several types of $_{vs}$(MOM) might be present in the matrix suggesting a possible bonding between the Nd^{3+} ion and the matrix.

Moreover the band at 5285cm^{-1} was very sharp with a broad shoulder for Ndsol-gel (9.48wt%). This shoulder decreased as the concentration of the dopant decreased. The shoulder was not observed in the normal sol-gel.

As the band at 5285cm^{-1} arose from water molecules hydrogen bonded to silanol groups, the increase of the shoulder corresponded to an increase in the amount of water molecules. These water molecules were not bonded to silanol groups, as an increase in intensity of the band would have been noticed, but are bonded to another metal ion which is Nd^{3+} confirming the presence of Nd^{3+} in the matrix.

Finally, the last band at 7143cm^{-1}, in the presence of dopant, appeared as two distinct bands at 7333cm^{-1} and at 6900cm^{-1}. The shoulder at 7333cm^{-1} is a combination of the first overtones of the stretching modes of SiOH and H_2O. The increase of this band in the presence of Nd^{3+} metal ion, showed an increase of water (which has been already shown by midIR studies). This band decreased as the concentration of the metal ion decreased.

Moreover a shift (50cm^{-1}) toward longer wavelength was observed in the presence of a high concentration of dopant (9.48wt%) in the sol-gel. Both vicinal free OH groups and isolated free OH groups contributed to the band at 7143cm^{-1}. The observed shift means that more vicinal free OH groups were present in the matrix which could be due to the presence of the dopant.

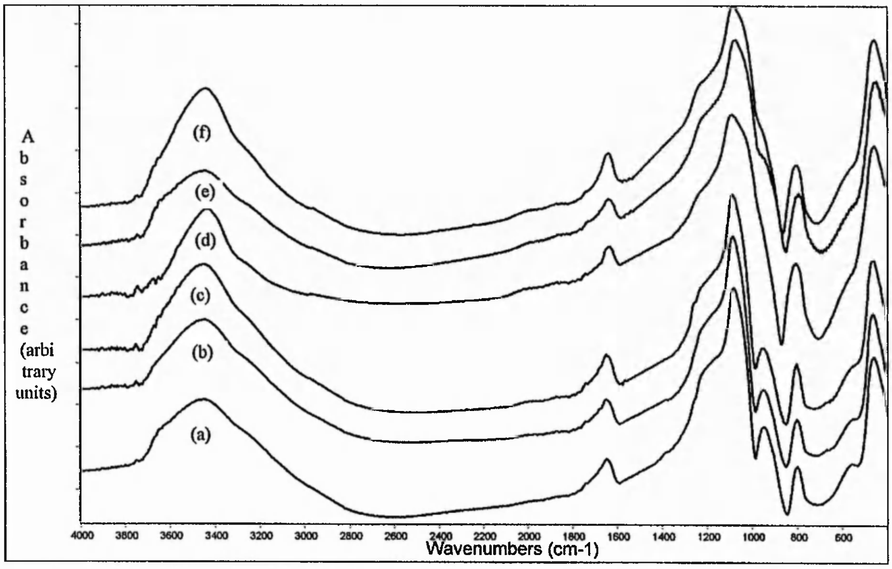

Figure 3.8: FTIR spectra of doped and undoped sol-gels,a) Normal sol-gel dried at 40°C b) $CeCl_3.6H_2O$ 8.99wt% sol-gel dried at 40°C, c) $CeCl_3.6H_2O$ 0.128wt% sol-gel dried at 40°C, d) Normal sol-gel heated to 800°C, e) $CeCl_3.6H_2O$ 8.99wt% sol-gel heated to 800°C, f) $CeCl_3.6H_2O$ 0.128wt% sol-gel heated to 800°C

In comparison with normal sol-gels, the presence of Ce^{3+} metal ion in the sol-gel matrix did not seem to have an effect on the matrix structure. The only difference observed was a broadening of the band at 3550cm^{-1} in the presence of the metal ion in the silica matrix. However when the samples were thermally treated, differences in the structure were observed between doped and undoped sol-gels. The band at 3550cm^{-1} was broader and a shoulder at 970cm^{-1} was observed.

This corresponds, as it has already been observed with Nd^{3+}, to only a partial dehydration of the silica matrix, whereas with normal sol-gels dehydration is more complete on heating to 800°C.

Ce^{3+} ions were present in the matrix and their effects on the hydroxyl species could be observed but unlike material prepared with Nd^{3+} ions and NO_3^- ions it was not possible to detect the Cl^- ligands associated with the metal ion.

3.3.2.1.2-Discussion

MidIR spectroscopy has been used to confirm the influence of the dopant on the silica matrix as changes in the structures were observed (LO and TO modes increase, hydroxyl functionalities decrease).

These results suggest that the dopant could be bonded to the OSi bonds forming Nd-O-Si linkages with a consequent decrease in the level of -OH groups.

The hydroxyl functionalities were studied more in depth using NIR spectroscopy.

In the presence of the dopant, different types of overtone and combination bands were observed in NIR which corresponded to different molecular vibrations in the midIR. Consequently the OH groups and adsorbed water molecules came from more than one molecular group when the glass was doped. Some of the water molecules could have come from the ligands of the Nd^{3+} metal ion.

The spectroscopic changes observed suggested a molecular interaction between the gel-glass and the metal ions.

To know if this interaction occurs during the drying process or as soon as the precursors have been mixed together further infrared studies were performed.

3.3.2.2-Study of the drying process of sol-gels by midIR

3.3.2.2.1-Results

The samples were measured each day in order to study the evolution of the structure during the drying process. This study showed distinct structural development according to the presence and concentration of the metal ion or not.

Figures 3.9.a and 3.9.b represent the development of the structure from sol-gel solution until dried as represented for a normal sol-gel.

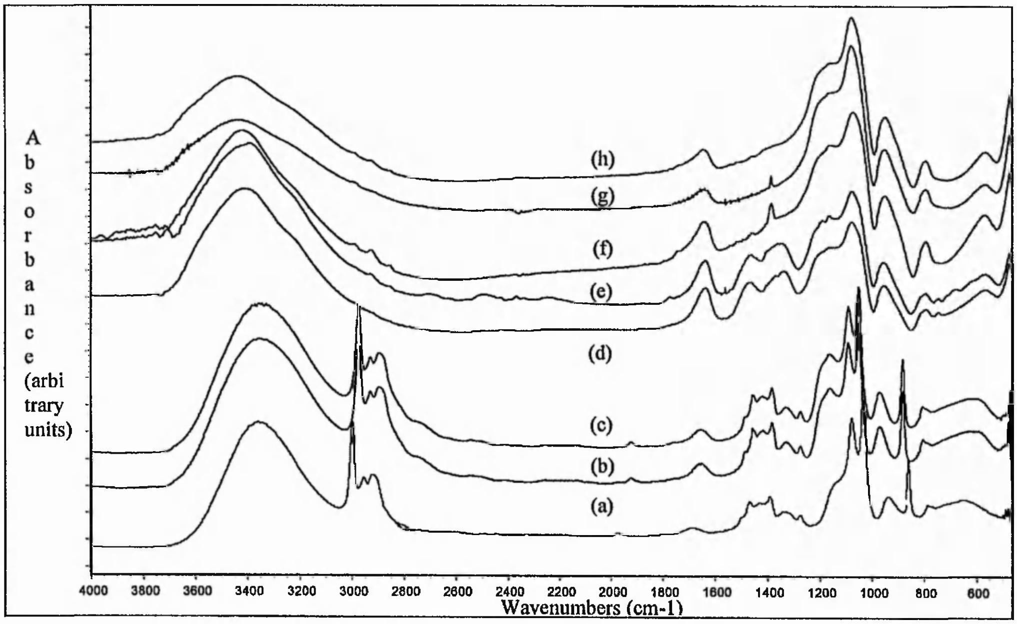

Figure 3.9.a: The structure development of normal sol-gel during the drying process, a) as soon as the precursors have been mixed together-**Stage 1**, b) after 1 day of drying, c) 4 days, d) 5 days-**Stage 2**, e) 6 days, f) 7 days-**Stage 3**, g) 10 days, h) 15 days

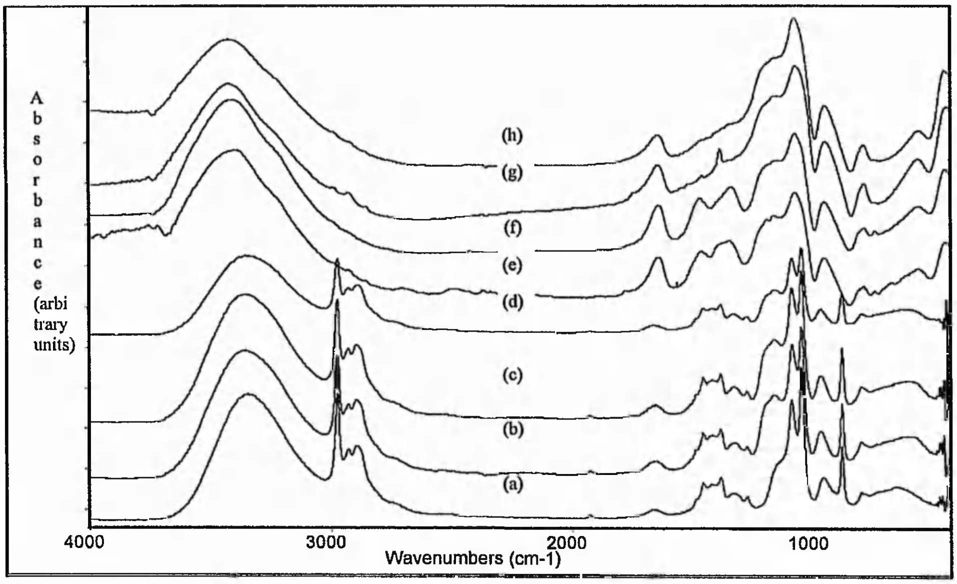

Figure 3.9.b: The structure development of Ndsol-gel solution (0.128wt%) during the drying process, a) soon as the precursors have been mixed together-**Stage 1**, b) after 1 day of drying, c) 3 days, d) 4 days, e) 5 days-**Stage 2**, f) 6 days, g) 7 days-**Stage 3**, h) 18 days

Stage 1 refers to the structure in the initial stage. The sol-gels had been put in the oven to dry, the solvent had started to evaporate but it was still present in the system, and copolymerisation was occurring. The spectrum contained bands arising from the precursors, TEOS and ethanol, (see Table 3.4). The solution started to gel with a slow formation of the matrix.

Table 3.4 gives the FTIR values of the different chemical groups present in the precursors [44,45].

Wavenumbers(cm^{-1})	**Groups**
880	skeletal vibration(from EtOH)
1050	CO stretching vibration (EtOH)
1111	SiOC asymmetrical stretching vibration (TEOS)
1167	SiOSi rocking (TEOS)
1275	CH twisting, Wagging in CH_2 (TEOS, EtOH)
1416,1324	-OH in plane bending coupled with CH, wagging in CH_2 (from EtOH)
1381	symmetrical CH bending vibration in CH_3 (TEOS, EtOH)
1446	asymmetrical CH bending vibration in CH_3 (TEOS, EtOH)
2892	symmetrical CH stretching (TEOS, EtOH)
2930	asymmetrical CH stretching vibration in CH_2 (TEOS, EtOH)
2974	asymmetrical CH stretching vibration in CH_3 (TEOS, EtOH)

Table 3.4: FTIR values of the different chemical groups present in the precursors.

At Stage 2 the sol had been aging for several days, the structure of the matrix was slowly forming. A decrease or partial absence of the bands characteristic of carbon containing compounds mostly was observed (bands between 1275cm^{-1} and 2974cm^{-1}). The excess of solvent started to be removed. The structure of the matrix with its characteristic peaks appeared. At the same time the appearance of bands characteristic of Si-O-Si, Si-OH bonds (between 800cm^{-1} and 1200cm^{-1}) corresponding to the silica network was apparent.

At stage 3 the matrix was nearly formed. The final structure was observable. Bands characteristic of the 3D-network were observed together with a decrease of the bands from the solvent (3500cm^{-1}, 1650cm^{-1}) which is a lot slower when the matrix has formed as the solvent is trapped in the pores. At this stage the silica network has formed and most of solvent has been removed.

In order to follow the development of the structure from sol-gel solution until dry sol-gel, the weight loss of the doped and undoped sol-gel was monitored prior to FTIR analysis. For every %weight of each type of sol-gel, three samples were analysed with consistent results.

	Stage 1 **weight of the sol-gel solution (%)**	**Stage 2** **weight of the sol-gel solution (%)**	**Stage 3** **weight of the sol-gel solution (%)**
Normal sol-gel solution	100%→65% 1→5 days	65% 6 days	below 63% 7 days
Ndsol-gel solution: **0.128wt%**	100%→71% 1→4 days	71%→66% 5 days	below 65% 7 days
0.0128wt%	100%→70% 1→4 days	70%→63% 6 days	below 62% 7 days
0.00128WT%	100%→70% 1→5 days	70%→65% 6 days	below 62% 7 days
1.128.0^{-5}M	100%→70% 1→5days	70%→65% 6 days	below 61% 7 days

Table 3.5:Evolution of the structure with time. The word 'days' corresponds to the number of days since the samples had been prepared.

Table 3.5 shows the evolution of the silica structure with time. The structure of the sol-gel is dependent on the time of drying. An effect on the time of drying necessary to have structural formation of the silica network was observed with Nd^{3+} ion in the sol-gel in comparison with normal sol-gel.

In the presence of the dopant at high concentration (0.128wt%), the formation of the silica matrix (stages 2 & 3) was quicker than with normal sol-gel or doped sol-gel at low concentrations (below 0.0128wt%). Moreover the high concentration doped sol-gel losses weight slower than the other type of sol-gels which was shown when the drying process was studied (Figure 3.1). Differences in the structure of the sol-gel was noticed during this period of time (from 100wt% to 70wt%).

The decrease of the band at 880cm^{-1} (EtOH band) and the increase of the band at 980cm^{-1} (SiOH) was faster in normal sol-gels than in Ndsol-gel (0.128 wt%). The same behaviour was observed for the bands between 1050cm^{-1} and 1200cm^{-1} characteristic of the formation of the silica network. Then after this first period, the structure formation of the sol-gel was faster in the presence of dopant.

At the beginning of the drying process, the doped sol-gel took longer to lose some weight but the formation of the silica matrix was quicker as Stages1 and 2 were observed earlier in the drying process than for normal sol-gels.

For lower concentrations of the dopant (below 0.0128wt%), the time taken for the silica matrix to form became similar to normal sol-gels as the concentration of the dopant decreased.

3.3.2.2.2-Discussion

By studying the evolution of the structure with time, the dopant affects the formation of the matrix and the rate of the removal of the solvent.

In principal it could be expected that all doped samples would behave in an identical fashion with the solvent being retained by the structure because of the solvation of the additional cations and anions in the system. This perhaps is the effect observed at the start of the drying period for the doped sol-gels. However, this behaviour was not observed throughout and the presence of the metal ions aids in the stabilisation of the gel-structure and removal of the solvent phase.

To identify if these interactions occur initially when the precursors were mixed together during the formation of the glass, the first hour of hydrolysis and condensation reactions was studied for normal sol-gels and doped sol-gels with the initial concentration of the dopant being from 1.10^{-6} M up to 1M (as at lower concentration the drying process does not seem to be affected by the presence of the dopant).

3.3.2.3-FTIR experiment during the very early stages of silica formation

Several studies by other workers have been performed on the hydrolysis and condensation reactions with variations of the precursors (solvents, catalysts etc..) using FTIR techniques [19,46,47]. From these studies, the increase of the hydrolysis and condensation rates with increasing amounts of water was shown as well as the effect of temperature on the development of the silica matrix. The experiments were designed to look at the specific effect of the Nd^{3+} dopant on the development of the silica matrix.

3.3.2.3.1-Results

To interpret the spectra obtained during these experiments, the spectra of TEOS and dry ethanol were recorded. They were compared with the spectrum of a normal sol-gel solution after 30 seconds of hydrolysis and condensation reactions (Figure 3.10).

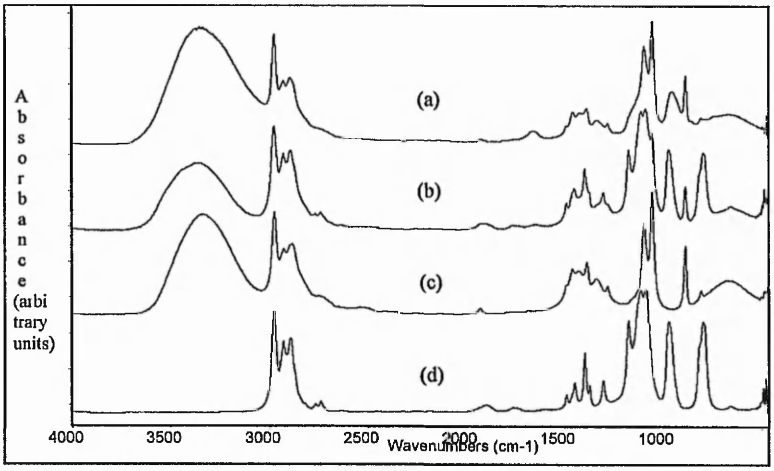

Figure 3.10: FTIR spectra of a) Normal sol-gel after 30 seconds of hydrolysis, b) TEOS :ethanol with a molar ratio of 1:4, c) dry ethanol, d) TEOS

The bands characteristic of EtOH and TEOS were observed (see Table 3.4 for assignments).

Some of the bands associated with vibrational structures of TEOS and dry ethanol have the same position which means that their separate identification is difficult especially when the matrix starts to form and the precursors disappear.

Certain bands of TEOS (1167 cm^{-1} and 950 cm^{-1}) did not appear when normal sol-gel had been hydrolysed for 30 seconds showing that the hydrolysis reaction occurs as soon as the precursors are mixed together.

Similar behaviour was observed for normal and doped sol-gels.

The spectra were recorded at up to one hour of reaction but Figure 3.11 shows only the spectra obtained during the first 10 minutes as most of the changes in the spectra were observed during that time period.

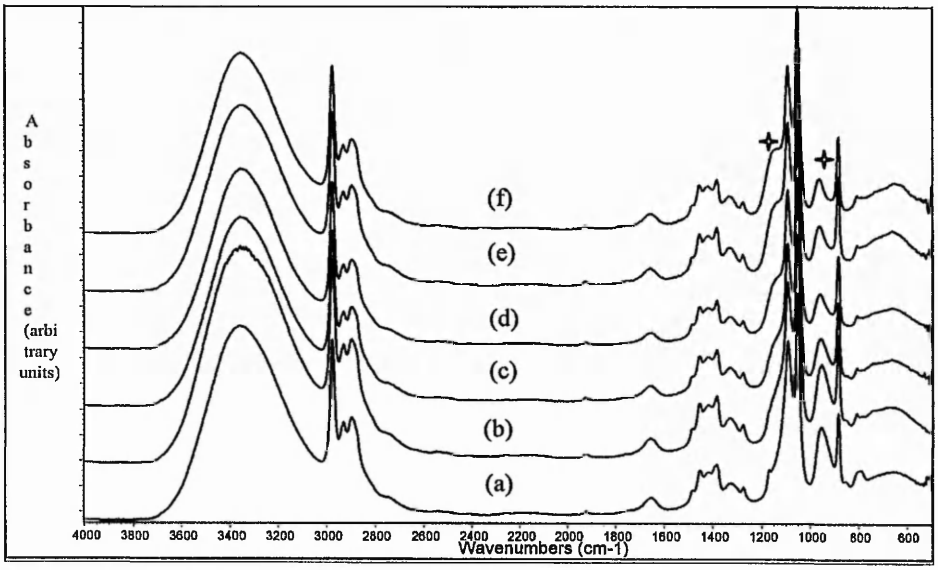

Figure 3.11: FTIR of normal sol-gel at different times of hydrolysis and condensation reactions a) 30 seconds, b) 45 seconds, c) 1 minute, d) 2 minutes, e) 5 minutes, f) 10 minutes

The most significant changes were the disappearance of the peak at 1191cm^{-1} (SiOSi rocking made from TEOS) after 30 seconds and the formation of a broad shoulder at 1141cm^{-1}. One of the peaks characteristic of TEOS had disappeared as it was used in the formation of the silica network. The decrease of the band at 980cm^{-1} was noticed as well. This band corresponds to Si-OH groups which have been used during the formation of the silica network.

The other changes correspond to variations with time in the intensity of the peaks.

In order to gain an understanding of the effect of Nd^{3+} ions on the evolution of the matrix, the intensity of the most important vibrational bands was recorded and plotted versus time.

Figure 3.12 shows only the characteristic plot of the first band at 883cm^{-1}. Changes in the other bands are in Appendix 2.

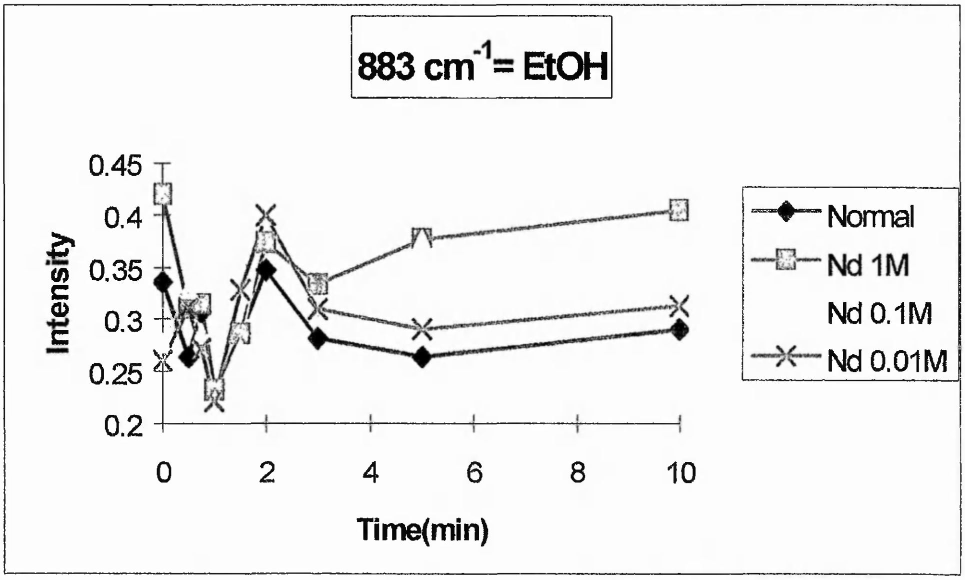

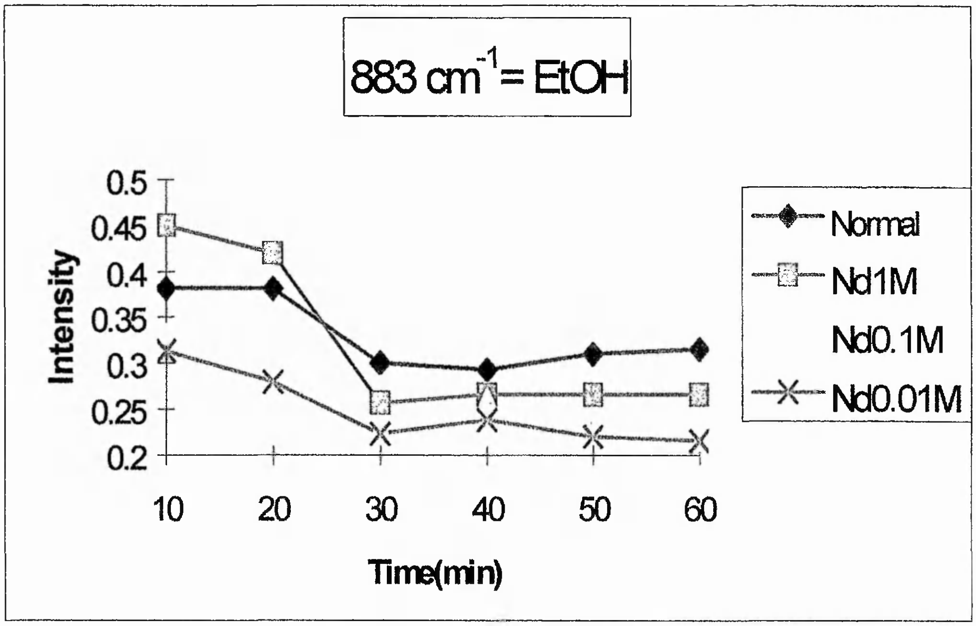

Figure 3.12: Changes in intensity for the band at 883 cm^{-1} in the presence of various concentrations of Nd^{3+}

The first aim was to try to identify the different bands which appeared in the spectra.

It was relatively difficult to assign the bands to the correct species as TEOS and dry ethanol (which still contains some water), have bands at very similar wavenumbers.

The first band appears at 665cm^{-1} and was very broad at the beginning of the reaction during the first 10 minutes and then became sharper implying that several types of bonds were present under the broad band and then these species were used during the hydrolysis and condensation reactions and consequently the number of species present was reduced and so the band was narrower. The band comes from the dry ethanol for the major part, a very low intensity band at this value was observed for TEOS.

The band at 966cm^{-1} corresponds to the CH_3 rocking vibration of TEOS [20]. This band disappeared during the hydrolysis and condensation reactions as the species were used, especially for the polymerisation reaction and the formation of the silica network with Si-O-Si bonds.

This band was replaced by another one very close by, at 960cm^{-1} from $_{v}$(SiOH) non bridging O stretch formed during the condensation reaction and which was part of the sol-gel matrix.

This change of bands was very difficult to detect and could be mistaken by a slight shift of one of the bands.

The two bands respectively at 1050cm^{-1} and 1091cm^{-1} correspond to vibrations from the ethanol and TEOS precursors.

A decrease of these bands was observed which meant that the species represented by these bands were used during the hydrolysis and condensation reactions in order for polycondensation and formation of the silica network to occur.

A very small band was observed at 1191cm^{-1} during the first seconds of the reactions and then disappeared. It could correspond to some C-OH stretching bonds of ethanol immediately used during the reactions.

The sharp band observed at 883cm^{-1} corresponded at the beginning of the reaction to the C-C-O symmetric stretching bonds coming from ethanol [48].

Then as the reaction proceeded, the band was still there which meant that an other species was identified at the same wavenumber. This bond was ν(SiO) oxygen bending frequencies from the formation of the silica network [22]

These ideas were strengthened by the changes in intensity of this band at $883cm^{-1}$ during the first hour of reaction. First a decrease of the intensity was observed. Then a slow increase in intensity of the band at $883cm^{-1}$ was noticed as the reactions proceeded. The silica network was forming.

It has to be said that in our case both hydrolysis and condensation reactions and the formation of the silica network were relatively fast as the reaction medium was very acidic. When a spectrum of the just mixed precursors at a time of hydrolysis of 30 seconds and a spectrum of the dry sol-gel were compared we observed that the peaks corresponding to the TO and LO Si-O-Si bonds were actually at slightly higher wavenumbers [49]. So the bands observed at $1050cm^{-1}$ and $1091cm^{-1}$ really correspond to the precursors.

In addition, it was not possible that after only one hour of hydrolysis and condensation reaction, all the TO and LO Si-O-Si bonds had formed.

After 2 minutes a band (more like a shoulder) appeared at $1141cm^{-1}$which corresponded as mentioned above to the TO Si-O-Si and so as soon as 2 min of reaction the silica network is already forming.

Moreover the band corresponding to the LO Si-O-Si is usually observed at around $1090cm^{-1}$ and so this band observed in our spectrum could well be the longitudinal optic mode of vibration of Si-O-Si species, even after a few minutes of hydrolysis and condensation reactions.

Finally the last important band observed was the one at $3350cm^{-1}$ corresponding to water species coming mainly from diluted HCl.

Water species are an important part of the hydrolysis reaction. First a decrease of the intensity of the bands arising from water was observed as it was consumed, then a further amount was released during the condensation reaction so an increase of the intensity was observed, then in the band intensity a decrease was observed as these new species formed were used for further hydrolysis reactions. Also, a shift of the band was observed as the reactions proceeded. The band became broader as the reactions were carried out which means that the water species are used and other species are formed. Hence the band at $3540cm^{-1}$ corresponds to the silanol groups linked to molecular water through hydrogen bonds, $_{\nu OH}$(SiOH,H) [33]. The band at $3500\text{-}3400cm^{-1}$ corresponds to the absorbed water represented as $_{\nu OH}(H_2O,P)$.

Finally the band at $3738cm^{-1}$ which represents free SiOH on the surface of the gel, appeared when the sample was dry.

3.3.2.3.2-Discussion

Once the different bands were characterised it was possible to investigate if the dopant had any effect on the formation of the matrix and on its structure (Figure 3.12 + Appendix 2). First the variation of the intensity with time was compared between doped and undoped sol-gels. The same type of behaviour was observed for all the samples.

During the first minute of reaction a decrease of the intensity of every band was observed which corresponds to a use of the precursors for the reaction. Then after 1 minute an increase of the intensity was observed with a maximum observed at 2 minutes. The intensity decreased to 5 minutes, then an increase was again noticed up to 20 minutes followed by a decrease of the intensities for the rest of the first hour of the hydrolysis and condensation reactions.

The variation of intensity of the bands with time for doped and undoped sol-gels is related to the hydrolysis and condensation reactions. The decrease of intensity at the beginning of the reaction corresponded to the consumption of the precursors by the hydrolysis reaction , then the increase of intensity of the bands as the reactions proceeded was due to the formation of new silica species, the silica matrix, by the condensation reaction.

Finally the intensity of every band was compared for doped and undoped sol-gels.

For all the bands, the highest intensity was noticed for normal sol-gels, specially for the water bands.

The major difference observed was the appearance of the LO Si-O-Si bonds (1200cm^{-1}) earlier in the reaction (a few seconds) with dopant than without dopant. This effect was concentration dependent and decreased as the concentration of the dopant in the sol-gel solution decreased. This could mean that the dopant speeded up the reaction.

This method of analysis contains certain limitations as the high intensity of certain bands can overlap other bands having low intensity but corresponding to characteristic bonds. Consequently it is necessary to use a method where all the species will have different characteristic bands without any overlapping.

To know the different species present in the system more accurately, a study of gelation point was made and ^{29}SiNMR spectroscopy experiments were carried out.

3.3.3-Studies of the effect of hydrolysis time on gelation using a two stage acid/base sol-gel process

3.3.3.1-Results

In order to complete the study of the drying process, the study of the gelation point for normal sol-gels and doped sol-gels was performed as it enabled us to identify if the dopants were interacting with the precursors during the first hour of reaction or later in the development of the sol-gel matrix.

Nd^{3+} dopant at concentrations from $1.28.10^{-7}$M to 0.128M of the metal ion in the sol-gel solution was used as well as Ce^{3+} dopant at concentrations from $1.28.10^{-4}$M to 0.0897M in the sol-gel solution were used.

Figures 3.12.a,b shows the time of gelation (t_G) versus the time of hydrolysis (t_H) for normal and Nd doped sol-gels.

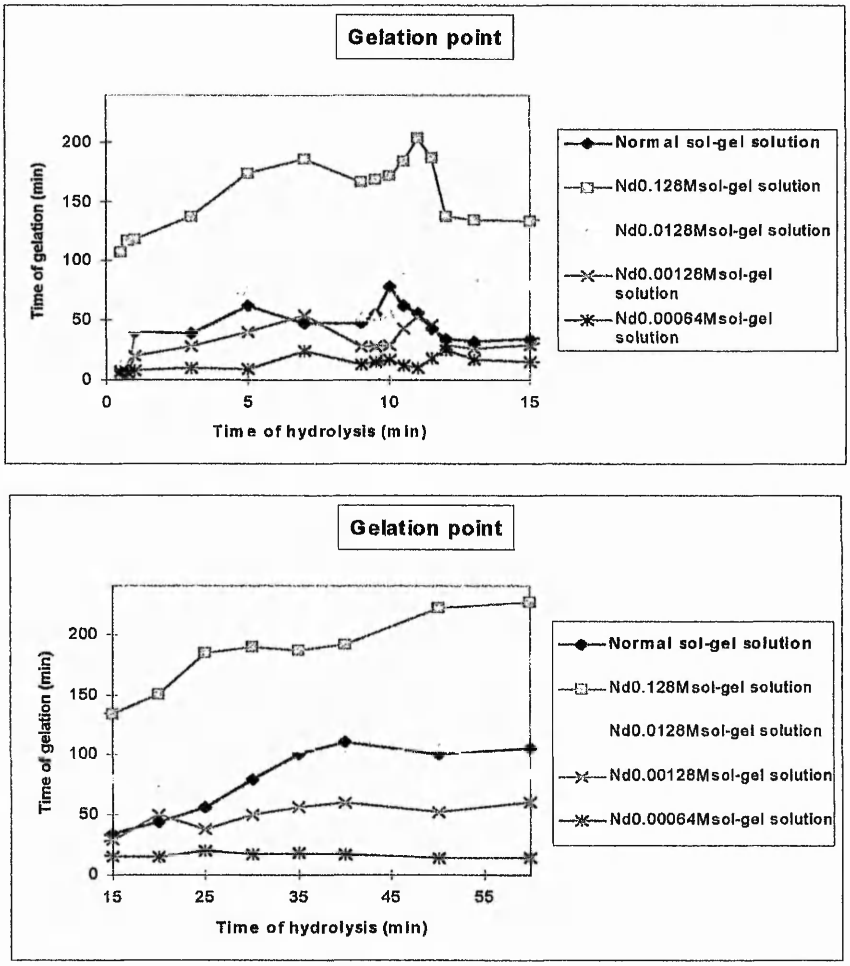

Figure 3.12.a.: Gelation point versus hydrolysis time for Nd^{3+} doped (from $6.4.10^{-4}$M up to 0.128M) and undoped sol-gels

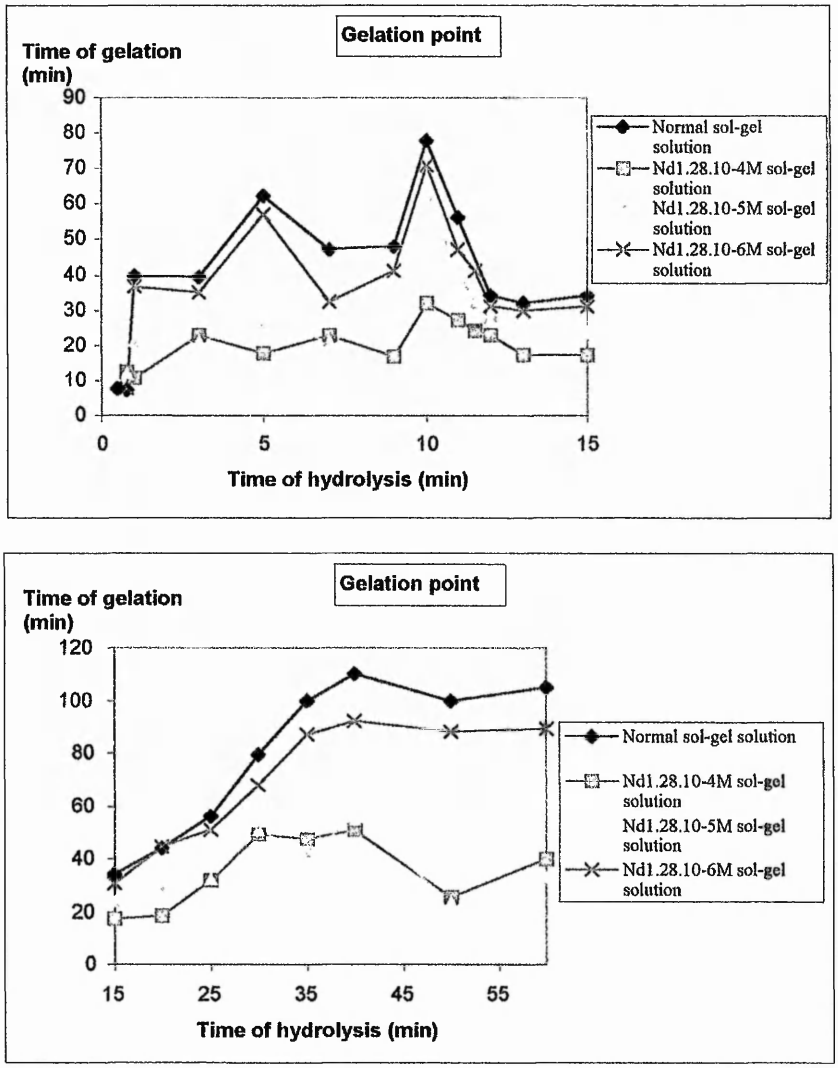

Figure 3.12.b: Gelation point versus hydrolysis time for Nd^{3+} doped ($1.28.10^{-6}$M up to $1.28.10^{-4}$M) and undoped sol-gels

Statistical analysis using the student t-test was carried out on every data point of the curve using an average of 8 measurements. The results of the calculations can be found in the Appendix 3-Tables 1,2,3.

In a normal sol-gel solution, when the precursors were mixed and the ammonia added (t_H=35sec), a very short gelation time was observed. At longer hydrolysis times (t_H=45seconds-8 minutes) an increase of the gelation time was observed.

However, the increase of the gelation time was not linear with time of hydrolysis.

After a small decrease of the gelation time (at t_H=9-10 minutes) a large increase was noticed (at t_H=11 minutes) followed again by a large decrease (between t_H=12-15minutes). Finally, a regular increase of the gelation time was observed as the reaction proceeded. When the dopant was added to the sol-gel all the curves had the same shape.

A displacement of the t_G-t_H curve was observed toward longer gelation time in the presence of the dopant. The displacement of the curve changed with the amount of Nd^{3+} in the system. At high concentrations of the metal ion in the sol-gel solution (0.128M-0.0128M), a larger gelation time was obtained in comparison to the normal sol-gel system.

The increase of gelation time was displaced toward shorter hydrolysis time when the concentration of the dopant decreased. Furthermore with low concentrations of the dopants, the gelation time was faster than for normal sol-gel but the effect of this dopant was noticed only down to a certain concentration of dopant in the system. Below 0.00064M, the gelation time started to increase again and at $1.28.10^{-6}$M, the gelation curve of the doped sol-gel was similar to the gelation curve of the normal sol-gel.

The effect of cerium ions on gelation was also investigated in order to see if the effect observed for neodymium ion might be common for other lanthanide elements. The drying process has already shown a difference of the drying rate in the presence of cerium ions in the silica matrix instead of neodymium ions.

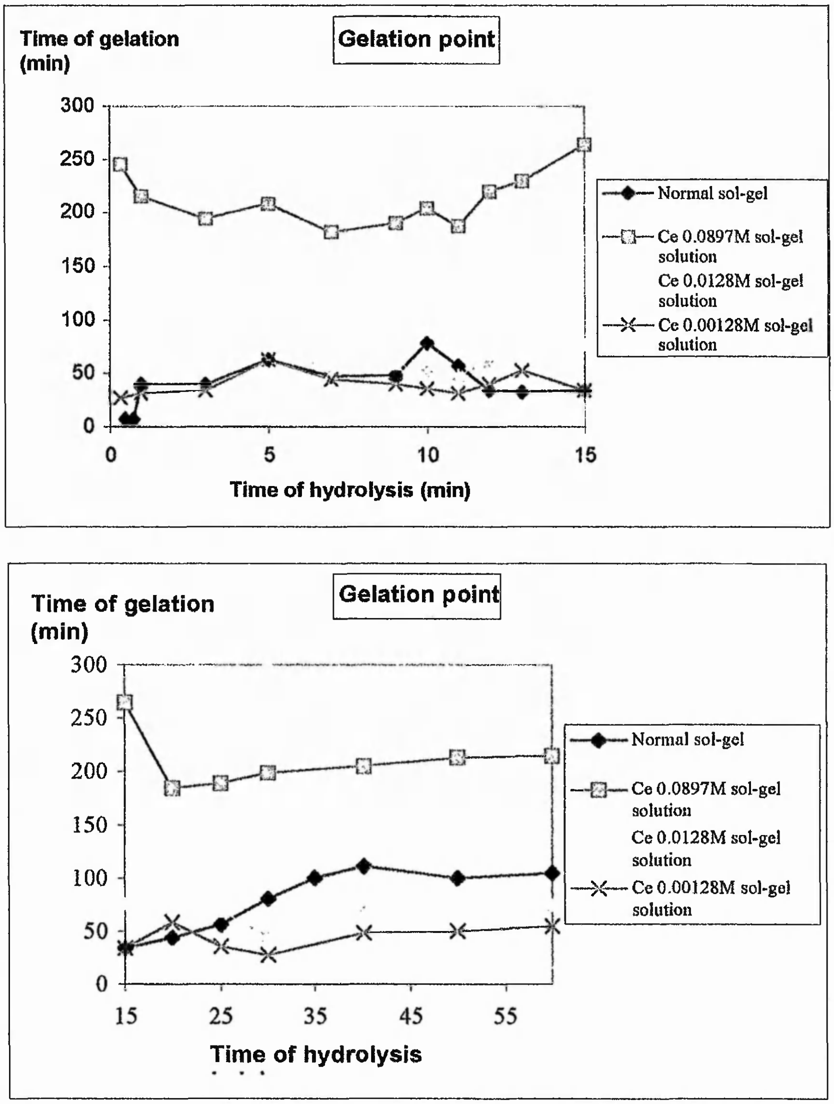

Figure 3.13: Gelation point versus hydrolysis time for Ce^{3+} doped (0.00128M up to 0.0897M) and undoped sol-gels

Statistical analysis using the student t-test were carried out on every data point of the curve using an average of 8 measurements. The results of the calculations can be found in the Appendix 3-Table 4.

The t_G-t_H curve of cerium doped sol-gel solutions showed a decrease of the gelation time for the first 10 min of hydrolysis. Then a rapid increase of the gelation time was observed (t_H= 11-16 min), followed by a decrease (t_H=20 min) and finally a regular increase of the gelation time.

Moreover in the presence of cerium ions in the sol-gel solution, the gelation time was longer that for normal sol-gels. As the concentration of the metal ion in the sol-gel solution decreased, the gelation time decreased and became very similar to the gelation time of normal sol-gel solutions for a concentration of 1.28.10^{-4}M Ce^{3+}.

When comparing the curves of Nd^{3+} and Ce^{3+} sol-gel solutions (Figure 3.14), differences in the t_G-t_H curves can be observed.

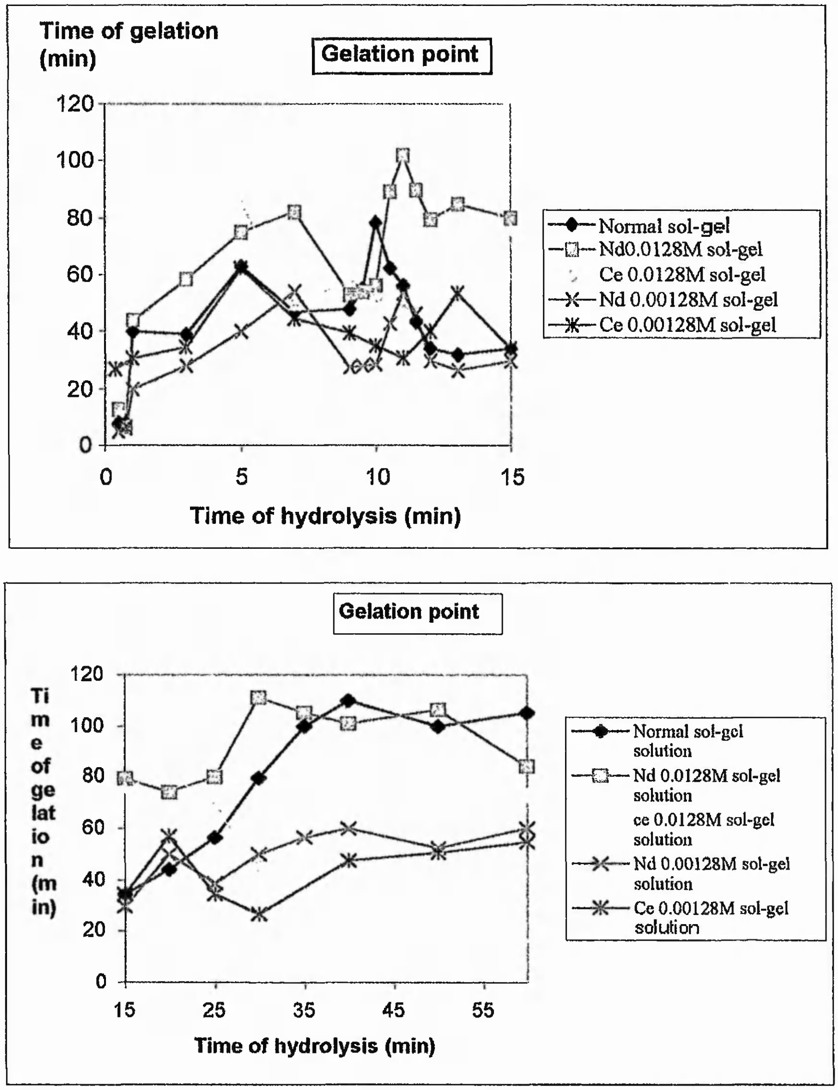

Figure 3.14: Gelation point versus hydrolysis time for Nd^{3+} and Ce^{3+} doped (0.00128M up to 0.0128M) and undoped sol-gels

For the first 15 minutes of the hydrolysis reaction, the sol-gel solutions with high concentration of Ce^{3+} and Nd^{3+} (0.0128M) had a higher gelation time than normal sol-gel solutions. Moreover at this concentration (0.0128M), Ce^{3+} sol-gel solution required a longer gelation time than Nd^{3+} sol-gel solution for the first 5 minutes, then the Nd^{3+} sol-gel solution exhibited the longest gelation time.

Between 15 and 20 minutes the sol-gel solutions with high concentrations of Nd^{3+} and Ce^{3+} needed a very similar gelation time, still longer than normal sol-gel. Then after 25 minutes the gelation time of Ce^{3+} sol-gel solutions was lower than for normal sol-gel solutions and Nd^{3+} sol-gel solutions.

At lower concentration of the Ce^{3+} and Nd^{3+} (0.00128M) sol-gel solutions, the gelation time was shorter than for normal sol-gel solution. Between 30 seconds and 15 minutes, the Ce^{3+} sol-gel solution required a longer gelation time, closer to the normal sol-gel, than the Nd^{3+} sol-gel solution. After 15 minutes, the Nd^{3+} sol-gel solution had the longest gelation time, very close to the normal sol-gel solution.

Both metal ions affected the gelation time of the sol-gel solution. However, for the same concentration of metal ion in the sol-gel solution, different gelation times were observed in the presence of either Ce^{3+} or Nd^{3+} metal ions. This effect was as well concentration dependent.

Both metal ions do not have the same effect on the hydrolysis and condensation reactions.

3.3.3.2-Discussion

The trend of the t_G-t_H curves observed for our sol-gel system is affected by the presence of the dopant.

In a normal sol-gel solution, the very short gelation time observed at t_H=35sec is a consequence of the -OH containing species present in the system which are numerous. They are mainly coming from the product of the hydrolysis reaction of the precursors. As the medium is very acidic (pH≈2), the hydrolysis reaction is very fast, consequently on addition of base gelation is fast.

As hydrolysis proceeds (longer t_H) the silanol groups are consumed by the condensation reaction and fewer silanol groups are therefore available for the ammonia to react with and consequently an increase of the gelation time is observed (t_H=45 seconds-8 minutes). Then again, as the concentration of the silanols increases (as hydrolysis of partially condensed oligomers occurs), the gelation time decreases (t_H=12-15 minutes at which the silanol concentration is a maximum).

In the presence of the dopant (0.128M-0.0128M), an increase of the gelation time was observed which decreased as the concentration of the dopant decreased in the system. This means that fewer silanol groups were present in the system [10], suggesting that the dopant might interact with TEOS at the beginning of the reaction.

So the possibility of cross-linking between hydrolysed TEOS molecules during condensation is considerably reduced. The formation of a network of cross-linked chains is an essential requirement for gelation and the time for gelation will therefore be increased.

However, the gelation time was lower than for normal sol-gels for low concentrations of the dopant (from 0.00128M down to 0.00064M) suggesting that the formation of silanol groups is speeded up when a small amount of the dopant is added to the sol-gel and consequently Nd^{3+} ions may act as a catalyst for hydrolysis.

Strangely it seems that when only a very low level of Nd^{3+} is added into the system that the gelation time is reduced for all hydrolysis time points and gelation is quicker than for normal sol-gels. More silanol groups must be present in the system suggesting quicker hydrolysis and condensation reactions. Between a certain range of concentrations, the metal ion can act as a catalyst.

With this experiment, the catalytic effect of the metal ion at high concentration is relatively fast as a long gelation time is required. The amount of silanol groups present in the system is low. As soon as the silanol species are formed, they are used by the condensation reaction. Both hydrolysis and condensation reactions are fast.

Furthermore an effect of the dopant on the sol-gel was also observed when a different metal ion was used.

As explained for the neodymium doped sol-gel, this behaviour relates to the number of silanol groups present in the sol-gel solution and consequently to the extent of the hydrolysis and condensation reactions.

Cerium ions interact with the matrix as well as neodymium ions.

At high concentrations of the metal ion (0.0128M), the gelation time of the sol-gel solution was longer than in the presence of high concentrations of Nd^{3+} (0.0128M).

Cerium ions interact with the matrix and hence the number of silanol groups available in the system is reduced. At lower concentration ranges, the gelation time of the sol-gel solution was lower than in the presence of Nd^{3+}.

It seems that the metal ions play a catalytic role which speed up the reactions and reduce the number of silanol species present in the system. Moreover the reduction of available silanol groups for the doped sol-gels compared to normal sol-gels shows a possibility of interaction between Nd^{3+} ion and the silanol groups. The metal ion could be electrostatically attracted and bonded to the silica matrix.

The high gelation time required for the doped sol-gels could explain the relatively slow loss of solvent at the beginning of the drying process and so the observation of the three stage drying process. The suggested catalytic effect of Nd^{3+} and Ce^{3+} may be the cause of a quicker drying time observed for sol-gels prepared in the presence of the dopant.

To confirm these explanations, it is necessary to look at the different silica species present during the hydrolysis and condensation reactions. This will help to understand the interaction between the dopants and the precursors/initial polymeric species and then to look at any possible catalytic effect of the dopant on the formation of the silica matrix.

3.3.4-^{29}SiNMR

3.3.4.1-Results

^{29}SiNMR is a useful tool to study the early stages of hydrolysis and condensation reactions in the formation of sol-gels. It allows the characterisation of small molecular weight silica species present at any particular time point.

Analyse of the ^{29}SiNMR spectra of the sol-gel solutions at different reaction times showed several groups of species which were identified by comparison with literature [12-19] (Table 3.6).

Table 3.6: Identity of the different silica species observed.

Shift (ppm)	Species	Groups
-73.87	$Si(OH)_4$	Q^0
-75.37	$Si(OC_2H_5)(OH)_3$	
-77.06	$Si(OC_2H_5)_2(OH)_2$	
-79.1	$Si(OC_2H_5)_3(OH)$	
-81.78	**$Si(OC_2H_5)_4$ (TEOS)**	
-83.21	$\equiv SiOSi(OH)_3$	Q^1
-83.42	$\equiv SiOSi(OH)_3$	
-84.82	$\equiv SiOSi(OC_2H_5)(OH)_2$	
-84.99	$\equiv SiOSi(OC_2H_5)(OH)_2$	
-86.31	$\equiv SiOSi(OC_2H_5)_2(OH)$ linear	
-86.83	$\equiv SiOSi(OC_2H_5)_2(OH)$ cyclic	
-92.22	$(\equiv SiO)_2Si(OH)_2$ linear	Q^2
-92.97	$(\equiv SiO)_2Si(OH)(OC_2H_5)$ cyclic	
-93.96	$(\equiv SiO)_2Si(OH)(OC_2H_5)$ linear	
-94.69	$(\equiv SiO)_2Si(OC_2H_5)_2$cyclic	
-100.46	$(\equiv SiO)_3Si(OH)(OC_2H_5)$	Q^3
-101.88	$(\equiv SiO)_3Si(OC_2H_5)$	
-102.05	$(\equiv SiO)_3Si(OH)$	
-110	$(\equiv SiO)_4Si$	Q^4

Q^0 groups correspond to monomer species with no bridging oxygen. These species appear at the beginning of the hydrolysis reaction.

Q^1 groups represent the end group species with bridging oxygen (monosubstituted).

Q^2 groups are the middle group species with two bridging oxygens (disubstituted).

Q^3 are the trifunctional branching species with three bridging oxygens (trisubstituted).

Q^4 groups correspond to tetrafunctional branching species with four bridging oxygens (tetrasubstituted).

Q^4 species cannot be observed in our case as the glass tube used for the analysis gave a very broad peak in this region (-110ppm).

3.3.4.1.1-Qualitative analysis of NMR data

Detection of these species and comparison with the type of sol-gels (undoped or doped with different concentrations of the metal ions) enabled us to understand how the dopant and the precursors interact at the molecular level during the first hour of reaction and what role the dopant may play in the formation of the matrix. Analysis was carried out for normal sol-gels and Ndsol-gel solutions (0.128M-1.28.10^{-7} M). The data were generally collected between 10 seconds and 20 minutes after the start of the reaction. All the data are shown for normal sol-gel on Figure 3.14. The data for Ndsol-gel solutions (0.128M-1.28.10^{-3}M) can be found in Appendix 4. For the doped sol-gel solutions with dopant concentrations below 1.28.10^{-3}M, spectra were collected for only 10 and 30 seconds of reaction as the major differences between doped and undoped sol-gels appeared only during the first 30 seconds of reactions. The data are also shown in Appendix 4.

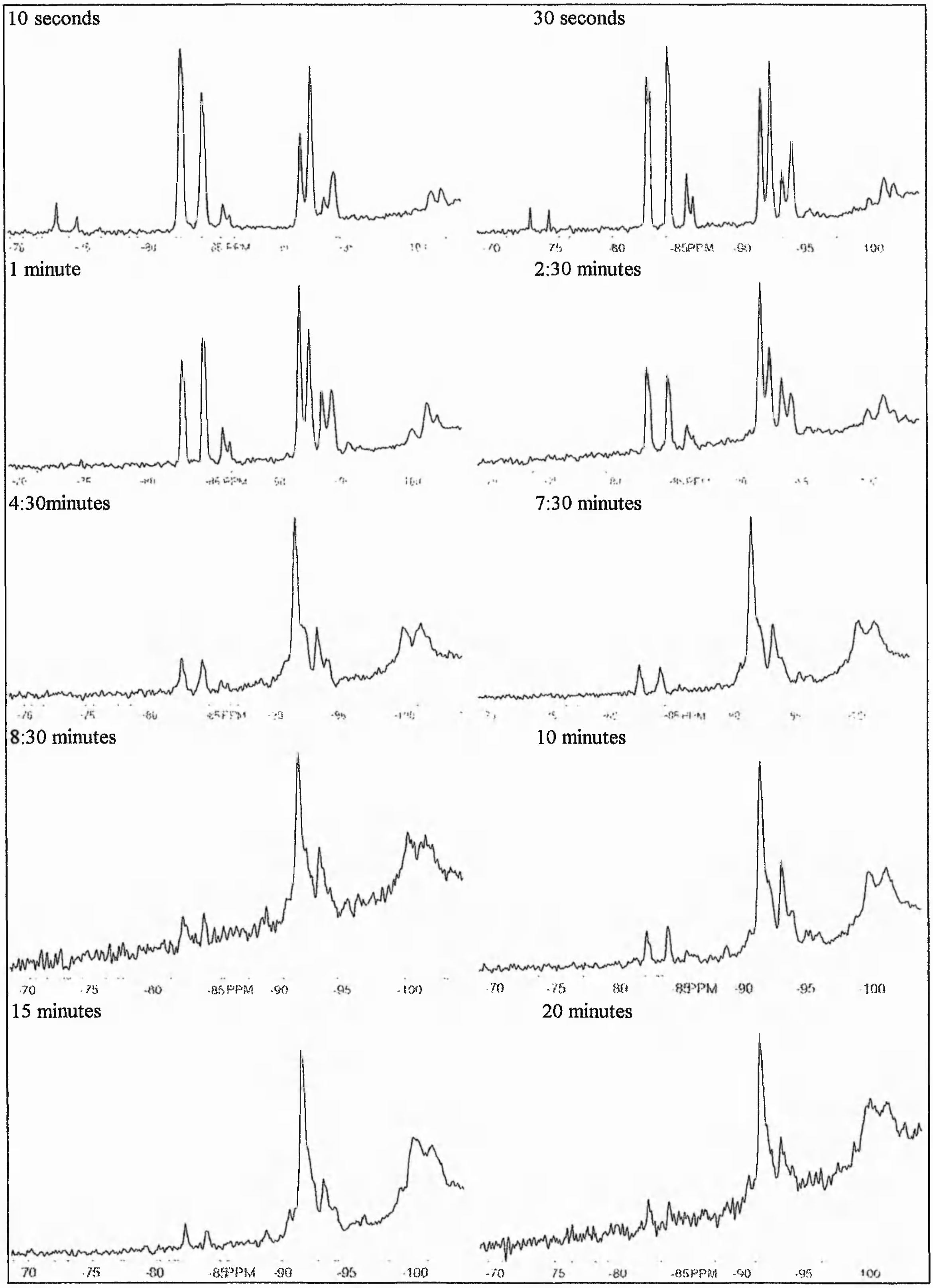

Figure 3.14: Normal sol-gel (ppm from -70 to -110 ppm)

When Nd^{3+} was present in the sol-gel mixture, a shift of the peaks toward lower field was observed, the shift increasing as the concentration of the dopant increased (Figure 3.15). With concentrations of $1.28.10^{-5}$M and below of the metal ion in the sol-gel solution, the shift was no longer observed.

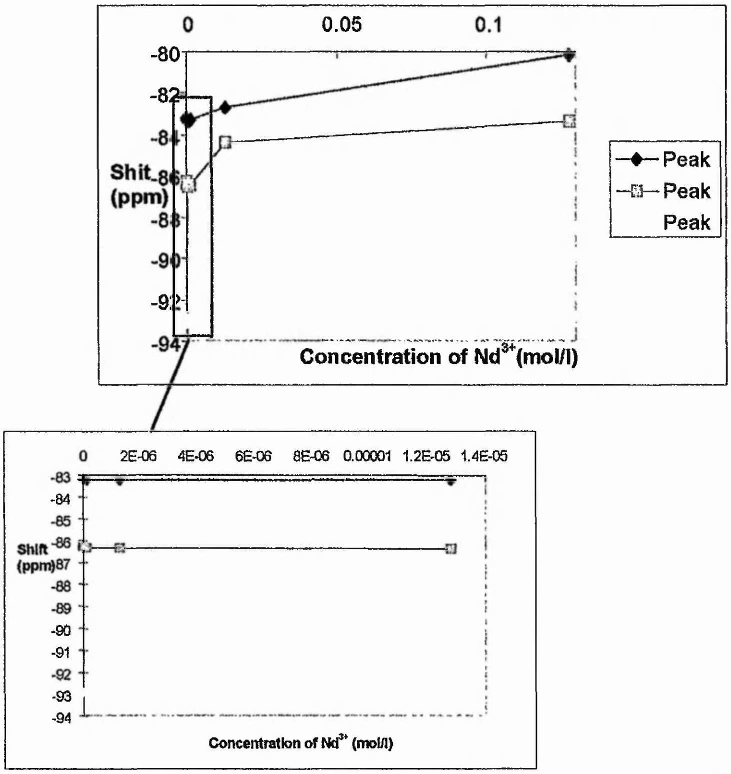

Figure 3.15: Effect of the concentration of Nd^{3+} doped in the sol-gel on the shift of the peaks with peak 1corresponding to Q^1 species $\equiv SiOSi(OH)_3$, peak 2 corresponding to Q^1 species $\equiv SiOSi(OC_2H_5)(OH)$ and peak 3 corresponding to Q^2 species $(\equiv SiO)_2Si(OH)(OC_2H_5)$

This shift corresponds to deshielded Si nuclei which precess more quickly than highly shielded Si nuclei. It is due to the electronegative effect of Nd^{3+}. It reduces the local diamagnetic shielding in the vicinity of the Si nuclei because it reduces the electronegativity around the Si nuclei[50].

This again suggests that the Nd^{3+} ions are in close proximity to silicon nuclei. N.B.the presence of $Cr(acac)_3$ had no effect on the chemical shift position of Si species.

A qualitative analysis was performed to identify the different silica species present in normal sol-gel solutions and doped sol-gel solutions at various times of the hydrolysis reaction.

Q^0 species were observed between -73.5 and –82.0ppm.

A peak arising from TEOS was not observed as the medium was very acidic and hydrolysis of TEOS was almost instantaneous. Q^0 species were present for the normal sol-gel during the first 30 seconds of hydrolysis. Only $Si(OH)_4$ and $Si(OC_2H_5)(OH)_3$ species were present. With Nd^{3+} present at a concentration of 0.128M, no Q^o species were detected after 30 seconds of reaction, showing an advancement in the extent of the hydrolysis and condensation reactions.

For lower concentrations of the dopant, eg. Nd 0.0128M, all the Q^o species could be observed after 30 seconds of reaction and the TEOS peak was observed for Nd1.28.10^{-3}M and Nd6.4.10^{-4}M sol-gel solutions suggesting a lesser extent of the hydrolysis and condensation reactions than in the presence of high concentrations of the dopant.

Q^1 species were observed between –83.0 and 87.02ppm for doped and undoped sol-gels after 10 seconds of hydrolysis and condensation reactions. For the peaks at -83.21 and 83.42ppm, the same assignment is given ($\equiv SiOSi(OC_2H_5)_2(OH)$) . The peaks are very close together and the difference in shift corresponds to two different species bound with the $\equiv$Si group. The same phenomenon is observed for the peaks at -84.82 and -84.99ppm forming a doublet. It is different for the peaks at -86.31 and -86.83ppm (group 1) where the first peak represents a linear species and the second a cyclic species [12-19].

Q^1 species were present at up to 7.5min of reaction. After 10min of reaction for doped and undoped sol-gels they were absent. The Q^1 species were no longer observable as they had been used in the formation of Q^2, Q^3 and Q^4 species and therefore in the formation of the silica matrix.

Q^2 species were observed between –92.0 and –95.0ppm. The peaks at -92.22ppm and at –93.66ppm correspond to linear species whereas the peaks at -92.97 and -94.69ppm (group 2) correspond to cyclic species (group 3). Q^2 species were already present after 10 seconds of hydrolysis and condensation reactions. After 4.30 minutes, a decrease of the peaks occured. The Q^2 species were observed during the whole 20 minutes of the reaction.

In normal sol-gel solutions, the relative intensities of the linear and cyclic peaks for the apparent doublets at -86.31, -86,83 ppm (group 1); -92.22, -92.97 ppm (group 2), -93.96, -94.69 ppm (group 3), change with time. For group 1, the linear species had a higher intensity than the cyclic species at the beginning of the reaction. As the reaction proceeded, the difference in intensity between the peaks reduced and then at 4:30 minutes their intensity was equal.

At the beginning of the reaction (for the first 30 seconds), the cyclic species had a higher intensity for the peaks of groups 2 and 3. The intensity of the linear species increased as the reaction proceeded and at 1 min their intensity was higher than for cyclic species, for group 2 and equal for group 1. This higher intensity for linear species in comparison with cyclic species was observed for the whole reaction and at 20 min, the cyclic species were only observed as shoulders on the peaks arising from linear species.

In the presence of high concentrations of the Nd^{3+} dopant (0.128M), the relative intensity of group 1 was similar to that of the normal sol-gel, but for group 2 after 10 seconds the linear species already had a higher intensity than the cyclic species. With group 3, the cyclic species had a higher intensity than linear species at the beginning of the reaction and at 2:30 minutes, the linear species had the highest intensity.

In comparison with normal sol-gel solutions, at high concentrations of dopant the linear species were more numerous at the beginning of the reaction. As the concentration of the dopant was decreased (0.0128M and lower), the relative intensity of the linear and cyclic species became more like the relative intensities found with the normal sol-gel solutions.

Finally the Q^3 species were observed between -100 and -103ppm. They appeared with a very low intensity after 10 seconds of reaction and increased in intensity with time of reaction.

3.3.4.1.2- Semi-quantitative analysis of NMR data

Having identified all the peaks, a more detailed comparison was made between doped and undoped sol-gel solutions. GRAMS/32 software was used to measure the peak areas of the various silica species and by using the TMS peak for reference, the number of moles of silica species was calculated (see Appendix 5 for details of the calculation). It was possible to compare the evolution of the species during the first hour of hydrolysis and condensation reactions for doped and undoped sol-gels. For every data point an average of 2-3 measurements was done. Good reproducibility of the peak areas was obtained after 1 minute of hydrolysis and condensation reactions. For the 1st minute of reaction up to 4 measurements were necessary in order to obtain reproducible results. This was due to the very fast reactions in the system and to the rapidity of the manipulation as the sample had to be frozen at 10 and 30 seconds precisely.

In this section of the results, normal sol-gels and Nd doped sol-gels were considered. The concentration of the metal ion in the sol-gel solution was between 0.128M and 0.00128M. Lower concentrations of the metal ion were looked at later on (see page 56).

During the drying process, below 0.00128M, the behaviour of the sol-gel sample became more and more similar to that of normal sol-gels.

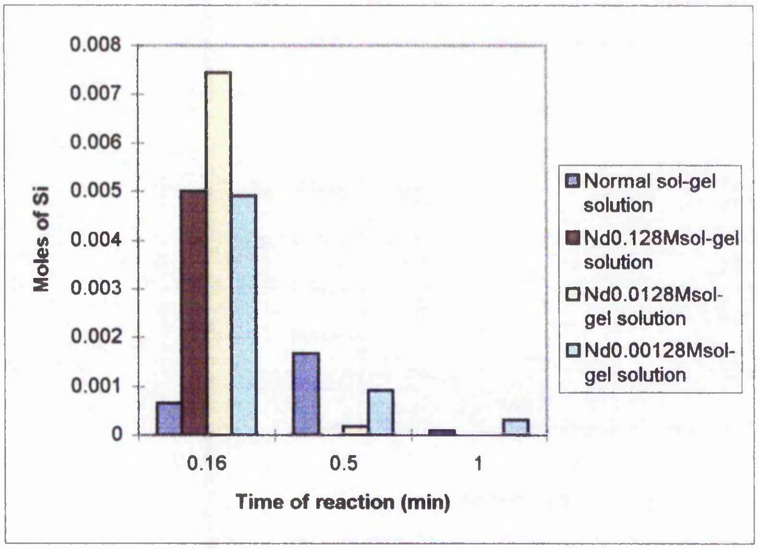

Figure 3.16 :Variation of the Q^0 species with time of reaction

Q^0 species could only be observed for the first minute of hydrolysis regardless of the concentration of the dopant in the sol-gel solution.

A lower number of moles of Q^0 Si species were present in normal sol-gel solutions than in the presence of the dopant.

The level of Q^0 species was at its maximum at 10 seconds of reaction and then decreased rapidly with time. In the presence of the dopant (0.128M-0.00128M), the number of moles of Q^0 species was higher at 10 seconds than for normal sol-gel solutions.

The variation of the level of Q^0 species in doped sol-gel solutions was dependent on the concentration of the dopant in the sol-gel solution. At high concentrations (0.128M) Q^0 species disappeared faster than at low concentrations (0.0128M-0.00128M).

At 10 seconds, the highest concentration of Q^0 species was observed for Nd0.0128M doped sol-gel solution.

At 30 seconds, an increase of the Q^0 species was noticed for normal sol-gel solutions whereas the number of moles of Q^0 Si species decreased for doped sol-gel solutions. The same data were obtained for three different runs.

At 1 minute, Q^0 species were only observed for normal sol-gels and Nd0.00128M sol-gel solutions.

The Q^0 species in doped sol-gel solutions were no longer observable at a shorter time of hydrolysis than the Q^0 species in normal sol-gel. They had been used during the hydrolysis and condensation reactions more quickly.

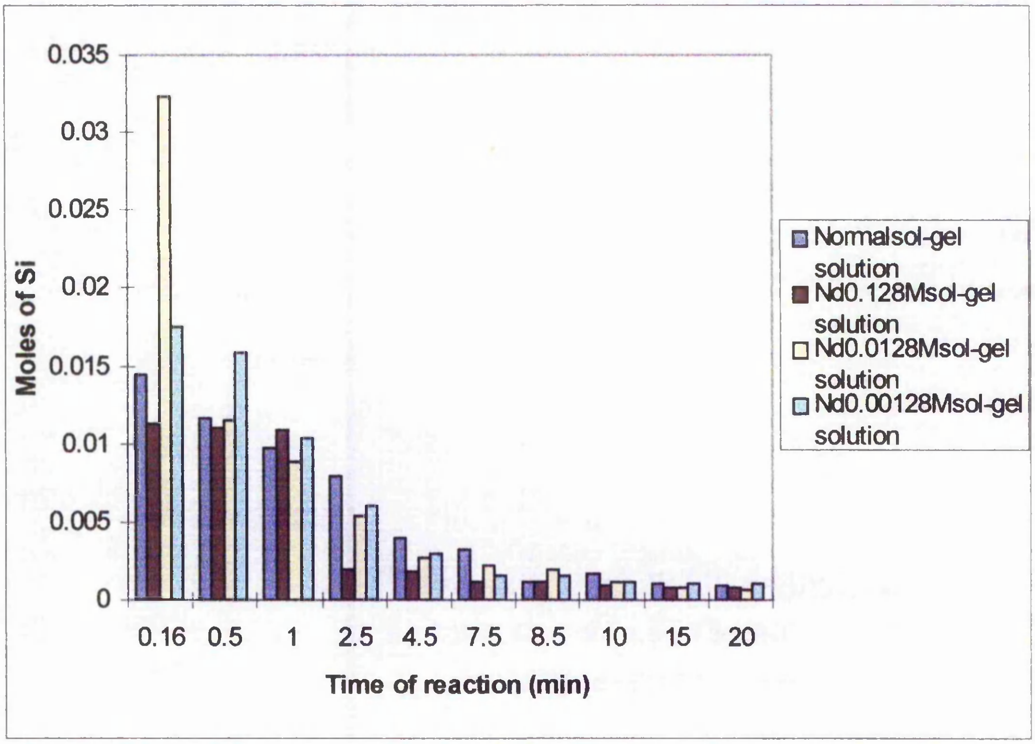

Figure 3.17:Variation of Q^1 species with the time of reaction

When the number of moles of Q^1 species present was plotted versus time, a decrease with time was noticed. However after 20 minutes of reaction Q^1 species were still present in the system (at a very low level).

For normal sol-gel solutions, a gradual decrease of the Q^1 species with time was noticed. For doped sol-gel solutions at high concentration (0.128M) a rapid drop was noticed after 1min of reaction. The level of Q^1 silica species was lower than for normal sol-gel solutions. At lower concentrations (0.0128M) of the dopant, a sudden drop was noticed after 10 seconds followed by a slow but gradual decrease in the number of Q^1 species in the system. The number of moles of silica species (Q^1) was higher than normal sol-gel solution at 15 seconds and then became lower after 30 seconds.

A decrease in the amount of silica species was also observed after 30 seconds for low concentrations (0.00128M) of the dopant. The number of moles of Q^1 species was higher than normal sol-gel solution for 1min and then became lower.

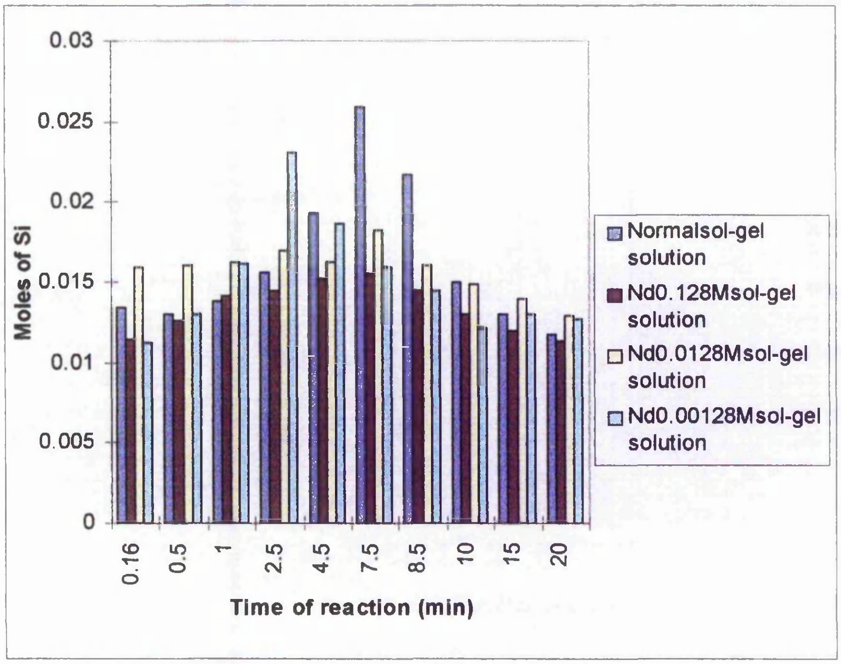

Figure 3.18:Variation of Q^2 species with the time of reaction

For Q^2 species for all experimental systems an increase in the number of moles measured was observed followed by a decrease.

For normal sol-gel solutions, the increase of the Q^2 species to a maximum concentration at 7:30 minutes was noticed.

For doped sol-gel solutions the same behaviour was observed with variation of the maximum of silica species according to the concentration of the dopant in the system.

For Nd0.128M sol-gel solution, a maximum was noticed at 7:30 min. For this concentration the level of Q^2 species was more constant until 7:30 min than for the other sol-gels where a more pronounced increase of the Q^2 species was noticed.

For Nd0.00128M sol-gel solution a maximum was noticed at 2:30 min.

For the whole 20 minutes, the number of Q^2 Si species in Nd0.128M sol-gel solution was lower than in the normal sol-gel solution or in Nd (0.0128M-0.00128M) sol-gel solutions.

For the first 2:30 minutes the low concentration (0.0128M-0.00128M) Nd doped sol-gels have a higher number of Q^2 Si species than normal sol-gel solutions. Then between 4:30 and 10 minutes, the normal sol-gel solution had the highest level. After 10 minutes, again the low doped sol-gel solutions have a higher number of Q^2 Si species than normal sol-gel solutions.

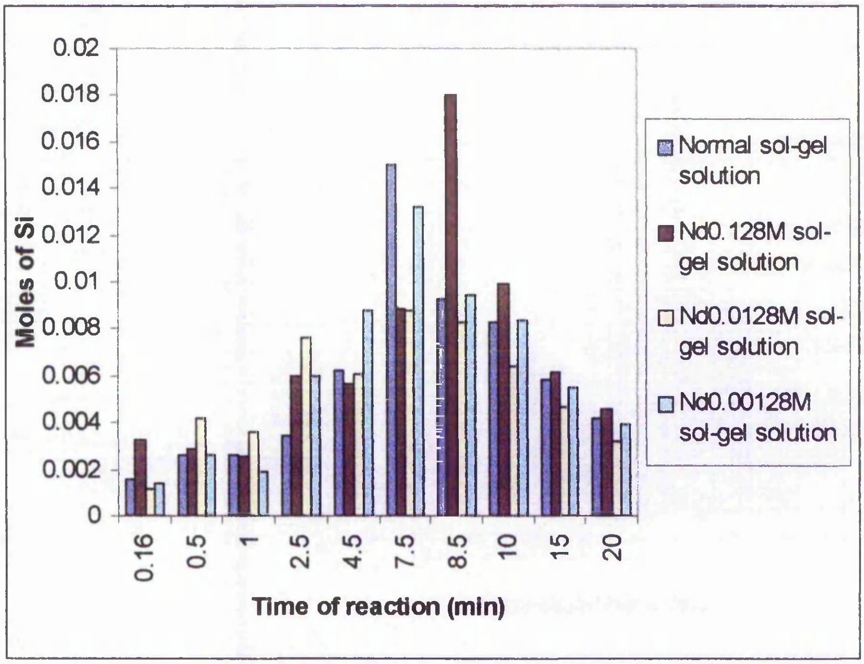

Figure 3.19:Variation of Q^3 species with the time of reaction

As for the Q^2 species, an increase of the Q^3 species with time followed by a decrease was noticed.

The number of moles of Q^3 species was a lot lower than for Q^2 species at the beginning of the reaction (at 10 seconds for normal sol-gel, 0.014moles of Q^2 Si were present whereas 0.0018moles Q^3 Si).

Maximum concentrations were found at 7:30 minutes for normal sol-gel solutions, 8:30 minutes for Nd0.128M sol-gel solutions and 7:30 minutes for Nd0.0128M and Nd0.00128M sol-gel solutions.

As for the Q^2 species, the level of Q^3 species in a Nd0.0128M sol-gel solution, showed the least change in concentration with time than for any other sol-gel system.

The presence of the dopant has an effect on the hydrolysis and condensation reactions. The dopant seems to have a catalytic effect as Q^2 and Q^3 species are observed at earlier hydrolysis times in comparison with normal sol-gels. This catalytic effect has already been suggested from the gelation studies.

To know the minimum concentration of dopant required to observe a catalytic effect, ^{29}SiNMR spectra were collected for a series of Nd^{3+} doped sol-gels at 10 seconds and 30 seconds reaction time where Q^0 species would still be observed. The spectra collected are presented in Appendix 3.

The data showed three different types of behaviour according to the concentration of dopant in the sol-gel (Figure 3.20, 3.21). As for the previous studies, an average of 3-4 measurements were collected in order to obtain reproducible peak areas. As the results were consistent, an average of the peak areas for every reaction time is presented for each concentration.

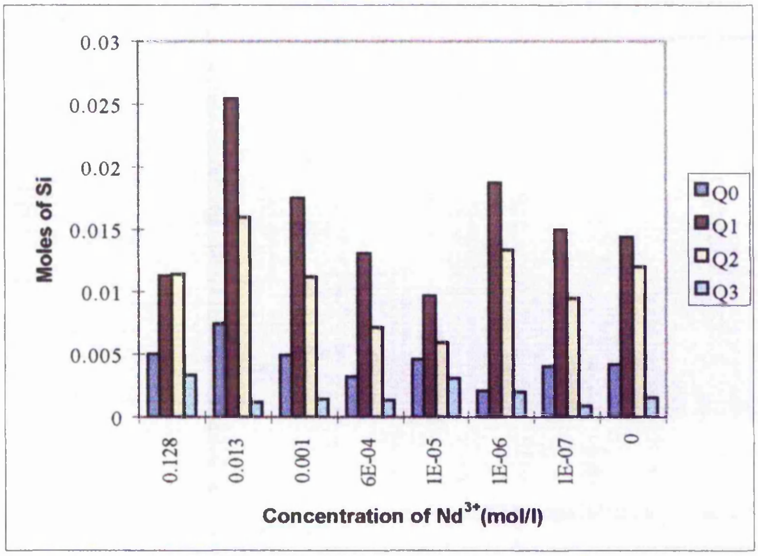

Figure 3.20: Variation of the silica species with the concentration of Nd^{3+} metal ion at 10 seconds of reaction

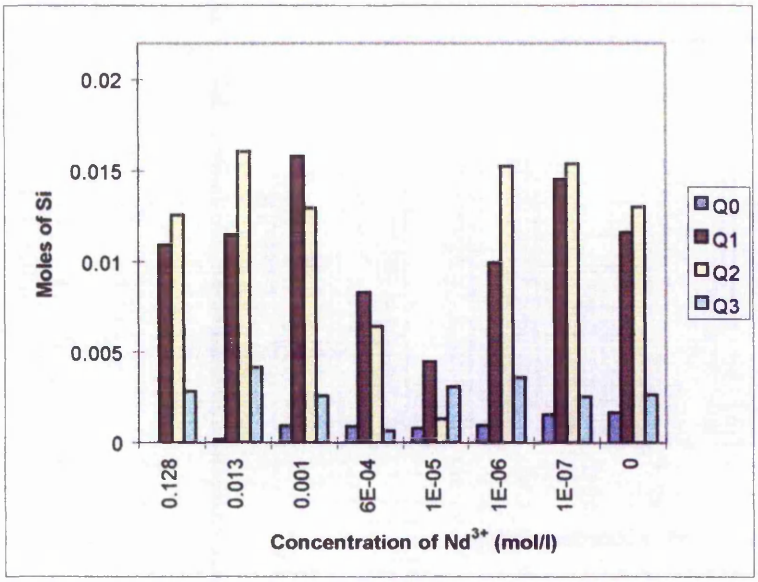

Figure 3.21:Variation of silica species with the concentration of Nd^{3+} metal ion at 30 seconds of reaction.

With or without dopants in the sol-gel solutions, hydrolysis and condensation reactions were relatively fast. Q^0, Q^1, Q^2 and Q^3 species was observed after 10 seconds of reaction. Regardless of the concentration of the metal ion in the sol-gel solution, the number of moles of $Q^1$and Q^2 Si species was higher than the number of moles of Q^0 and Q^3 Si species. However, as the concentration of the metal ion in the sol-gel solution increased the number of moles of Q^3 Si species increased as well with a value of 0.004moles for Nd^{3+} 0.128M sol-gel solution in comparison with 0.002moles for normal sol-gel solutions. Two different patterns in the formation of Si species were observed. At high concentrations of the metal ion in the sol-gel solution (0.128M), the reaction was well advanced as Q^3 species were already observed and the number of Q^1 and Q^2 Si species was lower than for normal sol-gels or lower concentrations of the metal ion in the sol-gel solution.

For a lower concentration (0.0128M) of the metal ion in the sol-gel solution, the number of Q^0, Q^1 and Q^2 Si species was higher than for high concentrations (0.128M) of the metal ion and normal sol-gel solutions. Furthermore, the number of Q^3 species was lower. Then as the concentration of Nd^{3+} metal ion in the sol-gel solution decreased down to $1.28.10^{-5}$M, the number of moles of Q^0, Q^1 and Q^2 decreased and the number of moles of Q^3 increased.

Finally, for concentrations of the metal ion in the sol-gel solution between 1.28.10^{-6}M and 1.28.10^{-7}M, the number of moles of Q^0,Q^1,Q^2 and Q^3 species became very similar to that of normal sol-gel solutions.

At 30 seconds, regardless of the concentration of the metal ion in the sol-gel solution, the number of moles of $Q^1$and Q^3 Si species was higher than the number of moles of Q^0 and Q^3 species.

For higher concentrations of the metal ion in the sol-gel solution (0.128M), Q^0 species were no longer observed and the amount of Q^3 species remained the same suggesting that some of the Q^0 became Q^1, some Q^1 became Q^2 (an increase of the number of moles was noticed), some Q^2 became Q^3 and some Q^3 became Q^4 (Q^4 cannot be observed with our NMR technique).

As the concentrations of dopant decreased the number of moles of Q^0 Si species increased with a maximum for 1.28.10^{-7}M and normal sol-gel solutions. At concentrations between 0.0128M and 1.28.10^{-5}M of the metal ion in the sol-gel solution, the number of moles of Q^1 and Q^2 Si species decreased and the number of moles of Q^3 Si species increased. At these concentrations of the dopant in the sol-gel solution, the condensation reaction appeared slower than for higher concentrations of the dopant. Due to this a higher number of moles of Q^0, Q^1 and Q^2 species were observed in comparison with the Nd^{3+} 0.128M sol-gel solution.

At concentrations 1.28.10^{-7}M of the metal ion, the number of moles of Q^0,Q^1,Q^2 and Q^3 was very similar to the one of normal sol-gel.

The extent of hydrolysis was dependent on the concentration of the dopant in the sol-gel solution.

Below 1.28.10^{-5}M, the hydrolysis and condensation reactions were slowed down in comparison with higher concentrations of the metal ion in the sol-gel solution. However, differences were still observed in comparison with normal sol-gel solutions. However, at Nd^{3+} concentration of 1.28.10^{-7}M, no noticeable effect of the metal ion on the precursors was observed.

To know if the effect of the metal ion on the sol-gel process as shown by ^{29}SiNMR was due to the type of metal ion or only to the fact that a metal ion was present in the system, Ce^{3+} ions were used also. In our study, the Ce^{3+} metal ion was used as it possessed bands in the UV region and could be used as a potential standard (see Chapter 5). As stated previously, Ce^{3+} metal ions affected the drying rate and the gelation process. ^{29}SiNMR data were collected for Ce doped sol-gels for the following concentrations of the metal ion in the sol-gel solution: 0.0897M-0.0128M-0.00128M. The maximum concentration was 0.0897M due to solubility limitations. The spectra of Ce sol-gel solutions (0.0897M-0.00128M) can be found in Appendix 5.

A shift of the peaks was observed with Ce^{3+} sol-gel solutions as compared to normal sol-gel solutions.

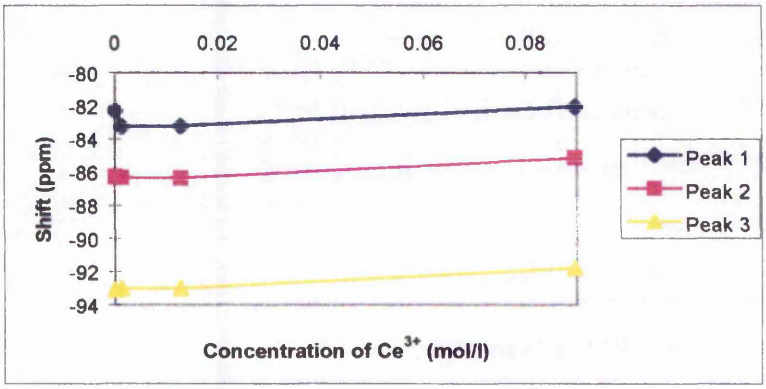

Figure 3.22: Effect of the concentration of Ce^{3+} doping in the sol-gel on the shift of the peaks with peak 1corresponding to Q^1 species $\equiv SiOSi(OH)_3$, peak 2 corresponding to Q^1 species $\equiv SiOSi(OC_2H_5)(OH)$ and peak 3 corresponding to Q^2 species $(\equiv SiO)_2Si(OH)(OC_2H_5)$

A shift toward lower ppm was observed as the concentration of the dopant increased in the sol-gel solution. However, a shift toward lower ppm was observed between a concentration of the metal ion of 0.0128M and normal sol-gel solution for peak 1 and peak 2, and a shift toward higher ppm was observed for peak 3.

The effect of the dopant on the silica species present was studied.

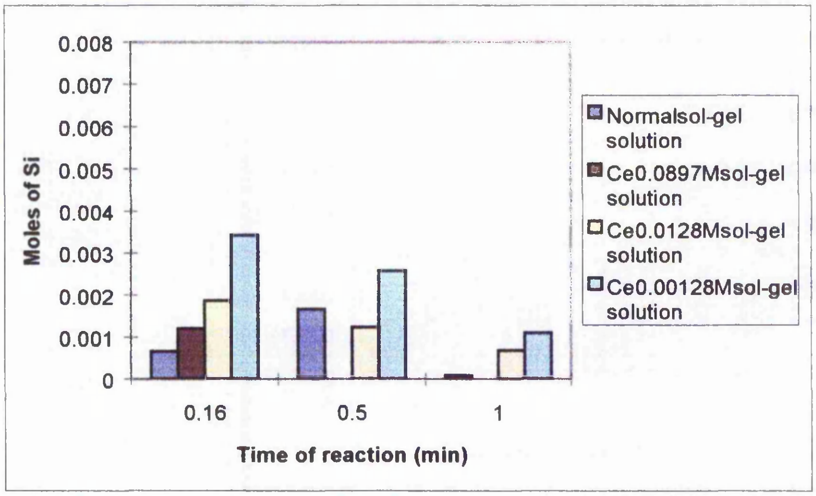

Figure 3.23:Variation of Q^0 species with the time of reaction

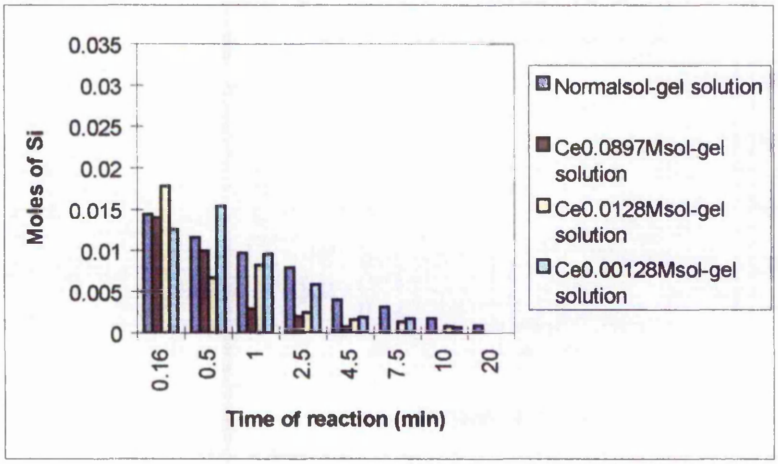

Figure 3.24: Variation of Q^1 species with the time of reaction

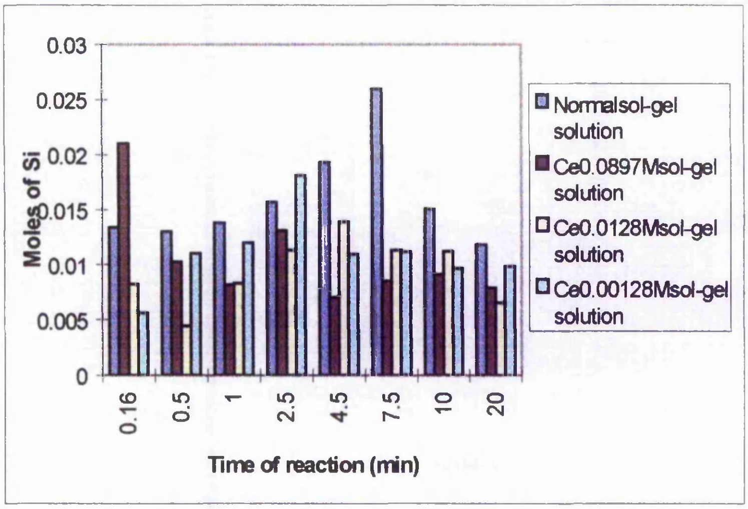

Figure 3.25: Variation of Q^2 species with the time of reaction

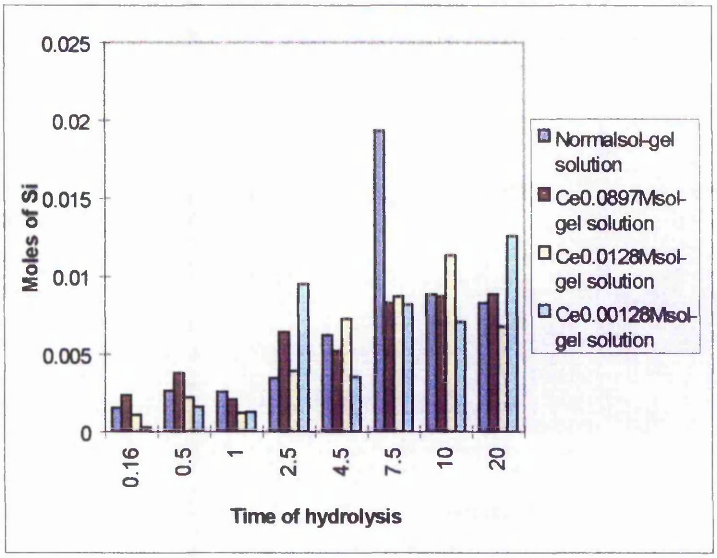

Figure 3.26: Variation of Q^3 species with the time of reaction

Ce^{3+} metal ions affect the pattern of silica species present at the different analysis points. In comparison with normal sol-gels, the number of moles of Q^0, Q^1, Q^2 and Q^3 Si species was affected by the presence of the Ce^{3+} ion. As the concentration of the metal ion in the sol-gel solution decreased, the silica speciation pattern became similar to normal sol-gel solutions.

The number of moles of Q^0 Si species was only observed for the first minute of hydrolysis and condensation reactions. Afterward Q^0 species were no longer present.

At 10 seconds of reaction, the number of Q^0 species was higher in the presence of dopant than with normal sol-gels. At 30 seconds, a decrease of the Q^0 species for doped sol-gels was observed whereas the Q^0 species of normal sol-gels had increased. At 1 minute, the number of moles of Q^0 species for normal sol-gels and Ce^{3+} doped sol-gels had considerably decreased, although the Ce^{3+} doped solutions at 0.0128M and 0.00128M still contained higher levels than for the normal sol-gel solutions.

A decrease of Q^1 species was observed as the reaction proceeded. At 20 min, only Q^1 species for the normal sol-gel were detected. The Q^1 species of Ce^{3+} doped sol-gels were no longer observable.

An increase of the Q^2 species was noticed during the first 4:30 minutes followed by a decrease.

An increase of the Q^3 species during the whole 20 minutes was noticed also. The number of moles of Q^2 species was higher in the normal sol-gel solution whereas the number of moles of Q^3 species was higher in doped sol-gel solutions.

By comparing the effect of Nd^{3+} and Ce^{3+} ions on the precursors, it is possible to see that fewer Q^0 and Q^1 species were present in the system when Ce^{3+} ion was the dopant regardless of the concentration used.

Q^2 and Q^3 species were present at higher levels at the first time point analysed in the reaction with Ce^{3+} rather than with Nd^{3+}.

When the sol-gel was doped with Ce^{3+} a different pattern of the silica speciation was apparent in comparison with the sol-gel doped solution with Nd^{3+}.

An increase of the Q^2 species was noticed followed by a decrease after 4:30 minutes whereas the decrease in the Nd sol-gel was noticed after 7:30 minutes.

An increase of the Q^3 species was noticed with the time of reaction for the sol-gel solution doped with Ce^{3+}. The increase of the Q^3 species was higher than with Nd sol-gel solution. Moreover the total amount of silica species detected for the Q^2 and Q^3 species was lower for the Ce^{3+} system than Nd sol-gel solution meaning that a lot more Q^4 species had already formed in the system containing Ce^{3+} (ie. the reaction has gone further).

3.3.4.2-Discussion

The study of the variation of the different silica species present in normal sol-gel solutions and Nd^{3+} sol-gel solutions was carried out in order to understand the molecular changes occurring within the system in the presence of specific dopant metal ion. Knowing the effect of the dopant on the silica precursors will help to prepare sol-gels with specific optical properties.

The interpretation of this data did not allow a comparison between the total number of moles of Si introduced in the system and the total number of the different silica species detected in the system. This is due to the fact that some silica species are detected more than once, for example the Q^1 species being at the end chain of Q^2 species, or some silica species being already Q^4 and not being observable in our system. Consequently, only the number of moles of the different species could be used for comparison.

When comparing the number of moles of Q^0 and Q^1 species present in the system, it was noticed that the levels were dependent on the concentration of the Nd^{3+} dopant in the system.

The higher the concentration of the dopant, the lower the number of moles of Q^0 and Q^1 species.

Q^0 and Q^1 species decreased with time whereas Q^2 and Q^3 species increased and then decreased during the formation of the silica network (Q^4 species).

Q^0 and Q^1 species were used during the hydrolysis and condensation reactions to form Q^2 and Q^3 species.

The formation of these groups of silica species varied with the concentration of the dopant in the sol-gel solution.

At a high concentration (0.128M) of the dopant in the sol-gel solution hydrolysis and condensation reactions occur quickly as Q^2 and Q^3 species are already observed at 15 seconds of reaction and their levels are higher than for undoped sol-gels or doped sol-gels with low concentrations of dopant (below 0.0128M).

For undoped sol-gels and sol-gels with low concentrations (below 0.0128M) of dopant, Q^0 species disappear very quickly and Q^1, Q^2 and Q^3 speices are present in the system at 10 seconds. The formation of the silica matrix is already occurring at 10 seconds. Consequently hydrolysis occurs very fast.

Moreover the condensation reaction is slower for sol-gel solutions with low concentration of dopant (below 0.0128M) than for high concentrations of dopant as it took longer for the Q^0 species to disappear and be used in the formation of Q^1 species.

Consequently we can say that the presence of the dopant in the sol-gel acts as a catalyst but a certain amount of dopant is needed to act as a catalyst not only for the hydrolysis reaction but for the condensation reactions as well.

The pattern of change in the number of moles of silica species present at different time points is characteristic of the formation of the silica matrix.

Q^0 species were completely used after 30 seconds and no longer observable for normal sol-gel solutions and low concentration doped sol-gel solutions (below 0.0128M). They had been used in the condensation reaction to form Q^1 species.

For high concentrations of the dopant, no Q^0 species could be observed. This suggests that they were used as soon as the precursors were mixed together during the hydrolysis and condensation reactions. Consequently the dopant (0.128M) increases the rate of hydrolysis and condensation reactions.

Moreover for low concentration doped sol-gels (below 0.0128M) more Q^0 species could be observed than for normal sol-gel solutions meaning that the rate of hydrolysis has been increased but not the rate of condensation otherwise the species formed by hydrolysis reactions would have been immediately used to produce condensed species.

As the concentration of the dopant decreased in the reaction medium the amount of Q^0 species observable increased. So a certain amount of metal ions in the reaction medium could serve to increase the hydrolysis rate. When the concentration of the dopant was too low (below 0.0128M), only the hydrolysis rate was increased. The metal ions act as a catalyst for this process. The condensation rate was also increased for doped sol-gel solutions at higher concentration (above 0.0128M) as no Q^0 species were observed.

For the Q^1 species, the intensity of the peaks was higher for the first 1min for the Nd 0.128M sol-gel solution and the normal sol-gel solution than for Nd 0.0128-0.00128M sol-gel solutions meaning that the formation of these species was quicker due to the catalytic effect of the metal ions. Consequently the intensity of these peaks became lower for doped sol-gel solutions (0.128M) than doped sol-gel solutions (below 0.0128M) after a minute as these molecular species were used for the formation of Q^2 species.

The peaks at –83.21ppm and –83.42ppm (Q^1 species) correspond to two types of silanol species with different linear chains. These peaks were observed only at low concentrations of dopant in the sol-gel solutions and for normal sol-gel solutions. For high concentrations one peak only was observed at -83.42ppm. The relative intensity of one peak in relation to the other increased as the concentration of the dopant decreased. Consequently it is possible to assign the peaks and say that the peak at -83.21ppm corresponds to silanol groups dominant when the presence of the metal ion is low or non existent and the peak at -83.42ppm is dominant when the concentration of the dopant is high.

The condensation reaction to form silica used the linear species at a slower rate than the cyclic species. Moreover, the decrease in intensity of the cyclic species was quicker in the presence of dopant in the sol-gel solution in comparison with normal sol-gel solutions again suggesting an effect on the rate of hydrolysis and condensation reactions.

For Q^2 groups the same behaviour was observed as for Q^1 as these species were used for the formation of Q^3 species.

After 7:30minutes the same speciation pattern (decrease of Q^0, Q^1, Q^2 and Q^3 species) was observed for doped and undoped sol-gels meaning that the metal ions affect the precursors only at the beginning of the reaction where initial hydrolysis and condensation reactions take place.

The ^{29}SiNMR data of Ce^{3+} doped sol-gels have shown that this dopant also has an effect on the silica precursors. In the presence of the dopant, the formation and then disappearance of Q^0 and Q^1 species was quicker and the formation of Q^2 and then Q^3 species faster than for normal sol-gel solutions. At high concentrations (0.0897M) of the metal ion in the sol-gel solution, Q^0 species were no longer observable after 10 seconds and Q^1 species after 4:30 minutes. These silica species were used during the hydrolysis and condensation reactions for the formation of Q^2 and Q^3 species. The number of Q^2 species was already high at 10 seconds of reaction meaning that in this system the hydrolysis and condensation reactions are very fast, even faster than for the Nd^{3+} doped system.

So the Ce^{3+} ion had an effect on the precursors and the silica formation as the formation of the Q^2 and Q^3 species were faster in their presence.

The effect of the Ce^{3+} ion on the precursors had a catalytic effect in the same way as for the Nd^{3+} ion. The rate of the hydrolysis and condensation reactions was quicker for the sol-gel doped with Ce^{3+} instead of Nd^{3+}as measured by the shift in emphasis of the Q^1 signal in the NMR spectrum.

The disappearance of the Q^2 species was noticed at 7 minutes and 30 seconds for Ce^{3+} (0.0897M) sol-gel whereas for the Nd^{3+}sol-gel at 20 minutes Q^2 species could still be observed.

The same behaviour was observed for all the silica species and at all concentrations of the metal ion investigated.

Consequently Ce^{3+} has a more pronounced catalytic effect than Nd^{3+}.

In conclusion, the dopants affect both the rate of hydrolysis and the rate of condensation of the silica precursors in the formation of silica matrix.

A certain concentration of metal ions is required to increase the hydrolysis rate but not the condensation rate as for low concentration (below 0.00128M for Nd^{3+} and below 0.0128M for Ce^{3+}) doped sol-gel solutions only the hydrolysis rate was increased and increases in levels of Q^0 species could be observed.

However for high concentrations of the dopant (0.128M for Nd^{3+} and 0.0897M for Ce^{3+}), Q^0 species were not observed. At these concentrations, the metal ions interact with the Q^0 and Q^1 species as soon as they are formed enhancing the condensation pathway.

As the Q^1 species contain silanol species it is more likely that the remaining metal ions not used in a catalytic mode for the hydrolysis reaction, interact with the silanol groups present on the developing polymer chain and probably bond electrostatically to the silicon atom via the oxygen groups.

To know if the observed catalytic effect was due to a variation of pH and/or due to the metal ion and its ligands, a study of pH was carried out using normal sol-gel solutions and Ndsol-gel solutions.

3.3.5-Study of the variation of the pH in the sol-gel system in the presence of Nd^{3+} at a range of concentrations

3.3.5.1-Results

As has been seen in the previous paragraph, the dopant has a direct effect on the hydrolysis and condensation reactions involved in forming the silica gel matrix. This effect could either result from a modification of the pH of the system (H^+ catalysis) and/or an effect of the metal ion (metal ion catalysis). For a better understanding of the nature of this interaction a study of pH changes in the sol-gel system during the early stages of reaction was carried out.

The pH of the neodymium salt in ethanolic solution was measured at different concentrations (Figure 3.27). The measurement of pH in ethanolic solvent was performed as the dopant was prepared in this solvent for the formation of the sol-gel material.

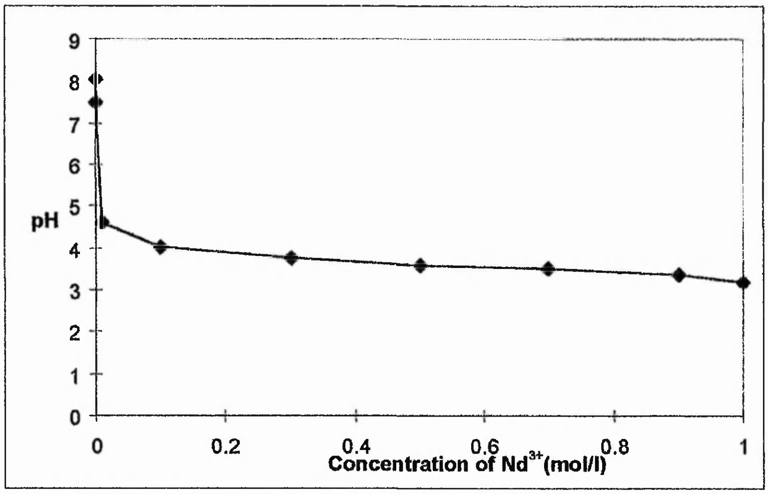

Figure 3.27: pH of neodymium ion in ethanol solution at different concentrations

The pH of the Nd^{3+} containing solution was relatively acidic. A decrease of the acidity (an increase in pH) was observed with decreasing concentration of the metal ion. Solutions of the metal ion (1M-10^{-3}M) were more acidic than TEOS (pH=8.34) and ethanol (pH=8.18). The theoretical value of the pH of dry ethanol was 8 (calculated from the pK_a=16) [50]. Consequently it could affect the sol-gel process as even a very small variation in pH can affect the rate of the hydrolysis and condensation reactions.

For example, increasing the pH by 0.5 of a unit has been found to double the rate of gelling, an end indication of the speed of the hydrolysis and condensation reactions [51]. It was also possible that the amount of dopant added would not be enough to affect the pH of the precursors in an acidic medium. To know the lowest concentration of dopant at which the pH of the precursors (without the acid catalyst) was no longer affected by the dopant, the pH of solutions containing only TEOS and ethanol, and solutions containing TEOS, ethanol and Nd^{3+} at various concentrations, were measured for one hour (Figure 3.28). Two sets of pH measurements for every solution were carried out to obtain reproducible results. The concentrations of the metal ions in solution used correspond to the concentration of the metal ion in sol-gel solution studied during the NMR experiments.

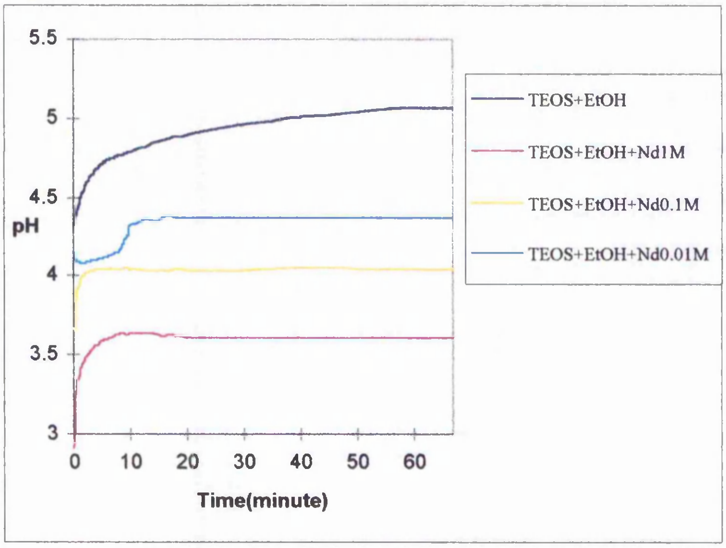

Figure 3.28: Variation of the pH with TEOS, EtOH and the Nd^{3+} ion at different concentrations (1M-0.01M)

When the dopant was added to a solution containing TEOS and ethanol, the pH of the solution was affected. The pH decreased when the concentration of the dopant was increased. The decrease in acidity corresponds to the decrease of the pH of the metal ion at different concentrations.

The dopant had an effect on the pH of the EtOH+TEOS solution even without acid. It affects the pH of the whole solution. To observe any effect it was necessary to have a concentration of neodymium ions in ethanol starting from 10^{-4}M, below that limit the dopant's concentration was too low to see any effect on the pH which became similar to that of solutions containing TEOS+EtOH only.

When the catalyst (HCl- 0.5M) was added to the precursors, the pH of the sol-gel solution became very acidic.

The pH of normal sol-gel solutions and doped sol-gel solutions were recorded for the first hour of reaction (Figures 3.25a→i) to identify the effect of the dopant on the pH of the reaction medium in the presence of acid (the pH was measured every 5 seconds). After one hour, the viscosity of the sol-gel solution had increased and made it difficult to make pH measurements. Two runs were made for every sol-gel solution to ensure for reproducibility.

The drop of pH observed for every sol-gel solutions (doped and undoped) at the beginning of the reaction corresponded to the addition of the acid catalyst into the system.

Figures 3.29:Variation of the pH with time for sol-gel reactions carried out in the presence of different concentrations of Nd^{3+}

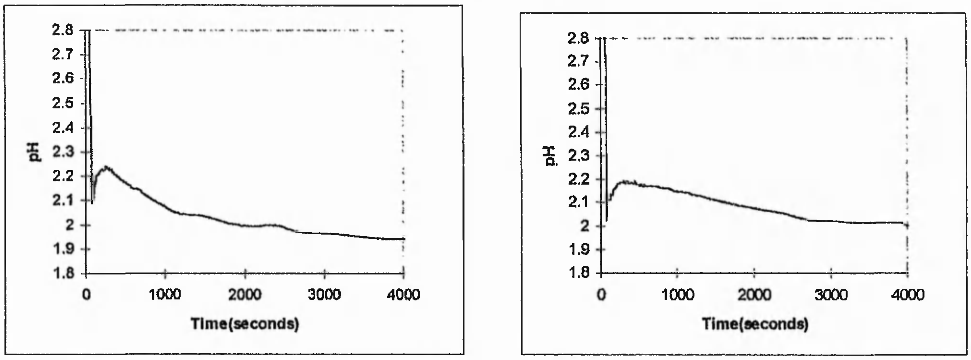

Figure 3.29.a: Normalsol-gel solution Figure 3.29.b: Nd0.128Msol-gel solution

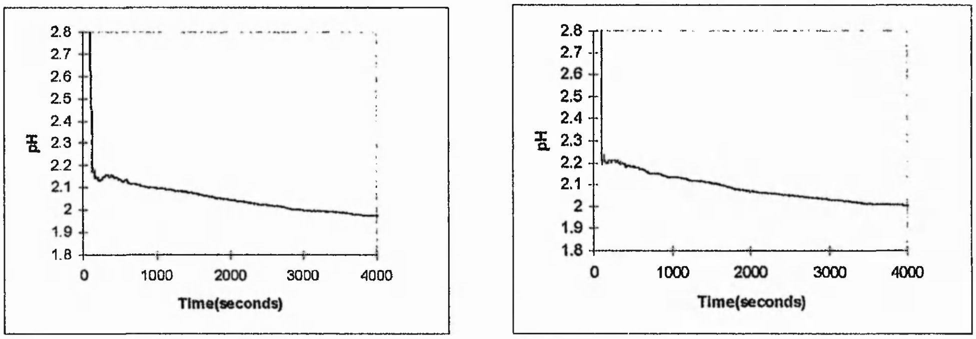

Figure 3.29.c: Nd0.115Msol-gel solution Figure 3.29.d: Nd0.0897Msol-gel solution

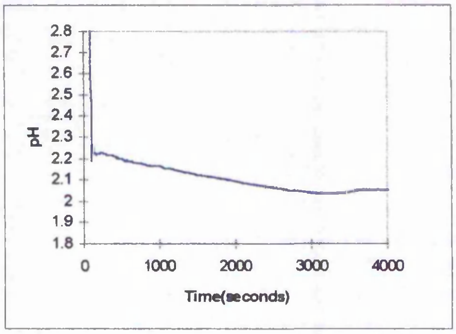

Figure 3.29.e: Nd0.064Msol-gel solution

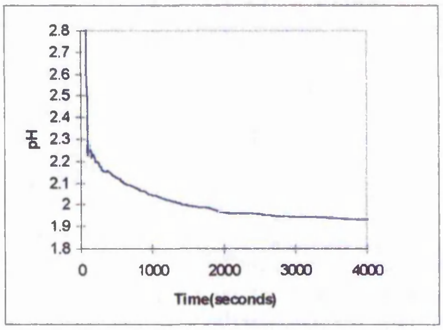

Figure 3.29.f: Nd0.038Msol-gel solution

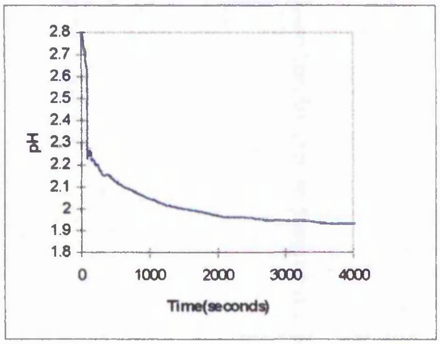

Figure 3.29.g: Nd0.0128Msol-gelsolution

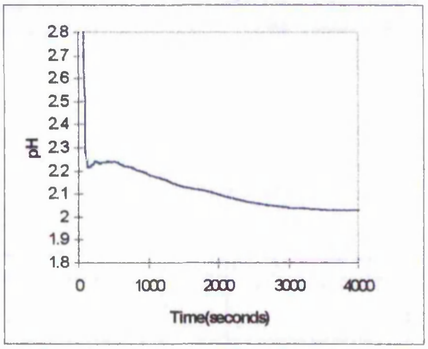

Figure 3.29.h: Nd0.00128Msol-gelsolution

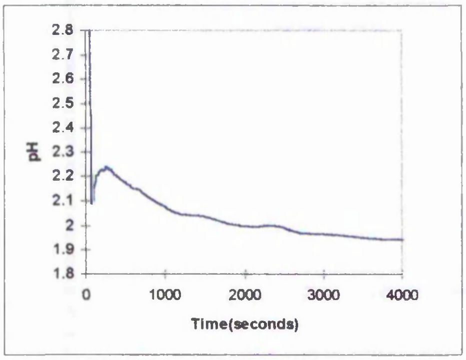

Figure 3.29.i: Nd1.28.10^{-5}Msol-gel solution

The pH of the sol-gel solution changed with the time of reaction.

The variation of the pH of normal sol-gel solutions showed two different regions. When the acid had been added to the solution containing TEOS and ethanol, the pH of the solution dropped. As soon as they have been mixed together an increase of the pH was measured reaching a maximum at 4:30 min. Finally the pH decreased to reach a stable pH after 25min.

At high concentrations of the dopant in the sol-gel solution, the pH behaviour was of the same pattern as for normal sol-gels. After addition and mixing of the acid with the precursors an increase of the pH with a maximum at 4:30 min followed by a slower decrease of pH than for normal sol-gels was observed.

A lower pH was observed for the first 10 min of reaction in the presence of Nd^{3+} (0.128M) in the sol-gel solution in comparison with normal sol-gels. Then after these 10 minutes, a lower acidity than for normal sol-gels was observed. The difference between the highest pH at 4:30 min and the stabilised pH after 25 min, was 0.17 units for Nd^{3+} (0.128M) sol-gel solutions and of 0.28 units for normal sol-gel solutions.

So a difference of 0.1 unit was noticed between the highest concentration (0.128M) of the dopant in the sol-gel solution and the normal sol-gel solution.

When the concentration of the dopant was decreased, the acidity of the sol-gel solution increased. At concentrations of the metal ion between 0.115M and 0.0128M of the metal ion in the sol-gel solution, the increase of pH observed at the beginning of the reaction was not as significant as for high concentrations of the metal ion in the sol-gel solution and normal sol-gel solutions. The initial pH (as soon as the precursors have been mixed together) was already higher.

At low concentrations (from 0.00128M) of the metal ion in the sol-gel solution, the curve became similar to that obtained for normal sol-gels (figure 3.28).

The ^{29}SiNMR data have shown a difference in silica species with time according to the dopant introduced in the system.

The pH of Nd^{3+} metal ion varies according to its concentration in solution and hence influences the pH of the sol-gel solution.

For comparison, the pH of the Ce^{3+} metal ion in ethanol solution at various concentrations was measured (figure 3.30).

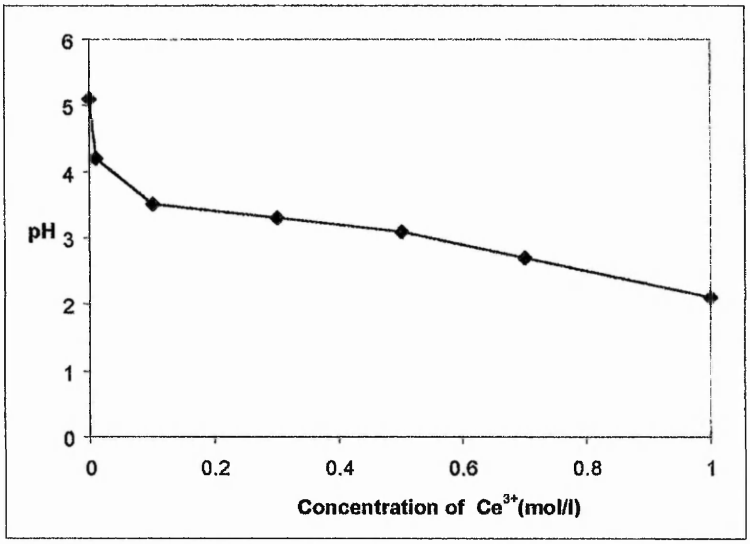

Figure 3.30: pH measurement of Ce^{3+} in ethanol solution

When compared with the pH of neodymium ion in solution, the pH of cerium ion in solution was more acidic.

Consequently the increase in acidity could cause an increase in the speed of the hydrolysis and condensation reactions. So cerium ions could be a better catalyst than neodymium ion due to its higher acidity.

3.3.5.2-Discussion

At the beginning of the reaction, the acid is used by the hydrolysis and the condensation reactions and a decrease of pH was observed. Then as the reaction proceeded the acid was used and the pH decreased corresponding to the combined acidity of the different silanol groups present in the system. The acidity of the whole reaction was above pH=2 and so the rate of the condensation reaction which involves an ionic mechanism was proportional to the concentration of OH^-. Active anionic silica was generated [1] and then used in the condensation reaction.

After 25 min, the pH was relatively stable which meant that the species forming in the silica network have the same acid dissociation constant. As seen by ^{29}SiNMR, after 20 min the most important species present were Q^3 and Q^4 species. The monomers had polymerised to form dimers and higher molecular weight species of silicic acid (trimer, tetramer and much higher species).

The variation of pH observed in the system used for the generation of sol-gel absorbance standards was of the order of 0.1 unit pH for the largest differences between the normal sol-gel solution and sol-gel solutions with the highest concentration of dopant (0.128M). As the pH of Nd^{3+} is acidic, this small change of acidity could come from the metal ion introduced into the solution. Acting as a catalyst, the metal ion speeds up the hydrolysis and condensation reactions involving a higher consumption of acid and catalyst thus explaining the higher pH of doped sol-gel solutions in comparison with normal sol-gel solutions at the beginning of the reaction. The NMR data have shown that a difference in the speed of the hydrolysis and condensation reactions is observed according to the metal ion present in the system. Consequently the effect of the dopant on the hydrolysis and condensation reactions is due to the metal ion itself and its acidity but the ligands around the metal ion could also play a role in the observed effect.

3.3.6- Effect of the metal ion on the precursors

3.3.6.1-Results

To know if the catalytic effect observed is due to the metal ion and its ligands or only due to its acidity, the exact number of ligands around the metal ion was determined.
Nd^{3+} salts in water contain Nd^{3+} ions which possess an inner sphere of ligands which are water.

The dopant is Neodymium metal ions surrounded by a sphere of water ions.
Using the Karl Fisher method, the water present around the metal ion was titrated.
After titration, 6 moles of water were found in the system for $Nd(NO_3)_3.xH_2O$ dissolved in dry ethanol. This does not imply that they are bonded to the metal ion, they can be in solution as well as part of the solvent and not boned any longer to the metal ion.
In order to know if the water ligands had the observed catalytic effect on the precursors, normal sol-gels were prepared with an excess of water corresponding to the amount required to account for the water ligands around the metal ion at a particular dopant concentration. For a concentration of 0.128M neodymium ion in the precursors, the number of water moles from the metal ion complex is 0.01823moles and for a concentration of 0.0128M the number of water moles is 0.001823moles.

Normal sol-gels were prepared with an additional amount of water corresponding to the amount of water present around the metal ion at concentrations of 0.128M and 0.0128M. The pH of the sol-gel solutions were studied (Figure 3.30)

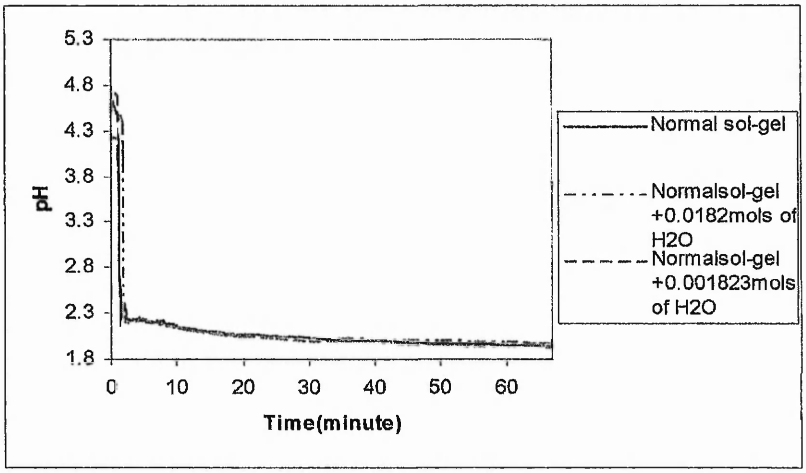

Figure 3.30: Normal sol-gel pH with variation of the amount of water

The three curves had the same shape and pH.

The addition of water did not affect the pH of the sol-gel during the first hour of reaction. The changes observed on the pH according to the concentration of the metal ion dopant in the sol-gel solution were consequently due to the metal ion itself.

This change of pH was very low and the effect of the dopant observed by ^{29}SiNMR spectroscopy was very important. So there was also a possibility that the water ligands around the metal ion interact with the precursors when mixed with them. Consequently the catalytic effect could have been due to either the metal ion or to the water associated with the metal ion.

^{29}SiNMR spectra were collected at 10 seconds and 30 seconds for sol-gel solutions to which had been added an amount of water corresponding to that measured for the Nd^{3+} ion from $Nd(NO_3)_3.6H_2O$ in solution.

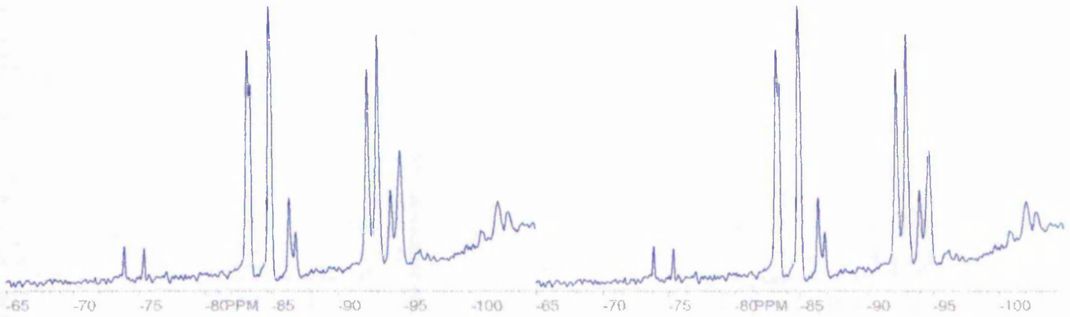

a) b)

Figure 3.31: At 10 seconds of reaction
a)Normal sol-gel + addition of 0.01823 moles of water, b)Normal sol-gel

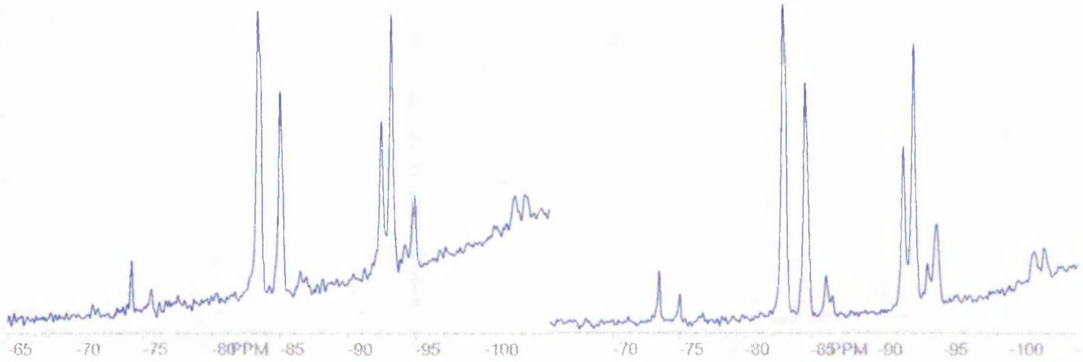

a) b)

Figure 3.32: At 30 seconds,
a)Normal sol-gel + addition of 0.01823 moles of water, b)Normal sol-gel

The same spectra were obtained. Q^0,Q^1,Q^2,Q^3 species were present at the same chemical shifts. The only difference observed was a slightly lower intensity in the peaks for normal sol-gel (comparison done by GRAMS 32). This could have beeen due to the detection of the spectrometer (two runs for every time of hydrolysis and sol-gel were made).

3.3.6.2-Discussion

The water ligands around the metal ion do not affect the pH of the sol-gel solution.

As the same type of chemical species were observed for normal sol-gels and normal sol-gels with additional water, the water ligands around the metal ion do not have any catalytic effect on the precursors. The ligands are covalently bonded to the metal ion and do not interact with the environment surrounding the metal ion.

The catalytic effect of the metal ion on the precursors is consequently due to the presence of the hydrated metal ion itself.

The cationic effect of the metal ion must be the cause of the catalytic effect.

3.4-Conclusions

Through these studies, it has been shown that the metal ion affects the drying process of the sol-gels suggesting a direct interaction between the gel matrix and the metal ions themselves. FTIR (midIR and NIR) of the silica sol-gel solutions and glasses have shown that the intensity of the hydroxyl species is higher in the presence of dopant. Moreover, the metal ion is present in the silica matrix and its NO^{-}_{3} groups can be observed.

This shows that the dopant has an effect on the matrix.

The gelation point study has demonstrated the fact that the dopant interacts with the precursors as soon as they are mixed to form the matrix. The gelation time was a lot longer with high concentrations of the dopant in the sol-gel than with low concentrations of the dopant or no dopant at all. The difference in gelation is due to the presence of silanol groups which are less numerous with high concentrations of the dopant as the dopant interacts with the precursors.

^{29}SiNMR showed that the dopant has two roles in the hydrolysis and condensation reactions. First it acts as a catalyst to speed up the reactions and second it interacts with the silanol precursors to be covalently bonded with the matrix.

By recording the pH of the sol-gel solutions with the pH and different concentrations of the dopant, it was demonstrated that the effects observed during the hydrolysis and condensation reactions could be affected by the pH changes from the metal ion only and not its ligands.

According to the metal ion and its acidity, the hydrolysis and condensation reactions were affected in a different manner.

In conclusion, the dopant first interacts with the precursors as soon as the reaction is initiated and not when the solution becomes a gel or dry.

This understanding will help in the preparation of the doped sol-gel.

In the future it will be possible to add the dopant during the preparation of the sol-gel in a more accurate way according to the desirable effects of the dopant on the precursors or on the sol-gel and as well according to the desired changes of the structure of the matrix. Glasses will then be prepared with a better understanding of their desired properties.

REFERENCES

[1] E.M.Rabinovich, *Sol-Gel Optic Processing Optics*, (publishers Kluwer Academic, New York), 1, (1993)

[2] L.L.Hench, Ceramics International, **17**, 206, (1990)

[3] C.C.Perry, *Sol-gel Technology-Sira Technology Centre* , (one day course not published), (1997)

[4] L.L.Hench, J.K.West, Chem.Rev., **90**, 33, (1990)

[5] C.J.Brinker, G.W.Scherer, *Sol-Gel Science*, (publishers Academic Press inc, London), (1990)

[6] G.H.Engelhart, W.Atlenburg, Z.Anorg.Alg.Chem., **43**, 428, (1977)

[7] R.K.Hanis, C.T.G.Knight, J.Chem.Soc.,Chem.Commun., **421**, 726, (1980)

[8] P.F.James, J.Non-Cryst.Solids, **100**, 93, (1988)

[9] T.N.M.Bernards, PhD Thesis, (publishers Ponsen & Loojens, Wageningen), (1997)

[10] A.H.Boonstra, T.N.M.Bernards, J.Non-Cryst.Solids, **105**, 207, (1988)

[11] W.Atlenburg, D.Hoebbel, W.Wicker, Z.Anorg.Alg.Chem., **428**, 43, (1977)

[12] J.C.Pouxviel, J.P.Boilot, J.Non-Cryst.Solids, **89**, 345, (1987)

[13] R.A.Assink, B.D.Kay, Abstr. of papers of the Amer.Chem.Soc., **202**, 256, (1991)

[14] R.A.Assink, B.D.Kay, Abstr. of papers of the Amer.Chem.Soc., **200**, 144, (1990)

[15] R.A.Assink, B.D.Kay, Abstr. of papers of the Amer.Chem.Soc., **193**, 318, (1987)

[16] J.Jonas, Molec.Liquids, **48**, 233, (1991)

[17] I.Artaki, S.Sinka, A.D.Irwin, J.Non-Cryst.Solids, **72**, 391, (1985)

[18] I.Artaki, M.Bradley, T.W.Zerda, J.Phys.Chem., **89**, 4399, (1985)

[19] I.Artaki, T.W.Zerda, Mat.Lett., **12**, 493, (1985)

[20] G.Öye, F.Olav Libnau, J.Sjoblon, S.E.Friberg, Colloids Surfaces A:Physicochem.Eng.Aspects, **123**, 329, (1997)

[21] D.A.Skoog, D.M.West, *Fundamentals of Analytical Chemistry*, 4th edition, (publisher Saunders College, London), (1982)

[22] F.L.Galeener, J.C.Mickelson, J.Phys.Rev.B, **23**, 5527, (1981)

[23] H.Yoshino, F.Kamiya, H.Nasu, J.Non-Cryst.Solids, **126**, 68, (1990)

[24] D.L.Wood, E.M.Rabinovich, D.W.Johnson, J.B.Machesney, E.M.Vogel, J.Am.Ceram.Soc., **66**, 693, (1983)

[25] A.Duran, C.Serna, V.Fornes, J.R.Fernandez Navarro, J.Non-Cryst.Solids, **82**, 69, (1986)

[26] A.Bertoluzza, C.Fagnano, M.A.Morelli, J.Non-Cryst.Solids, **48**, 117, (1982)

[27] D.L.Wood, E.M.Rabinovich, Applied Spectroscopy, **43**, 2, (1989)

[28] R.M.Almeida, T.A.Guiton, C.G.Pantano, J.Non-Cryst.Solids, **121**, 193, (1990)

[29] C.C.Perry, X.Li, J.Chem.Soc.Faraday-Trans., **87**, 761, (1991)

[30] C.C.Perry, X.Li, J.Chem.Soc.Faraday-Trans., **87**, 3857, (1991)

[31] F.L.Galeener, G.Lucosky, Physical Review Letters, **37**, 22, (1976)

[32] C.Kittel, *Quantum Theory of Solids*, 2nd edition, (publisher J.Wiley & Sons, New York), (1987)

[33] X.Li, PhD Thesis, Brunel University, (1991)

[34] M.Arora, M.M.Pradham, Indian J.Pure & Applied Physics, **31**, 409, (1993)

[35] M.Arora, M.M.Pradham, Infrared Physics, **34**, 49, (1993)

[36] A.Bernson, J.lindgren, Solid State Ionics, **86**, 369, (1996)

[37] S.S.Wang, Y.Zhou, Y.L.Lam, Mater.Res.Innova., **1**, 92, (1997)

[38] L.J.Bellamy, *The Infrared Spectra of Complex Molecules*, 3rd edition, (publisher Chapman & Hall, London), (1975)

[39] P.Hite, R.Kramansky, J.K.Thomas, J.Phys.Chem., **90**, 5795, (1986)

[40] F.Orgaz, H.Rawson, J.Non-Cryst.Solids, **82**, 57, (1986)

[41] J.H.Anderson, J.R & K.A.Wickersheim, J.Surface Science, **2**, 252, (1964)

[42] D.L.Wood, E.M.Rabinovich, J.Non-Cryst.Solids, **82**, 171, (1986)

[43] J.Kratochvila, Z.Salajka, A.Kazda, J.Non-Cryst.Solids, **116**, 93, (1990)

[44] P.Y.Chu, D.E.Clark, Spectroscopy Letters, **25**(2), 201, (1992)

[45] J.Y.Ying, J.B.Benziger, J.Non-Cryst.Solids, **147-148**, 222, (1992)

[46] A.Bertoluzza, C.Fagmano, M.A.Morelli, J.Non-Cryst.Solids, **48**, 117, (1982)

[47] M.H.Selle, F.Fredrisksen, J.Sjoblon, A.Christy, Acta.Chem.Scand., **50**, 12, (1996)

[48] G.W.Scherer, Mat.Res.Soc.Sym.Proc., **271**, 527, (1992)

[49] G.Orcel, J.Phalippou, L.L.Hench, J.Non-Cryst.Solids, **88**, 114, (1986)

[50] D.L.Pavia, G.R.Lampman, G.S.Kriz, *Introduction to Spectroscopy*, 2nd edition, (Harcourt Brace College publishers, London), (1996)

[51] R.K.Iler, *The Chemistry of Silica*, (publishers J.Wiley & Sons, New York), (1979)

Chapter 4: Effect of the Precursors and the Sol-Gel Matrix on the Coordination Chemistry of the Dopant Metal Ions

4.1- Introduction

The sol-gel process can be used for the preparation of glass with high optical quality and high purity [1].

Using this method, the preparation of the glass can be controlled from the beginning of the production process. Consequently the composition of the glass can be changed by introducing dopants which may be organic, inorganic and even biological such as enzymes [2]. The sol-gel process is widely used and enables the preparation of glassy materials in different forms such as thin films [3], monoliths [4] (xerogels and aerogels) and powders [5].

Zink et al. [6] studied the optical properties of the dopants (pyranine, europium(III) and terbium(III)) as the matrix evolves during the gelation, aging and drying stages.

Our work is concerned with the study of metal ion dopants in monolithic (xerogels) sol-gels and their effect on the drying process and on the sol-gel matrix.

The glass can be doped with metal ions as well as with organic compounds using the *pre-doped method*, which consists of doping the glass during its preparation. The pre-doped method has been used for encapsulating molecules for optical applications (laser radiation or semiconducteurs). Nogami [7] reported the preparation of glass doped with different semiconductors (CdS, ZnS, PbS) at low temperature, which was not possible with the melting method.

Yamane et al. [8,9] and Hench et al. [10] have shown a particular interest in the production of sol-gel glasses containing a controlled concentration of metal ions, very useful for the preparation of Gradient-index (GRIN) materials.

Shahriari et al. [11] have reviewed the different studies done on the sol-gel process allowing the immobilisation of organic macromolecules in inorganic glass networks for the preparation of fibre optic chemical sensors.

All these different works carried out using the sol-gel process used various dopants in order to obtain materials with different properties and hence applications.

In our work, neodymium ions, were principally used as a dopant in the glass. The metal ion was doped into the glass using the pre-doped method.

The neodymium ion has been widely used as a doping agent in the sol-gel glasses with one of the points of interest being its quality as a laser with action at ambient temperature [12-15].

To understand the behaviour of the dopant in the glass it is necessary to understand its spectroscopic behaviour.

The electronic configuration of Nd^{3+} is $4f^3$. The electronic transitions in f^q configurations are parity forbidden but in crystals and solutions, there arise weak so-called "forced" electric-dipole transitions [16]. As the observed spectra arise directly from crystal-field induced electric-dipole transitions, a change in neodymium environment [17,18] may be expected to give rise to changes in observed spectral features. The complex fine structure of the spectra arise from a number of transitions from the ground level ($^4I_{9/2}$) to excited levels. The "*hypersensitive transitions*" are $^4I_{9/2}\leftarrow{}^4G_{5/2},{}^2G_{7/2}$ (575nm and 580nm). They are the most sensitive to any change in the environment of Nd^{3+} ions. The following transitions were considered to be insensitive to the environment and were called "*insensitive transitions*"":$^4I_{9/2}\leftarrow{}^4G_{7/2}$ (520nm), $^4I_{9/2}\leftarrow{}^4S_{3/2},{}^4F_{7/2}$ (740nm), $^4I_{9/2}\leftarrow{}^4F_{5/2},{}^2H_{9/2}$ (800nm) [17,18]. Further studies [19,20] showed that in fact these transitions have substantial sensitivity toward changes in the coordination environment of neodymium ions and are called "*pseudo hypersensitive*" transitions.

In this chapter it is shown and try to explain that the coordination chemistry of the neodymium (III) ion varies depending on whether the rare earth element is in a crystal, in solution or in the solid, especially for glasses prepared by the sol-gel process (see method in chapter III). Variations in the coordination chemistry of neodymium are characterised by changes in the shape of spectral peaks in the (UV)-VIS spectrum [20] and that from solution to glass, the intensity of the Nd^{3+} ion spectrum changes as well.

Single crystal structure analysis on crystals as well as Extended X-ray Absorption Fine Structure (EXAFS) analysis on crystals, solutions and glasses will allow the determination of the coordination chemistry of Nd^{3+} reliably.

Previous workers have shown changes in the coordination chemistry of different rare earth fluorides contained in a glass by performing EXAFS analysis [21].

The coordination chemistry of Nd^{3+} containing crystals has also been studied by Rocca et al. [22]. They demonstrated that neodymium ions are mainly located near the oxygen sites, whereas Prieto et al. [23] determined the location of the excess of oxygen between the consecutive Nd^{3+} layers in the lattices using EXAFS techniques.

This understanding will help to dope sol-gel materials according to the effect of the matrix on the dopant and hence obtain sol-gel glasses with specific optical properties.

4.2- Method

4.2.1-Crystal preparation and analysis

Crystals were prepared using $Nd(NO_3)_3.6H_2O$, $NdCl_3.6H_2O$ and anhydrous $NdCl_3$ from Aldrich as precursors. The powders were dissolved in different solvents. The solutions were saturated and heated up to 100°C. The crystals formed when the solution was cooled down and left at room temperature.

The crystals were prepared in ethanol, dry ethanol (distilled from 95% ethanol over magnesium) and distilled deionised water.

They were analysed by single crystal x-ray structure analysis using a Brucker SMART CCD system with MoKα (0.71073Å) radiation and the data analyses were carried out using a commercial SHELXTL package and powder X-ray diffraction using a Philips X50 diffractometer operating with CuKα (1.5418Å) radiation, at Loughborough University in collaboration with Dr A.Slawin.

The crystals were also analysed by UV-VIS spectroscopy using a UNICAM UV2 UV-VIS spectrometer (scan speed 600nm/min, data interval 0.5nm).

As the crystals had different thickness and shape it was only possible to do a qualitative analysis and not quantitative analysis using this technique.

In this work, results are presented for $Nd(NO_3)_3.6H_2O$ crystals prepared from ethanol, water and dry ethanol and $NdCl_3.6H_2O$ crystals prepared from H_2O, ethanol and dry ethanol.

4.2.2-Sol-gel preparation

Nd^{3+} solutions were prepared using $NdCl_3.6H_2O$ (Aldrich) and $Nd(NO_3)_3.6H_2O$ (Aldrich). The compounds were dissolved in either dry ethanol (dried over magnesium) or distilled deionised water to obtain a range of concentrations (1M-0.01M).

Doped sol-gels were prepared using tetraethylorthosilicate (98%TEOS) (Aldrich), dry ethanol (dried over magnesium) and 0.5M HCl (diluted from concentrated HCl

Aldrich).

The precursors were mixed together in the following molar ratios:

1TEOS: 4EtOH: $4H_2O$: 0.04HCl

The dopant being added either in the ethanolic or aqueous phase at room temperature (21°C±2°C).

After mixing the precursors for one hour, 4ml of the solution was pipetted into petri dishes (Nunc brand products 3cm diameter) covered with Nesco film® in which 5 holes (0.6mm diameter) had been made and left to dry in a fan assisted oven at 40°C. Sample weight loss was monitored. When the samples were dry as assessed by no further measurable weight loss, they were analysed by UV-VIS spectroscopy using a UNICAM UV2 UV-VIS spectrometer (scan speed 600nm/min, data interval 0.5nm). The glasses (around 1.05mm thickness) were analysed in the bulk using a metallic holder.

The same analyses were performed on Nd^{3+} in solution using a 2mm pathlength quartz cell (Starna). Calculations were made in order to have values of absorbance in solution for a 1mm pathlength cell and hence be able to compare the results with the absorbance of the sol-gel samples.

Samples were also investigated as dried pieces of glass, immediately after dehydration by subjecting the samples to a vacuum pressure of 6mbar (measured by an Edwards Pirani 10 pressure sensor) for 18 hours and after thermal treatment at 700°C (with a ramp temperature of 0.1°C/min) for 24 hours using a Carbolite programmable furnace. The samples were cooled down at a ramp temperature of 5°C/min, the whole heating process taking 36 hours.

The various bands of the UV-VIS spectrum of solutions were used to calculate the covalency factor. Using the following equation [24], the covalency factor of the solvent ethanol was calculated in comparison with water as the solvent.

$$\delta = (1-\beta)/\beta \cdot 100$$

δ is the covalency parameter expressed in percent.

β is the average value of the ratio $\lambda comp/\lambda ref$ using as many wavelengths as possible.

In this case the reference sample corresponds to the metal ion in water and has a covalency factor of 0.

The covalency factor gives us information about the metal-ligand covalent binding.

If the factor is positive, the type of bond is more covalent than with water and if the factor is negative the type of bond is more ionic than with water.

When the sol-gels were dried, the concentration of the metal ion in the glass was expressed in %wt of the metal ion itself without its ligands.

Concentration of Nd^{3+} in solution (mol/l)	**%weight of Nd^{3+} in the glass**
1	9.48
0.6	5.69
0.3	2.844
0.1	0.948
0.05	0.474
10^{-2}	0.0948
10^{-3}	$9.48.10^{-3}$
10^{-4}	$9.48.10^{-4}$
10^{-5}	$9.48.10^{-5}$
10^{-6}	$9.48.10^{-6}$

Table 4.1: Nd^{3+} concentration in solution and in the sol-gel glass

4.2.3- EXAFS analysis

The experiments were carried out using synchrotron radiation emitted by the storage ring at Daresbury running between 2-2.5GeV with an average current of 200mA on the station 8.1. A Si(111) crystal allowed monochromatization of the incoming beam. Spectra were obtained at room temperature for Nd L_{III}- edge energy.

In the transmittance mode, the samples were mounted at 90° to the direct beam and in the fluorescence mode at 45°.

Nd^{3+} containing crystals were ground to a fine powder and placed as a thin layer between two films of Sellotape® for analysis in the transmittance mode. 3 scans were recorded for every sample.

Nd^{3+} solutions were injected into a polycarbonate cell. The window was covered with Mylar film glued to the cell. For every sample, 4 scans were recorded in the fluorescence mode.

Nd^{3+} sol-gels were analysed as a monolith placed on a metallic holder. The spectra were collected in the fluorescence mode, 8 scans were necessary for every sample.

For all the samples, the scans recorded were very noisy due to a lot of disorder around the metal ion.

The data were analysed using a UNIX computer system operating with the software packages EXCALIB, EXBROOK and EXCURV98 developed by the Daresbury Laboratory.

4.2.4- Karl Fischer experiment

A Karl Fischer experiment was carried out on $Nd(NO_3)_3.6H_2O$ in solution in order to know the number of water ligands in the inner sphere of the metal ion and to know if the water ligands around the metal ion stay covalently bound or react with the environment when in solution.

The technique used was as described by Skoog et al. [25].

The apparatus used was a Model 602 Karl Fischer from Analysis Automation Ltd Oxford. The apparatus was thoroughly dried to avoid any contamination from the moisture of the air.

For the titration, a Karl Fischer reagent (from Fisher) was used.

The solvent, dry ethanol, was titrated in case of presence of water. Then a calibration of water was done. Finally neodymium containing solutions were titrated.

The titrations were repeated until three results were obtained with an error of ±2%.

4.3- Results and Discussion

4.3.1- Results

The effect of the environment of the Nd^{3+} ion on its coordination chemistry and electronic transitions can be studied by looking at the behaviour of Nd^{3+} in crystals, in solution and entrapped in the sol-gel glass.

The UV-VIS spectrum of Nd^{3+} arises from electronic transitions of the metal ion which are affected by its environment.

By monitoring the changes in the UV-VIS spectrum the effect of the local environment on the metal ion was studied.

The electronic transitions and different energy levels need to be known to allow this study. From the work done by Wybourne [26], it was possible to plot the following diagram.

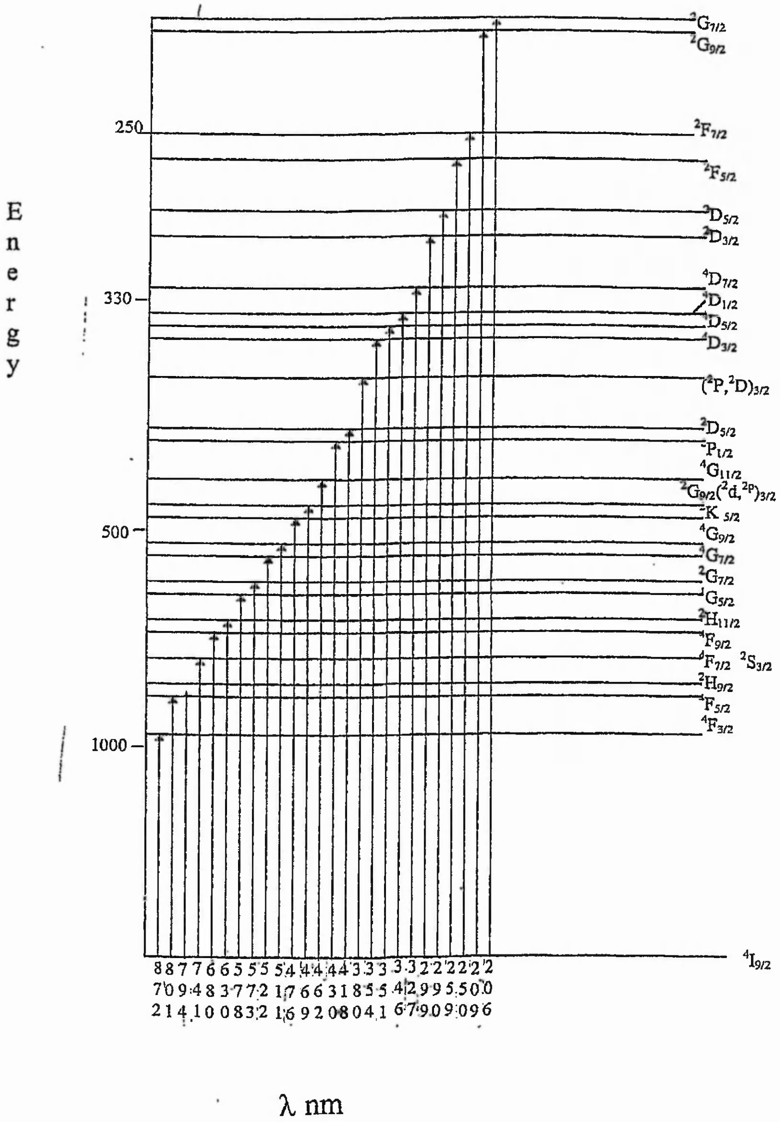

Figure 4.1: The different electronic transitions of the crystal spectra of Nd^{3+} ion.

By doing Single Crystal analysis, UV-VIS and EXAFS analysis, the coordination number of Nd^{3+} ion as a crystal, in solution and in the glass, was determined.

UV-VIS spectra of Nd^{3+} sol-gels show a shift toward longer wavelengths of the cut off as the concentration of the metal ion in the glass increased. The metal ion affects the optical transparency of the sol-gel glass.

Once the crystals were prepared, they were analysed by UV-VIS spectroscopy.

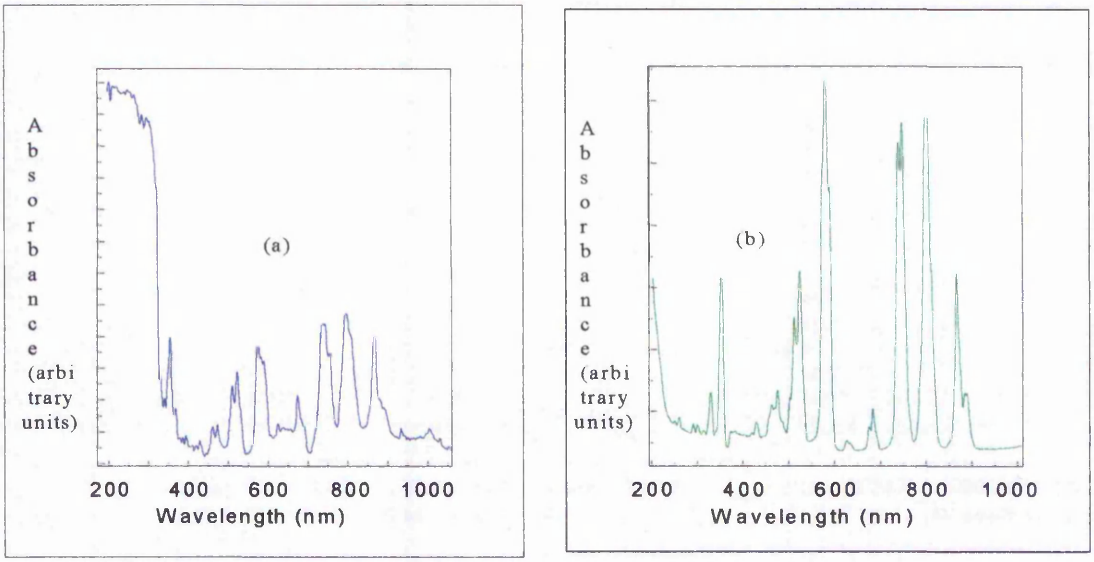

Figure 4.2: UV-Vis spectra of crystals, a) $Nd(NO_3)_3.6H_2O$ made from H_2O, b) $NdCl_3.6H_2O$ made from H_2O

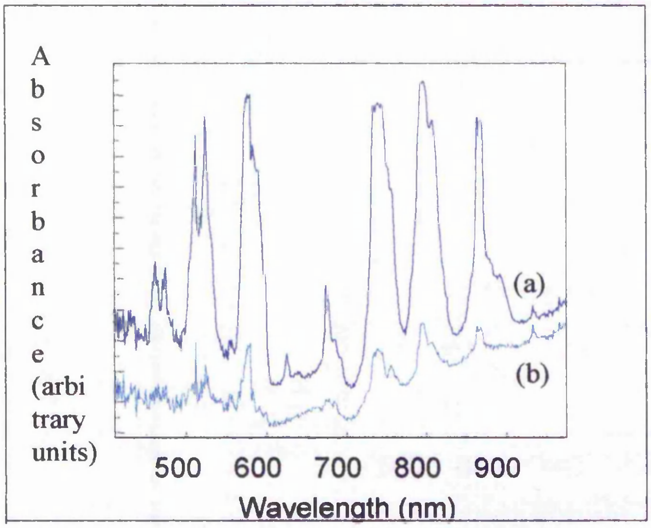

Figure 4.3: UV-Vis spectra of crystals a) $Nd(NO_3)_3.6H_2O$ made from EtOH, b) $Nd(NO_3)_3.6H_2O$ made from dry EtOH

The intensity of the peaks differs from one crystal to another as the thickness and the geometry of the crystal used were different and consequently some peaks appear to be present for certain crystals and not for others (eg: with crystal b being the thickest one) in figure 4.3. Moreover, due to the same reason, figure 4.2 and figure 4.3 are not on the same scale. Thus, it was not possible to do quantitative analysis but only a qualitative comparison of the data.

The exact wavelength of the peak maxima which correspond to the most sensitive (hypersensitive and pseudohypersensitive) electronic transitions to the environment, were measured.

Table 4.1: Wavelengths of the principal peaks from the different crystals (nm)

A	579	581	589	734	737	741	749	798	800	868
B	579	583	589	734	739	745	756	798	807	869
C	578	583	588	734	739	743	755	796	807	868
D	578	583	590	734	740		756	796	807	869

A: $NdCl_3.6H_2O$ crystal made from H_2O.

B: $Nd(NO_3)_3.6H_2O$ crystal made from H_2O.

C: $Nd(NO_3)_3.6H_2O$ crystal made from ethanol.

D: $Nd(NO_3)_3.6H_2O$ crystal made from dry ethanol.

When comparing the wavelengths of the different crystals together, shifts of the peaks for certain crystals were observed.

The wavelengths of crystals made from the same compound ($Nd(NO_3)_3.6H_2O$) regardless of the solvent used for the preparation of the crystals, were the same. No shift was noticed. However when the precursor was changed, $NdCl_3.6H_2O$ instead of $Nd(NO_3)_3.6H_2O$ for the same solvent, blue shifts were observed.

Taking the spectrum from $Nd(NO_3)_3.6H_2O$ crystals prepared in water as a reference and comparing it with the spectrum obtained from $NdCl_3.6H_2O$ crystals prepared in water, blue shifts (toward shorter wavelengths) were observed for the following peaks: 581nm (-2nm),

737nm (-2nm), 741nm (-3nm), 749nm (-7nm), 800nm (-7nm).
No red shift (toward longer wavelength) was observed.
The peaks showing a blue shift correspond to both the hypersensitive transitions and the pseudohypersensitive transitions.

The changes in the spectra correspond to the electronic transitions of the metal ion which change with its environment (different counterions).
The solvents in which the crystals have been prepared do not have an effect on the electronic transitions of neodymium ions in the crystal phase.

To know the coordination number of Nd^{3+} in the crystals, single crystal structure analysis was done. The structure of the molecule using PLATON software is drawn below.
For the crystals prepared with $Nd(NO_3)_3.6H_2O$ the coordination number was 10 (see Figure 4.4) regardless of the solvent used in the preparation of the crystals (ethanol, extensively dried ethanol or water).

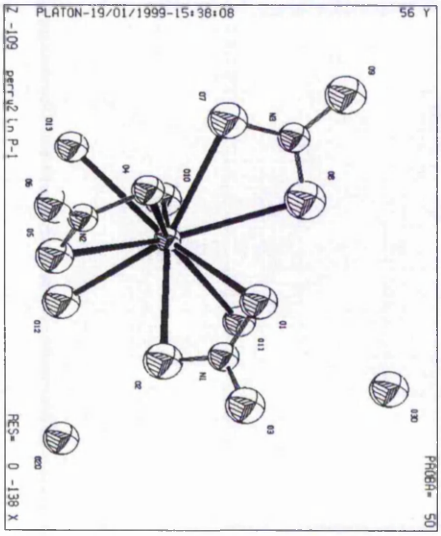

Figure 4.4: $Nd(NO_3)_3.6H_2O$ crystals

The three nitrate and six water ligands coming from the powder used to prepare the crystal are present in the unit cell. The three NO_3^- ligands are bonded to the metal ion as well as 4 H_2O ligands. The two other water ligands are trapped within the crystal lattice at distances further from the Nd^{3+} ion.

The average bond distance between Nd-O(NO_2) was 2.55Å, Nd-O(H_2) was 2.45 Å and O-N was 1.25 Å. The crystal was triclinic.

Similar results were obtained by Hirashima et al. [27] who studied Nd^{3+} crystals with nitrate ligands and found a coordination number of 10 with a bond distance of 2.55Å for Nd-O(NO_2).

For the crystals prepared with $NdCl_3.6H_2O$ the coordination number was 8 (see Figure 4.5).

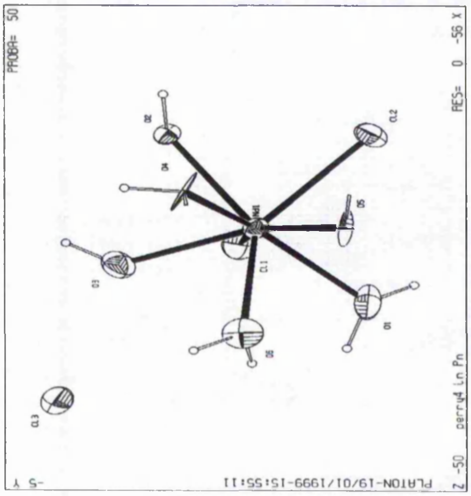

Figure 4.5: $NdCl_3.6H_2O$ crystals

Two of the three Cl^- ligands from the salt used to prepare the crystal were covalently bonded to the metal ion. One Cl^- was situated further from the metal centre, trapped in the lattice. 6 of the water ligands were bonded to the metal ion. The bond distance between Nd-Cl was 2.82Å, Nd-O(H_2) was 2.45Å. The crystal was monoclinic. These results are similar to Habenschuss et al. [28] who proposed a coordination number of 8 with a bond distance of 2.45Å for Nd-O(H_2) when looking at Nd^{3+} containing crystals with Cl^- counterions.

When the XRD spectra of the single crystals were ground and run as powders, the same spectrum was obtained for $Nd(NO_3)_3.6H_2O$ regardless of the solvent in which the crystal was prepared. The samples gave stable results with time. The data shows a very noisy spectrum as the material was disordered. In contrast, with a starting material of

$NdCl_3.6H_2O$ or anhydrous $NdCl_3$ the spectra were changing with time. The results can be seen in Appendix 6.

From the data obtained from the single crystal structure analysis, the bond distance between the metal ion and the chloride ligand was longer than the bond distance between the metal ion and the nitrate ligand.

The NO_3^- ions are covalently bonded to the metal ion, via a chelate type of bonding which is very stable. The Cl^- ions are more weakly bonded to the metal ion and consequently they could be replaced by the H_2O and CO_2^- from the air. To overcome this problem, the crystal has to be kept away from air and when analysed, it had to be covered by a thin film of parrafin oil.

The results obtained with the single crystal structure X-ray analysis complemented information obtained with the UV-VIS spectroscopy study when only changes in the spectrum occurred with changes in the type of ligands and not the type of solvent.

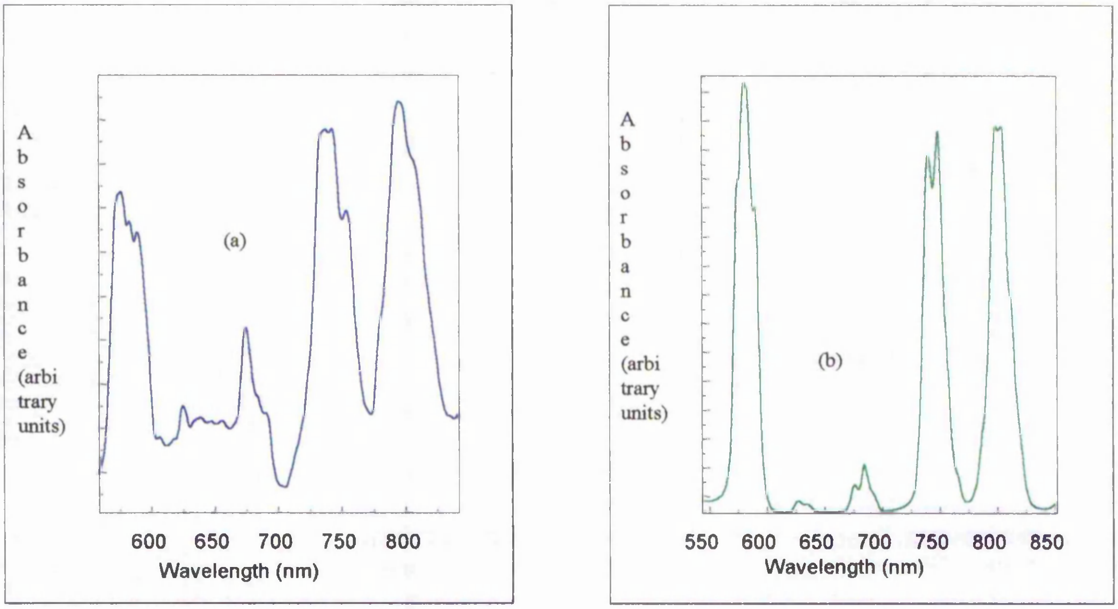

Figure 4.6:VIS spectrum of Nd^{3+} crystals prepared in H_2O with
a) $Nd(NO_3)_3.6H_2O$, b) $NdCl_3.6H_2O$ (covered with a thin film of paraffin oil)

Nd^{3+} containing crystals prepared with $Nd(NO_3)_3.6H_2O$ were very thick and good definition of the peaks was difficult to obtain.

By looking at the peaks arising from the electronic transitions which are the most sensitive to the environment, a change in the peak shapes occurred as well as a shift of the peaks when there was a change in the ligands present during the preparation of the crystals.
The changes in the peak shapes corresponds to a variation in the coordination number of the metal ion, 10 for Nd^{3+} crystals prepared with $Nd(NO_3)_3.6H_2O$ and 8 for Nd^{3+} crystals prepared with $NdCl_3.6H_2O$.
For confirmation of the coordination chemistry of the crystals and for comparison with the metal ion behaviour in solution and in the sol-gel glass, EXAFS analysis was carried out on $Nd(NO_3)_3.6H_2O$ crystals prepared in water and in ethanol, $NdCl_3.6H_2O$ crystals prepared in water, ethanol and dry ethanol and finally anhydrous $NdCl_3$ crystals prepared in dry ethanol.

To get a good fitting of the observed spectrum with the calculated one, the coordination number was varied. The Debye-Waller factor has acceptable values between 0.015 and 0.050Å^2 as the data collected were very noisy. The Debye-Waller factor σ contains important structural and chemical information. It has two components σ_{stat} and σ_{vib} due to static disorder and thermal vibrations, respectively. Large disorder can lead to a reduction of the EXAFS amplitude and hence the apparent coordination numbers. Moreover the residual index should be lower than 20 for data collected into transmittance mode but as our samples were very noisy the residual index could be allowed to go up to 40. For data collected in the fluorescence mode, the residual index should be between 30 and 40. In the fitting, O atom was entered as directly bonded to the metal ion in the case of $Nd(NO_3)_3.6H_2O$ and both O and Cl atoms in the presence of $NdCl_3.6H_2O$. As the bond distances between Nd-O (2.45Å) and Nd-Cl (2.82Å) are not very different from one another , the data obtained were exactly the same whether O or Cl atoms were entered as directly bonded to the metal ion.
A contour map for every data set analysed allows the determination of the error in the coordination number found which should be in the 10% error circle in order to be correct. The spectra recorded were noisy due to a highly disordered coordination environment around the metal ion. Moreover, a second shell analysis was tried using multiple scattering without any success suggesting the presence of only one ordered shell around the metal ion.

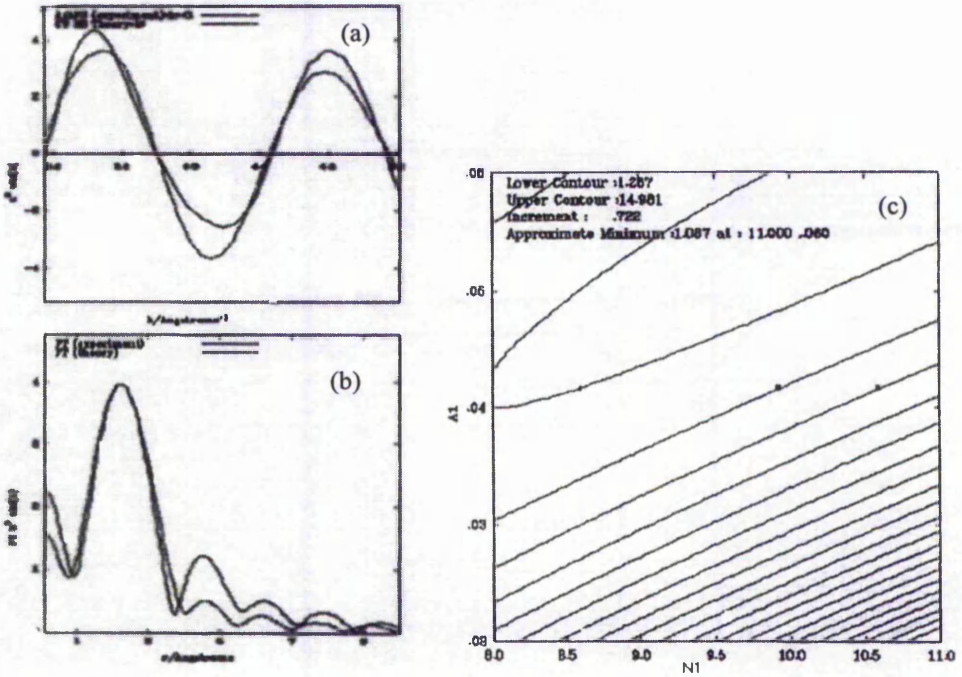

Figure 4.7: $Nd(NO_3)_3.6H_2O$ crystal prepared in water, a) k^3 K-edge EXAFS spectra,
b) Fourier transform magnitude of k^3 K-edge EXAFS spectra,
c) contour map of k^3 K-edge EXAFS spectra

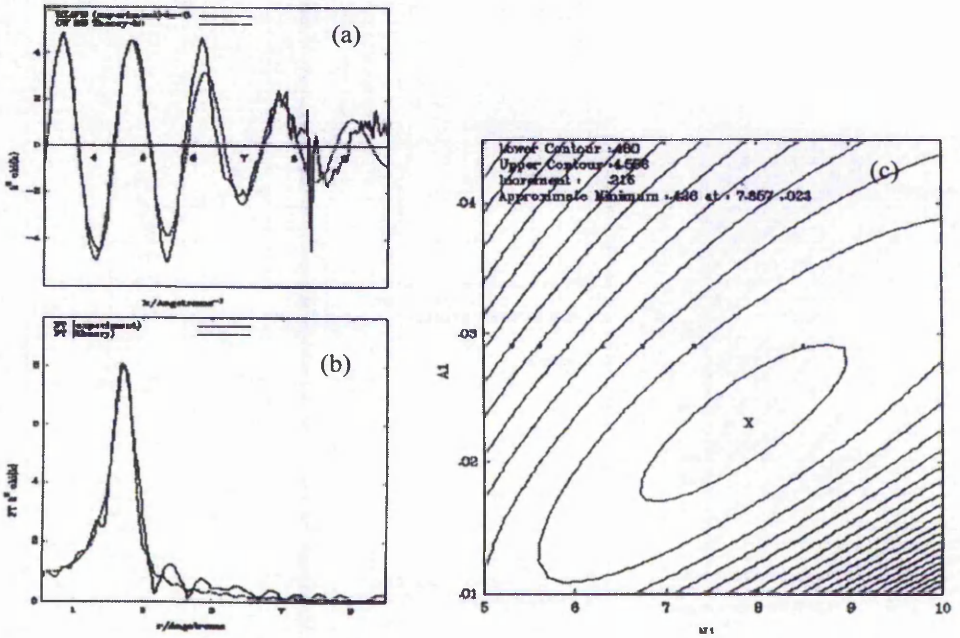

Figure 4.8: $NdCl_3.6H_2O$ crystal prepared in water, a) k^3 K-edge EXAFS spectra,
b) Fourier transform magnitude of k^3 K-edge EXAFS spectra,
c) contour map of k^3 K-edge EXAFS spectra

Table 4.2 summarises the values of the coordination numbers, bond distances and Debye-Waller factors for the different crystals analysed.

Table 4.2

Crystals	Coordination number (N)	Bond distance between Nd-O (r/Å)	Debye-Waller factor (σ/Å^2)	Residual index (R/%)
$Nd(NO_3)_3.6H_2O$ prepared in water	10	2.549	0.051	23.24
$Nd(NO_3)_3.6H_2O$ prepared in ethanol	10	2.549	0.054	37.15
$NdCl_3.6H_2O$ prepared in ethanol	7.7	2.516	0.022	24.1
$NdCl_3.6H_2O$ prepared in water	7.7	2.514	0.024	33.2
$NdCl_3.6H_2O$ prepared in dry ethanol	7.8	2.514	0.024	29.00
$NdCl_3$ anhydrous prepared in dry ethanol	7.7	2.516	0.023	23.98

The data analysis showed that a coordination number of 10 is obtained for $Nd(NO_3)_3.6H_2O$ crystals (Figure 4.7) regardless of the solvent used in their preparation and a coordination number of 8 was found for $NdCl_3.6H_2O$ (Figure 4.8) and $NdCl_3$ anhydrous regardless of the solvent used.

These values fit with the results from the single crystal structure analysis.

The bond distance between Nd-O is identical to that found by X-ray diffraction for $Nd(NO_3)_3.6H_2O$ crystal and slightly smaller for $NdCl_3.6H_2O$ crystals.

The Debye-Waller factor is higher for crystals with NO_3^- as a ligand than Cl^- which corresponds to a more distorted environment around the metal ion in the presence of NO_3^- ligands.

4.3.1.2-Nd^{3+} salts in solutions

Nd^{3+} containing solutions were prepared. They were used for the preparation of Nd^{3+} doped sol-gel materials. UV-VIS spectra were obtained from the samples.

Different effects were observed according to the counterions present and the solvents.

The most important changes were observed for the peaks at 575, 580, 740 and 800 nm which correspond to the electronic transitions which are the most sensitive to the environment.

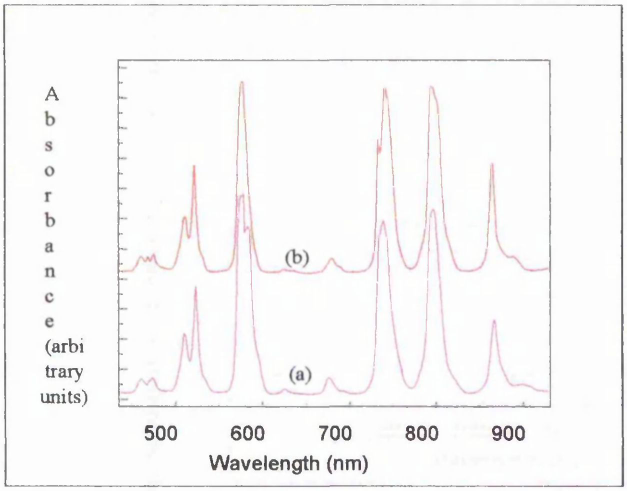

Figure 4.9: Effect of the solvent on Nd^{3+} spectrum (solution prepared with $Nd(NO_3)_3.6H_2O$ (1M)), a) in ethanol, b) in water

The Nd^{3+} ion is sensitive to the type of solvent used.

A shift toward longer wavelength was observed when the metal ion was in water rather than ethanol.

Table 4.3: Wavelengths of $Nd(NO_3)_3.6H_2O$ solutions in water and ethanol (nm)

H_2O	428	462	476	512	524	578	580	622	679	741	797	866	892
EtOH	428	462	474	511	524	579	585	626	676	739	797	868	902

A red shift (toward longer wavelengths) was observed for the following peaks: 476nm (+2nm), 512nm (+1nm), 679nm (+3nm), 741nm (+3nm).

A blue shift (toward shorter wavelengths) was observed for the following peaks: 578nm (-1nm), 580nm (-5nm), 622nm (-4nm), 866nm (-2nm), 892nm (-10nm).

The electronic transitions of the metal ion were very sensitive to the change of solvent. This time not only the hypersensitive and pseudohypersensitive transitions showed some shifts in the spectrum but the transitions which were normally insensitive to the environment, showed shifts as well.

Using the spectral shifts of the two spectra, it was possible to calculate the covalency of the metal-ligand with the two different solvents (section 4.2.2).

For a covalency factor of 0 when the solvent is in water, the covalency factor is -0.0389 when the solvent is ethanol. This means that water is more covalently bonded to the metal ion than ethanol which is more ionically bonded.

Moreover, some splitting in the spectral peaks occurred for the different solvents suggesting that the environment around the neodymium ions changed when ethanol or water was the solvent.

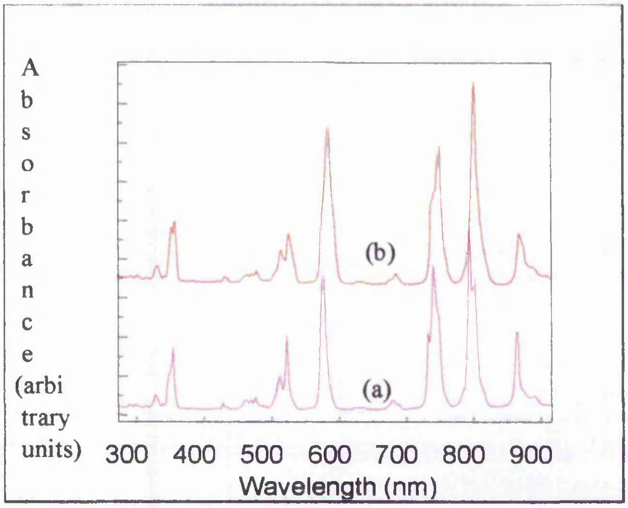

Figure 4.10: Effect of the solvent on $NdCl_3.6H_2O$ from Aldrich (0.3M), a) in water, b) in ethanol

Table 4.4: Wavelengths of $NdCl_3.6H_2O$ solutions in water and ethanol (nm)

EtOH	429	460	513	525	579	585	749		802	868	889
H_2O	430	462	512	522	576		740	794	802	866	888

As with $Nd(NO_3)_3.6H_2O$ solutions in ethanol and water, the spectra of $NdCl_3.6H_2O$ solutions in ethanol and water showed some differences.

By comparing the spectrum with ethanol for the solvent to the spectrum with water for the solvent, red shifts were observed: 513nm (+1nm), 525nm (+3nm), 579nm (+3nm), 749m (+9nm), 868nm (+2nm), 889nm (+1nm).

Blue shifts were observed as well: 429nm (-1nm), 460nm (-2nm).

The red shifts occurred with the peaks corresponding to the electronic transitions which are the most sensitive to the environment and the blue shifts occurred for the electronic transitions which are the least sensitive to the environment.

This same behaviour had already been described for $Nd(NO_3)_3.6H_2O$ solutions.

The covalency factor was also calculated to find out if the ligand can affect the interaction between the metal and the solvent.

As with the NO_3^- ligands, the covalency factor is negative (-0.239) meaning that the water solvent is more covalently bonded than the ethanol solvent.

Both covalency factors were different from one another, so each ligand has its own specific covalency factor and consequently the ligand affects the metal ion and its environment.

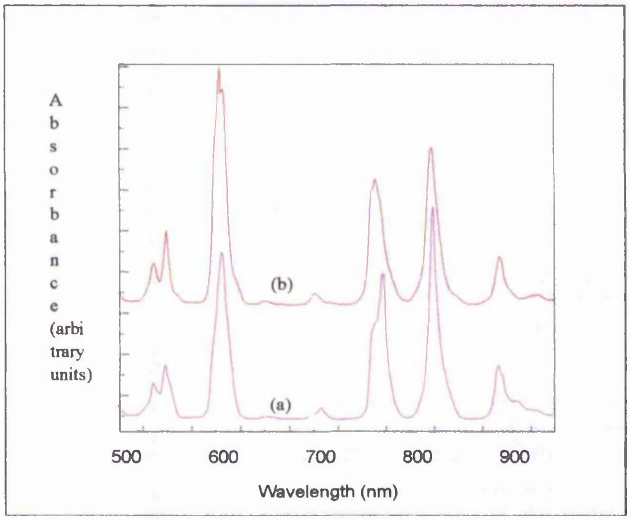

Figure 4.11: Effect of the ligands on Nd^{3+} spectrum in ethanol (1M), a) Cl^- ligand, b) NO_3^- ligand

From the figure above, shifts of the spectra were observed when the counterion was Cl^- or NO_3^-.

A splitting of the peaks at 581nm in the presence of NO_3^- ligands and at 802nm a broader peak was noticed with NO_3^- rather than with Cl^-. The appearance of a shoulder at 794nm and a broadening of the shoulder was noticed with Cl^- in comparison with NO_3^-. However the effect of the ligands seem to be less significant than the effect of the solvent as the ligands are in the outer sphere of the metal ion and are only ionically bonded.

Spectra of neodymium ions in different solvents were recorded to see if other solvents affect the electronic transitions of the metal ion or only water or ethanol were able to make the electronic transitions sensitive to the environment.

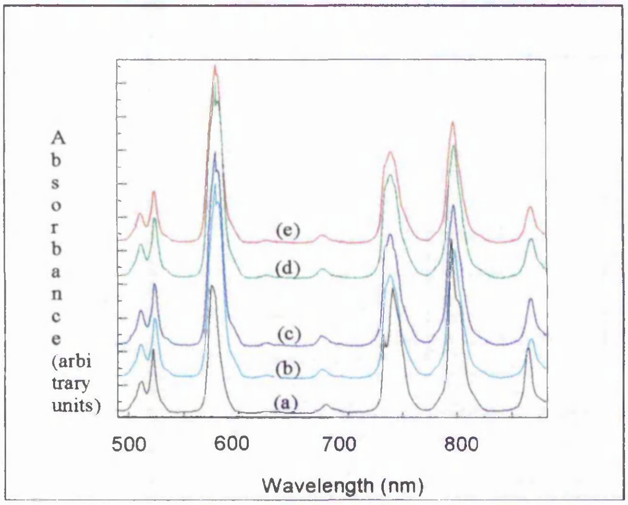

Figure 4.12: $Nd(NO_3)_3.6H_2O$ 0.3M in, a) water, b) ethanol, c) methanol, d) butan-2-ol, e) isopropanol

Table 4.5: Wavelengths of $Nd(NO_3)_3.6H_2O$ solutions in different solvents (nm)

A	511	524	579	585	676	739	797	867
B	512	524	579	584	676	739	798	869
C	511	524	579	584	675	739	797	868
D	511	524	579	585	676	740	797	868
E	512	524	577	580	679	741	797	866

A: Isopropanol

B: Butan-2-ol

C: Methanol

D: Ethanol

E: Water

By looking at the spectra, two types of behaviour were observed. Ethanol, methanol, isopropanol and butan-2-ol have similar spectra whereas water has a different spectrum. In the presence of water a shift of the whole spectrum was observed.

By calculating the covalency factor for the different solvents using the water as reference, it was possible to know if the solvents have a more covalent or ionic effect toward the metal ion than water.

The following classification was found:

Butan-2-ol < Isopropanol < Ethanol < Methanol < Water

-0.099 < -0.049 < -0.038 < -0.0245 < 0

All the solvents have a tendency to be more ionically bonded to the metal ion than water. Methanol, ethanol and isopropanol have nearly the same covalency factor whereas butan-2-ol has a lower covalency factor which would mean that this solvent is even less covalently bonded than the others.

Water as a solvent was more covalently bonded to the metal ion than any other solvent.

Finally a variation in the intensity of the peaks was observed according to the different types of solvent.

A variation of the area of the peaks (measured using the area of groups of peaks) was observed according to the solvent.

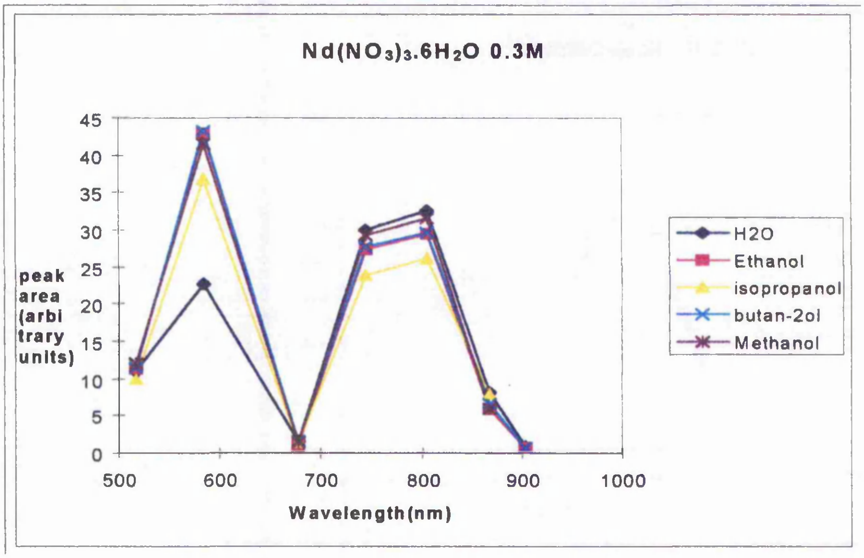

Figure 4.13 : Peak areas of neodymium ion in solution with various solvents

The peak areas for the spectra of neodymium ions in different solvents were plotted.
All the solvents had similar peak areas for the peaks corresponding to the insensitive electronic transitions (these transitions were not affected by the environment around the metal ion). Changes in peak areas from one solvent to another were observed for the peaks corresponding to the hypersensitive transitions and the pseudohypersensitive transitions.
The area of the peaks at 584nm, 744nm and 806nm were affected by the solvent which means that the environment around the metal ion is affected by the solvent.
By looking at the variation of the areas, the behaviour of Nd^{3+} ions in water was very different from the other solvent.
When the peak areas of the three sensitive transitions for every solvent were combined and the ratio calculated (Table 4.6) methanol, ethanol, butan-2-ol and isopropanol have very similar peak areas (as a proportion of the whole) whereas a very different pattern was found for water.
However, when the sum of the three peak areas was calculated for every solvent, it was noticed that water and isopropanol possessed a similar peak area of 84, whereas methanol and ethanol a peak area of 99 and butan-2-ol a peak area of 97.
The peak areas could be linked to the symmetry of the solvent and its interaction with the metal ions. Water and isopropanol probably form the most symmetric solvent metal ion complexes (Table 4.6).

Table 4.6: Peak areas of Nd^{3+} spectra with different solvents (arbitrary units)

	584nm	744nm	806nm
H_2O	0.26	0.36	0.38
MeOH	0.41	0.29	0.31
EtOH	0.43	0.28	0.30
IPA	0.42	0.27	0.31
Bu-2-ol	0.43	0.27	0.29

The first peak at 584nm showed the most differences according to the solvent. It corresponds to the hypersensitive transition whereas the other peaks at 744nm and 806nm (pseudohypersensitive transition) showed less difference between the water solvent and the other solvents.

Due to its higher covalent property water interacts more strongly with the metal ion in both its inner and outer sphere than the other solvents.

Consequently the electronic transitions are sensitive to this environment and changes in the spectrum of the metal ion appear.

This understanding will help us to study the coordination number of the metal ion in the different solvents and later in the sol-gel glass environment.

Finally, the variation of the absorbance with the concentrations of the metal ion in solution was plotted in order to see if Nd^{3+} ions follow the Beer Lambert law.

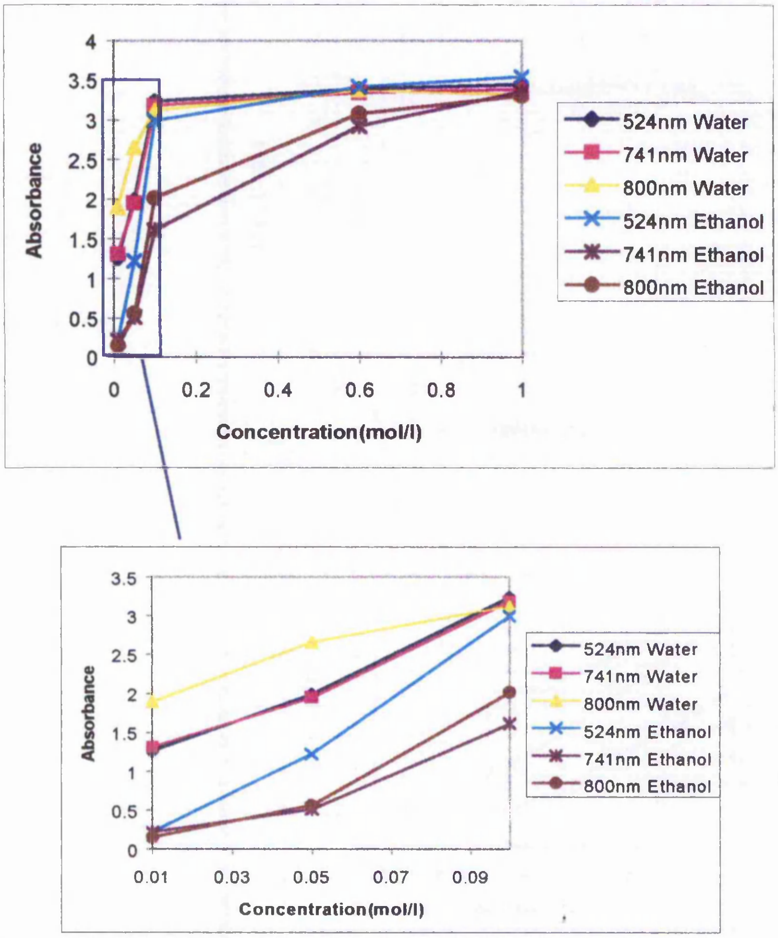

Figure 4.14: Variation of the absorbance with concentration for $Nd(NO_3)_3.6H_2O$ solutions

To plot Figure 4.14, the absorbance of the peaks corresponding to the hypersensitive transitions was used because they are the most sensitive to the environment and consequently they allow a better monitoring of the effect of the environment on the metal ion. The graph shows that the metal ion does not follow the Beer Lambert Law over the whole concentration range used; but appeared to have two regions of linear behaviour, the first with low concentrations (up to 0.1M) and the second with higher concentrations (from 0.1M).

The deviation from the Beer Lambert law could be due to a change in chemical equilibria which affects the absorbing species, possibly a molecular association of the solute at high concentrations [29]. Moreover a difference in absorbance was noticed when the solvent was changed.

The metal ion showed a lower absorbance when the solvent used was ethanol.

At a certain concentration of the metal ion, when in water as the solvent, the intensity of the peaks did not change very much whereas when the metal ion was in ethanol as the solvent the intensity between the three peaks changes.

When replacing the water as solvent, by ethanol as solvent, the intensity of the peak at 524nm did not change, but a large decrease of the absorbance was noticed for the peaks at 741nm and 800nm.

These two peaks and consequently these two electronic transitions are the most affected by the change in the environment of the metal ion.

The variation of the absorbance for $NdCl_3.6H_2O$ solutions was plotted and compared with $Nd(NO_3)_3.6H_2O$ solutions.

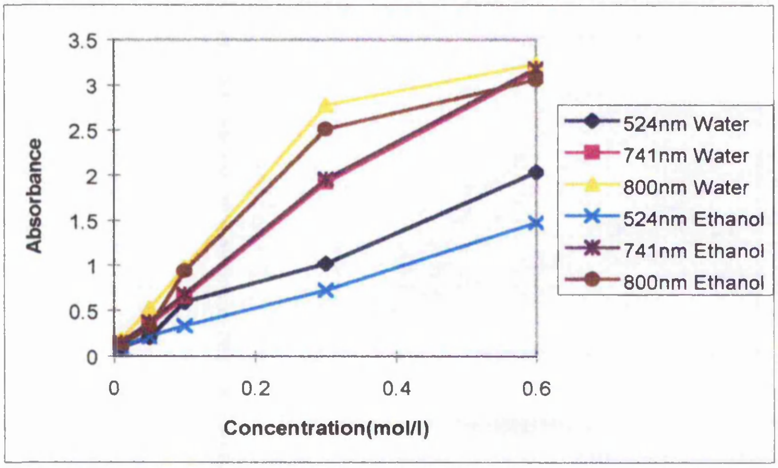

Figure 4.15: Variation of the absorbance with the concentration of $NdCl_3.6H_2O$ solution

As with the $Nd(NO_3)_3.6H_2O$ solutions, $NdCl_3.6H_2O$ solutions did not follow the Beer Lambert Law. Two different regions of linear behaviour were observed, one with concentrations up to 0.3M and one with concentrations ≥0.3M.

As for $Nd(NO_3)_3.6H_2O$ solutions, the solvents affect the absorbance of the peaks for $NdCl_3.6H_2O$ solutions.

The intensity of the peaks was higher with water as the solvent and lower with ethanol as the solvent but in this case the absorbance of the three peaks chosen for comparison were different from one another.

To determine the coordination chemistry of Nd^{3+} ion in solution, the spectra of Nd^{3+} metal ion solutions were compared.

In several publications [30,31], Karraker has shown that the shape of the absorption bands of the neodymium ion can be correlated with the coordination number of the ion.

The peaks taken into consideration were those most sensitive to the environment at 580nm, 750nm and 800nm.

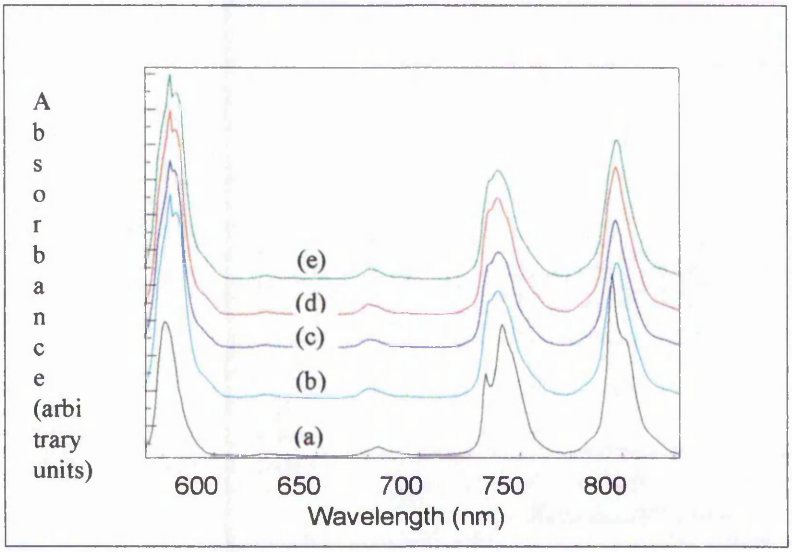

Figure 4.16: VIS spectrum of $Nd(NO_3)_3.6H_2O$ in solution with a) water, b) ethanol, c) isopropanol, d) methanol, e) butan-2-ol

As stated in the previous section we can see that the salts in the presence of the solvents ethanol, methanol, butan-2-ol and isopropanol have the same spectrum.

They have the same coordination number of 7.

The spectroscopic evidence (comparison of changes of the hypersensitive bands in the UV

VIS region spectrum of Nd^{3+} with the crystal spectra and UV-VIS spectra of Karraker [18]) suggests that Nd^{3+} ion in ethanol can only fit 7 ligands around it.

For water, a coordination of 9 is found. Wilkinson [32] and Stephens [33] suggest that the complex is $[Nd(H_2O)_9]^{3+}$ which has a tricapped trigonal prism geometry.

Cossy et al. found a coordination number of 9 for Nd^{3+} in water solution with water molecules in the first coordination sphere by doing UV-VIS and XRD analysis [34]. Moreover the UV-VIS spectrum of Nd^{3+} in water was also compared with the spectrum proposed by Karraker [18] for a coordination number of 9.

EXAFS analysis were carried out on Nd^{3+} solutions with NO_3^- or Cl^- as counterions and ethanol or water as solvents.

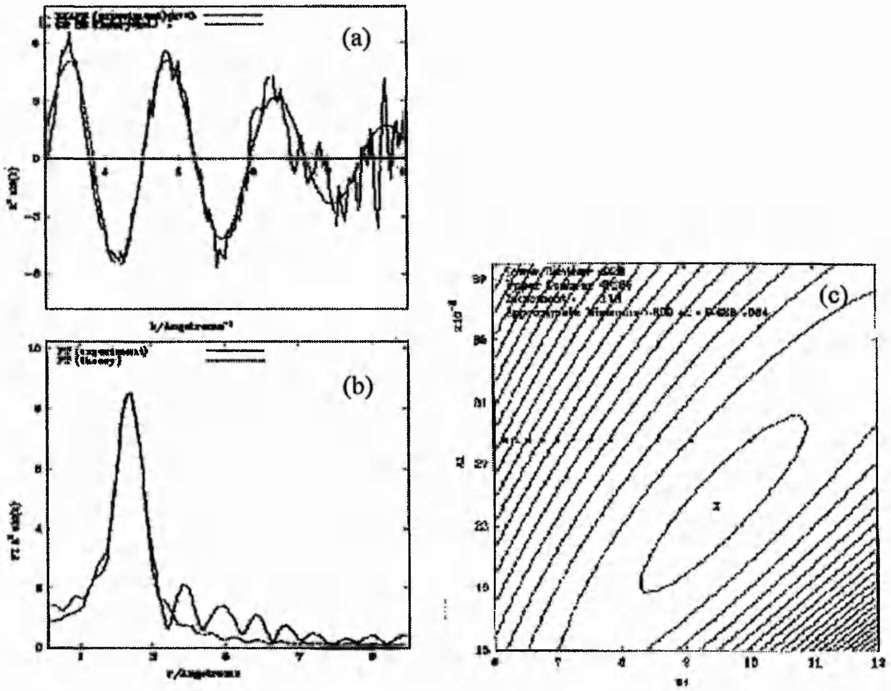

Figure 4.17: Nd^{3+} solution in water prepared with $Nd(NO_3)_3.6H_2O$,

a) k^3 K-edge EXAFS spectra,

b) Fourier transform magnitude of k^3 K-edge EXAFS spectra,

c) contour map of k^3 K-edge EXAFS spectra

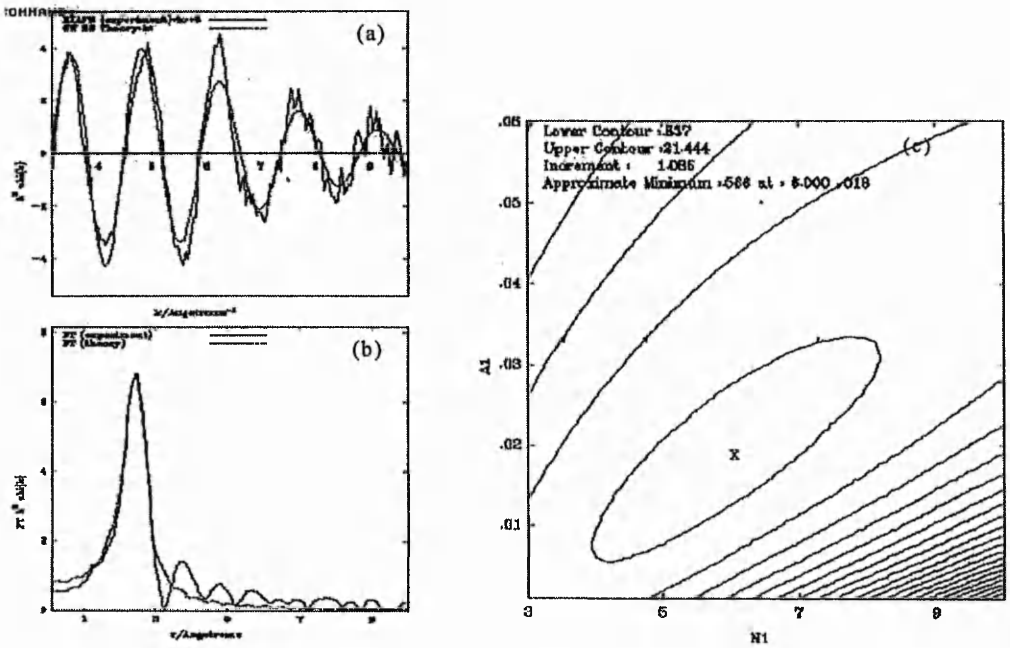

Figure 4.18: Nd^{3+} solution in ethanol prepared with $NdCl_3.6H_2O$,

a) k^3 K-edge EXAFS spectra,

b) Fourier transform magnitude of k^3 K-edge EXAFS spectra,

c) contour map of k^3 K-edge EXAFS spectra

Table 4.7 gives values of the coordination number, bond length and Debye-Waller factor from EXAFS analysis of Nd^{3+} in solution.

Table 4.7

Solutions	Coordination number (N)	Bond distance between Nd-O (r/Å)	Debye-Waller factor (σ/Å^2)	Residual index (R/%)
$Nd(NO_3)_3.6H_2O$ in water	9	2.535	0.025	31.15
$NdCl_3.6H_2O$ in water	8.9	2.522	0.024	32.28
$Nd(NO_3)_3.6H_2O$ in ethanol	7	2.548	0.037	39.86
$NdCl_3.6H_2O$ in ethanol	7	2.527	0.025	28.72

The coordination number obtained from the EXAFS analysis was 9 for the metal ion in water irrespective of the ligands used and 7 for the metal ion in ethanol irrespective of the initial ligands.

These data are in agreement with the UV-VIS analysis carried out. The bond distance was smaller in the presence of Cl^- rather than in the presence of NO_3^-. The Debye-Waller factors fit the contour map.

In water solution, the complex is more likely to have the following structure: $[Nd(NO_3)_3.3H_2O]^{3+}$ as the NO_3^- ligands are strongly covalently bonded to the metal ion.

As the sample is $Nd(NO_3)_3.6H_2O$ when it is dissolved in ethanol there are both water and ethanol molecules present in the system.

A Karl Fisher experiment was carried out to measure the amount of water present in the system.

For that, the metal ion (from $Nd(NO_3)_3.6H_2O$ from Aldrich) was prepared as a solution in methanol, first, to calibrate the apparatus and then in dry ethanol.

To make certain that the water titrated came only from the metal ion and not the solvent, dry ethanol was first titrated. The solvent was completely dry, no water was detected in the system.

After titration of the metal ion, it was found that in dry ethanol, 6 moles of water were present in the solution whether the ligand was Cl^- or NO_3^-.

Using the structure of the crystals, the complex in ethanol solution was determined and more likely to have the following structure: $[Nd(NO_3)_3(H_2O)]^{3+}$ and $[Nd(Cl)_2(H_2O)_5]^{3+}$ with the remaining water being in solution as a solvent.

4.3.1.3-Nd^{3+} salts in sol-gels

When the Nd^{3+} ion was used as a dopant for the preparation of sol-gel glasses, the study of the UV-VIS spectrum showed that the electronic transitions were not affected by the type of counterion or solvent used in the preparation process.

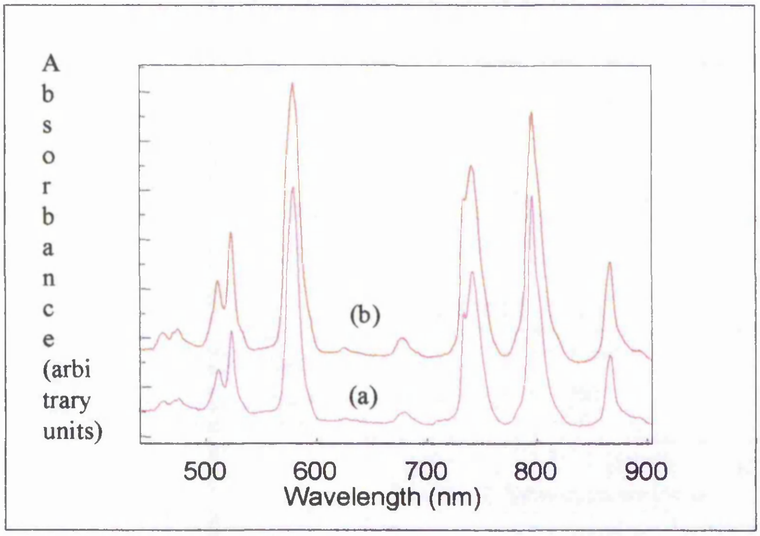

Figure 4.19: Spectra of Nd^{3+} (9.48wt%) sol-gel prepared in ethanol with a)Cl^- counterions, b) NO_3^- counterions

The same spectrum was observed whether the species in the outer sphere of Nd^{3+} ion was Cl^- or NO_3^- and whether the solvent was water or ethanol. The intensity of the peaks was also not affected by the ligands.

No shift of the peaks was observed.

In the glass the electronic transitions were not affected as much as in solution.

The nature of the electronic transitions did not change regardless of the solvent in which the metal ion was prepared and regardless of its counterions.

In the sol-gel, the intensity of the peaks did not follow the Beer-Lambert law as was also observed when the metal ion was in solution.

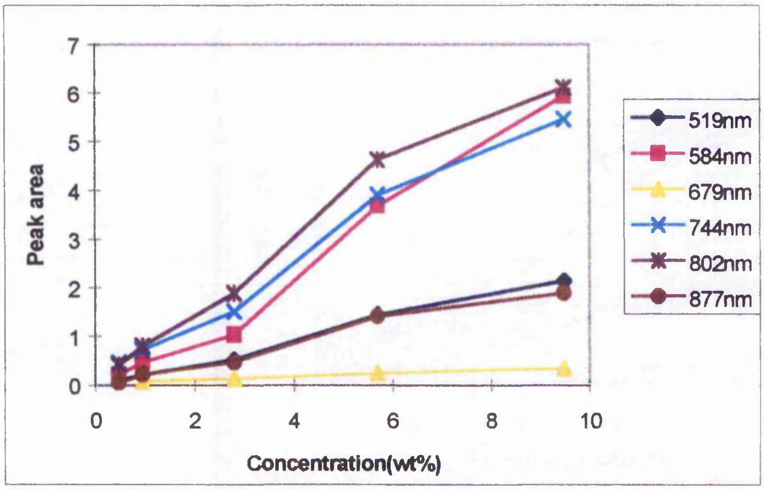

Figure 4.20: $Nd(NO_3)_3.6H_2O$ sol-gel prepared in water

Figure 4.20 shows that the peak area follows a linear scale for low concentrations (up to 5.69wt%) of dopant then a second linear scale is approximately followed for high concentration (from 5.69wt%) of dopant.

This behaviour was observed especially for the peaks at 584nm, 744nm and 802nm which correspond to the electronic transitions which are the most sensitive to the environment.

To know if the metal ion undergoes changes in coordination/ environment in the sol-gel, different treatments were carried out on the glass.

First the samples were evacuated for 24 hours then rehydrated for 24 hours and finally they were thermally treated at 800°C. The samples were assessed by UV-VIS spectroscopy before and after each treatment.

When the doped sol-gels were treated (vacuum and thermally), changes in its UV-VIS spectrum were observed.

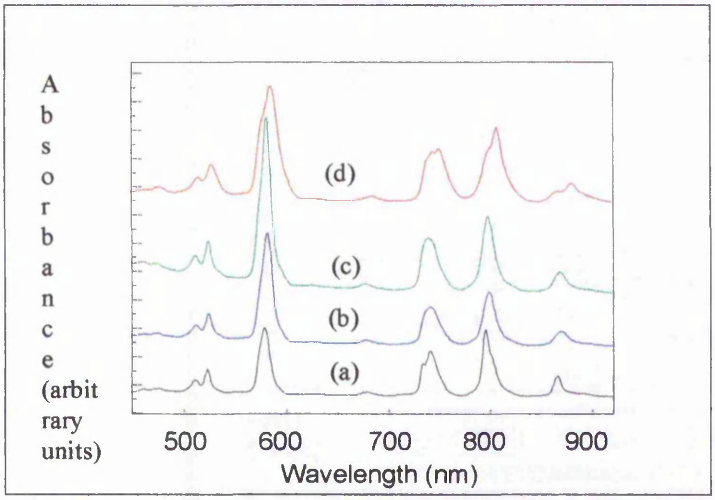

Figure 4.21: $NdCl_3.6H_2O$ (5.45wt%) sol-gel, a)dried at 40°C, b) after evacuation for 24 hrs, c) after rehydration for 24 hrs, d) after heating 800°C

Table 4.9: Wavelengths of $NdCl_3.6H_2O$ sol-gel after different treatments (nm).

Dried at 40°C	354	512	522	576.4	680	741	748	795.2	800.6	866.2	886.2
Vacuum	354	514	526.5	586	685.5	749.5			804.5	878	
Rehydration	352	512	524	578	680	744			798	866	
Heated	354	512.5	527	584.5	683.5	743.5	749		805	865.5	878.5

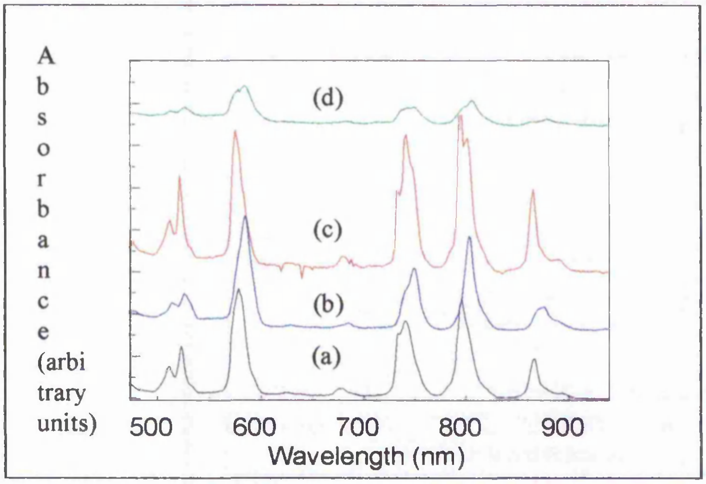

Figure 4.22: $Nd(NO_3)_3.6H_2O$ (5.45wt%) sol-gel a) dried at 40°C, b) after evacuation for 24hrs, c) rehydrated for 24 hrs, d) heated up to 800°C

During the different treatments applied on the sol-gel samples, the metal ion reacted in the same way regardless of the ligands and of the solvent as the same effect on the spectra were observed.

When the samples were put under vacuum, a red shift of the peaks was observed.

After rehydration, a blue shift was observed, the spectrum returning to that measured prior to dehydration.

After heating the sample, a red shift was observed similar to the red shift of the spectrum just after being evacuated.

The doped sol-gel contains water in its pores which is largely removed when the sample is put under vacuum and thermally treated.

The data presented show that the electronic transitions of Nd^{3+} are sensitive to water in the pores of the sol-gel glass. This could imply that the water is in the proximity of the metal ion and can consequently be part of its local environment.

Moreover not only a peak shift was observed according to the different treatments inflicted on the samples but a change in the shape of the peaks was also observed corresponding to a change in the coordination chemistry of the metal ion.

A change in the intensity of the peaks was also observed after the samples had been thermally treated to 800°C.

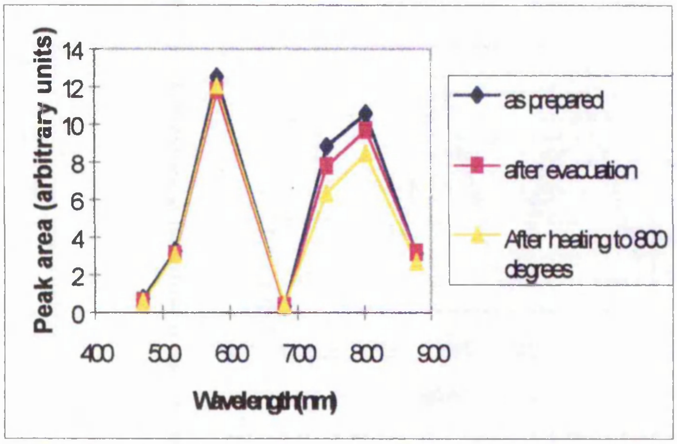

Figure 4.23: $Nd(NO_3)_3.6H_2O$ (9.48wt%) sol-gel prepared in ethanol

A decrease in the peak areas was noticed for the peaks corresponding to the electronic pseudohypersensitive-transitions at 750nm and 800nm.

A very small decrease in peak area was observed for the hypersensitive transition at 580nm.

When comparing the effect of the environment of the metal ion on its electronic transitions, differences in intensity of the peaks were observed according to whether the metal ion was in solution or in the glass.

To compare the intensity of the peaks of the metal ion in solution and in the sol-gel, it was necessary to have the same pathlength.

The exact concentration of the metal ion in the sol-gel glass was calculated using weight of the metal ion added and the weight of the glass. Similar concentrations were prepared for the metal ion in solution. The thickness of the sol-gel monolith was measured using a Vernier micrometer and an average of 1mm±0.01mm was found.

For the solutions, a 2mm quartz cuvette was used. Correction of the absorbance were made for comparison with 1mm pathlength used for the sol-gel glasses.

The intensity of the peaks at 580nm (hypersensitive transition) and at 750nm and 800nm (pseudohypersensitive transitions) were measured for Nd^{3+} ions in solution and in the sol-gel.

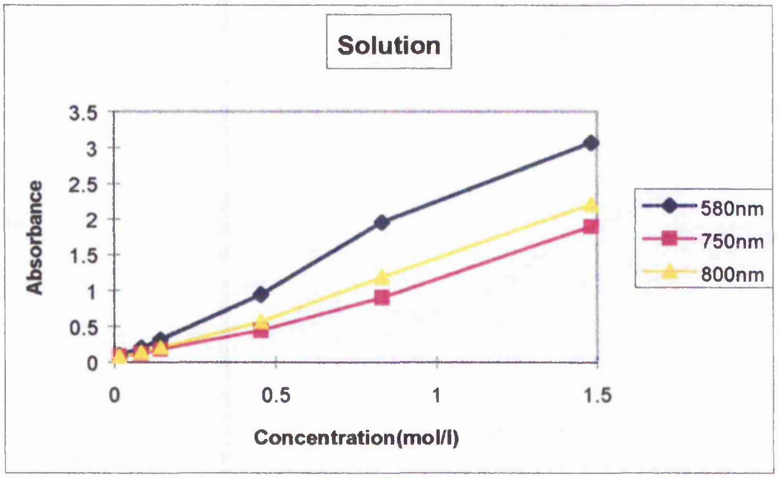

Figure 4.24: $Nd(NO_3)_3.6H_2O$ solution prepared in ethanol

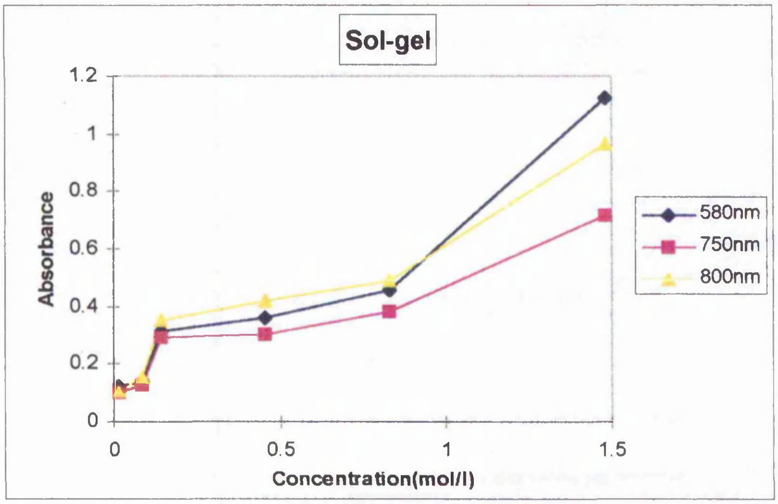

Figure 4.25: $Nd(NO_3)_3.6H_2O$ sol-gel prepared in ethanol

In the sol-gel, as well as in solution, the variation of the absorbance of the metal ion did not follow the Beer-Lambert law.

As described previously (section 4.3.2.1), in solution two linear regions of behaviour were observed whereas in the sol-gel three regions could be defined.

With low concentrations of the metal ion (0.0154-0.1433M) in the sol-gel a non linear increase of the absorbance with concentration was noticed. As the concentration increased (0.1433-0.829M) a linear region was observed. Finally with high concentration of the metal ion in the sol-gel (1.482M), a large increase of the absorbance occurred which did not follow any linear pattern with the absorbance of lower concentrations.

A decrease of the intensity of the peaks was observed when the metal ion was in the glass compared to the intensity of the peaks of the metal ion in solution.

In solution, the highest intensity was observed for the peak at 580nm, then came the peak at 800nm, the lowest intensity was for the peak at 750nm regardless of the concentration of the metal ion in solution. However in the sol-gel, for concentrations of the metal ion in the glass between 0.0154M and 0.829M, the highest intensity was observed for the peak at 800nm, then for the peak at 580nm and the lowest intensity was measured for the peak at 750nm. For a high concentration (1.482M) the order changed and the highest intensity was observed for the peak at 580nm followed by the peak at 800nm and then at 750nm.

Different effects on the electronic transitions were observed according to the environment of the metal ion.

The coordination chemistry of the metal ion in the sol-gel was studied by UV-VIS and EXAFS analysis.

Vis spectrum of Nd^{3+} sol-gels with Cl$^-$ ligands or NO$_3^-$ ligands are presented in Figure 4.26.

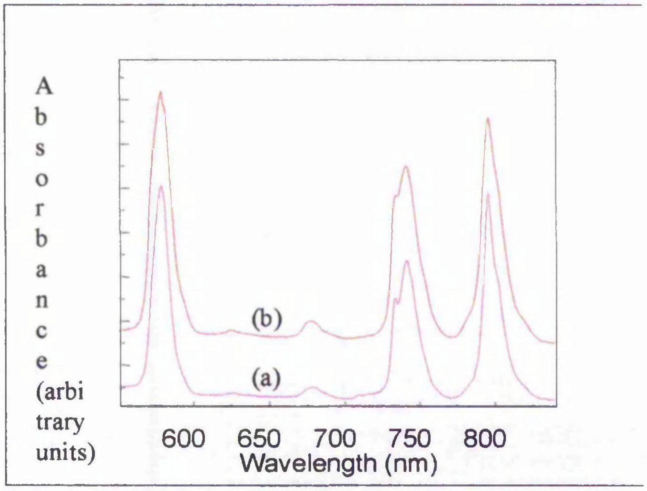

Figure 4.26:Vis spectrum of Nd^{3+} sol-gel with a) Cl$^-$ ligands, b) NO$_3^-$ ligands

The same spectrum of Nd^{3+} ion in the sol-gel was observed regardless of the type of ligands. The coordination number of the metal ion in the sol-gel was not affected by the type of ligands around Nd^{3+}.

Changes in the spectrum were observed when the samples were put under vacuum and thermally treated involving a probable change in the coordination number of Nd^{3+} (Figure 4.27).

By comparing the spectra obtained for the samples dried at 40°C , the spectra obtained from the samples put under vacuum, rehydrated and finally heated up to 800°C, several changes were noticed.

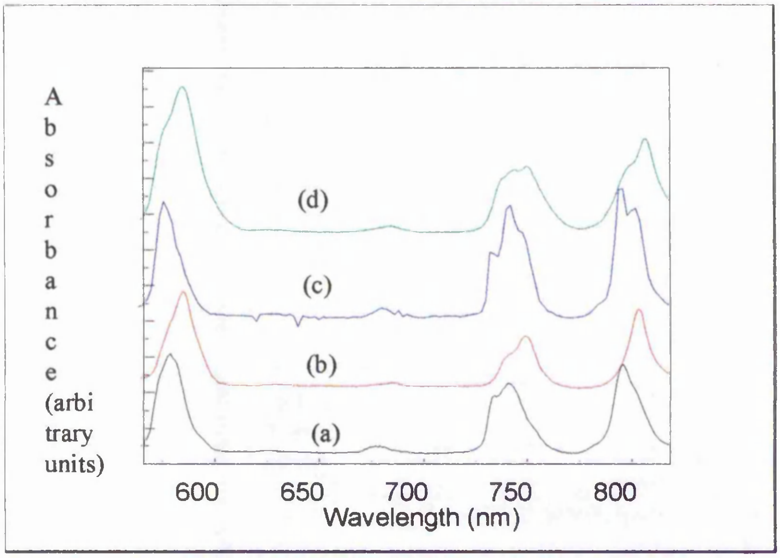

Figure 4.27: Vis of $Nd(NO_3)_3.6H_2O$ sol-gel a) dried at 40°C, b) after evacuation, c) after rehydration, d) after heating up to 800°C

Changes in the spectra correspond to changes in the matrix structure and in the coordination chemistry around the metal ion.

When the samples were put under vacuum they lost the remaining solvent which was trapped in the pores. The removal of some solvent was confirmed by a sample loss of weight of around 7% after vacuum treatment.

After this the samples were heated up to 800°C and at this temperature all the water which was present in the glass (as well as any solvent which could have stayed even after vacuum treatment) was eliminated (by ca. 180°C). The organic compounds were eliminated at around 400-600°C and finally at high temperature (800°C) the pores started to collapse and the glass to sinter.

Consequently the environment around the Nd^{3+} ion has changed during the vacuum and thermal treatment compared to the initial sample.

The change in the shape of the peaks showed that a coordination number of 7 was present in the glass as prepared, regardless of the initial solvent in which the metal ion was added to the sol-gel solution by comparison with the UV-VIS spectra proposed by Karraker [18]. After evacuation, a shift of the peaks was observed involving a change to a coordination number of 6 which after rehydration for 24 hours went back to 7 by comparison with the

UV-VIS spectra proposed by Karraker [18].

After thermal treatment was applied, a change in coordination number was observed which could not be interpreted by UV-VIS analysis alone.

EXAFS experiments were carried out to confirm the proposed coordination numbers.

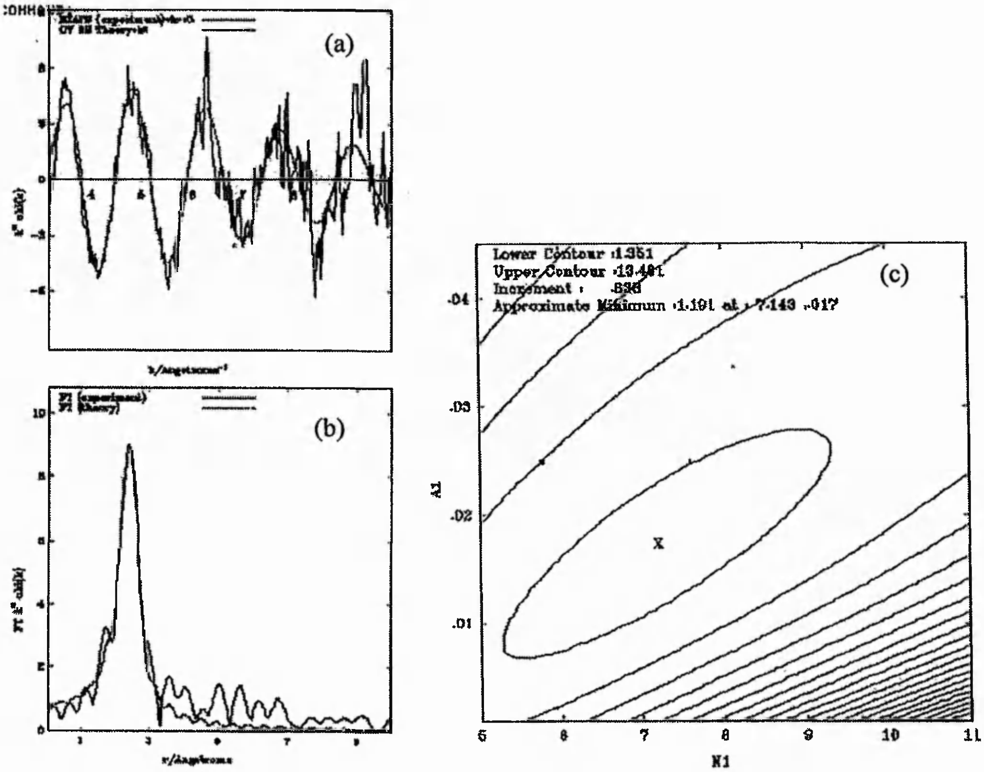

Figure 4.28: Nd^{3+} sol-gel dried at 40°C prepared with Nd(NO$_3$)$_3$.6H$_2$O,

a) k^3 K-edge EXAFS spectra,

b) Fourier transform magnitude of k^3 K-edge EXAFS spectra,

c) contour map of k^3 K-edge EXAFS spectra

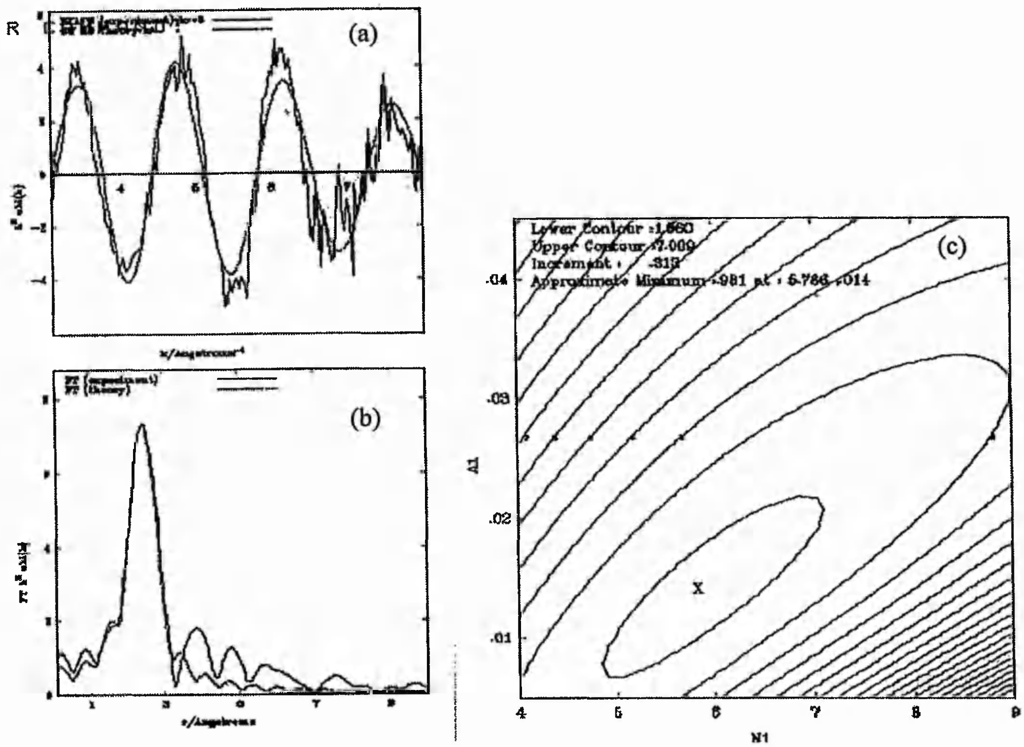

Figure 4.29: Nd^{3+} sol-gel evacuated, prepared with $Nd(NO_3)_3.6H_2O$,

a) k^3 K-edge EXAFS spectra,

b) Fourier transform magnitude of k^3 K-edge EXAFS spectra,

c) contour map of k^3 K-edge EXAFS spectra

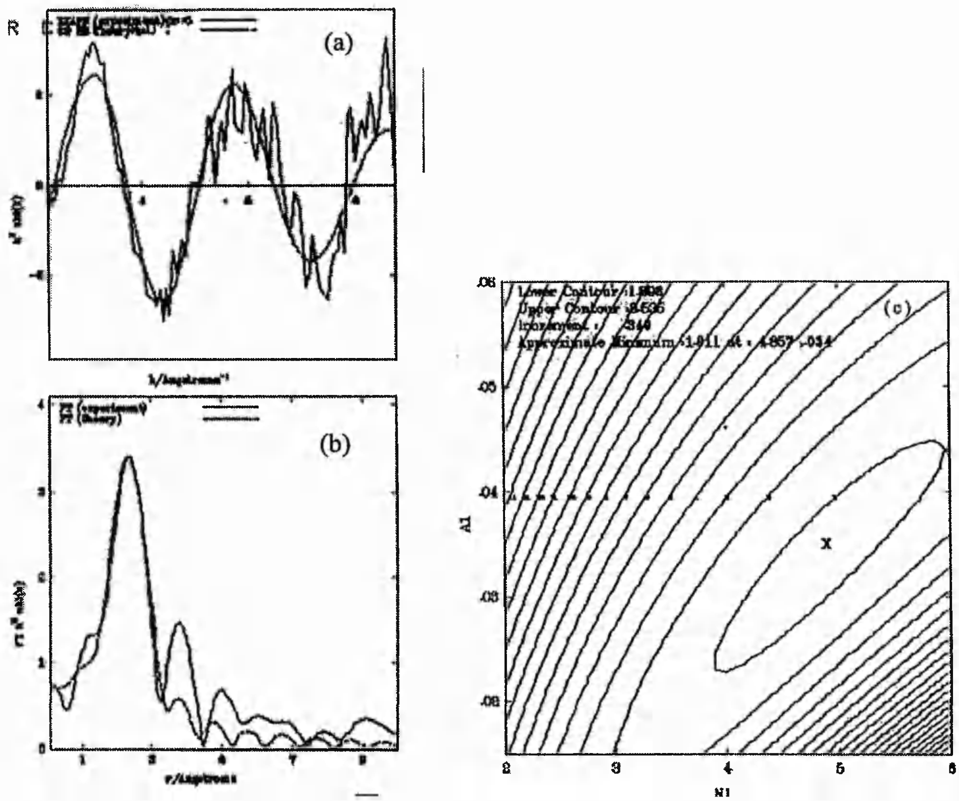

Figure 4.30: Nd^{3+} sol-gel heated to 800°C, prepared with $Nd(NO_3)_3.6H_2O$,

a) k^3 K-edge EXAFS spectra,

b) Fourier transform magnitude of k^3 K-edge EXAFS spectra,

c) contour map of k^3 K-edge EXAFS spectra

Table 4.9 shows the values of the coordination number, bond distance and Debye-Waller factors for Nd^{3+} sol-gels as prepared, evacuated and thermally treated to 800°C.

Table 4.9

Sol-gels	**Coordination number (N)**	**Bond distance between Nd-O (r/Å)**	**Debye-Waller factor (σ/Å²)**	**Residual indice (R/%)**
as prepared	7.2	2.55	0.025	37.52
evacuated	5.9	2.549	0.014	32.03
heated to 800°C	4	2.495	0.025	36.76

A coordination number of 7 was observed for Nd^{3+} ion in the sol-gel, after evacuation the coordination number became 6 and 4 after heat treatment.

The bond distance decreases with the coordination number suggesting a potential change in the type of ligands. All data were fitted using oxygen in the first coordination sphere.

4.3.2- Discussion

In the present study, the UV-VIS spectra of Nd^{3+} ions in crystals show differences in the shape of the peaks when different counterions are associated with the metal ion.

No effect on the metal ion UV-VIS spectrum occured when the solvent was changed (water or ethanol) in the preparation of the crystals.

For the crystals examined, the coordination number changes only according to the counterions and not to the solvents used in their preparation. The counterions are strongly covalently bonded to the metal ion. A shorter bond distance between the metal ion and the oxygen from the water was observed than the bond distance between the metal ion and the oxygen from the nitrate or between the metal ion and the chloride. The variation in the bond distances between the metal ion and the ligands was due to a variation in the electronegativity of the ions. According to Pauling classification [35], Nd^{3+} has an electronegativity of $1.14\chi^P$, O of $3.44\chi^P$, H of $2.2\chi^P$, N of $3.04\chi^P$, Cl of $3.16\chi^P$. Also the ionic radii of Cl^- is 1.81Å whereas the ionic radii of oxygen is 1.40Å. Consequently, the bond distance between Nd^{3+} and Cl^- is longer than the bond distance between Nd^{3+} and oxygen.

In solution, some changes in the position of the peaks were noticed according to the ligands and to the solvents around the metal ion.

A red shift of the peaks occurred which happens when the energy of the excited states is lowered more that that of the ground state or when the energy of the ground state is raised more that that of the excited state. The blue shift is characteristic of the reverse phenomenom [36]. These changes were produced by structural changes on introducing a substituent or on altering the environment of the metal ion. Nd^{3+} ions possess two spheres of ligands. The inner sphere which is directly bonded to the metal ion and the outer sphere not directly bonded to the metal [30]. Small systematic shifts (around 2nm) of the bands to longer wavelengths were observed when Nd^{3+} was in solution and the NO_3^- ligand was replaced by Cl^-. Nitrate ions affect the spectrum of the rare earth element differently from chloride ions. As the metal-ligand bond is changing, there is an alteration of the strength and symmetry of the ligand field surrounding the metal ion. Cl^- is an anion of a strong acid which contains no oxygen and forms relatively weak outer sphere complexes with the metal ion, whereas NO_3^- contains O atoms and is strongly bonded to the metal ion.

which contains no oxygen and forms relatively weak outer sphere complexes with the metal ion, whereas NO_3^- contains O atoms and is strongly bonded to the metal ion. Change in the shape of the spectral peaks occurs corresponding to the variation of new electronic transitions [37].

As well as the ligand, the solvent had a direct effect on the Nd^{3+} spectrum when the metal ion was in solution [38]. The spectrum of the Nd^{3+} ion is influenced by its environment. The band intensities of Nd^{3+} increase as the electron donating ability of the solvent increase [39]. The solvent affects the environment of the metal ion and consequently its electronic transitions [40].

Variation in the peak areas of the various electronic transitions affected by the metal ion environment was observed according to the solvent. Water had a higher covalency factor than the other solvents suggesting a stronger metal-ligand interaction. This is due to the solvation and covalency capability of the solvent.

The intensity changes and peak area changes for the hypersensitive transitions and pseudohypersensitive transitions are due to an enhancement of the quadrupole transitions by the dielectric constant due to the inhomogeneities in the media [41,42].

Hypersensitivity owes its existence to the inhomogeneous polarizability of the solvent which enhances the variations of the electric vector of the electromagnetic radiation across the rare-earth ion, thereby increasing the intensities of the quadrupole transitions. In solution, as well as the solvent, the ligands in the outer sphere of the metal ion affect the environment of the metal ion and its electronic transitions.

In solution, the coordination number changes with the type of solvent which can be correlated with its donor capability. A coordination number of 9 is found in the presence of water and a coordination number of 7 with ethanol.

In water Nd^{3+} ions with NO_3^- and H_2O ligands loses one ligand and Nd^{3+} with Cl^- and H_2O ligands gains one.

Water ligands are bonded to the metal ion by one oxygen but two oxygens bond nitrate ligands, so nitrate ligands are more stably bound than the water ligands. Consequently in water, the metal ion loses a water ligand in the presence of nitrate.

In the presence of chloride the metal ion gains a water ligand.

The electronegativity of the oxygen ion is higher than the electronegativity of the chloride ion and consequently the water ligand is more attracted to the metal ion than the chloride that stays in the medium. Moreover as the solvent is water, the concentration of water in the solution is higher than the concentration of chloride ion in the solution.

χP	χP	χP
Nd: 1.17	Cl: 3.16	O: 3.44 [35]

In water, the coordination number of 9 for Nd^{3+} complex is the more thermodynamically stable and is observed in most cases [32-34,43].

In ethanol, a coordination number of 7 is found. In the current system, both ethanol and water are present.

Nd^{3+} is a hard metal due to its high positive charge +3 [44] and subsequently the metal-ligand bonding possesses a high degree of ionic character.

This has an effect on the type of ligands with which the metal ion prefers to interact. A hard metal ion will favor ligands containing donor atoms which are highly electronegative. Water has a higher donor property than ethanol and a higher polarity [45,46] and Nd^{3+} has a negative pK_a value of -8.5 which means that it is a strong acid, with proton transfer lying in favour of donation to water. The water ligands were not replaced by the ethanol solvent. In ethanol, the Nd^{3+} complex containing H_2O and NO_3^- ligands loses 3 ligands as compared to the coordination found in the X-ray analysis of the crystalline form of neodymium nitrate hexahydrate.

An electrostatic interaction can occur between the water ligand and the ethanol present in the system due to the presence of the –OH group.

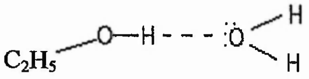

So the metal ion is probably bonded to three NO_3^- ions and one H_2O ligand.

The coordination number of 7 being more thermodynamically stable than 9 in ethanol. The Nd^{3+} complex containing Cl^- counterions and water ligands loses one ligand in the presence of ethanol as compared to the solid state. As water is more electronegative than chloride ions, it is likely that the complex loses one chloride ion when ethanol is the solvent.

$Nd(NO_3)_3.6H_2O$ salt in ethanol was used for the preparation of sol-gel glasses.

When in the glass, the same UV-VIS spectrum was observed regardless of the counterion associated with the metal ion and the type of solvent used.

The electronic transitions were not sensitive to the solvent in which the metal ion had been prepared as a solution, suggesting that the same solvent/environment is present around the metal ion. In the glass, the electronic transitions are still sensitive to the environment of the metal ion which is not only the solvent but also the silica matrix. Therefore, shifts of the peaks and changes in the shape of the spectral bands are observed when different treatments are done on the samples.

A decrease in the intensities of the peaks corresponding to the sensitive electronic transitions was observed when the metal ion was in the glass and no longer in solution. The intensity of the spectrum when Nd^{3+} is in the glass decreased an average of 35-40% for each peak compared to Nd^{3+} in solution. This decrease of absorbance was observed for low as well as high concentrations of the dopant.

This change in absorbance could be associated with a change of coordination chemistry and consequently a change of environment around the metal ion.

In the glass, according to the treatment carried out on the samples, changes are observed in the UV-VIS spectra associated with a change in the crystal field of the metal ion.

A coordination number of 7 was found for the as prepared gel, identical to the coordination number in ethanol solution. Rao et al. [47] reported a coordination number of 7 as well in a conventionally prepared Nd^{3+} doped glass by doing EXAFS and XANES analysis.

In the glass, the coordination chemistry is not affected by the local chemical environment around the metal ion. Both nitrate and water ligands are strongly covalently bonded to the metal ion.

By looking at the UV-VIS spectra of Nd^{3+} in ethanol solution (7 coordinate) and Nd^{3+} in the as prepared sol-gel, differences in the band shapes were noticed corresponding to a different environment around the metal ion which must be associated with the proximity of silica to the metal ion in the glass. The Nd^{3+} complex is trapped in the glass and could be electrostatically bonded to the matrix by the silanol groups as was suggested in Chapter 3.

After dehydration, a coordination number of 6 was found for the glass sample. The complex loses one ligand. The samples were put under vacuum in order to remove the remaining solvent and water. As the water was not as strongly bonded to the metal ion as the nitrate ligands, a water ligand was removed.

When the samples were rehydrated, the coordination number went back to 7, gaining one water ligand. It shows that for the Nd^{3+} complex trapped in the matrix, the coordination number of 7 is more thermodynamically stable than a coordination number of 6 which can only be maintained if the sample is kept out of air.

Finally, when the sol-gel samples were heated up to 800ºC, a coordination number of 4 was found.

FTIR analysis of the glasses (Chapter 3) has shown that, at this temperature, the nitrate ligands have been removed from the matrix.

The EXAFS analysis have shown that after heating the sample, a shorter bond distance is observed between Nd-O.

Consequently, different ligands are around the metal ion after heat treatment.

The nitrate ligands are eliminated and the metal ion bonds to the matrix by the silanol groups as siloxane groups and so is bonded to 4 O-Si≡ groups.

Previous work done by Chabrabarti et al. [48] and Pope et al. [49] have also shown the possibility of direct covalent bonds between Nd^{3+} and O-Si≡ groups in the sol-gel glass system.

4.4- Conclusions

The neodymium ion is influenced by its environment.

The electronic transitions of the metal ion are affected by the coordination number.

A coordination number of 10 was observed for crystals of neodymium salts when the counterion was NO_3^- and a coordination number of 8 was observed with Cl^-.

However the solvent used to prepare the crystals did not affect the metal ion and its environment as identical crystal structures were observed for sample preparation from various solvents.

In solution a different behaviour was observed. The solvent has a stronger effect on the electronic spectrum of the metal ion than the counterion. Only changes in the type of solvents produced a variation of the coordination number. In water a coordination number of 9 was found whereas in ethanol a coordination number of 7 was present. The donor capability of the solvent as well as its covalent properties affect the coordination chemistry of the metal ion.

In the glass matrix, the electronic transitions of Nd^{3+} were sensitive to the local environment of the metal ion.

The solvent and the salts from which the glass had been prepared had no effect on the coordination chemistry of the metal ion.

As the same spectrum and hence same coordination chemistry was found for various counterions and solvents. The metal ion in the glass as prepared exhibited a coordination number of 7.

After evacuation of the glass, a coordination number of 6 was present.

During evacuation, water and solvent remaining in the pores are removed and the metal ion loses a water ligand.

After heat treatment, the metal ions have a coordination number of 4.

The metal ion before any treatment, is entrapped in the matrix. After heat treatment, a change of ligands occurred and the metal ion was covalently bonded to the silica matrix by the OSi≡ groups.

REFERENCES

[1] L.L.Hench, *Ceramics International*, **17**, 206 (1990)

[2] D.Avnir, S.Braun, M.Ottolengh, ACS Sym.Series 499, (Am.Chem.Soc, Washington DC Publishers), 384, (1992)

[3] C.J.Brinker, C.J.Hurd, J.Non-Cryst.Solids, **121**.294, (1990)

[4] L.L.Hench, J.K.West, Chemical Review, **90**, 33, (1990)

[5] S.J.Sakka, J.Non-Cryst.Solids, **121**, 294, (1990)

[6] J.I.Zink, B.Dun, J.Mater.Chem., **1**(6), 903, (1991)

[7] N.Nogami, *Sol-Gel Optics*, (Kluwer Academic Publishers, New York), (1993)

[8] M.Yamane, *Ultrastructure Processing Advanced Materials*, (publishers Wiley, New York), 509, (1992)

[9] M.Yamane, J.B.Caldwell, D.T.Moore, *Better Ceramics Through Chemistry II*, (publishers North-Holland, Amsterdam), 765, (1986)

[10] L.LHench, G.P de La Torre, S.Donovan, Sol-Gel Optics II, 94, (1992)

[11] M.R.Shahriari, J.Y.Ding, *Sol-Gel Optics*, (Kluwer Academic Publishers, New York), (1993)

[12] E.Snitzer, Phys.Rev.Lett., **7**, 444, (1961)

[13] O.Suelto, *Principles of Lasers*, (Plenum Press, New York), (1989)

[14] R.M.Almeida, X.Orignac, D.Barbier, J.of Sol-Gel Science & Technology, **2**, 465, (1994)

[15] L.E.Ageeva, V.I.Arbuzov, E.I.Galent, Sov.J.Glass.Phys.Chem., **13**, 221, (1988)

[16] B.G.Wybourne, *Spectroscopic Properties of Rare Earths*, (Interscience Publishers, London), (1965)

[17] D.G.Karraker, Inorg.Chem., **7**, 473, (1968)

[18] D.G.Karraker, Inorg.Chem., **6**, 1863, (1967)

[19] S.N.Missa, S.B.Metha, Bulletin Chem.Soc.Jpn., **64**, 3653, (1991)

[20] S.Davis, M.F.Reid, E.M.Stephens, Inorg.Chem., **23**, 4607, (1984)

[21] W.C.Wang, Y.Chen, T.Dhu, J.Appl.Phys., **7**, 79, (1996)

[22] F.Rocca, A.Kutzmin, J.Purans, G.Mariotto, Solid State Ionics, **70/71**, 465, (1994)

[23] C.Prieto, A.Andres, M.Medarde, J.L.Martinez, Solid State Comm., **80**, 975, (1991)

[24] S.P.Sinha, Spectrochimica Acta, **22**, 57, (1966)

[25] D.A.Skoog, D.M.West, *Fundamentals of Analytical Chemistry*, 4th edition, (publisher Saunders College), (1982)

[26] B.G.Wybourne, J.Chem.Phys., **32**, 3, (1960)

[27] B.K.Teo, *EXAFS Spectroscopy techniques and Application*, (publisher Plenum Press, New York), (1981)

[27] Y.Hirashima, T.Tsutsui, J.Shiokowa, Chem.Lett., 1405, (1982)

[28] A.Habenschuss, F.H.Speeding, J.Chem.Phys., **70**, 81, (1979)

[29] C.N.R.Rao, *Ultra-Violet and Visible Spectroscopy*, 3rd edition, (publisher Butterworths, London), (1975)

[30] D.G.Karraker, Inorg.Chem., **7**, 3, (1968)

[31] D.G.Karraker, Inorg.Nucl.Chem., **31**, 2815, (1969)

[32] G.Wilkinson, R.D.Gillard, J.A.McCleverty, *Coordination Chemistry*,(publisher Pergamon press, Oxford), **1**, (1987)

[33] E.M.Stephens, S.Davis, Inorg.Chem., **23**, 1641, (1984)

[34] A.Cossy, L.Helm, D.H.Powell, A.E.Merbach, New Journal of Chemistry, **19**, 27, (1995)

[35] J.E.Huhey, E.A.Keiter, R.L.Keiter, *Inorganic Chemistry*, 4th edition, (publisher HarperCollins College, New York), 187, (1993)

[36] S.K.Freeman, *Interpretive Spectroscopy*, (publishers Reinhold, New York), (1965)

[37] D.R.Browning, *Spectroscopy*, (publishers Mc Graw-Hill, London), (1969)

[38] G.R.Choppin, D.E.Henrie, K.Buijs, Inorg.Chem., **5**, 10, (1996)

[39] D.F.Henrie, R.L.Fellows, G.R.Choppin, Coord.Chem.Reviews, **18**, 199, (1976)

[40] L.L.Quill, P.W.Selewood, B.S.Hopkins, J.Am.Chem.Soc., **50**, 2929, (1928)

[41] B.R.Judd, Phys.Rev., **127**, 750, (1962)

[42] B.R.Judd, ACS Sym.series (Lanthanide Actinide Chemical Spectroscopy), **131**, 267, (1980)

[43] G.Oczko, M.Zalewicz, J.Molecular Structure, **407**, 63, (1997)

[44] F.W.Atkins, G.H.Langford, *Inorganic Chemistry*, (publishers Oxford), (1990)

[45] B.M.Antipenko, L.A.Batayaev, Zh.Neorg.Khim., **20**, 12, (1975)

[46] C.E.Housecroft, E.C.Constable, *Chemistry; an Integrated Approach*, (publishers Longman, Harlow), (1997)

[47] K.J.Rao, J.Wong, M.J.Weber, J.Chem.Phys., **78**, 6628, (1983)

[48] S.Chabrabarti, J.Sahu, M.Chakraborty, H.N.Acharya, J.Non-Cryst.Solids, **180**, 196, (1994)

[49] E.J.A.Pope, J.D.Mackenzie, J.Non-Cryst.Solids, **106**, 236, (1988)

Chapter 5: Solid Absorbance Standards

5.1- Introduction

Standards are necessary for calibration. They can be used at any absorbance level in an instrument's range[1]. Two types of standards exist: liquid standards and solid standards. In ultraviolet spectroscopy, currently the only available standard in solution is potassium dichromate in sulphuric acid [2]. Inorganic compounds such as potassium nitrate can also be used as can organic compounds including nicotine or acridine solutions [2]. With these solutions, some problems such as fluorescence and absorption of water occur which reduce the efficiency of the standards [3,4].

Solid standards are used to determine the intrinsic performance of the instrument. The standards currently used are glass standards [5] such as National British Standard glass filters [6,7]. These standards are however difficult to calibrate, unstable with time, a decrease of the transmittance with time being observed.

Stable solid standards are required which must have a high transmittance and must be highly stable with time. In order to achieve this objective, solid UV absorbance standards have been prepared.

The following specifications were required.

- They had to be used at wavelengths between 230-350nm.
- They had to be flat and homogeneous, available in a range of absorbance values (from 0.5 to 2A) and exhibit a long term stability of spectral response.
- The suitable bands in the UV region need to have a width of around 6nm.

To prepare solid standards, the sol-gel process was used to produce materials with high purity, homogeneity and excellent optical characteristics. The sol-gel process allows the preparation of the glass at room temperature and hence allows the dopant to retain its intrinsic chemical and structural properties.

To use the UV absorbance standards as a calibration material, the UV spectrum of the standards need to show some bands in the UV region between 230-350nm.

Organic compounds showing bands in the UV region when in solution such as histidine, pyrazole or 4-isopropylpyridine, were not suitable for this purpose as they were found to react with the precursors used to make the sol-gel material with the consequence that their bands in the UV region were no longer observable.

A study of the lanthanide elements was then performed as they are known to be relatively stable elements and possess bands in the UV region.

Cerium, neodymium, samarium and gadolinium ions were considered to be the most suitable candidates as they possess electronic transitions in the UV region [8].

5.2-Method

5.2.1- Preparation of Solutions

Solutions containing various dopants ($Nd(NO_3)_3.6H_2O$, $CeCl_3.7H_2O$, $Ce(NO_3)_3.6H_2O$, $GdCl_3.6H_2O$, $SmCl_3.6H_2O$, 4-isopropylpyridine, 4-ethoxyatephenone, pyrazole and histidine, all from Aldrich) were prepared in dry ethanol (distilled from 95% ethanol over magnesium) and distilled deionised water.

The solutions were analysed by UV-VIS spectroscopy using an UNICAM UV2 UV-VIS spectrometer (scan speed 600nm/min, data interval 0.5mm).

5.2.2- Sol-gel preparation

Using the sol-gel process silica monoliths were prepared.

Non-doped and doped silica gel glasses were made using tetraethylorthosilicate 98% (Aldrich) mixed with dry ethanol (distilled from 95% ethanol over magnesium) and stirred gently for a few seconds to obtain an homogeneous solution. Then, if necessary, the dopant was added. Finally, 0.5M HCl (prepared from 11.3M HCl (Fisher)) was added at the following molar ratio:

For normal sol-gels:

1 TEOS:4 EtOH:4 H_2O:0.045 HCl

For doped sol-gels:

The molar ratio was the same as above with the dopant at a range of concentrations from 0.7M to 10^{-3}M in the initial solutions (water or ethanol) with Ce^{3+} ion (from $CeCl_3.7H_2O$ from Aldrich) used as dopant (Ce^{4+} doesn't have any bands in the UV region).

The solution was mixed at room temperature for one hour before being put (4ml) in petri dishes (diameter 3.5cm, depth 1cm from Nunc) covered with Nesco film® in which 5 holes (0.6mm diameter) had been made before being placed in a fan assisted oven at 40°C to dry. The method of drying the samples was determined after a series of trials including various containers and heating temperatures was carried out. In order to obtain good optical quality the heating temperature had to be low to get an efficient removal of water and solvents which reduce the transmittance in the UV region.

For every type of sol-gel, a batch of 8 samples was prepared simultaneously.

Samples were weighed daily (%weight loss versus time was plotted). Statistical analysis using the student's t-test was performed in order to assess the significance of variations measured. When the samples showed no measurable weight loss, they were analysed by UV-VIS spectroscopy using a UNICAM UV2 UV-VIS spectrometer (scan speed 600nm/min, data interval 0.5nm). The glasses (around 1.05mm thickness) were analysed in the bulk supported by a metallic holder. Samples were also investigated as dried pieces of glass, immediately after dehydration by subjecting the samples to a vacuum pressure of 6mbar (measured by an Edwards Pirani 10 pressure sensor) for 18 hours, and after thermal treatment (with a ramp temperature of 0.1°C/min) for 4 hours at 800°C. The samples were cooled down at a ramp temperature of 5°C/min, the whole process taking 36 hours. A Carbolite programmable furnace was used.

5.2.3- Further Treatments of Doped Sol-Gel Materials for use as absorbance standards.

The suitable solid standards need to be stable with time. The transmittance of the material has to remain the same. Preliminary studies were carried out on the dry samples.

First an attempt was made to try to protect the glass from the outside environment and from absorption of moisture, then an aging of the samples under various conditions was carried out.

5.2.3.1- To Prevent absorption of moisture

The samples, when dry, were immersed in a solution containing hydrolysed TEOS. Hydrolysed TEOS was made by mixing and stirring TEOS (from Aldrich 98%) and HCl (from Fisher 11.3mol/l) with a molar ratio of 38 TEOS: 1 HCl for one minute. Then the sol-gel glass was immersed in the solution for 24 hours.

UV-VIS spectra were obtained from the samples before and after the treatment using a UNICAM UV2 UV-VIS spectrometer with a scan speed of 1200nm/min and a data interval of 1nm.

5.2.2.2- Stablity studies

To study the stability of the samples with time, several measurements were carried out. For these measurements, two type of samples were used. The ones which were immersed in hydrolysed TEOS and the ones which did not have any treatment as this will allow us to compare which method of sample production is the most suitable.

A bench stability test was done which consisted of leaving the samples on the bench and recording the UV-VIS spectrum every week to notice any changes. The spectra obtained were correlated with atmospheric changes (temperature in the laboratory, humidity).

Another series of experiments involved irradiation of the samples. A UV lamp (pen lamp, 220V, spectra output between 200nm and 500nm) from UNICAM was used. The lamp was placed at a distance of 1cm from the samples.

They were irradiated 24 hours a day and UV-VIS measurements were done every week. The stability of their spectra with time was studied.

A study of sample stability at low temperature was also performed. Samples were put in a freezer at -16°C. UV-VIS spectra were recorded every week.

The appearance and the resistance of the sol-gel glass to these treatments were also observed.

5.3- Results and Discussion

5.3.1- The choice of standards

Metal ions were prepared in solution and then doped in the sol-gel. Figure 5.1 shows the UV-VIS spectra of the metal ions in solution. UV-VIS spectra were obtained from the dried doped sol-gels in order to know if the metal ions maintain their spectroscopic properties in the sol-gel.

To observe the UV spectrum of the samarium(III) ion it was necessary to prepare a very high concentration of the solution (above 3M). At lower concentrations (1M), bands in the visible are observed. The electronic configuration of samarium is ($4f^6$) with the ground state at $^6F_{5/2}$. In solution (figure 5.1), the characteristic bands are observed at 363nm, 375nm and 402nm. The bands are too close to the visible region. The metal ion does not possess bands between 250nm and 350nm. Moreover in the sol-gel (figure 5.2), only one band characteristic of samarium was observed at 400nm with a very low intensity. This metal ion was not thought suitable for the preparation of an UV standard.

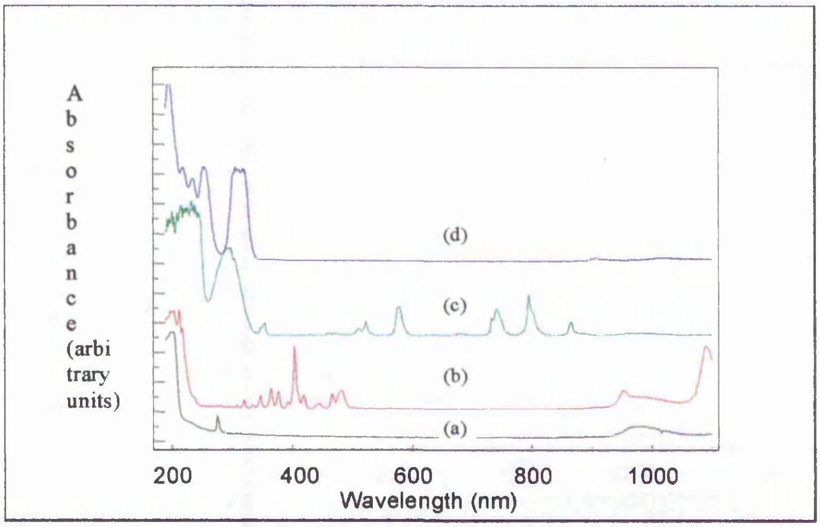

Figure 5.1: UV-VIS spectra of various metal ions in water solution

a) Gd^{3+} 0.9M, b) Sm^{3+} 1M, c) Nd^{3+} 1M, d) Ce^{3+} 0.7M

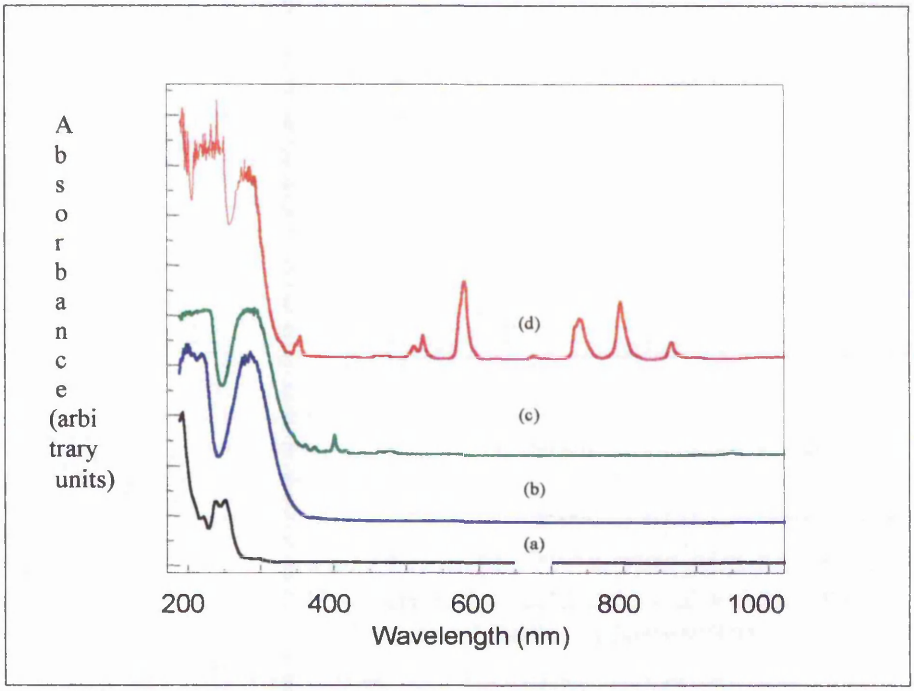

Figure 5.2: UV-VIS spectra of various metal ions in the sol-gel

a) Ce^{3+} 10^{-2}M, b) Gd^{3+} 0.9M, c) Sm^{3+} 1M, d) Nd^{3+} 1M

The gadolinium ion in solution (Figure 5.1) possesses a band at 280nm. Its electronic configuration is ($4f^7$), the ground state being $^8S_{7/2}$. This band is too sharp (0.01nm width) to be used as standard for calibration. The highest concentration of the metal ion which could be dissolved in solution was 0.9M as the metal ion is not very soluble. Due to the low intensity of the band in solution, the band characteristics of gadolinium (III) were no longer observable in the sol-gel (Figure 5.2).

The neodymium (III) ion possesses only one band at 325nm, not ideal for a UV standards as a series of bands is desired. All the bands characteristic of Nd^{3+} are situated in the visible region.

Finally, the cerium(III) ion was used and showed a series of bands in the UV region both in solution and in the glass. This metal ion was chosen for further investigation as a standard in the UV region.

5.3.2- Characterisation of the standards

5.3.2.1- Results

Figure 5.3 shows spectra of $CeCl_3.7H_2O$ solutions in either ethanol or water at various concentrations and also of $Ce(NO_3)_3.6H_2O$ in water. $CeCl_3.7H_2O$ at a concentration of 0.01M in ethanol shows bands at 201nm, 213nm, 230nm, 252nm and at 309nm.

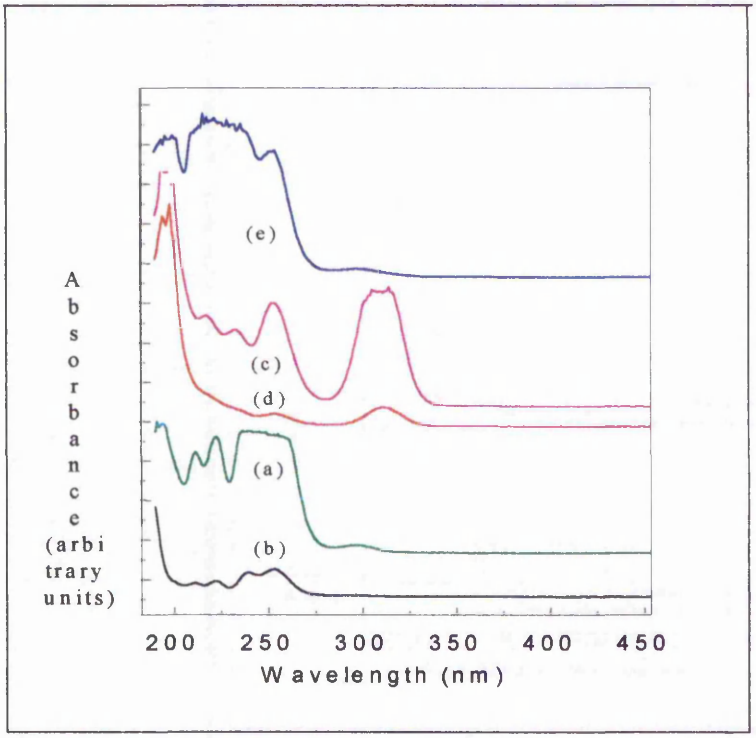

Figure 5.3:UV-VIS spectra of (a-d) $CeCl_3.7H_2O$ solutions a) 0.01M and b) 0.001M in water, c) 0.01M and d) 0.001M in ethanol, e) $Ce(NO_3).6H_2O$ 0.01M in water

The band at 309nm is due to an interaction between the solvent and the metal ion that could be related to the polarity of the solvent which affects the environment around the metal ion and gives rise to a new electronic transition.

At a solution concentration of 0.001M, the intensity of the bands is very low (figure 5.3b) and hence more difficult to observe. $CeCl_3.7H_2O$ in water shows bands at 200nm, 208nm, 223nm. The band which was observed at 252nm in ethanolic solution is observed as two bands at 239nm and 253nm. Moreover the band observed at 309nm in ethanol is shifted in water and observed at 298nm but at a lower intensity than in ethanol. Solutions of $Ce(NO_3)_3.6H_2O$ only show one band at 250nm. The broad and noisy band observed in the UV region between 205nm and 240nm corresponds to charge transfer between the metal ion and the ligands. The very close proximity of the charge transfer and bands arising from electronic transitions prevent a clear assignment of the bands.

Doped sol-gels were prepared with Ce^{3+} (Figure 5.4). The samples prepared with $Ce(NO_3)_3.6H_2O$ metal ion did not show a band in the UV region when in the sol-gel and hence were studied no further.

When the sol-gels were dried, the presence of Ce^{3+} was detected by its UV-VIS spectrum. The characteristic bands of Ce^{3+} (from $CeCl_3.7H_2O$) (at 200nm, 208nm, 222nm, 245nm, 298nm) in the UV region were observed (figure 5.4).

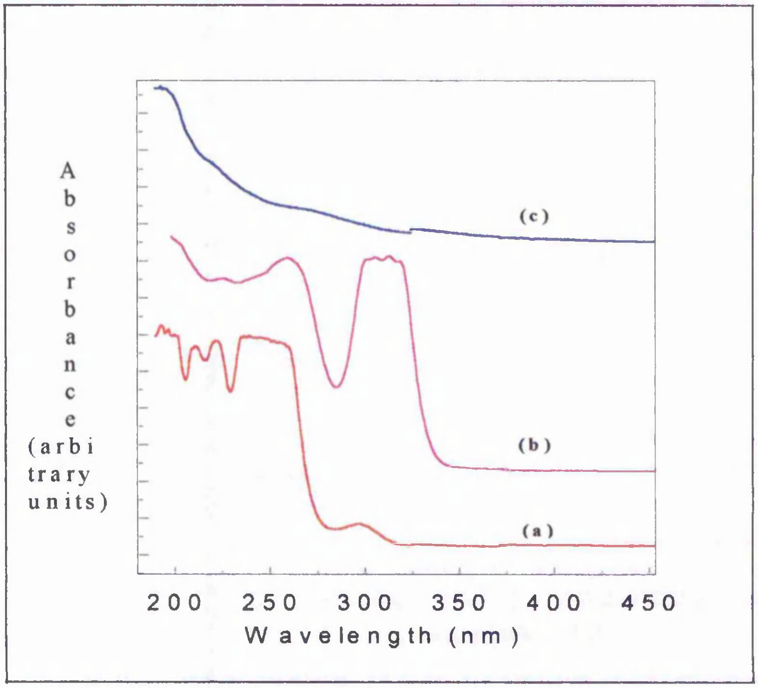

Figure 5.4: Ce^{3+} sol-gel (8.99wt%) prepared using 0.7M solution of $CeCl_3.7H_2O$, a) dried, b) after evacuation, c) after heating to 800°C

In comparison with Ce^{3+} in solution, the spectrum of Ce^{3+} in the sol-gel corresponded to the spectrum of Ce^{3+} in water regardless of the solvent in which the metal ion had been added to the sol-gel mixture, suggesting the presence of water in the first coordination sphere around the metal ion in the sol-gel glass.

After evacuation (figure 5.4b), a change in the bands characteristic of Ce^{3+} could be observed. A very low intensity band was detected at 242nm. A band was detected at 269nm and another one at 315.5nm. A shift of the bands toward higher wavelength was noticed.

Moreover when the sample was thermally treated, the signal arising from the presence of cerium(III) was no longer observable (figure 5.4c).

However, it was possible to use this metal ion as a dopant in the preparation of UV standards as even after dehydration a band was observable in the UV region.

The bands at 238nm and 252nm were used as standards as they can be observed at high concentrations (0.05M) and at low concentrations (0.005M) of the metal ion in the sol-gel whereas the bands at 200nm, 208nm cannot be observed at low concentration of the metal ion in solution (below 0.009M). The band at 223nm could also be used as measurement for the standards as it is observed at high and low concentrations of the metal ion in the sol-gel.

To be used as standards, the doped sol-gels needed to be prepared at a range of nominal absorbances: i.e.0.5, 1, 1.5, 2, 2.5.

Ce^{3+} solutions were prepared in ethanol and water. The variation of the intensity of the bands at 232nm and 248nm versus the concentration of the metal ion in solution was plotted

(Figure 5.5). The solution concentrations have been converted to weight% Ce^{3+} for comparison with the sol-gel doped glasses.

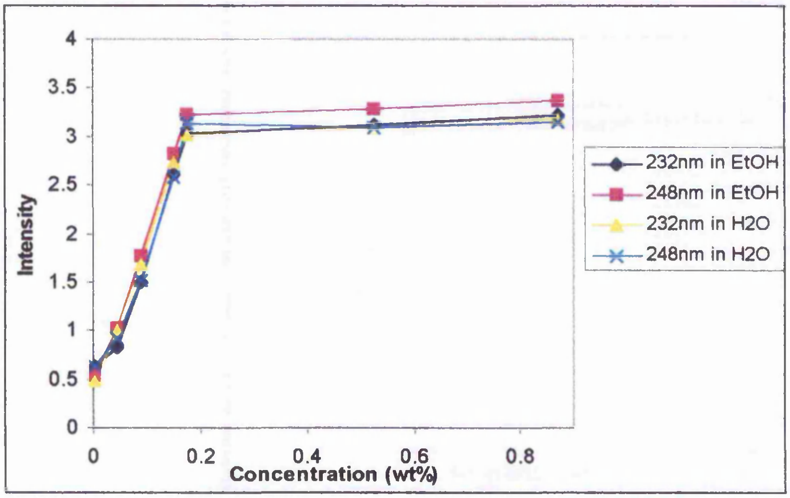

Figure 5.5: Variation of the intensity of the bands of Ce^{3+} solutions at various concentrations in ethanol and water solvents.

The intensity of the absorbance of the bands characteristic of Ce(III) increase with the concentration of the metal ion in solution. The type of solvent does slightly affect the absorbance of Ce(III). The intensity of the bands is slightly higher in the presence of ethanol in comparison to water.

The solvent has an effect on the environment of the metal ion and on the energy of the electronic transitions involved. The metal ion did not follow the Beer Lambert Law over the whole concentration range studied. At low concentrations (up to 0.01M) a linear behaviour was observed. At concentrations above 0.01M the increase of the absorbance is less obvious and a nearly constant behaviour is observed.

Using this variation of the intensity with the concentration of the metal ion in solution, Ce^{3+} doped sol-gels were prepared at a range of solution concentrations from 0.005M up to 0.05M.

As a decrease in the intensity of the bands characteristic of Ce^{3+} was noticed when the metal ion was in the sol-gel instead of being in solution, the values of the intensity at various concentrations were measured in the glass. These values were measured for the bands at 238nm and 252nm as they are observed even at low concentrations of the dopant (figure 5.6).

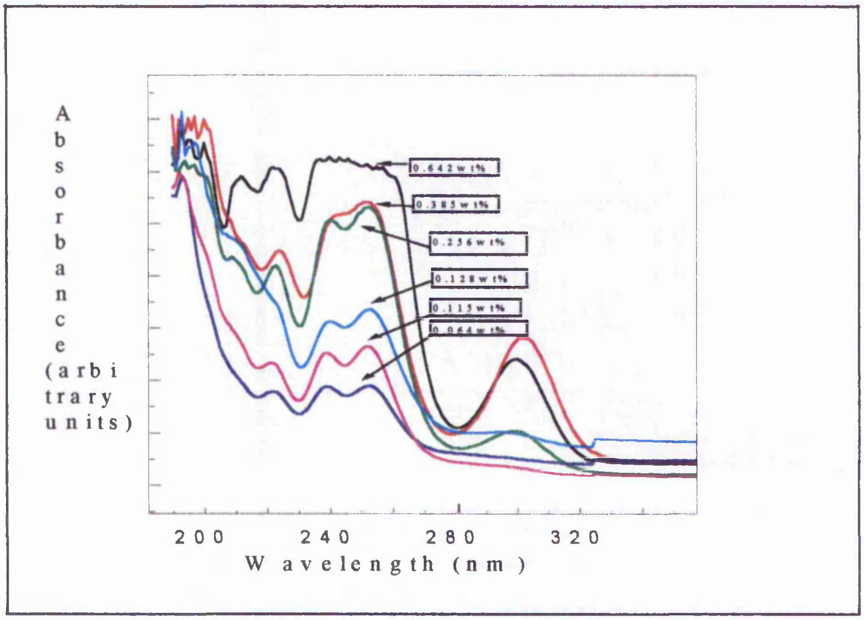

Figure 5.6: UV spectra of Ce^{3+} doped sol-gels prepared with various concentrations of the dopant in solution (0.05M=0.642wt%, 0.03M=0.385wt%, 0.02M=0.256wt%, 0.01M=0.128wt%, 0.009M=0.115wt%, 0.005M=0.064wt%)

By plotting the concentration of the metal ion in solution (converted to units of wt%) versus the intensity of the bands at 232nm and 248nm it was possible to determine which concentration of the metal ion in the initial solution give rise to absorbance at 0.5, 1, 1.5, 2 and 2.5 units in the sol-gel (figure 5.7) and hence to prepare the required UV standards.

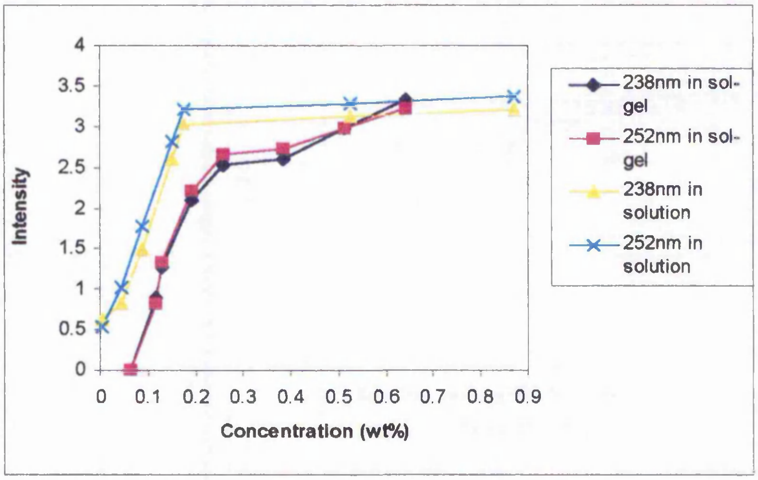

Figure 5.7: Variation of the intensity of the bands of Ce^{3+} in the sol-gel and in the solution versus the %weight of the metal ion in the sol-gel glass and in the solution.

In the sol-gel, the variation of the intensity of the bands versus the concentration of the metal ion was not linear. The metal ion did not appear to follow the Beer Lamber law. Two different types of behaviours were observed.

At low %weight (up to 0.256wt%), the variation of the intensity follows an approximately linear pattern but for higher %weight (from 0.256wt%), the linear pattern is no longer observable. Fortunately, the linear behaviour is observed for intensity of the absorbance up to 2.8A. So by using this graph it was possible to determine the %weight and hence the concentrations required of the metal ions to have a series of standards with increasing intensity.

A decrease in the intensity of the bands was noticed when the metal ion was in the sol-gel rather than in solution for a same %weight of the metal ion in the medium. The electronic transitions of Ce^{3+} are sensitive to its environment and consequently a change from a solution environment to a glass environment could lead to the decrease in intensity observed.

Moreover the bands characteristic of the metal ion could no longer be observable below

0.06wt% in the sol-gel whereas in the solution, it is only below 0.001wt% of the metal ion that the bands could no longer be detected.

Finally, the variation of the intensity with the %weight of the metal ion is very similar in solution and in the sol-gel. At low %weight (up to 025-0.3wt%) they followed an approximately linear increase.

By measuring the known absorbance of the bands at 238nm and 252nm for these samples, it is possible to prepare standards (Figure 5.8) and study the behaviour of the materials.

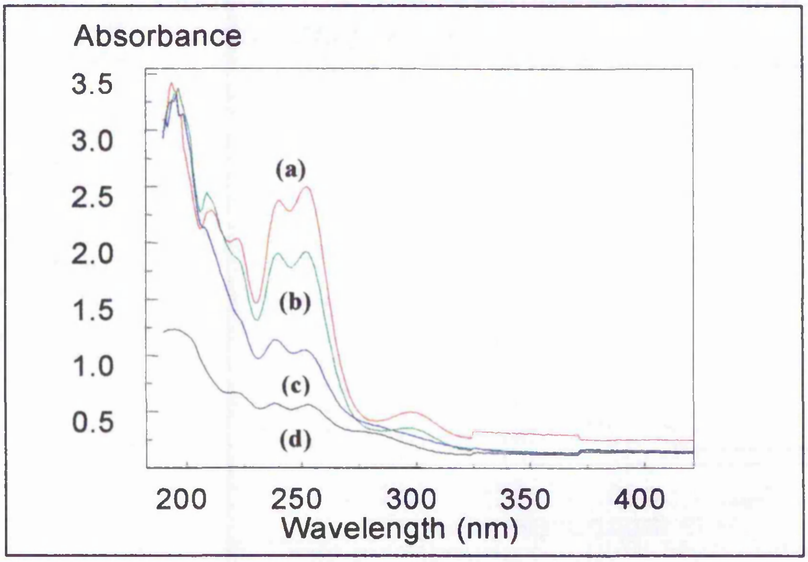

Figure 5.8: Series of standards with Ce^{3+} sol-gel a) 0.32wt%, b) 0.19wt%, c) 0.0924wt%, d) 0.0485wt%

Figure 5.9 shows the series of solid standards prepared for the UV region.

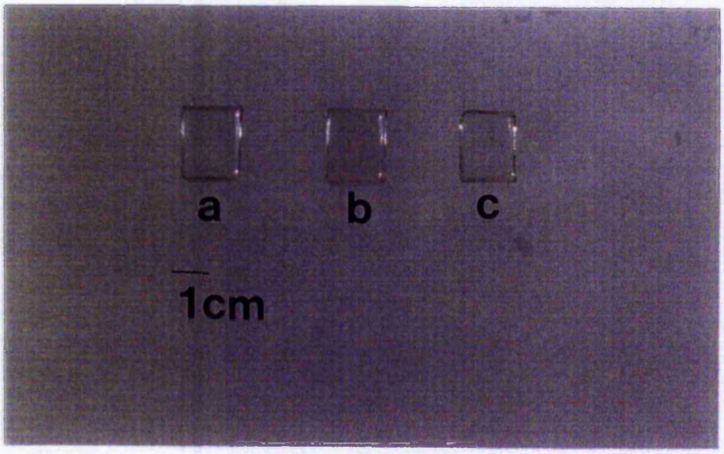

Figure 5.9: Ce^{3+} sol-gels a) 0.32wt%, b) 0.19wt%, c) 0.0924wt%

Following the success in the preparation of Ce^{3+} doped sol-gel materials having a spectroscopic signature in the UV region we attempted to prepare doped sol-gels with spectroscopic signatures in both the UV and Visible regions. From our previous studies (chapter 3, [6]) neodymium ions are suitable for use as a dopant in the preparation of optical standards in the visible region. It was, therefore decided to investigate if it was possible to incorporate metal ions which would give bands which could be used in both the UV and visible regions. For this reason solutions and sol-gel glasses containing both Ce^{3+} and Nd^{3+} were prepared. Several solutions were prepared containing $CeCl_3.7H_2O$ and $Nd(NO_3)_3.6H_2O$ at various concentrations in both water and ethanol. Figure 5.10 shows UV-VIS spectra from various solutions containing Ce^{3+} and Nd^{3+} metal ions with similar behaviour being observed in the two solvents.

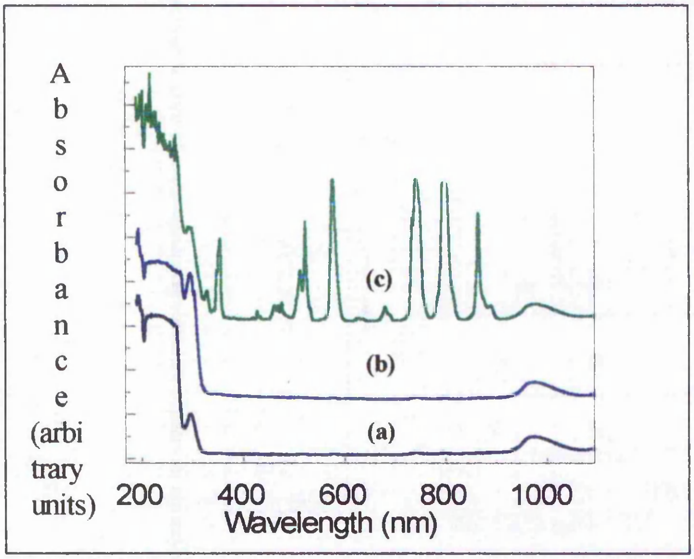

Figure 5.10: UV-VIS spectra of Ce^{3+} and Nd^{3+} ions in water a) Ce^{3+} 0.1M + Nd^{3+} 0.01M, b) Ce^{3+} 0.7M + Nd^{3+} 0.01M, c) Ce^{3+} 0.1M + Nd^{3+} 1M

In the UV region, the bands characteristic of Ce^{3+} were masked by the signal from Nd^{3+}, even at very low concentrations of Nd^{3+}. The only band observed for Ce^{3+} was at 290nm where changes in intensity and shape were noticed as the concentration of the Ce^{3+} ion was varied.

Instead of having distinct bands in the UV region, a broad and noisy band was observed (charge transfer between the ligands and the metal ions) and even at low concentrations of Nd^{3+} (0.01M), all the bands of the Ce^{3+} ion were not observable.

When mixed with Nd^{3+} ion, the presence of Ce^{3+} in the glass was still masked with only Nd^{3+} being detected in the glass (Figure 5.11).

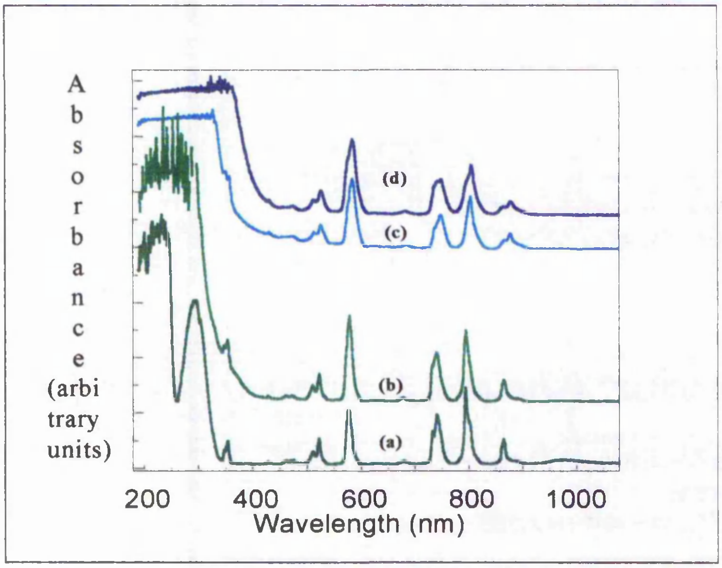

Figure 5.11: UV-VIS spectra of a) Nd^{3+} doped sol-gel using $Nd(NO_3)_3.6H_2O$,

(b-d) sol-gels prepared using $Nd(NO_3)_3.6H_2O$ (9.48wt%) + $CeCl_3.7H_2O$ (8.99wt%), b) dried, c) after evacuation, d) after heating to 800°C

When compared with the spectrum of Nd^{3+} only sol-gel [6], small differences in the shape of the bands was noticed, especially for the bands at 740nm and 800nm which correspond to electronic transitions very sensitive to the environment. No shift of the band was observed. When dehydrated and heated, the spectrum of Nd^{3+} in the Nd^{3+} /Ce^{3+} sol-gel was similar to that of Nd^{3+} only sol-gel. Consequently an interaction between the two metal ions occurs in the dried sol-gel which would explain the differences observed in the spectra. As stated previously, when evacuated and thermally treated, the coordination number of Ce(III) changed its environment as well (the bands characteristic of Ce(III) were no longer observable). It was suggested that after heating there is no further interaction between the two metal ions detectable using the methods employed in this study.

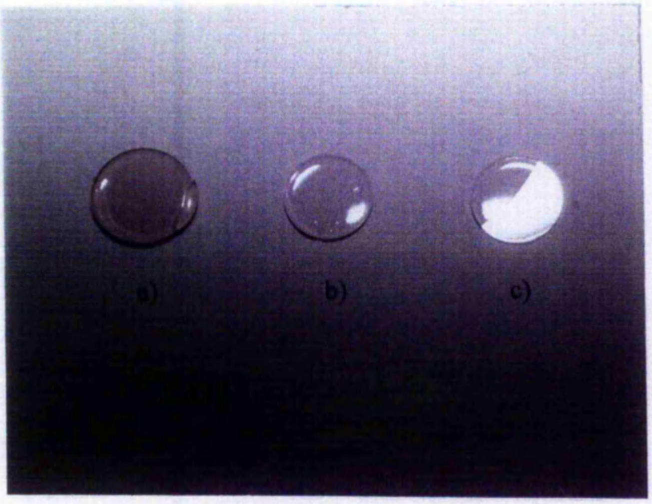

Figure 5.12: Sol-gels prepared using a) $Nd(NO_3)_3.6H_2O$ (9.48wt%) + $CeCl_3.7H_2O$ (8.99wt%), b) $Nd(NO_3)_3.6H_2O$ (0.948wt%) + $CeCl_3.7H_2O$ (1.28wt%), c) $Nd(NO_3)_3.6H_2O$ (0.0948wt%) + $CeCl_3.7H_2O$ (0.128wt%)

5.3.2.2- Discussion

The electronic spectrum of Ce(III) consists of a single transition between $^2F_{5/2}$ (ground state) and $^2F_{7/2}$ [7]. This transition could in principal be observed in the infrared region (5000nm) but is hidden by vibrational bands occurring in this region. The broad bands observed in the UV region are due to $4f^n \rightarrow 4f^{n-1}$ transitions [8].

The five bands observed correspond to the five Kramers doublets of ^2D ($5d^1$) [9].

In solution, the electronic transitions of the metal ion are influenced by the environment around the metal ion as a shift of the bands is observed in the presence of different solvents and in the presence of different anions in the second coordination sphere (Figure 5.3).

In the sol-gel, the bands characteristic of Ce^{3+} are shifted toward higher wavelengths by ca.5nm. From solution to sol-gel, the environment around the metal ion has changed. Due to the removal of water, the ligand field around the metal ion is weaker explaining the shift observed. During evacuation, the remaining water and the solvent contained in the pores of the sol-gel are removed. Once again the environment around the metal ion changes. The cerium ion could be bonded to some water ligands in its outer sphere which are eliminated during the evacuation thereby explaining the transformation in the UV spectrum. The energy of the transitions are very sensitive to the environment around the metal ion which in turn influences the 4f and 5d electronic configuration [10]. After evacuation no signal from Ce^{3+} is observed suggesting a transformation of Ce(III) into Ce(IV) which does not show a band in the UV region [11]. As the sample is heated up in air, oxidation of the metal ion could occur. Another possibility is that Ce(III) remains in the pores. Consequently during heat treatment up to 800°C, the silanol groups start to condense in the sol-gel matrix, Ce(III) bonds with the silica, changing its oxidation state becoming cerium(IV).

The coordination number for Nd^{3+} in the materials prepared with Ce^{3+} and Nd^{3+} is the same as for the materials prepared with Nd^{3+} alone. The environment sensitive bands of Nd^{3+} show small changes in their intensity in the presence of Ce^{3+} in the sol-gel glass. The intensity of the electronic transitions is not similar to Nd^{3+} sol-gel and then decrease of some shoulders of the bands most sensitive to the environment are observed. In the sol-gel with Nd^{3+} and Ce^{3+}, the environment around Nd^{3+} ions is different from the Nd^{3+} only sol-gels, due to the presence of Ce^{3+}. The strength of the ligand field around the metal ion is different due to the presence of the other metal ion and its ligands changing the energy of the electronic transitions of Nd^{3+} and consequently the bands which correspond to the electronic transitions most sensitive to the environment are affected. There is a possibility of interaction between the two metal ions which does not allow the electronic transitions of the cerium ions to be observed.

From the data presented it is apparent that the metal ions interact with the gel network as it is formed, ages and dries. Due to the interaction between Nd^{3+} and Ce^{3+} ions in the sol-gel system, it is not possible at present to prepare a combined rare earth doped standard for use in the visible and UV region using sol-gel technology. It is possible that another system with different metal ions might have the necessary characteristics for such an optical standard.

Finally, to fulfil the requirements for the preparation of a series of standards, it is necessary to have the prepared materials stable with time with no changes in the absorbance of the metal ion. For that, stability studies on the samples were carried out.

5.5.3- Initial Stability Studies

In order to obtain samples which are stable with time, it was thought necessary to reduce the porosity of the glasses. Consequently the glass samples were immersed, after evacuation, in a solution containing hydrolysed TEOS.

UV-VIS spectra of the samples were collected in order to see the effect of the second gel treatment on the glasses.

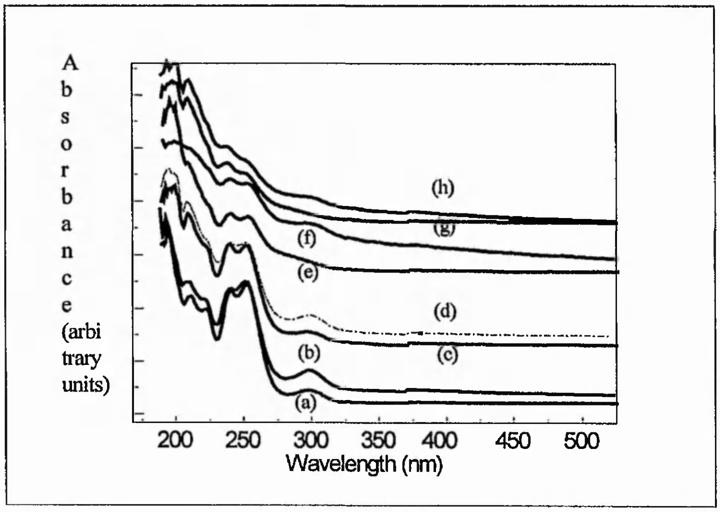

Figure 5.13: Effect of the second gel treatment on the UV-VIS spectra of Ce^{3+} sol-gel at various %weight of the metal ion in the glass; Spectra before treatment a) 0.321wt%, c) 0.193wt%, e) 0.0924wt%, g) 0.00485wt%; Spectra after treatment b) 0.321wt%,d) 0.0193wt%, f) 0.0924wt%, h) 0.00485wt%

After the treatment, the samples had lost some of their transparency (increase of absorbance) as some hydrolysed TEOS was on the surface of the glass.

The spectrum of the Ce^{3+} metal ion did not appear to be affected by this doping as bands characteristic of the metal ion were observable after treatment. Due to the loss of transparency of the material, a change in intensity of the bands was noticed.

So this method of porosity reduction was not perfect as the optical quality of the material was damaged. The polymer by being doped in the matrix stayed in the pores and hence reduced the optical quality of the material.

However, in order to know if the doping of the sol-gel matrix with a polymer is in principal a valid method, the stability of the material with time after UV irradiation and cold treatment in comparison with samples not doped with TEOS was investigated.

5.5.3.1- UV radiation

UV radiation was applied to the sol-gel samples as a method of fast aging.

Normal sol-gels and Ce(III) doped sol-gels were put under UV radiation for 4 months in order to study their stability when UV irradiated.

Two sets of samples were analysed. The samples which had been immersed in hydrolysed TEOS and the untreated samples.

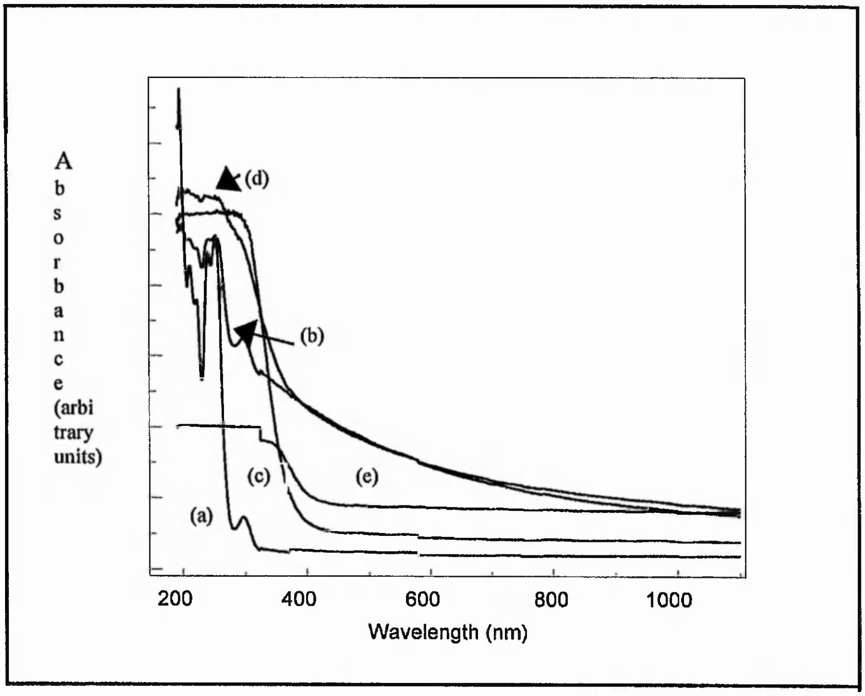

Figure 5.14: Effect of the UV radiation on the UV-VIS spectra of Ce^{3+} sol-gel glass (0.32wt%); a) untreated before radiation; b-c after 2 months of radiation b) pretreated with TEOS, c) untreated; d-e after 4 months of radiation d) pretreated with TEOS, e) untreated

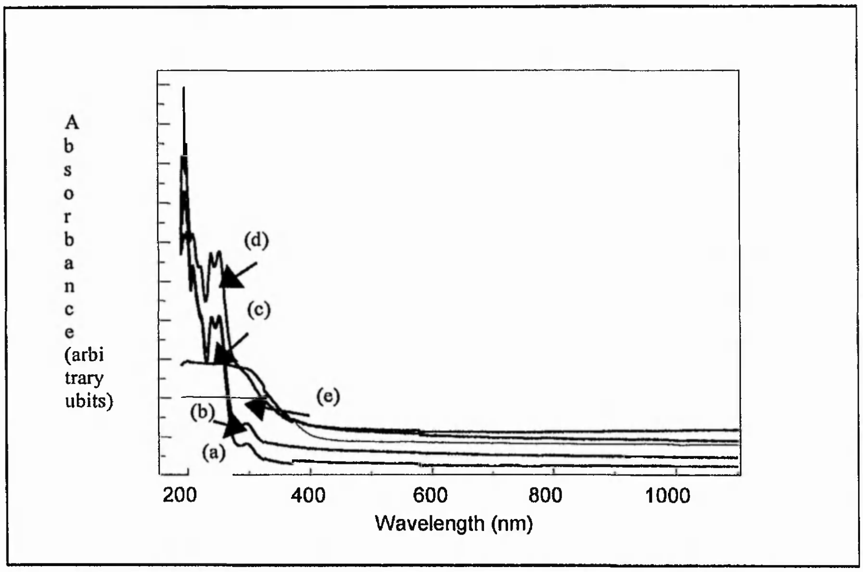

Figure 5.15: Effect of the UV radiation on the UV-VIS spectra of Ce^{3+} sol-gel glass (0.192wt%); a) untreated before radiation; b-c after 2 months of radiation b) pretreated with TEOS, c) untreated; d-e after 4 months of radiation d) pretreated with TEOS, e) untreated

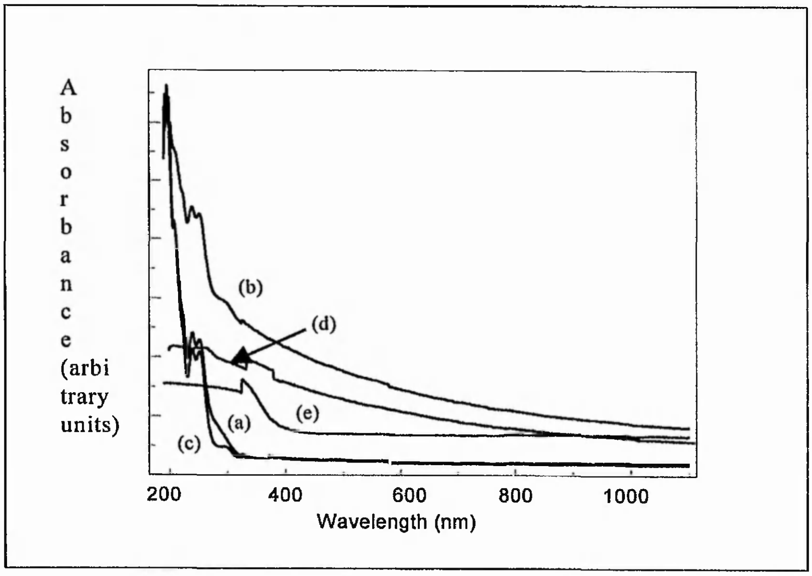

Figure 5.16: Effect of the UV radiation on the UV-VIS spectra of Ce^{3+} sol-gel glass (0.0924wt%); a) untreated before radiation; b-c after 2 months of radiation b) pretreated with TEOS, c) untreated; d-e after 4 months of radiation d) pretreated with TEOS, e) untreated

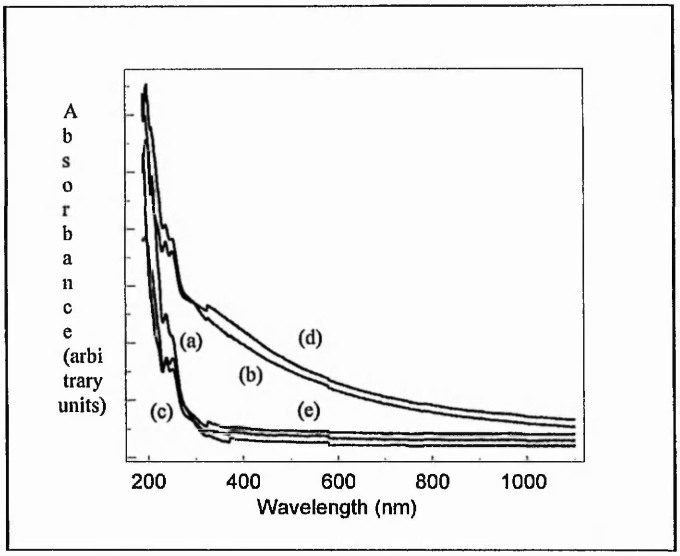

Figure 5.17: Effect of the UV radiation on the UV-VIS spectra of Ce^{3+} sol-gel glass (0.0485wt%); a) untreated before radiation; b-c after 2 months of radiation b) pretreated with TEOS, c) untreated; d-e after 4 months of radiation d) pretreated with TEOS, e) untreated

When irradiated the samples did not resist very well irrespective of the concentration of metal ion in the glass. An increase of the absorbance was noticed as the samples were progressively irradiated. Moreover some of the samples crazed and cracked under UV radiation.

The increase in the absorbance was probably due to internal cracks which could not be observed by the naked eye.

The filling of the pores with TEOS did not prevent the samples from cracking and being damaged by UV radiation.

So to use this material as solid standard it would be necessary to find another way of protecting the samples from UV radiation.

5.5.3.2- Cold treatment

Cold treatment was performed on the samples in order to study their aging under extreme conditions.

The samples treated with TEOS and the untreated samples were put in a freezer at -18°C and their UV-VIS spectrum measured each week for a period of 4 months.

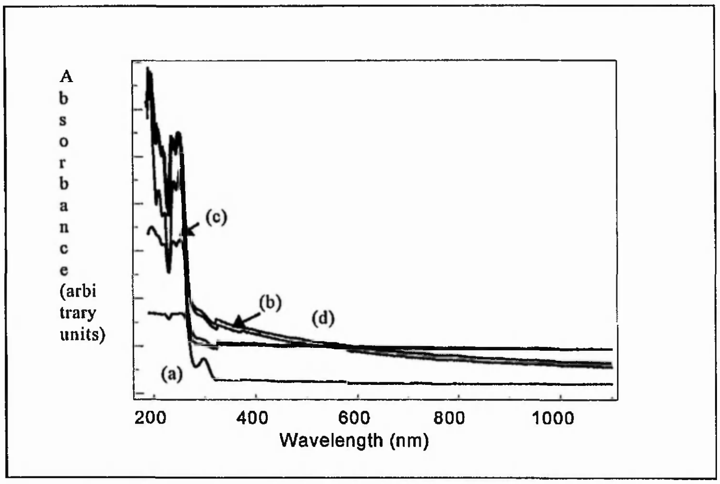

Figure 5.18: Effect of the low temperature on the UV-VIS spectra of Ce^{3+} sol-gel glass (0.32wt%); a) untreated before radiation; b-c after 2 months of radiation b) pretreated with TEOS, c) untreated; d-e after 4 months of radiation d) pretreated with TEOS, e) untreated

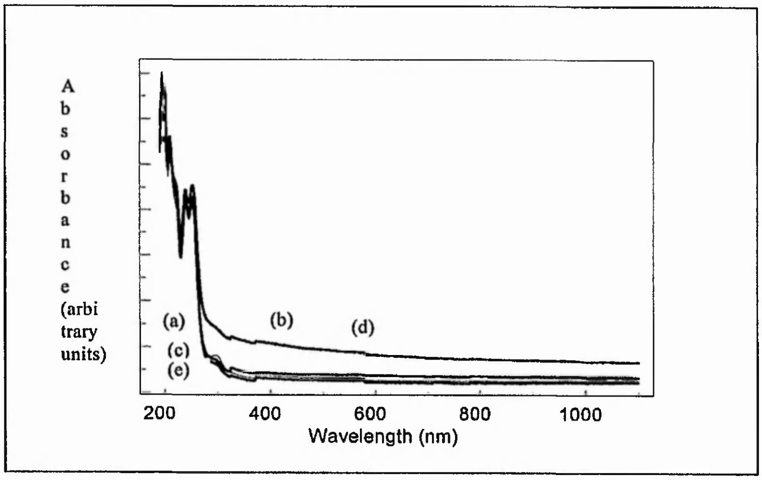

Figure 5.19: Effect of the low temperature on the UV-VIS spectra of Ce^{3+} sol-gel glass (0.19wt%); a) untreated before radiation; b-c after 2 months of radiation b) pretreated with TEOS, c) untreated; d-e after 4 months of radiation d) pretreated with TEOS, e) untreated

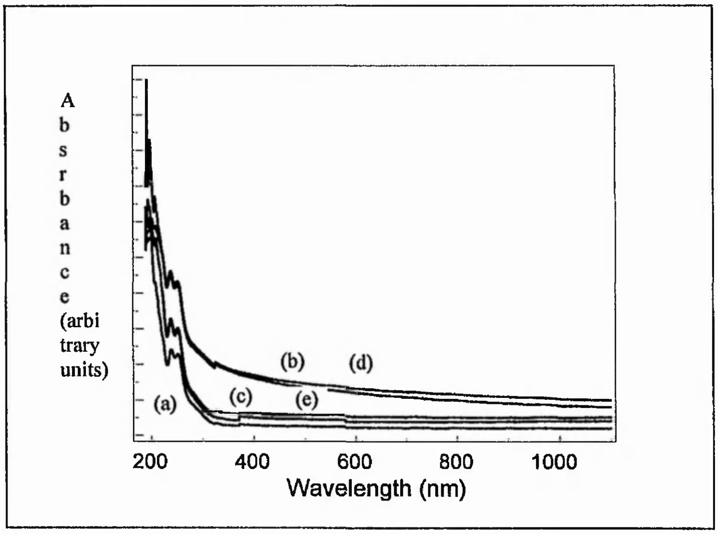

Figure 5.20: Effect of the low temperature on the UV-VIS spectra of Ce^{3+} sol-gel glass (0.0924wt%); a) untreated before radiation; b-c after 2 months of radiation b) pretreated with TEOS, c) untreated; d-e after 4 months of radiation d) pretreated with TEOS, e) untreated

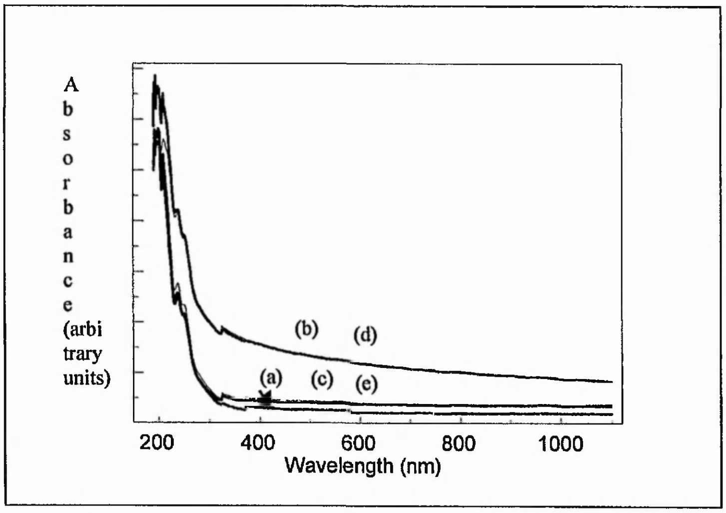

Figure 5.21: Effect of the low temperature on the UV-VIS spectra of Ce^{3+} sol-gel glass (0.0485wt%); a) untreated before radiation; b-c after 2 months of radiation b) pretreated with TEOS, c) untreated; d-e after 4 months of radiation d) pretreated with TEOS, e) untreated

For the samples untreated (c & e), a very small increase (2%) of the absorbance was noticed. The samples resisted very well at cold temperatures.

For the samples treated with TEOS (b & d), no change in absorbance was noticed.

The cold had no effect on the samples.

Consequently when the samples were untreated with addition of TEOS they were able to absorb a small quantity of moisture coming from the freezer which could explain the increase in absorbance measured.

When the samples had been treated, the pores were filled with hydrolysed TEOS and then no moisture was absorbed. No increase in absorbance was noticed.

5.5.3.3- Bench stability

The treated and non treated samples were left on the bench for 4 months in order to see how the samples behaved with time, changes in temperature, pressure.

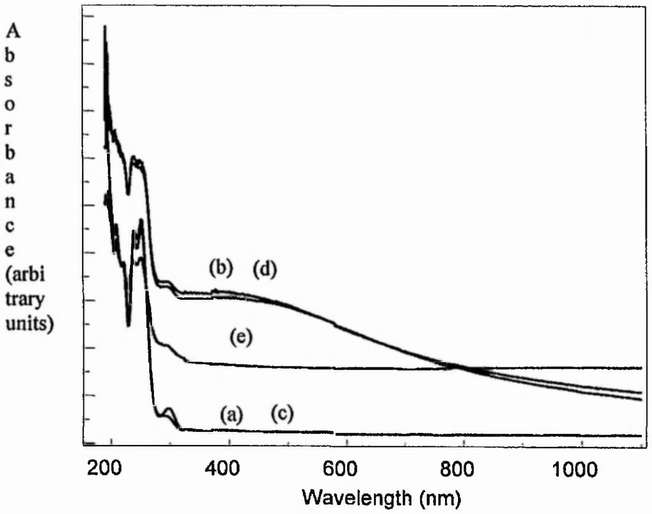

Figure 5.22: Effect of aging at RT on the UV-VIS spectra of Ce^{3+} sol-gel glass (0.32wt%); a) untreated before radiation; b-c after 2 months of radiation b) pretreated with TEOS, c) untreated; d-e after 4 months of radiation d) pretreated with TEOS, e) untreated

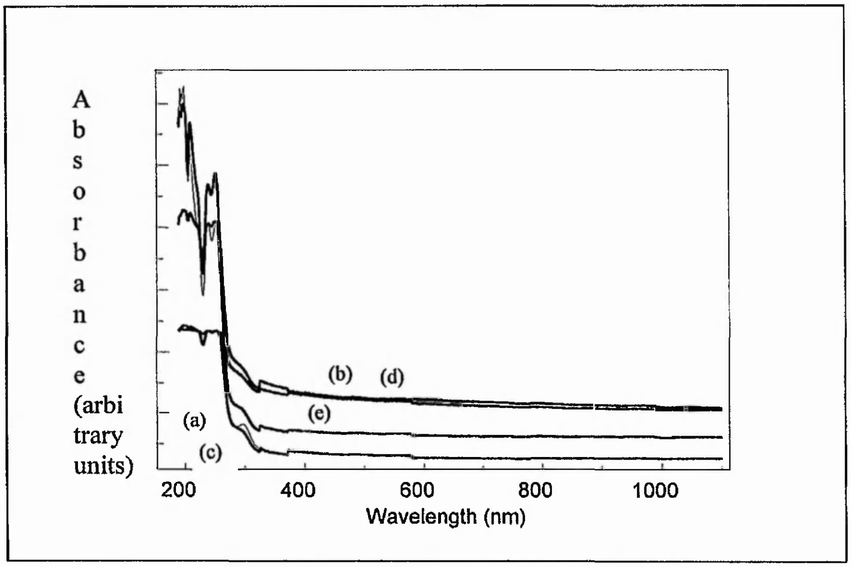

Figure 5.23: Effect of aging at RT on the UV-VIS spectra of Ce^{3+} sol-gel glass (0.19wt%); a) untreated before radiation; b-c after 2 months of radiation b) pretreated with TEOS, c) untreated; d-e after 4 months of radiation d) pretreated with TEOS, e) untreated

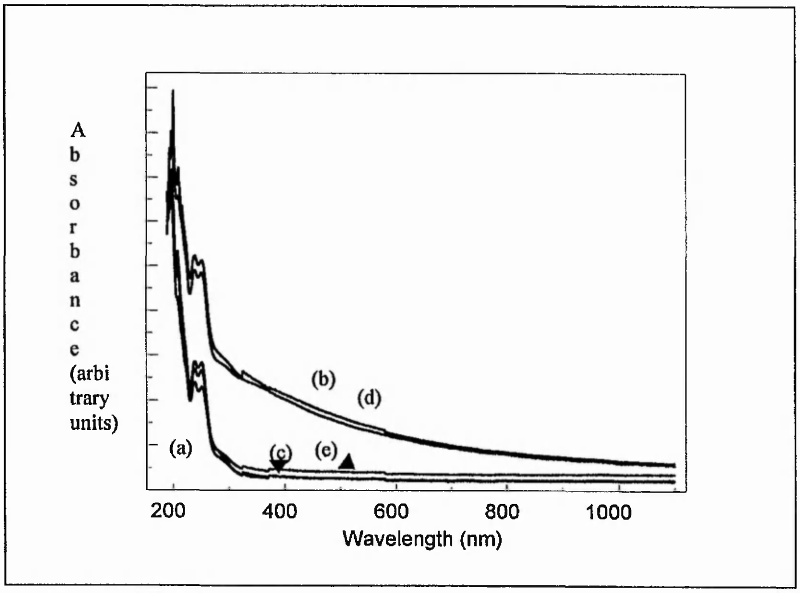

Figure 5.24: Effect of aging at RT on the UV-VIS spectra of Ce^{3+} sol-gel glass (0.0925wt%); a) untreated before radiation; b-c after 2 months of radiation b) pretreated with TEOS, c) untreated; d-e after 4 months of radiation d) pretreated with TEOS, e) untreated

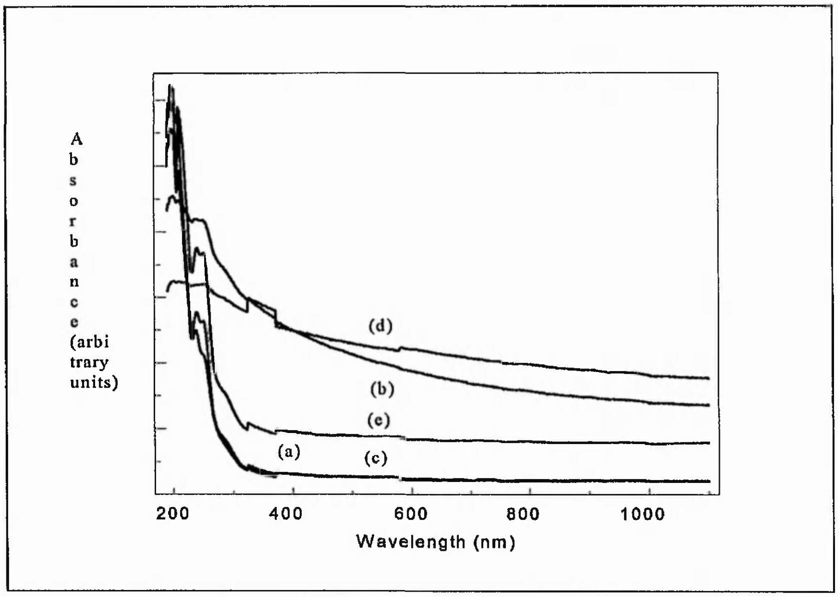

Figure 5.25: Effect of aging at RT on the UV-VIS spectra of Ce^{3+} sol-gel glass (0.0485wt%); a) untreated before radiation; b-c after 2 months of radiation b) pretreated with TEOS, c) untreated; d-e after 4 months of radiation d) pretreated with TEOS, e) untreated

In general, the samples did not show any changes in their absorbance for the first two months (samples b & c). Then for the non treated samples (samples e), a large increase of the absorbance was noticed regardless of the concentration of the metal ion in the sol-gel solution.

After 4 months, the increase was relatively important (20%) which was mainly due to the absorption of moisture from the air. At that time, the humidity in the air was relatively high compared with the previous months.

However, the samples treated with TEOS (samples b & d) showed only a very small increase of the absorbance after two months. These samples did not absorb moisture as much as the untreated samples, the pores and the surface of the materials being protected by the hydrolysed TEOS, and consequently the sol-gel glasses were more stable with time.

5.4- Conclusions & Future work

From this study the preparation of absorbance solid standards in the UV region was possible using Ce^{3+} metal ions doped in silica sol-gel glasses.

The energy of the transitions of the metal ion was very sensitive to its environment. Changes in the oxidation number of Ce^{3+} was observed when Ce^{3+} sol-gel glasses were evacuated and thermally treated. This effect of evacuation and thermal treatment on the metal ion in the glass was observed for all the samples regardless of the concentration of the metal ion.

The preparation of combined UV-VIS solid standards using Ce^{3+} and Nd^{3+} metal ions was not successful possibly due to molecular interactions between the two metals.

The absorbance solid standards needed to be stable with time. The sol-gel glasses were porous. To prevent the absorption of moisture from the air, even at low porosity, the sol-gel glasses must be protected.

Heat treatments during which the pores collapsed, were not possible as the Ce^{3+} ion is affected and consequently the glass cannot be any longer used as solid standard.

Another method was proposed which consist of filling the pores and surround the material with a polymer, in this case TEOS, and hence protect the material from any moisture. Unfortunately the filling of the pores involved a certain loss of transparency of the samples.

Moreover the treated samples were not very resistant to UV radiation (a model for accelerated aging), even if they did not absorb moisture with time or in the freezer.

A different method for treating the sample is necessary in order to obtain complete stable samples regardless of the treatment the glass has been subjected to.

In the future, the pores of the samples could be doped with another type of polymer which would not affect the transparency of the material and which would increase the hardness of the material, hence improving the resistance of the material to UV radiation.

References

[1] R.N.Rand, Clinical Chemistry, **5**, 9, (1969)

[2] G.Milazzo, S.Caroli, M.Palumbo-Doretti, N.Violante, Anal.Chem., **49**, 6, 711, (1977)

[3] D.Irish, *Standards in Absorption Spectrometry*, (publishers Chapman and Hall, London),1, (1981)

[4] Am.Nat.Bur.Standards (US), Circ. 552, 24, (1957)

[5] J.A.Dobrowolski, G.E.Marsh, Appl.Opt., 11, 594, (1990)

[6] K.S.Gibson, NBS Circular, 484, (1949)

[7] K.S.Gibson, M.M.Balcom, J.Res.Nat.Bur.Std., **38**, 601, (1947)

[8] T.Moeller, J.C.Brantley, Anal.Chem., **22**, 3, 433, (1950)

[9] C.C.Perry, S.Aubonnet, J.Sol-Gel Science and Technol., **13**, 593, (1998)

[10] S.F.Kettel, *Physical Inorganic Chemistry, A Coordination Chemistry Approach*, (publisher Oxford University Press), (1998)

[11] S.Cotton, *Lanthanides & Actinides*, (publishers Macmilland Education, London), (1991)

[12] K.Okada, Y.Kaizu, H.Kobayashi, J.Chem.Phys., **75**(3), 1577, (1981)

[13] A.A.Boiko, E.N.Poddenezhny, J.legendziewicz, J.Sokolnicki, E.Lukowiak, W.Strek, J.Applied Spectroscopy, **62**(4),18, (1995)

[14] A.Patra, D.Kundu, D.Ganguli, J.Sol-Gel Science and Technol., **9**, 65, (1997)

Chapter 6: 1^{st} Row transition metals as dopants in the visible region

6.1- Introduction

In this chapter, the preparation of solid standards in the visible region is proposed using transition metal ions (from Ti to Cu) as dopants.

The doping of sol-gel glasses with transition elements for electronic applications [1], magnetic devices [2], chemical active filters [3] and optical purposes [4] has been carried out. No attempt to prepare solid standards in the visible region using the sol-gel process has been found in the literature.

Cobalt has been extensively used as a dopant in sol-gel matrices with materials prepared by post doping [4,5] and pre-doping [1,2]. The surface interaction between the metal ion and the silica matrix has been studied as well as the coordination chemistry of the metal dopant.

Other transition elements of the first row have been used as dopants in the sol-gel process. In particular, Cu(II) has been used together with Ni(II) and Co(II) to study the effect of doping on the microscopic properties of the glass [2,3]. The coordination chemistry of Ni^{2+} in fluoride glasses has also been studied by optical absorption spectroscopy and EXAFS analysis [6].

Moreover codoping studies of $As_{12}Ge_{33}Se_{55}$ glass with transition elements (Fe, Cu, Mn, Cr) has been carried out to identify the effect of the impurities introduced during the glass preparation [7]. Transition metal alkoxides, such as titanium alkoxide, have also been used in sol-gel glasses as precursors [8].

In our work, the effect of local environment on the metal ions was studied by comparison of visible spectra and by calculation of the ligand field strength and covalency effects. Metal ions in solution (with different solvents), in the sol-gel glass prior to and after treatment were investigated. Finally, a transition element to be used as standard was proposed.

To study the effect of the metal ion environment on the d-d electronic transitions, Orgel diagrams [9] and Tanabe-Sugano diagrams [10] were used. From these diagrams, the ligand field strength Δ_o and/or the Racah inter-electron repulsion parameter B were calculated. The key idea of the crystal field theory and the ligand field theory is that the 5-

fold degeneracy of the metal d orbitals is lifted when a metal atom is surrounded by a set of negative charges or the negative end of dipoles. The pattern of energies produced depends on the symmetry of the arrangement of ligands. In weak field, the ligand field strength is smaller than the free ion energy group. In strong field, the opposite is observed. The effect of the field on the metal d-electron is much more important than the inner electron repulsion. The ligand field strength is classified, for certain ligands, ins spectrochemical series. For a 3d metal divalent ion, the ligands at the low end series gives a Δ_0 less than 10000cm^{-1} and the ligands at the high end gives a value higher than 25000cm^{-1}. The constant B is a direct result of covalency between the metal and the ligands within the complex. In an octahedral complex, the e_g electrons become σ antibonding and the t_{2g} electrons may be involved in π-bonding. The electrons are no longer pure metal electrons but are delocalised on to the ligands. This delocalisation increases the average separation between the various d electrons and reduces the value of B. The greater the reduction in the value of B, the greater the covalency of the metal ligand bond.

The preparation of solid standards for use in the visible region requires the presence of bands in this region coming from the transition metal ion doped in a sol-gel silica matrix. Scandium and zinc were eliminated as they do not show bands in the visible spectrum. The manganese ion required a highly concentrated solution (3mol/l) to show a very low intensity band in the visible region. Due to its high insolubility, this ion was not suitable for the preparation of standards.

Titanium isopropoxide was insoluble in water and ethanol, the solubility of titanium ethoxide was too low to use the metal ion as a potential standard and additionally, the alkoxide reacts with water.

Iron (III) in solution is yellow with a UV-VIS spectrum having only one broad and noisy band in the UV region which corresponds to a charge transfer transition between the metal and ligand. This electronic transition has strong low energy wings in the visible region that obscure the weak spin forbidden d-d electronic transitions [11,12]. The colour of the solution is due to an hydroxo species bonded to the metal ion [13].

Once in the sol-gel the yellow colour was still observed. However, because of the presence of the charge transfer band in the UV region, it was not suitable for the preparation of a solid standard.

In consequence for our study vanadium, chromium, cobalt, nickel and copper ions were used.

6.2- Methods & Techniques

6.2.1-Solution preparation

The chemical formulae of the transition element salts used were:$VOSO_4.3H_2O$, $(CH_3CO_2)_7Cr_3(OH)_2$, $Co(NO_3)_2.6H_2O$, $Ni(NO_3)_2.6H_2O$, $Cu(NO_3)_2.6H_2O$. The complexes were purchased from Aldrich.

($(CH_3CO_2)_7Cr_3(OH)_2$) was used due to the high insolubility of the other Cr^{3+} complexes ($Cr(NO_3)_3.9H_2O$ for example, 0.001M in water). Water and ethanol were used as solvents. To obtain solutions with a concentration of the salt high enough to show bands in the visible region when present in the sol-gel matrix, the concentration of the solutions used varied from one transition element to the other.

6.2.2-Sol-gel preparation

Using the sol-gel process, silica monoliths were prepared. Non-doped and doped silica gel glasses were made. Tetraethylorthosilicate 98% (Aldrich) was mixed with dry ethanol (distilled from 95% ethanol over magnesium) and stirred gently for few seconds to obtain homogeneous solution. Then, if necessary, the dopant was mixed with TEOS and dry ethanol. Finally, 0.5M HCl (prepared from HCl 11.3M Fisher) was added in the following molar ratio:

For normal sol-gels: 1TEOS: 4EtOH: $4H_2O$: 0.045HCl

For doped sol-gels: the molar ratio was the same as above with the dopant either in the aqueous or ethanolic phase.

Transition elements were used as the dopant at various concentrations of the metal ion in solution (V(IV) $1M-10^{-1}M-10^{-2}M$, Cr(III) $10^{-1}M-10^{-2}M$, Co(II) $1M-10^{-1}M-10^{-2}M$, Ni(II) $10^{-1}M-10^{-2}M$, Cu(II) $1M-10^{-1}M-10^{-2}M$).

The concentration of the dopant when mixed with the precursors in the sol-gel solution was calculated. The %weight of dopant in the glass was calculated using an average weight of the dry sol-gel and the number of moles of metal ions used to prepare the glass.

Table 6.1:Transition elements concentrations in solution and in the glass.

Transition elements	**Concentration in solution (mol/l)**	**Concentration in the glass (%wt)**
V(IV)	1	4.66
	10^{-1}	0.466
	10^{-2}	0.0466
Cr(III)	10^{-1}	0.475
	10^{-2}	0.0475
Co(II)	1	5.39
	10^{-1}	0.539
	10^{-2}	0.0539
Ni(II)	10-1	0.537
	10^{-2}	0.0537
Cu(II)	1	5.81
	10^{-1}	0.581
	10^{-2}	0.0581

The resulting sol-gel dopant solution was mixed at room temperature for one hour before being put (4ml) in petri dishes (diameter 3.5cm, depth 1cm from Nunc) covered with Nesco film® in which 5 holes (0.6mm diameter) had been made before being placed in a fan assisted oven at 40°C to dry.

The samples, when dry (the weight of the sol-gel glass became stable), were dehydrated by subjecting the samples to a vacuum pressure of 6mbar (measured by an Edwards Pirani 10 pressure sensor) for 18 hours. Samples were also heated up (with a ramp temperature of 0.1°C/min) and held for 4 hours at 800°C. The samples were cooled down at a ramp temperature of 5°C/min, the whole thermal treatment taking 36 hours. A Carbolite programmable tube furnace was used for the thermal treatment.

6.2.3-Spectral Analysis

Solutions and sol-gels (as prepared, dehydrated and thermally heated) were analysed using a UNICAM UV2 UV-VIS spectrometer between 190nm and 1100nm at a scan speed of 1200nm/min and a data interval of 1nm.

6.3- Results & Discussion

A blank sample (undoped sol-gel) was used to observe the optical changes in the matrix when the sample was evacuated and thermally treated.

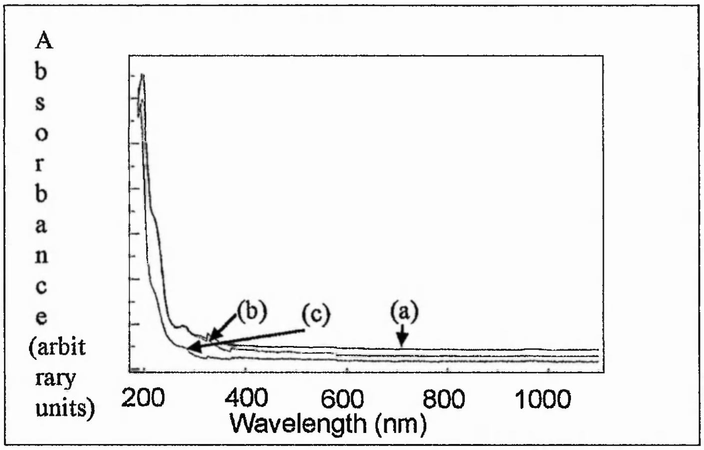

Figure 6.1: Normal sol-gel a) dried, b) evacuated, c) heated at 800°C

The spectrum of the normal sol-gel was not affected by the physical changes caused by evacuation or thermal treatment in the visible region. The only change observed was a small decrease in the absorbance when the sample was heated. The improvement in the optical quality of the sample was due to the removal of H_2O and -OH groups from the silica matrix. Consequently the changes that were observed for doped sol-gels were only due to the presence of the dopants.

6.3.1-Vanadium (IV): Results & Interpretation

Solutions of vanadium (IV) were recorded by UV-VIS spectroscopy.

The solution of vanadium (IV) 1M is not shown as the spectrum exhibited one very broad and noisy band from 500nm to 1000nm.

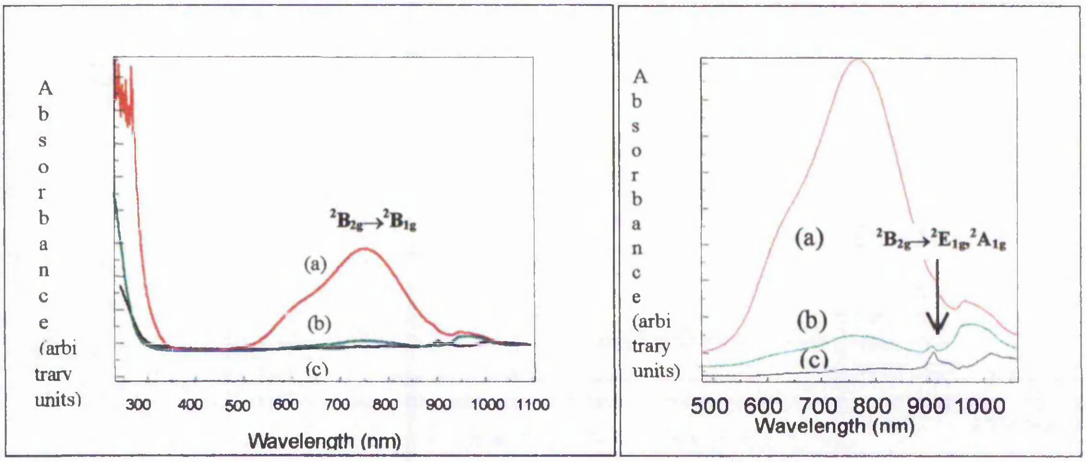

Figure 6.2: UV-VIS spectrum of Vanadium (IV) solution a) 10^{-1}M in water, b) 10^{-2}M in water, c) 10^{-2}M in ethanol

The metal ion in solution had a blue colour which decreased in intensity as the concentration of the metal ion decreased. At 10^{-1}M, an intense band was observed at 764nm with shoulders at 650nm and at 907nm. The intensity of the main band decreased with the concentration of the metal ion and the shoulders were not observable. The vanadium (IV) ion was not soluble in ethanol above 10^{-2}M with its spectrum showing a very low intensity band at 907nm.

Figures 6.3, 6.4 show respectively the color changes of vanadium (IV) ion in the sol-gels as prepared after heat treatment at various concentrations and prepared with different solvents.

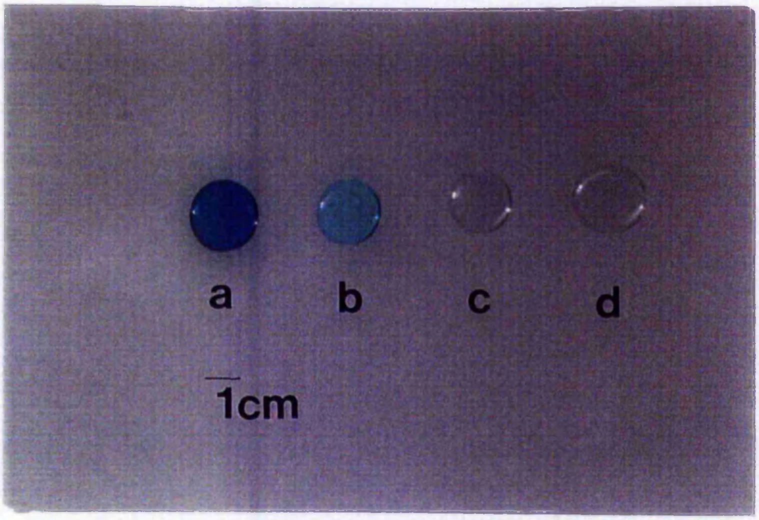

Figure 6.3: Sol-gel glasses doped with vanadium(IV) prepared in water solution a) 4.66wt%, b) 0.466wt%, c) 0.0466wt% ; prepared in ethanol solution d) 0.0466wt%

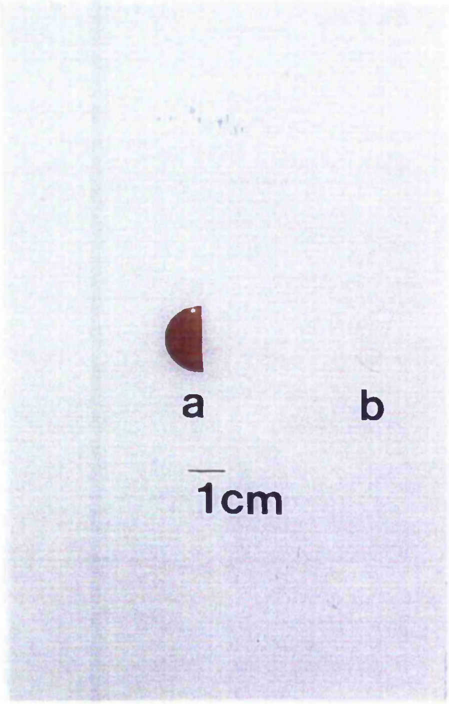

Figure 6.4: Sol-gel glasses heat treated to 800°C doped with vanadium(IV) prepared in water solution a) 4.66wt%, b) 0.466wt%

Changes in the spectrum of vanadium (IV) ion were observed when the metal ion was doped into the sol-gel and when the sol-gel was evacuated and thermally treated.

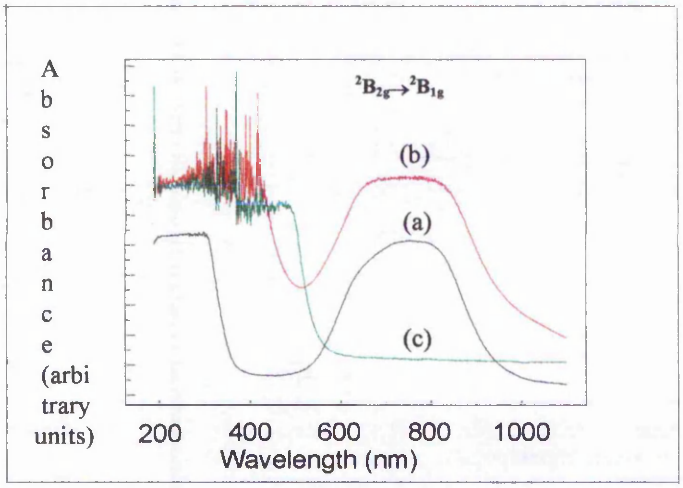

Figure 6.5: UV-VIS of vanadium (IV) (4.6wt%) sol-gel
a) dried, b) evacuated, c) heated

In the sol-gel matrix, the vanadium metal ion showed a broad band between 600 and 900nm. After evacuation, the intensity of the band decreased. The band was no longer observable after heat treatment.

A move of the cut off towards the visible was observed, from 300nm in the sol-gel to 500nm after evacuation and then to 580nm after heat treatment.

The following table (Table 6.2) summarises the effect on the metal ion observed when the metal ion was doped in the glass and when this glass had been evacuated and thermally treated.

Concentration in solution (mol/l)	**Solvent**	**Solution (nm)**	**Concentration in sol-gel (%wt)**	**Sol-gel dried (nm)**	**Sol-gel evacuated (nm)**	**Sol-gel heated (nm)**
1M	H_2O	550-1000 max 749	4.66	550-1000 max 749	broad 665-812	no peak observable
		deep blue		deep blue	dark green	orange
10^{-1}M		650s, 764 908s, 962	0.466	763	698	no peak observable
		blue		light blue	colorless	colorless
10^{-2}M		764 908s, 967	0.0466	no peak observable	no peak observable	no peak observable
		pale blue		colorless-blue glint	colorless	colorless
10^{-2}M	EtOH	907	0.0466	no peak observable	no peak observable	no peak observable
		pale blue		colorless	colorless	colorless

s=shoulder

Table 6.2: Bands of UV-VIS spectra of vanadium (IV) metal ion and its color changes in solution, in sol-gel glass prior and after evacuation and thermal treatment.

The variation of the ligand field strength was calculated for vanadium in solution and in the sol-gel, before and after treatment (Table 6.3).

Concentration in solution (mol/l)		**Solution** Δ_0 cm^{-1}	**Sol-gel dried** Δ_0 cm^{-1}	**Sol-gel evacuated** Δ_0 cm^{-1}	**Sol-gel heated** Δ_0 cm^{-1}
1M	H_2O	13351	13351	14326	no peak observable
10^{-1}M	H_2O	13089	13106	14326	no peak observable
10^{-2}M	H_2O	13089	no peak observable	no peak observable	no peak observable
10^{-2}M	EtOH	no peak observable	no peak observable	no peak observable	no peak observable

Table 6.3: Ligand field strengths of vanadium (IV)

The electronic configuration of vanadium(IV) is d^1. In a d^1 configuration, there is no constant B.

As very few bands were observed, it was difficult to do a comparison of Δ_0 of the metal ion at different stages of sample preparation (solution, sol-gel) and at different concentrations of the dopant.

In solution, the vanadium(IV) ion shows a blue color which corresponds to the octahedral form [12,14,15]. In solution,$VOSO_4.3H_2O$ contains VO^{2+} [17]. VO^{2+} unit ion is the most stable oxycation of the first row transition ions [16].

The electronic transitions allowed from the ground state $^2B_{2g}$ for an octahedral complex are ^2E_g, $^2A_{1g}$ and $^2B_{1g}$. The spin forbidden states were too weak to be observed. They correspond to $^3T_{1g}(F)$, ^1E_g, $^1T_{2g}$, $^3T_{2g}$, $^3T_{1g}(P)$ [11]. For high concentrations of the metal ion (1M), a broad band was observed at 764nm with a shoulder at 613nm. The band at 764nm corresponds to the $^2B_{2g} \rightarrow ^2B_{1g}$ transition.

The broadness of the band is due to the vibration of the metal ion. The ligand field varies between some maximum value corresponding to the minimum metal ligand distance, and to some minimum value corresponding to the maximum metal ligand distance.

Consequently the energy of the ground state of the complex varied between limiting values and so the transition to excited states gave rise to a broad band [10]. The concentration of the metal ion was high and consequently some spin forbidden transitions might have been strong enough to be seen and have also contributed to the broadness of the band.

When the concentration of the metal ion in solution was decreased, a band was observed at 908nm. This band is interpreted as transitions from the $^2B_{2g}$ ground term to $^2E_{1g}$ and $^2A_{1g}$ terms.

A decrease of the ligand crystal field was observed when the concentration of the metal ion in solution was decreased.

In the sol-gel, the metal ion gave the same appearance as in solution. The sulphate ions are strongly bonded to the metal ion. However, changes in the shape of the band were observed. The shoulder observed in solution at 613nm became more prominent and the band became broader. Some of the electronic transitions which were too weak to be observed in solution, were stronger in the sol-gel, due to a different environment around the metal ion explaining the change in the shape of the band observed.

After dehydration, the sample became colorless for low concentrations of the metal ion in the glass (0.0466%wt) and exhibited a band in the same region for higher concentrations (4.66-0.466%wt) as the band observed for the metal ion in the glass. The sol-gel glasses were colorless due to a low absorbance of the complex.

A dark green color was observed for high concentrations of the dopant in the dehydrated sol-gel glass. The change of color from blue to green could be a consequence of the evacuation and loss of water ligands which were around the metal ion. The sulphate $VO(SO_4)$ occurs in two forms, one hydrated ($VO(SO_4).3H_2O$) which gives a blue colour and the other one dehydrated ($VO(SO_4)$) which shows a green colour [17].

After thermal treatment, no bands were observed and the sample was colorless at low concentrations of the metal ion in the glass.

The metal ion was in the form VO^{2+} and was bonded to the silica matrix. The charge transfer band was too weak to be observed.

The slight orange colour of the sol-gel observed at high concentrations is more likely to correspond to V_2O_5 which is obtained by heat treatment of a V(IV) compound in an excess of oxygen [11].

In the sol-gel, at high concentration, Δ_0 remains the same value which however increased when the sample was evacuated.

Changes of Δ_0 were observed for lower concentrations when the metal ion was in solution, in the glass and after its evacuation.

The doped sol-gels after evacuation, had the same ligand crystal field regardless of the concentration of the metal ion suggesting that the environment around the metal ion was the same. The ligand field strength was however increased with the concentration of the metal ion in solution. An increase of the ligand field strength was observed when the complex was in the glass and after dehydration. It could be due to the entrapment of the complex in the matrix. The ligand field strength for vanadium complex was sensitive to changes in the environment of the metal ion.

6.3.2- Chromium (III):Results & Interpretation

UV-VIS spectra of Chromium (III) (from $(CH_3CO_2)_7Cr_3(OH)_2$) containing solutions were run. Above 10^{-2}M (H_2O and EtOH), only one broad and noisy band was detected which gave no useful spectral information.

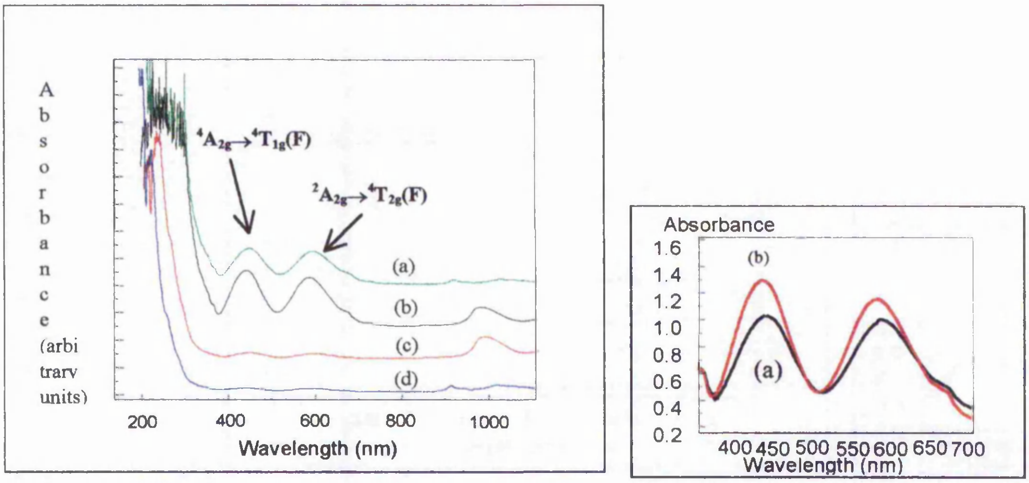

Figure 6.6:UV-VIS spectrum of chromium (III) solution a) 10^{-2}M in ethanol, b) 10^{-2}M in water, c) 10^{-3}M in ethanol, d) 10^{-3}M in water

In water and in ethanol, two main bands were observed in the visible region, one at 430nm and the other one at 580nm.

The spectrum of the metal ion in water and in ethanol were put on the same scale in order to compare their intensity.

The intensity of the bands was more intense in water than in ethanol.

A small shift of the band (2nm) toward longer wavelength was observed when water as solvent was replaced by ethanol due to changes in the environment around the metal ion.

When the metal ion was in water at 10^{-2}M and in ethanol at 10^{-3}M, a band appeared at 980nm. This band could also be observed at very low intensity for solutions at 10^{-3}M in H_2O. It is probably due to the solvent.

Figures 6.7, 6.8 represent respectively the color changes of chromium (II) ion in the sol-gels as prepared and after thermal treatment at various concentrations and prepared with different solvents.

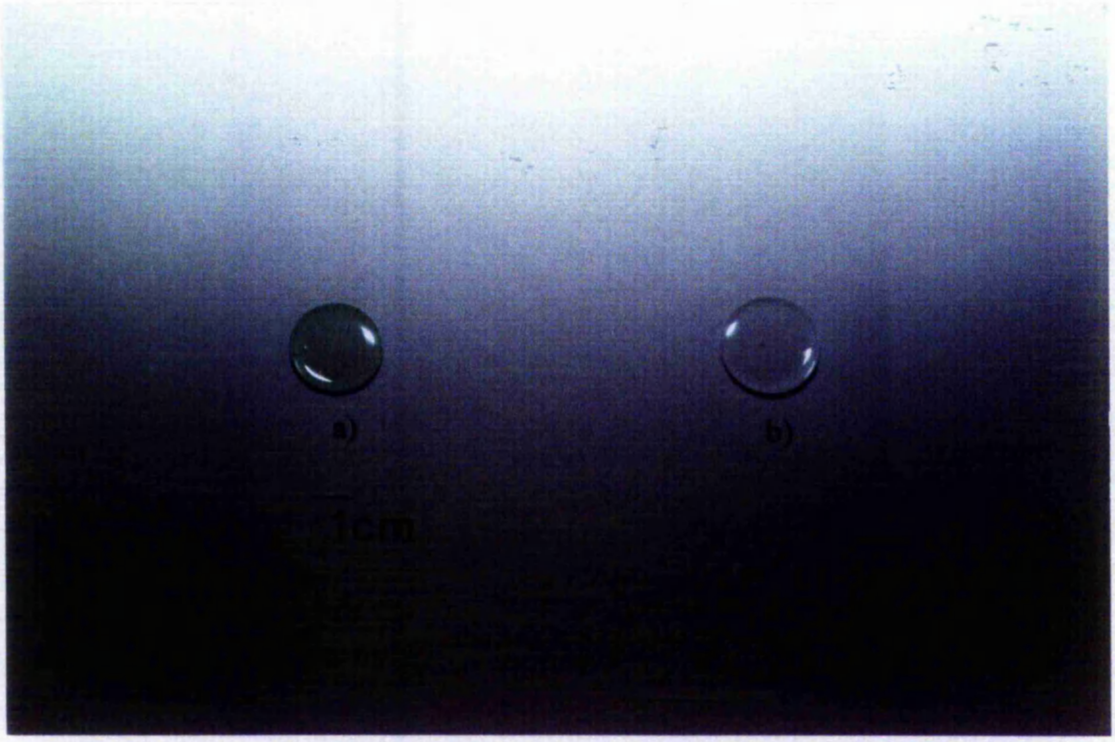

Figure 6.7: Sol-gel glasses doped with Cr(II) prepared in water solution a) 0.475wt%, b) 0.0475w%

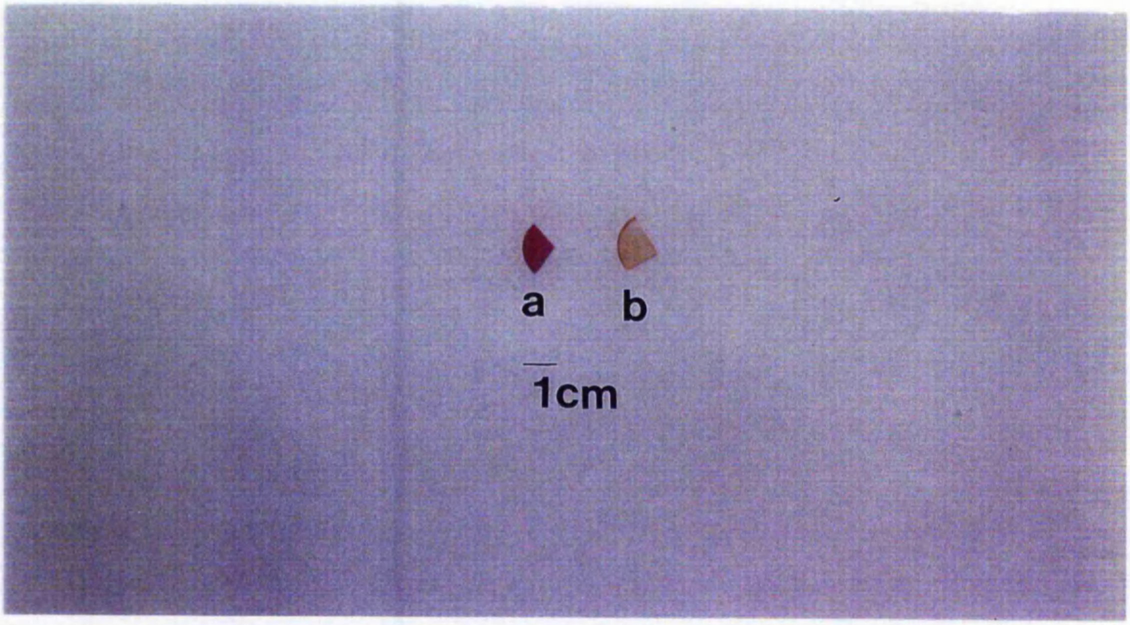

Figure 6.8: Sol-gel glasses heat treated to 800°C doped with Cr(II) prepared in water solution a) 0.475wt%, b) 0.0475w%

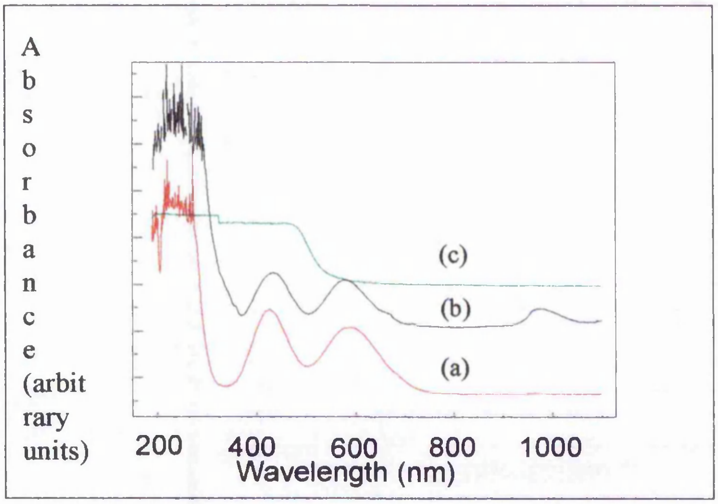

Figure 6.9: UV-VIS of Chromium (III) (0.475wt%) sol-gel

a) dried, b) evacuated, c) heated

Changes in the spectrum were observed as the doped sol-gel was treated (Table 6.4).

Concentration in solution (mol/l)	Solvent (nm)	Solution (nm)	Concentration in sol-gel (wt%)	Sol-gel dried (nm)	Sol-gel evacuated (nm)	Sol-gel heated (nm)
10^{-1}M	H_2O	broad band 500-1000	0.475	430 594	450 605	cut off 450
		dark green		green	green	red
10^{-2}M		430,580,680	0.0475	425,575	440,600	cut off 460
		green		light green	green	orange
10^{-1}M	EtOH	430,580	0.475	430,602	450,605	cut off 455
		green		green	green	red
10^{-2}M		434,580	0.0475	434,630	434,630	cut off 447
		green		green	green	orange

Table 6.4: Bands of UV-VIS spectra of Cr(III) metal ion and its color changes in solution, in sol-gel glass prior and after evacuation and thermal treatment

Δ_0 and B were calculated for the hydrated chromium (III) metal ion using the different electronic transitions.

Chromium (III) (free ion) has a B value of 918cm^{-1}.

$^4T_{2g}$= $(t_{2g})^2(e_g)$, $^4A_{2g}$=$(t_{2g})^3$, ^4T_1g=$(e_g)^3$ with e_g=3/5Δ_0 and t_{2g}=-2/5Δ_0.

E_1=430nm=1.2Δ_0 +0.6Δ_0-x=1.8Δ_0-x

E_2=580nm=1.2Δ_0-0.2Δ_0=Δ_0

So E_2=Δ_0=580nm= 17241.38cm^{-1}

Use of Tanabe-Sugano diagrams and the energy ratio of the two transitions (1.349), enabled B to be calculated. A value of 594.53cm^{-1} was found.

Calculation of Δ_0 and B was performed for each solution and for each doped sol-gel before and after treatment. The results are presented in table 6.5. A measure of β was also included. β is calculate by doing B complex/B freeion.

A decrease of β corresponds to an increase in the covalency.

Cr (III)		**Sol-gel dried**			**Sol-gel evacuated**			**Sol-gel heated**
		Δ_o (cm $^{-1}$)	**B (cm $^{-1}$)**	**β**	**Δ_o (cm $^{-1}$)**	**B (cm $^{-1}$)**	**β**	**Δ_o (cm $^{-1}$)**
10^{-1} M	H_2O	16835	909	0.99	15822	647	0.70	16667
10^{-2} M	H_2O	17391	589	0.64	16000	720	0.78	16398
10^{-1}M	EtOH	16611	679	0.74	15873	603	0.66	16531
10^{-2}M	EtOH	15873	793	0.86	15873	793	0.86	16750

In solutions, B has a value of 594.43cm^{-1}.

Table 6.5: Ligand field strengths of Cr (III) ion in sol-gels at different nominal concentration and after different treatments.

The electronic configuration of Cr^{3+} is high spin d^3 and is the most stable oxidation state of the metal ion.

In aqueous solution Cr^{3+} is always an octahedral hexaquo ion [15] which gives a green colour.

For an octahedral crystal field, there are three spin-allowed transitions from the ground state $^4A_{2g}$(F) to $^4T_{2g}$(F), $^4T_{1g}$(F) and $^4T_{1g}$(P) possible. Weak shoulders may appear in the visible spectrum, they would correspond to the spin-forbidden transitions from the ground state to ^2E_g(G), $^2T_{1g}$(G) and $^2T_{2g}$(G) [18].

In solution, the chromium (III) spectrum consisted of three bands.

One band appearing in the far UV was due to electronic transitions between metal ion and ligands and extends beyond the ultraviolet limit of the spectrometer at 190nm.

The other bands were observed at 430nm and 580nm. They were responsible for the color of the complex and were due to d-d transitions within the metal ion.

The band at 430nm corresponded to the $^4A_{2g} \rightarrow ^4T_{1g}(F)$ transition (E_1) and the band at 580nm corresponded to $^2A_{2g} \rightarrow ^4T_{2g}(F)$ transition (E_2).

At high concentrations, a broad band going from 550 to 605nm was observed.

This band could include not only the band at 580nm but the shoulder mentioned above coming from spin forbidden transitions.

The band became narrower as the concentration of the dopant in solution was decreased.

In comparison with water, the spectrum of the metal ion in ethanol was shifted toward higher wavelengths. This means that the metal ion was affected by its environment and consequently by water and ethanol as solvents. The intensity of the allowed transition corresponds to the symmetry of the species which links the ground and the excited states. In water, a more distorted structure exists compared to ethanol solution for the Chromium complex. It is confirmed by the higher intensity of the bands in the water solvent rather than in ethanol solvent.

In solution the ligand field strength did not seem to be affected by the concentration of the complex in solution or by the solvent. The metal ligands in the complex had a ligand field strength which did not vary. In solution, the ligand field strength was higher and the constant β lower than in the sol-gel, meaning that the metal ligands were more covalently bonded in solution than in the sol-gel.

In the glass, two bands were observed. They correspond to the same transitions existing for the metal ion in solution. The chromium complex was not affected by its environment. For confirmation the complex was prepared in acidic solution (0.5M HCl). By comparison its visible spectrum was identical to the visible spectrum of the same complex prepared in water. Consequently, the acetate ligands were still associated with the metal ion in its outer sphere.

When the samples were evacuated, the same band was observed with a shift toward longer wavelength with a weaker ligand field around the metal ion [19].

The environment around the metal ion changed. During dehydration, the remaining solvent and water were removed.

The same green color was observed for the metal ion in solution and in the glass which indicates that the metal ion had the same oxidation state.

When the samples were thermally treated, the spectrum showed only one band from 200nm to 450nm and the samples were red (most concentrated sol-gel glass) or yellow (lowest concentration of metal ion). The orange-red color was due to a charge transfer absorption. The change of color from green to red indicated a change in the oxidation state of the metal ion.

From Cr^{3+} the oxidation state transforms to Cr^{6+} [20].

Cr^{6+} is most commonly found in tetrahedral coordination [21]. The electronic configuration is d^{o}. At high temperature the acetate ligand was expected to be removed. Consequently the possible complex observed could be $[Cr_2O_7]^{2-}$ with some oxygen bonds coming from the matrix. For confirmation the spectrum of $[Cr_2O_7]^{2-}$ in solution was run. At 10^{-4}M a yellow solution in water showed two bands at 261nm and 359nm, in ethanol the bands were slightly shifted toward longer wavelengths at 268nm and 361nm.

As after treatment only a broad band was observed and the samples had a red-yellow color according to the concentration of the metal ion in the glass, it was possible that the bands coming from $[Cr_2O_7]^{2-}$ were present but could not be observed. The broad band was also a consequence of the heat treatment of the glass which can create internal scattering in the glass and consequently reduce the optical quality of the material with a cut off toward longer wavelength.

In the sol-gel, there is a possibility of bonding between the metal ion and the silica matrix creating a change in the symmetry, a geometrical rearrangement and consequently a lower field strength. After dehydration, a decrease of β was observed. Metal ligands were more covalently bonded due to a loss of certain ligands creating a higher symmetry and so a lower intensity of the bands in the visible spectrum.

After heating the sol-gel glass an increase in the ligand field strength was observed.

The ligands were strongly bonded to the metal ion.

6.3.3-Cobalt: Results & Interpretation

Cobalt (II) (from $Co(NO_3)_2.6H_2O$) was prepared in solution. UV-VIS spectra were run.

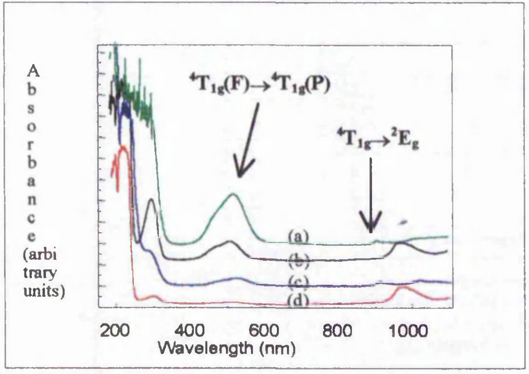

Figure 6.10:UV-VIS spectroscopy of Cobalt in solution a)10^{-1}M in ethanol, b)10^{-1}M in water, c) 10^{-2}M in ethanol, d) 10^{-2}M in water

The intensity of the bands varied with the solvent. For the same concentration of metal ion in solution, a higher intensity was found when the solvent was ethanol indicating a less symmetrical environment in the presence of ethanol.

In water, bands were observed at 300nm and 980nm which were due to the effect of the solvent on the metal ion.

In water and ethanol a band was observed at 515nm which was slightly shifted toward higher wavelengths when the concentration of the metal ion in solution was decreased.

A shoulder was observed at 471nm. A very small band was also observed at 890nm for the highest concentration of the metal ion in solution (10^{-1}M).

The metal ion was then used as a dopant in the glass.

Figures 6.11, 6.12 represent respectively the color changes of Co(II) in the sol-gels as prepared and after heat treatment at various concentrations of the metal ion prepared with different solvents.

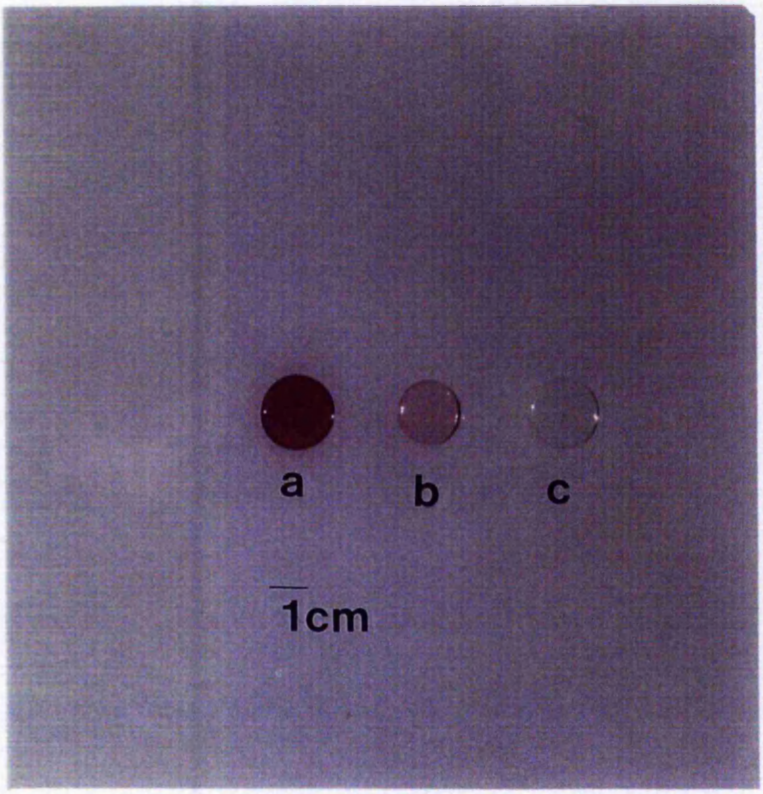

Figure 6.11: Sol-gel glasses doped Co(II) prepared in water solution

a) 5.39wt%, b) 0.539wt%, c) 0.0539wt%

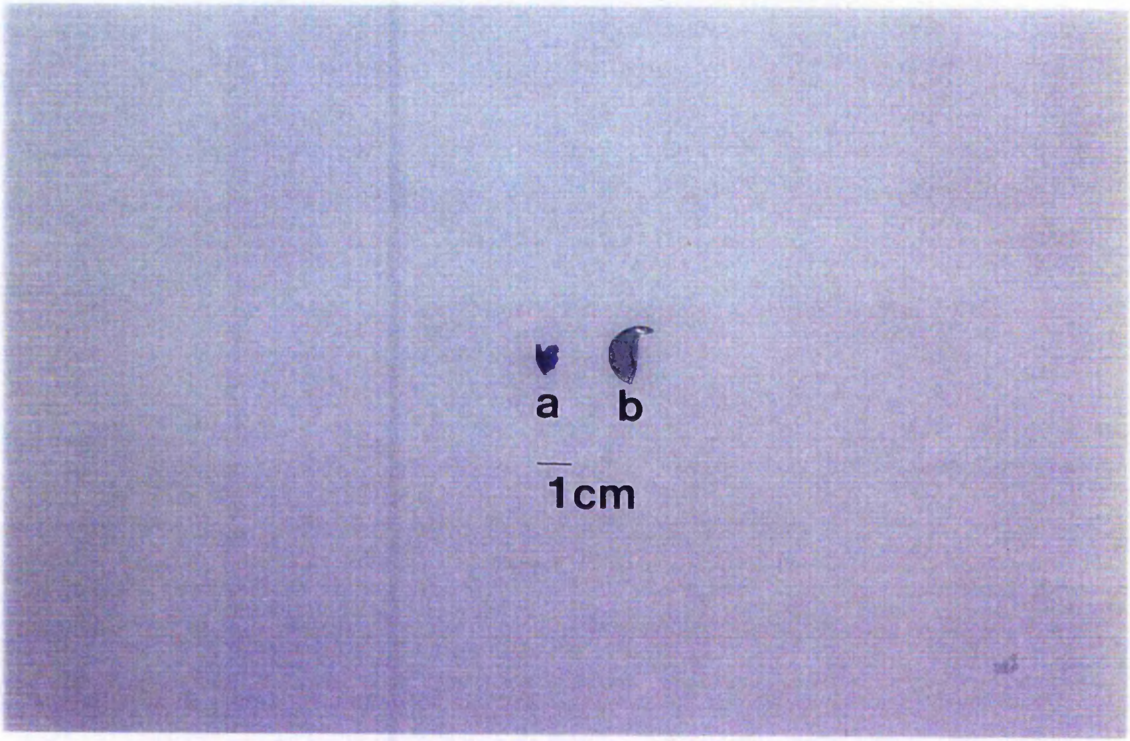

Figure 6.12: Sol-gel glasses heated to 800°C doped Co(II) prepared in water solution

a) 5.39wt%, b) 0.539wt%

The metal ion was studied in the glass and when the glass was dehydrated and thermally treated.

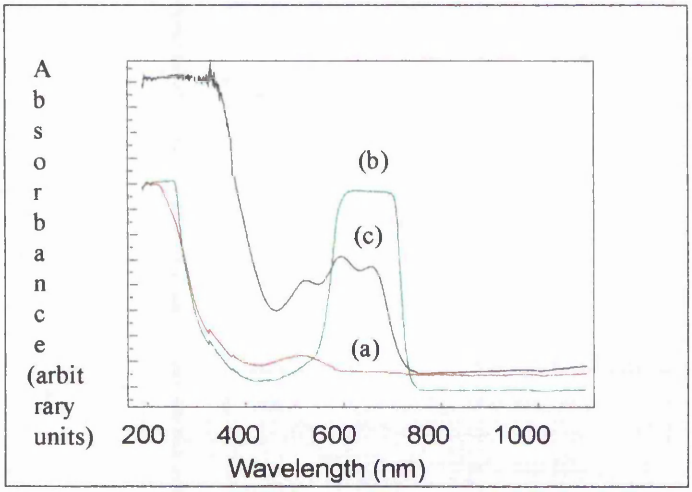

Figure 6.13.a: UV-VIS spectrum of cobalt (5.39wt%) sol-gel a) dried, b) evacuated, c) heated

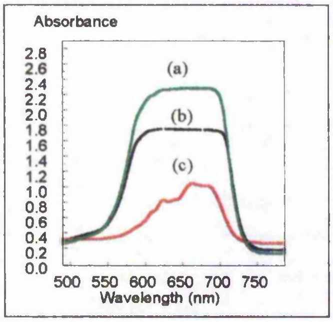

Figure 6.13.b: Visible spectrum of cobalt sol-gel evacuated a) 5.39wt%, b) 0.539wt%, c) 0.0539wt%

Concentration in solution (mol/l)	Solvent (nm)	Solution (nm)	Concentration in sol-gel (wt%)	Sol-gel dried (nm)	Sol-gel evacuated (nm)	Sol-gel heated (nm)
1M	H_2O	broad peak 510-890	5.39	515	broad peak 475-680	no peak observable
		dark red		dark pink	dark blue	blue
10^{-1}M		301,471, 511,890	0.539	broad peak 550-750	broad peak 609-698	515, 596, 656
		pale red		pale pink	pale blue	light blue
10^{-2}M		299, 471, 511, 950	0.0539	no peak observable	624, 659, 684	no peak observable
		pink		colorless-pink glint	light blue	light blue
10^{-1}M	EtOH	290,475, 518, 890	0.539	513	broad peak 623-691	535, 618, 661
		red		pale pink	pale blue	light blue
10^{-2}M		285, 518, 950	0.0539	no peak observable	626, 664	no peak observable
		pink		colorless-pink glint	light blue	light blue

Table 6.6: Bands of UV-VIS spectra of Co(II) metal ion and its color changes in solution, in sol-gel glass prior and after evacuation and thermal treatment

Δ_o and B were calculated for the metal ion in solution and in the sol-gel.

These parameters were very difficult to calculate as the spectrum of cobalt was difficult to monitor due to shoulders, overlapping bands and split bands.

In the sol-gel, after evacuation and after heat treatment, only one band was observed. Consequently it was not possible to find the different parameters as the Tanabe-Sugano diagrams used require at least two transitions.

The parameters were therefore only calculated for the metal ion in solution. The bands at 511nm and 890nm were used. The intensity ratio of the bands was calculated and then Δ_o and B were calculated.

In ethanol, the band at 511nm was slightly shifted and was found at 518nm.

Ethanol		Water	
B (cm^{-1})	β	B (cm^{-1})	β
897	0.924	890	0.9766

Table 6.7: ligand field strengths of cobalt(II)

The value of B was 897cm^{-1} in ethanol and 890cm^{-1} in water.

There was no shift of the bands at different concentrations of the metal ion in solution.

The value of B of the free ion was 971cm^{-1}.

β has a value of 0.924 in ethanol and 0.9766 in water.

In ethanol, the ligands were more covalently bonded to the metal ion than in water.

The electronic configuration of Co(II) is d^7. The octahedral complexes are characterised by a pink pale colour and the tetrahedral by a blue colour.

The transitions in the octahedral complex arise from either high spin or low spin configuration but only few low spins are present, as octahedral complexes occur at high values of the ligand field. The transitions are $^4T_{1g}(F) \rightarrow {}^4T_{2g}(F)$, $^4T_{1g}(F) \rightarrow {}^4A_{2g}(F)$, $^4T_{1g}(F) \rightarrow {}^4T_{1g}(P)$ [22].

In tetrahedral complexes, a high spin $e^4t_2^3$ configuration was observed.

The transitions are $^4A_2(F) \rightarrow {}^4T_2(F)$, $^4A_2(F) \rightarrow {}^4T_1(F)$, $^4A_2(F) \rightarrow {}^4T_1(P)$.

In most cases it is possible to have both octahedral and tetrahedral complexes due to the small stability difference between both of them. In solution, a red-pink solution was observed, the intensity of colour varying according to the concentration of the metal ion in solution. The complex was in an octahedral geometry with 6-coordinate Co^{2+}.

The transition $^4T_{1g}(F) \rightarrow {}^4T_{2g}(F)$ is observable only in the NIR at around 1250nm, the $^4T_{1g}(F) \rightarrow {}^4A_{2g}(F)$ is visually not observable. The intensity of the electronic transitions was not high enough to be detected by the spectrometer.

In water three bands were observed, one at 301nm which was due to the presence of water, the other one at 515nm which was characteristic of the $^4T_{1g}(F) \rightarrow {}^4T_{1g}(P)$ and the last one at 890nm corresponding to $^4T_{1g} \rightarrow {}^2E_g$.

A shoulder was observed at 490nm and corresponds to the spin forbidden transition derived from free-ion ^2G and ^2H terms [23]. In ethanol a shift toward longer wavelength was observed due to the presence of a lower ligand field.

In solution, from the literature [9], it is known that the $[Co(H_2O)_6]^{2+}$ complex was present with an amount of $[Co(H_2O)_4]^{2+}$ too low to be detected by UV-VIS spectroscopy. In the glass, a pink color appeared due to octahedral coordination of the metal ion.

In the sol-gel glass, the band observed was at 515nm which was the same band observed in solution.

After dehydration, a blue material was observed indicating the presence of tetrahedrally coordinated complexes. The presence of a tetrahedral complex was confirmed by the high increase of the intensity of the bands in comparison to the bands in the octahedral complex. The tetrahedral complex gave rise to more intense spectra than the octahedral complex as there is no centre of inversion and so the d-d transitions are spin allowed [24].

For tetrahedral complexes, the $^4A_2(F) \rightarrow {}^4T_2(F)$ transition is in the IR region (3000-5000nm) but is not detected due to its weakness and overlap by vibrational bands. The transition $^4A_2(F) \rightarrow {}^4T_1(F)$ is observable in the NIR.

After dehydration, a band was observed at 622nm corresponding to the $^4A_2(F) \rightarrow {}^4T_1(P)$ transition [11]. At low concentrations (from 0.0539wt%) two bands were observed at 622 and 659nm with a shoulder at 684nm which are characteristic of the tetrahedral complex. The intensity of the band was very high (4-5 times higher) compared to the intensity of the band observed prior to dehydration. This was a consequence of the tetrahedral bands which have higher intensity because the $e \rightarrow t_2$ transition has some d→p character to the p-orbitals possessing t_2 symmetry species. There was a possibility at low concentration of the dopant in the glass that there was also some octahedral complexes present but the intensity of the band was too low to be detected. After dehydration, the anions in the glass participate in the first coordination sphere of Co(II). The complex $[Co(NO_3)_2(H_2O)_4]$ is suggested [4].

At a high concentration (5.39wt%) of cobalt, a band was also observed at 552nm characteristic of octahedral complexes. At a high concentration of metal ion in the glass after dehydration, both octahedral and tetrahedral geometries were observed [4].

For lower concentration (0.539-0.0539wt%), no band was observed at 552nm, only the tetrahedral geometry was present.

The presence of tetrahedral complexes was due to the removal of the water during dehydration. The removal of water in doped sol-gel with high concentration was not total. After heat treatment, the sample was still blue showing once again the presence of tetrahedral complexes.

For high concentrations of dopant (5.39wt%), a dark blue sample was observed. No band could be recorded due to the strong colour of the sample and consequently the very low transparency of the glass.

For lower concentration (from and below 0.539wt%), three bands were observed, one at 515nm characteristic of octahedral complexes and the other ones at 596nm and 656nm characteristic of the tetrahedral complex.

So after thermal treatment, 4 and 6 coordinate complexes coexist.

There is a possibility of bonding with the silica matrix [25].

6.3.4-Nickel:Results & Interpretation

UV-VIS spectra of Nickel(II) (from $Ni(NO_3)_2.6H_2O$) in solution was run.

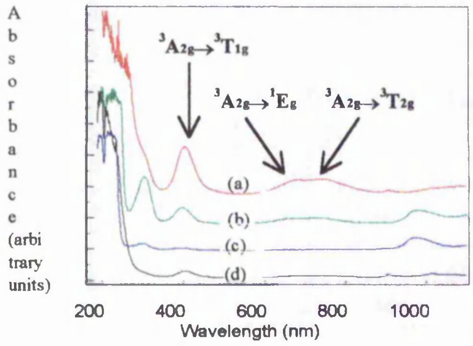

Figure 6.14: UV-VIS spectrum of nickel solution a) 10^{-1}M in ethanol, b) 10^{-1}M in water, c) 10^{-2}M in ethanol, d) 10^{-2}M in water

A sharp band was observed at 400nm and a broad band was observed between 700-800nm.

The intensity of the bands was higher in ethanol than in water. Bands corresponding to the water solvent were observed at 300nm. The metal ion doped in the glass was studied. The effect of evacuation and thermal treatment of the glass on the metal ion was studied as well.

effect of evacuation and thermal treatment of the glass on the metal ion was studied as well.

The complex was dissolved in solution to obtain a maximum concentration of 0.1M as the compound had limited solubility.

Figures 6.15, 6.16 represent respectively the color changes of Ni(II) ion in the sol-gels as prepared and after heat treatment at various concentrations.

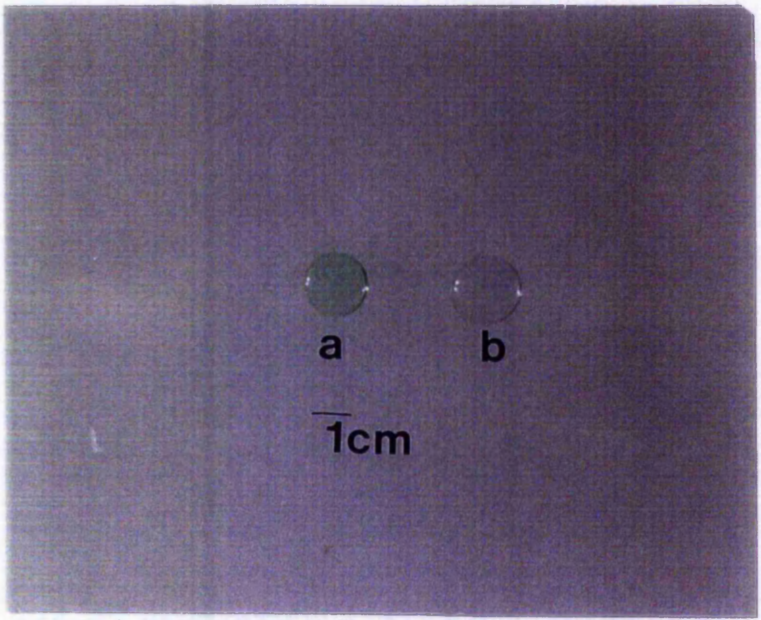

Figure 6.15: Sol-gel glasses doped with Ni(II) prepared in water solution a) 0.537wt%, b) 0.0537wt%

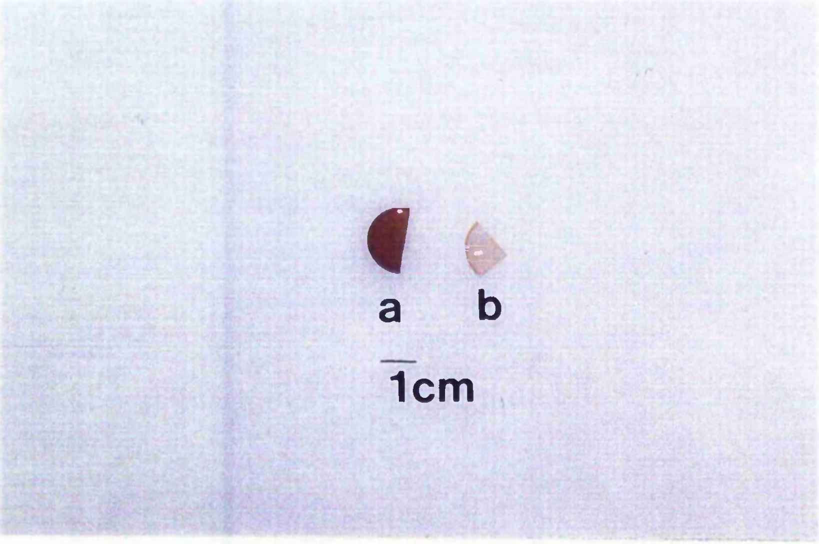

Figure 6.16: Sol-gel glasses heat treated to 800°C doped with Ni(II) prepared in water solution a) 0.537wt%, b) 0.0537wt%

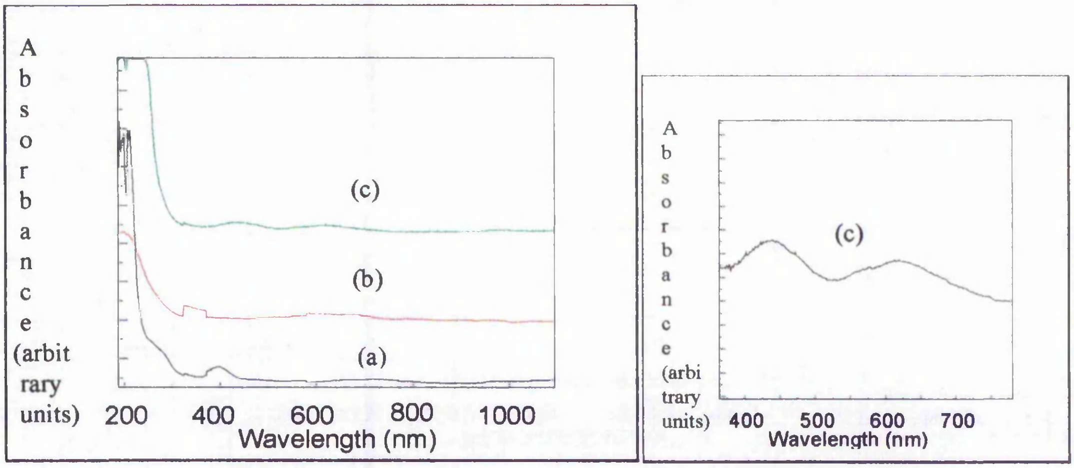

Figure 6.17: UV-VIS spectrum of Nickel (0.537wt%) sol-gel

a) dried, b) evacuated, c) heated

The intensity of the bands were not very high in the sol-gel but it was not possible to prepare higher concentrated doped solutions as nickel salts were not very soluble in water and ethanol solvents.

Concentration in solution (mol/l)	**Solvent (nm)**	**Solution (nm)**	**Concentration in sol-gel (wt%)**	**Sol-gel dried (nm)**	**Sol-gel evacuated (nm)**	**Sol-gel heated (nm)**
10^{-1}M	H_2O	395 broad band between 650-750	0.537	395 narrow band between 700-800	416	445-532-610
		green-blue		green	orange	brown
10^{-2}M	H_2O	300,395	0.0537	no peak observable	no peak observable	no peak observable
		green-blue		light green	yellow	light brown
10^{-1}M	EtOH	405,680, 745	0.537	394	394	462,550,610
		green-yellow		green	orange	brown
10^{-2}M	EtOH	402	0.0537	no peak observable	no peak observable	no peak observable
		green-yellow		light green	yellow	light brown

Table 6.8: Bands of UV-VIS spectra of Nickel (II) metal ion and its color changes in solution, in the sol-gel glass prior and after evacuation and thermal treatment.

The electronic configuration of Ni^{2+} is d^8.

Δ_o and B parameters were calculated using the bands at 395nm and at 740nm.

These bands were chosen because they appeared at different concentrations of the complex in both solvents.

The intensity ratio of the two bands was calculated and using the appropriate Tanabe-Sugano diagram it was possible to find the parameters.

The calculations were only possible in solution as in the sol-gel and after vacuum, the bands, if present, had too low intensity to be accurately measured.

After thermal treatment, bands appeared only at high concentrations of dopant.

Ethanol		Water	
Δ_o (cm^{-1})	B (cm^{-1})	Δ_o (cm^{-1})	B (cm^{-1})
7560	1030	9010	1001

Table 6.9: Ligand field strengths of Nickel(II); for the free ion B is 1030cm^{-1}.

In water, bands were observed for solutions prepared at 10^{-1}M. Δ_o has a value of 9010cm^{-1} and B of 1001cm^{-1}. In ethanol, bands were observed only for solutions prepared at 10^{-1} M. Δ_o has a value of 7560cm^{-1} and B of 1030cm^{-1}.

Ni^{2+} forms salts with virtually every anion and has an extensive aqueous chemistry based on the green $[Ni(H_2O)_6]^{2+}$ ion which is always present in the absence of strongly complexing ligands. Six-coordinated octahedral complexes of Ni^{2+} are often obtained from aqueous solutions by replacement of coordinated water especially with O-donor ligands [26].

For an octahedral field, there are three spin-allowed transitions from the ground state $^3A_{2g}(F)$ to $^3T_{2g}(F)$, $^3T_{1g}(F)$ and $^3T_{1g}(P)$ possible. Spin-forbidden transitions to the states $^1E_g(G)$, $^1A_{1g}(G)$ and $^1T_{1g}(G)$ may appear as shoulders on the spin allowed transitions [11,12].

In solution, the nickel spectrum consisted of three bands characteristic of octahedral coordination. Two of the bands were responsible for the colour of the complex and were due to d-d transitions within the metal ion. The band at 400nm corresponded to the

$^3A_{2g}\rightarrow{}^3T_{1g}$ (P) transition. A broad band was observed between 650nm and 750nm. The splitting in the middle of the band corresponds to a spin-orbit coupling that mixes the $^3T_{1g}$(F) and ^1E_g states which are very close in energy at the Δ_o given by H_2O. Prediction of the band position for $^3A_{2g}\rightarrow{}^3T_{1g}$(F) gave a value of 685nm. On the spectrum, the two bands which were observed, corresponded to the $^3A_{2g}\rightarrow{}^1E_g$ transition at 650nm and to $^3A_{2g}\rightarrow$ $^3T_{2g}$(F) transition at 745nm. The ^1E_g level was mixed through spin orbital coupling with $^3T_{1g}$(F).

The broad band included also some weaker absorption bands which correspond to spin-forbidden bands, that is transition from the $^3A_{2g}$ state to various singlet states [9]. The third band appears in the IR region and corresponds to the $^3A_{2g}\rightarrow{}^3T_{2g}$ transition.

For salts dissolved, in water a further band was observed at 300nm associated with the water solvent ($n\rightarrow\Pi^*$) transition. The band was no longer observed with ethanol as the solvent.

The solution of nickel nitrate in water was green-blue whereas in ethanol the solution was green-yellow with a small shift toward longer wavelength for the latter showing that the ligand field for nickel ion in ethanol was weaker than for nickel ion in water.

The sol-gel materials as prepared were green with a broad band between 700-800nm. Only the octahedral form of nickel(II) is present.

A shift toward longer wavelength was observed when the metal ion was in the glass indicating that the environment around the metal ion had changed.

When the glass had been evacuated a change in colour (from green to yellow) was observed but the position of the bands remained the same as before evacuation.

The thermally treated samples were brown and the spectra contained three bands close to each other with maxima at 445, 532, 610nm.

For nickel(II), the six-coordinate octahedral complexes have a green colour (for oxygen-containing ligands) whereas the four-coordinate, square planar complexes of divalent nickel are yellow or brown (the more the ligands are covalently bonded to the metal ion the darker the colour is) [27] and tetrahedral complexes are blue.

In aqueous solution, a green-yellow color was observed which shows the presence of six (octahedral) and four (square planar) coordinate complexes with a majority of six-nickel are yellow or brown (the more the ligands are covalently bonded to the metal ion the darker the colour is) [27] and tetrahedral complexes are blue.

In aqueous solution, a green-yellow color was observed which shows the presence of six (octahedral) and four (square planar) coordinate complexes with a majority of six-coordinate as the green colour was predominant. The absorption band for the square planar complex would have a medium intensity and its maximum situated between 450nm and 600nm.

In ethanol solution, a green-blue color was observed which was due to the presence of both four (tetrahedral) and six (octahedral) coordinate complexes.

Only six coordinate octahedral complexes were observed in the glass prior to dehydration as a strong green color was observed.

After dehydration the water and solvent were partially removed and an orange color corresponding to a predominance of four coordinate complexes was observed.

In the thermally, treated sol-gel glasses, the coordination state of Nickel is four-coordinate square planar. The removal of all the residual water was observed. The colour of the sample changed from orange after dehydration to brown after the thermal treatment. The darkening of the sample corresponds to the presence of ligands around the metal ion which are more covalently bonded than before thermal treatment.

6.3.5-Copper:Results & Interpretation

UV-VIS spectra of copper(II) (from $Cu(NO_3)_2.6H_2O$) solutions in water and ethanol were recorded, Figure 6.18.

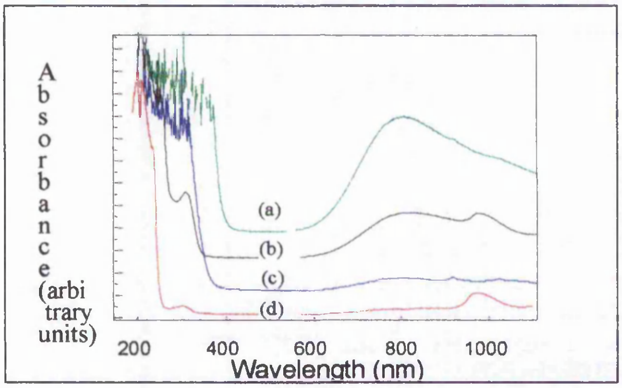

Figure 6.18: UV-VIS spectra of Copper (II) complex in solution
a) 10^{-1}M in ethanol, b) 10^{-1}M in water,
c) 10^{-2}M in ethanol, d) 10^{-2}M in water

In water three bands appeared at 300nm, 800nm and 980nm.

In ethanol, the cut off was observed at 350nm, so it was not possible to observe any band before. A broad band was noticed with the maximum at 820nm for high concentration of the metal ion in solution (10^{-1}M). At lower concentration (10^{-2}M), a small band was noticed at 900nm.

The intensity of the band was higher when the metal ion was in ethanol rather than in water.

The metal ion was studied when it was in the glass and after various treatment in the glass. Figures 6.19, 6.20 show respectively the color changes of Cu(II) ion in the sol-gels as prepared and after heat treatment at various concentrations.

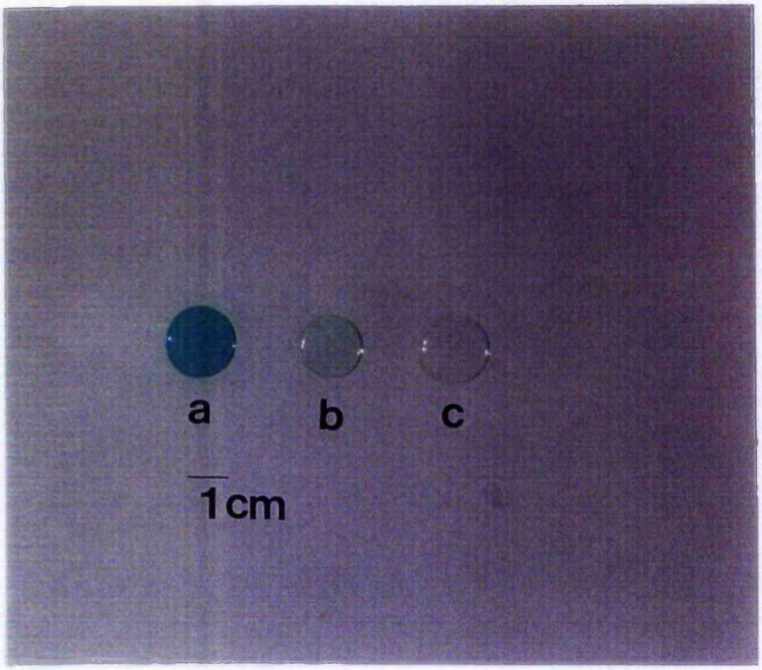

Figure 6.19: Sol-gel glasses doped with Cu(II) prepared in water solution

a) 5.81wt%, b) 0.581wt%, c) 0.0581wt%

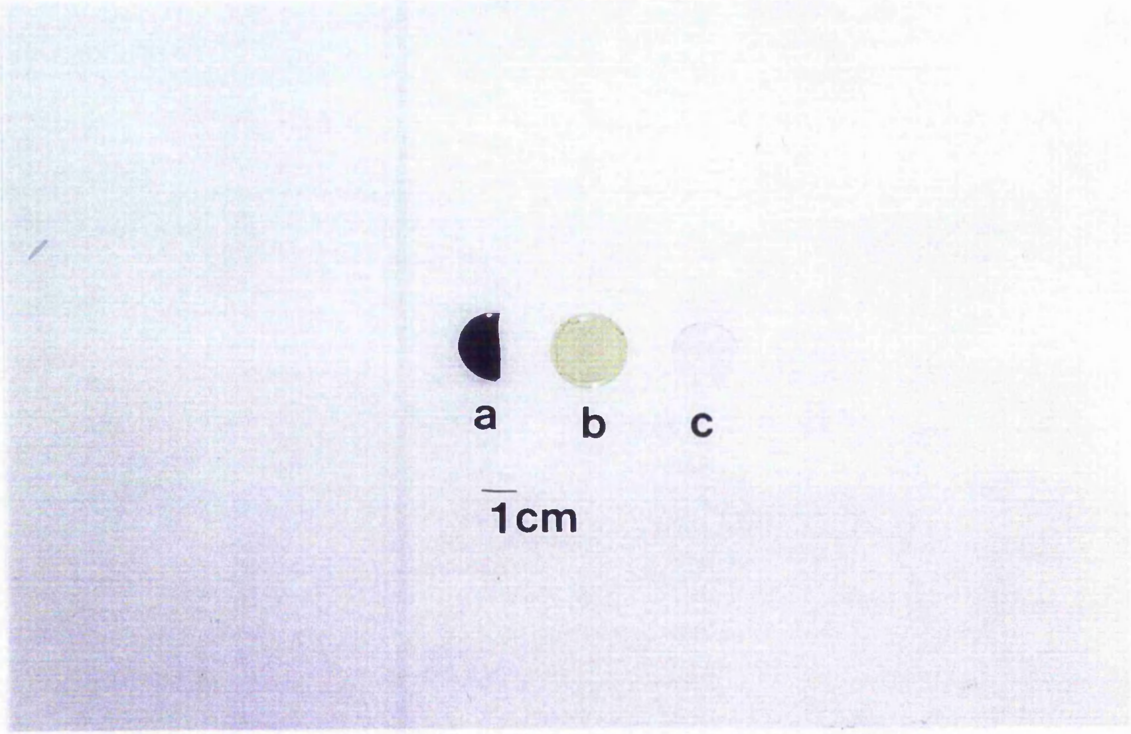

Figure 6.20: Sol-gel glasses heated to 800°C doped with Cu(II) prepared in water solution

a) 5.81wt%, b) 0.581wt%, c) 0.581wt%

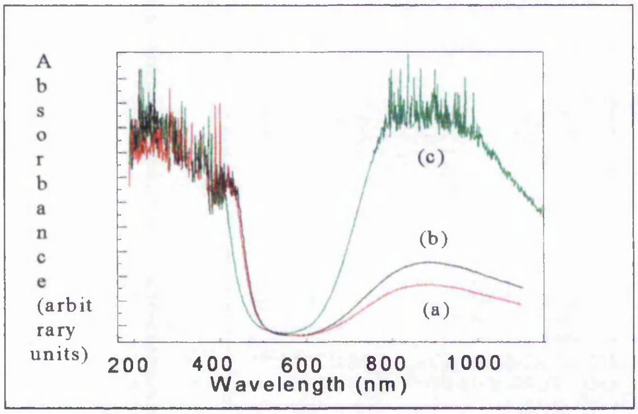

Figure 6.21: UV-VIS spectra of copper (II) (0.581wt%) sol-gel
a) dried, b) evacuated, c) heated

The spectrum of the doped sol-gel after heat treatment appeared to be very noisy. During heat treatment, some internal cracking occurred creating a scattering of the light when the sample was analysed. Consequently, the top of the main band in the visible region was very noisy.

Concentration in solution (mol/l)	**Solvent (nm)**	**Solution (nm)**	**Concentration in sol-gel (wt%)**	**Sol-gel dried (nm)**	**Sol-gel evacuated (nm)**	**Sol-gel heated (nm)**
1M	H_2O	301 798 broad	5.81	820	852	no peak observable
		Turquoise		green-blue	green	black
10^{-1}M	H_2O	242, 303, 798	0.581	844	869	869
		aqua blue		pale green	yellow green	yellow green
10^{-2}M	H_2O	233	0.0581	no peak observable	no peak observable	no peak observable
		colorless		colorless	colorless	colorless
10^{-1}M	EtOH	784 905	0.581	844	870	870
		turquoise		pale green	yellow green	brown
10^{-2}M	EtOH	784 905	0.0581	no peak observable	no peak observable	no peak observable
		light blue		colorless	colorless	colorless

Table 6.10: Bands of UV-VIS spectra of Cu(II) ion and its color changes in solution, in sol-gel glass prior and after evacuation and thermal treatment.

In solution of copper(II) only one broad band was observed, its wavelength corresponding to the ligand field strength.

Δ_o was calculated (table 6.11) As there is only band present it was not possible to calculate B.

Cu(II)		**Solution** Δ_o cm^{-1}	**Sol-gel dried** Δ_o cm^{-1}	**Sol-gel evacuated** Δ_o cm^{-1}	**Sol-gel dried** Δ_o cm^{-1}
1M	H_2O	12531	12195	11737	no peak observable
10^{-1}M	H_2O	12531	11848	11507	11507
10^{-2}M	H_2O	no peak observable	no peak observable	no peak observable	no peak observable
10^{-1}M	EtOH	12755	11848	11494	11494
10^{-2}M	EtOH	12755	no peak observable	no peak observable	no peak observable

Table 6.11: The crystal field strength for Cu(II) in different solutions/sol-gels and after different treatments.

The electronic configuration of Cu(II) is d^9 which gives rise to a Jahn-Teller distortion of the electronic transitions.

When, for example, the metal ion is in an octahedral configuration, the ion possesses one vacancy in the e_g orbitals, hence the electronic state of the ion is a degenerate E_g state [16]. The octahedron cannot remain perfectly symmetric at equilibrium and must be distorted.

In aqueous solution, the $[Cu(H_2O)_6]^{2+}$ complex forms when the Cu salts are dissolved in an excess of water [12] by producing a blue colour. Two of the water molecules are not as strongly bonded as the four others and are further away from the metal ion.

The band observed with a peak maximum at 798nm corresponds to the $^2E_g \rightarrow {}^2T_{2g}$ transition [10] which due to the Jahn-Teller distortion [10] is broad and includes several overlapping bands. This band involved transitions from the different occupied t_{2g} orbitals to the $d_{x^2-y^2}$ orbital which is only d orbital not doubly occupied [9].

In the sol-gel, a shift of the band to 820nm was noticed toward higher wavelength indicating a change in the environment of the metal ion producing a green glass.

During the formation of the sol-gel, the two water ligands away from the metal ion could be removed for certain complexes allowing the formation of tetrahedral complexes and the appearance of the green colour [11].

At that stage, the electronic transition might not be detected as it was overlapping with the electronic transition corresponding to the octahedral configuration.

After dehydration, a broad band was observed at 852nm corresponding to the $^2E_g \rightarrow ^2T_{2g}$ transition from the octahedral structure and to the $^2E \rightarrow ^2T_2$ transition from the tetrahedral structure [10].

The colour of the sample was green-yellow showing that the tetrahedral structure might be in the majority.

After heat treatment, a broad band was observed with a peak maxima at 869nm.

At low concentrations of the metal ion in the glass (0.581wt%- 0.0581wt%), the same colour is observed as that after dehydration suggesting the presence of a tetrahedral structure. However the intensity of the band is much higher (3 times) after thermal treatment than just after dehydration. The intensity of the band corresponding to tetrahedral complex is higher than the intensity corresponding to the octahedral complex. This suggests that after thermal treatment, there is no longer the octahedral structure and only the tetrahedral structure was present in the sol-gel glass.

At high concentration of the dopant (5.81wt%), a black colour was observed after thermal treatment. This black colour could be due to the formation of radical sites with strong absorptions which mask out the desired electronic transitions [28] or the thermal decomposition of the hydroxide ligands resulting in the formation of CuO compounds which are black.

In solution, the ligand field strength was higher for ethanol than for water. A higher intensity of the bands when the complex was in ethanol was observed. This suggests that a more organised structure was present in water solution rather than ethanol solution where the system was more disordered.

In the sol-gels, a higher ligand field strength was observed in the glass doped with the metal ion prepared in water as the solvent rather than ethanol as the solvent. However the ligand field strength was lower in the glass compared to the ligand field strength in solution.

After evacuation and heat treatment, the same ligand field strength was observed which was lower than in the sol-gel before treatment.

The decrease of the ligand field corresponds to a more disorganised structure present in the sol-gel glass.

6.4-Conclusions

The study of transition element in solution and as dopants for sol-gel silica based glasses has shown that the behaviour of the metal ion and its ligands varies according to its electronic configuration.

All of the transition metals studied were very sensitive to any changes in the environment of the metal ion.

By comparing their behaviour, it was possible to choose a transition element suitable as a dopant for the preparation of a solid standard in the visible region.

From the first row of the transition elements, it was proposed the use of either chromium or vanadium (Figure 6.22). Both transition elements when doped in the sol-gel glasses show bands in the visible region. The chromium complex has two separate bands in the visible region at 430nm and 594nm.

The complex possesses suitable bands in the visible region for use as a solid standard as the bands are relatively broad (6nm and 10nm) and suitable for standard measurements.

The vanadium complex has a broad band from 550nm to 900nm which can also be used as a standard.

In both complexes in the sol-gel glasses the transitions cannot be seen when the samples are dehydrated and after being thermally treated. Changes in environment around the metal ion, lead to changes in the electronic transitions which can no longer be observed in the visible region. Consequently, it is necessary to keep the ligands in order to conserve the properties of the complex in the visible region.

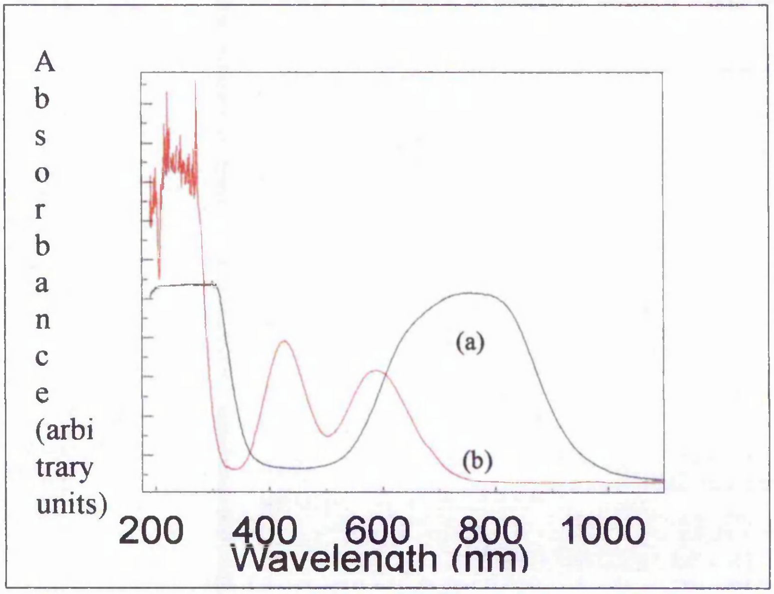

Figure 6.27 : UV-VIS spectra of a)Vanadium (1M) doped sol-gel, b)Chromium (10^{-1} M) doped sol-gel

To have stable compounds which do not absorb moisture it would be necessary to block the pores by doping the sol-gel glasses with hydrolysed TEOS to prevent changes to the gel glass with time. This was beyond the scope of the present project and should be investigated under further wok.

References

[1] A.Boos, G.Pourray, J.L.Rehspringer, J.L.Guille, J.Non-Cryst.Solids, **176**, 172, (1994)

[2] J.G.Darab, R.K.MacCrone, Physics & Chemistry of Glasses, **32**, 3, (1991)

[3] A.M.Buckley,M.Greenblatt, J.Non-Cryst.Solids, **146**, 97, (1992)

[4] C.C.Harrison, X.Li, I.Hopkinson, S.E.Stratford, A.G.Orpen, J.Chem.Soc.Faraday Trans., **89**, 4115, (1993)

[5] C.C.Harrison, J.K.Mc.Giveron, X.Li, J.of Sol-Gel Science & Technology, **2**, 855, (1994)

[6] H.Shigemura, M.Shojiya, R.Kanno, J.Phys.Chem.B, **102**, 1920, (1998)

[7] D.A.Turnbull, S.G.Bishop, J.Non-Cryst.Solids, **213**, 288, (1997)

[8] J.M.Barthez, F.Molino, J.Marignan, J.of Sol-Gel Science & Technology, **8**, 83, (1997)

[9] L.E.Orgel, *An Introduction to Transition-Metal Chemistry*, 2nd edition, (publishers Wiley, New York), (1966)

[10] D.Sutton, *Electronic Spectra of Transition Metal Complexes*, (publishers McGraw-Hill, London), (1968)

[11] F.Cotton, G.Wilkinson, *Advanced Inorganic Chemistry*, 4th edition, (publishers Wiley-Interscience, New York), (1980)

[12] D.Nicholls, *Complexes and First-Row Transition Elements*, (publishers Machmilan Press, London), (1974)

[13] T.J.Harrington, A.Earnshaw, *The Chemistry of the Transition Elements*, (publishers Oxford Press), (1973)

[14] C.D.Gowner, *Inorganic Chemistry of the Transition Elements*, (publishers The chemical society, London), **2**, 33, (1973)

[15] A.Bleuzen, F.Foglia, E.Furet, L.Helm, J.Am.Chem.Soc., **118**, 12777, (1996)

[16] L.F.Vilas.Boas, J.Costa.Pessoa, *Comprehensive Coordination Chemistry*, (publisher Pergamon Press, New York), **3**, 453, (1987)

[17] N.V.Sidgwick, *Chemical Elements and their Compounds*, (publisher Oxford-Clarendon Press, London), **1**, 804, (1950)

[18] J.E.Crooks, *The Spectrum Chemistry*, (Academic Press, London), (1978)

[19] S.Diaz-Moreno, A.Munoz-Paez, J.M.Martinez, J.Am.Chem.Soc., **118**, 12654, (1996)

[20] B.M.Weckhuysen, I.E.Wacks, R.A.Schoenheydt, Chem.Rev., **96**, 3327, (1996)

[21] M.J.Winter, *d-Block Chemistry*, (publishers Oxford university), (1994)

[22] X.Li, PhD Thesis, (Brunel Unversity), (1991)

[23] A.P.B.Lever, *Inorganic Electronic Spectroscopy*, (publisher Elsevier, Amsterdam), (1984)

[24] C.S.G.Phillips, R.J.P.Williams, *Inorganic Chemistry II Metals*, (publisher Clarendon press, London), (1966)

[25] J.Yan, A.M.Buckley, M.Greenblatt, J.Non-Cryst.Solids, **180**, 190, (1995)

[26] N.N.Greenwood, A.Earnshaw, *Chemistry of the Elements*, (publishers Pergamon Press, New York), (1984)

[27] F.A.Cotton, G.Wilkinson, *Advanced Inorganic Chemistry*, 3rd edition, (publishers Interscience, London), 528, (1972)

[28] J.G.Darab, R.K.MacCrone, Physics and Chemistry of glasses, **32**, 3, (1991)

Chapter 7: Conclusions

The research studies presented in this thesis have concentrated on the preparation of absorbance solid standards for the UV region. The standards were prepared using the sol-gel process with the pre-doping method with various rare earth metal ions being used as the dopant.

The drying process of the sol-gel glass was studied on doped sol-gels with Nd^{3+} or Ce^{3+} and undoped sol-gels.

The drying process of the sol-gel samples showed a difference in the drying rate according to the precursors used for the preparation of the glass. Both cerium and neodymium metal ions had an effect on the drying process.

With neodymium ions, the drying rate was slowed down only at high concentrations of the metal ion in the sol-gel glass (9.48wt%) whereas in the presence of cerium regardless of the concentration of the metal ion (from 0.00128wt% to 8.99wt%), the drying rate was slowed down.

For lower concentrations of Nd^{3+} in the glass (between $9.48.10^{-4}$wt% and 0.948wt%), the weight of the doped sol-gels stabilised more quickly than for undoped sol-gels. Below $9.48.10^{-5}$wt%, the dopant did not affect the sol-gel during the drying process.

The presence of dopant appeared to affect the stabilisation of the structure of the sol-gel material and the loss of solvent to the environment.

At this stage it was suspected a possible interaction between the dopant and the silica matrix.

Consequently, the structure of the sol-gel glasses was studied by mid infrared (midIR)and near infrared (NIR).

MidIR spectroscopy showed changes in the structures of the matrix under the influence of the dopant (Ce^{3+} and Nd^{3+}). Specially, the TO and LO modes of the SiOSi vibrations increased in intensity and the hydroxyl functionalities decreased in the presence of dopant in the glass. Before treatment of the glass, the NO_3^- counterions associated with the Nd^{3+} ions could be detected in the matrix.

NIR spectroscopy demonstrated that in the presence of a dopant, the OH groups and adsorbed water molecules present in the glass, came from more than one molecular group, possibly from the silica matrix and the dopants.

The study of the evolution of the structure with time using the FTIR technique, during the drying process, showed that the dopant affects the formation of the matrix and the rate of removal of the solvent.

The presence of the dopant enabled retention of the solvent at the beginning of the drying process, and the metal ions aided in the stabilisation of the gel-structure.

FTIR experiments during the very early stages of the silica gel formation showed that the dopant interacted with the precursors as soon as they had been mixed together.

The FTIR methods used to detect the effect of the dopant on the silica matrix were not sensitive enough to identify the different species present in the system.

Consequently, a study of the gelation point for normal sol-gels and doped sol-gels during the first hour of hydrolysis and condensation was carried out.

For high concentrations of the dopant in the sol-gel solution ($1.28.10^{-2}$M-0.128M for Nd^{3+}, 0.0897M for Ce^{3+}) an increase of the gelation time was observed which at the molecular level, corresponds to a decrease in silanol concentration in acidic environments. Due to the different gelation behaviour observed when the dopant was present, there was the suggestion of an interaction between the dopant involving changes in the structures. The formation of the silanol species is dependent on the speed of the hydrolysis and condensation reactions. The metal ion can be a catalyst. For qualitative analysis of the various silica species present during the first hour of reaction, ^{29}SiNMR experiments were performed on doped (Nd^{3+} and Ce^{3+}) and undoped sol-gels. When the formation and evolution of the different silica species was studied with the time of reaction, an effect of the dopant was noticed.

The Q^3 and Q^4 species, characteristic of the silica matrix, formed a lot quicker in the presence of a dopant. This effect increased as the concentration of the metal ion in the sol-gel solution increased. The dopant affected both the rate of hydrolysis and the rate of condensation reactions. A certain concentration of the metal ions was required to increase the hydrolysis rate but not the condensation rate as for the low concentration doped sol-gel solutions only the hydrolysis rate was increased and increases in levels of Q^0 species could be observed.

The study of pH variation in doped and undoped sol-gels during the first hour of hydrolysis and condensation reactions revealed that the catalytic effect observed was due to the metal ion itself and its acidity. ^{29}SiNMR confirmed that the water ligands present around the metal ion did not interact with the precursors, the metal ion alone was involved in the catalytic effect. In conclusion, the metal ion independently of its ligands acts as a catalyst on the sol-gel process. The catalytic effect is dependent on the concentration of the metal ion mixed with the precursors. At high concentrations of the metal ion, a catalytic effect on the hydrolysis and the condensation reactions is observed. At lower concentrations of the metal ion in the sol-gel solution, the catalytic effect is only observed for the hydrolysis reaction.

After looking at the effect of the dopant on the precursors, the effect of the environment on the metal ion and its ligands was studied.

UV-VIS spectroscopy of the Nd^{3+} in crystals, in solution and in the sol-gel glass, showed variation of the metal ion spectra according to the environment around the metal.

As a crystal, the electronic transitions of Nd^{3+} were not affected by the neighbouring ligands, here water and ethanol.

In solution, spectral changes were produced either by structural changes on introducing a substituent, or on altering the environment.

In the glass, the electronic transitions were insensitive to the solvent in which the metal ion was prepared as a solution, suggesting that the same solvent was present around the metal ion in the glass. Moreover single crystal X-ray analysis and Extended X-ray Absorption Fine Structure (EXAFS) analysis allowed the determination of the coordination number around the metal ion when present in crystals, in solution and in the sol-gel.

The coordination number of Nd^{3+} metal ions in a crystal form changed according to the ligands around the metal ion. A coordination number of 10 was found in the presence of NO_3^- with 3 nitrate and 4 water ligands covalently bonded to the metal ion. A coordination number of 8 in the presence of Cl^- was found with 2 chloride and 6 water ligands directly bonded to the metal ion.

In solution, a coordination number of 9 was found when the solvent was water and a coordination number of 7 when the solvent was ethanol regardless of the other ligands associated with the metal ion. The complexes in ethanol were suggested to be $[Nd(NO_3)_3(H_2O)]^{3+}$ and $[Nd(Cl)_2(H_2O)_5]^{3+}$.

In the glass, prior to any treatment, a coordination number of 7 was found. After dehydration, only 6 ligands were around the metal ion and only 4 ligands were bonded to the metal ion after heat treatment.

In the glass, prior to any treatment, the Nd^{3+} complex was trapped in the glass and could be electrostatically bonded to the silica matrix. The metal ion was strongly covalently bonded to three nitrate ligands. After evacuation, the complex loses one ligand. When the sample was rehydrated a coordination number of 7 was observed. So after dehydration the complex loses one water ligand.

After thermal treatment, a change in coordination number was observed. At 800°C, the nitrate ligands decomposed and were removed from their involvement with the metal ion. Consequently it was proposed that the metal ion bonds to the silica matrix via the oxygens of the siloxane groups.

By knowing the type of interaction between the matrix and the dopant and how they interact with each other, we were able to prepare standards.

Ce^{3+} metal ion was chosen as a possible dopant for the preparation of solid standards as it possesses four characteristic bands in the UV region. These four bands have a relatively high intensity at low concentration of the metal ion and the top of the spectroscopic bands are broad enough (4-6nm) for their uses as standards.

The electronic transitions of the metal ion were affected by the environment around the metal ion. When doped in the glass, a small shift of the bands was observed. Evacuation of the samples also affected the electronic transition of the metal ion. After heating up the sample, no bands were observed, from Ce^{3+} as the oxidation state became Ce^{4+}. In conclusion, Ce^{3+} metal ions can be used as a dopant as long as the glass does not undergo any further treatment. In consequence, it will be necessary to find a method allowing the protection of the metal ion from the external environment without losing the optical quality and transparency of the material.

By variation of the concentration of the metal ion in the sol-gel glass, a series of UV solid standards with absorbances between 0.5A and 2A was obtained.

The preparation of combined standards in the UV and Visible regions was also attempted using Ce^{3+} and Nd^{3+}. Unfortunately both metal ions interacted with each other and it was not possible to observe any bands in the UV region. Consequently, to prepare combined standards, it will be necessary to use two metal ions which do not interact with each other or a dopant which has bands in both the UV and the visible region.

A preliminary series of experiments were carried out to study the stability of the glass standards with time. At this stage of the work, the glasses are not completely stable with time and in the future a method should be found in order to obtain stable materials, for example by filling the pores of the glass to prevent absorption of moisture and a subsequent decrease of the transmittance with time.

Finally, the preparation of standards for the visible region was carried out. For this purpose, the transition elements of the first row were used. The effect of the silica matrix on the electronic transitions of the metal ions was studied.

All of the complexes were very sensitive to any changes in the environment of the metal ion. Transition elements suitable as dopants for the preparation of a solid standard in the visible region were chosen. Chromium(III) and vanadium(IV) were chosen.

For both complexes in the sol-gel glasses the bands due to electronic transitions could not be seen when the samples were dehydrated and thermally treated. Changes in environment around the metal ion lead to changes in the electronic transitions which could not be observed in the visible region.

In conclusion, as future work, methods to protect the dopants from the outside environment should be found. The chosen method should prevent the glass matrix from absorbing moisture, while maintaining optical transparency and clarity.

Appendices

For completeness, the appendices found in the following pages contain:

- Statistical analysis of the %weight loss with time for Nd^{3+} and Ce^{3+} doped sol-gels and undoped sol-gels.
- FTIR analysis of doped and undoped sol-gels.
- Statistical analysis of gelation time versus hydrolysis time for doped (Nd^{3+}, Ce^{3+}) and undoped sol-gels.
- ^{29}SiNMR spectra of doped sol-gels at various concentration of Nd^{3+} metal ion.
- Calculation of the moles of Si present for each type of species.
- ^{29}SiNMR spectra of doped sol-gels at various concentration of Ce^{3+} metal ion.
- Powder X-ray analysis of ground crystals

They are referred to but not included in the main body of the thesis.

Statistical analysis of the %weight loss with time for Nd^{3+} and Ce^{3+} doped sol-gels and undoped sol-gels

Time (day)	Normal $\bar{x}$	Error ±	Nd^{3+} 9.8wt% $\bar{x}$	Error ±	Nd^{3+} 0.948wt% $\bar{x}$	Error ±	Nd^{3+} 0.0948 wt% $\bar{x}$	Error ±
0	100	0	100	0	100	0	100	0
2	95	1.3	97.11	1.46	96	1.56	94.03	2.25
6	82	2.7	95.16	1.52	95.5	1.24	88.58	1.96
7	79.13	1.76	90.69	1.09	90	1.67	68.51	1.32
8	75	1.98	89	1.87	54.095	2.03	65	2.15
9	70.15	0.84	81	1.34	45.795	2.85	62.86	2.99
10	64.99	2.67	79	2.43	43.21	1.52	51.25	2.56
12	59	2.98	75	2.96	40.105	2.67	39	2.38
13	52.14	1.73	74	2.49	28.245	1.95	23.42	1.82
14	49.51	3.02	69	1.27	25.86	1.51	20.63	1.78
15	45.37	1.09	61	1.58	17.515	1.23	19.23	1.39
16	42.36	2.76	57	1.22	16.79	1.11	18.62	1.57
17	39.12	1.95	45	1.5	17.435	0.98	18.29	1.46
18	33.92	1.61	39	1.23	16.435	1.08	16.51	1.25
26	22.26	0.98	29	1.01	16.38	0.67	16.51	1.21
39	22.1	1.54	21	0.94	16.31	0.51	16.49	1.03
40	21.63	0.67	19.92	0.86	16.3	0.28	16.52	0.99
41	21.5	0.54	18	0.67	16.28	0.62	16.54	0.85
46	21.48	0.98	17.98	0.43	16.278	0.57	16.5	0.73
47	21.33	0.53	17.51	0.21	16.272	0.31	16.3	0.52
52	21	0.32	16.9	0.14	16.262	0.28	16.28	0.34

Table 1: statistical analysis using the student t-test for the %weight loss with time of Nd $^{3+}$ doped and undoped sol-gels (for each time point 8 samples were used)

Legend: $\bar{x}$: mean value

Time (day)	**Nd^{3+} 0.0948 wt%** $\bar{x}$	**Error** ±	**Nd^{3+} $9.48.10^{-4}$ wt%** $\bar{x}$	**Error** ±	**Nd^{3+} $9.48.10^{-5}$ wt%** $\bar{x}$	**Error** ±	**Nd^{3+} $9.48.10^{-6}$ wt%** $\bar{x}$	**Error** ±
0	100	0	100	0	100	0	100	0
2	94.03	2.51	98	2.01	91.286	1.94	94.98	2.67
6	88.58	1.74	95	2.58	79	2.61	81.68	2.94
7	68.51	2.98	90.86	1.67	75	2.57	79.13	2.81
8	65	2.37	89	2.39	69	2.46	74.87	1.96
9	62.86	1.91	87.61	1.86	59	1.92	70.15	1.75
10	51.25	1.63	45	1.34	57.24	1.54	65	1.94
12	39	1.25	35	1.59	48	1.37	58.71	1.67
13	23.42	1.02	26.74	1.16	42.27	1.51	52.31	1.38
14	20.63	0.98	25	1.35	41.25	1.39	49.51	1.65
15	19.23	0.82	24	0.96	36	1.27	45.68	1.49
16	18.62	0.51	21.69	0.74	34.98	1.13	42.36	1.01
17	18.29	0.49	20.25	0.53	32.23	1.02	39.12	1.25
18	16.51	0.37	19.97	0.61	29.49	0.65	33.98	1.11
26	16.51	0.28	18.51	0.37	21.98	0.54	22.31	0.67
39	16.49	0.17	17.71	0.19	18.09	0.38	22.1	0.61
40	16.52	0.22	17.54	0.24	17.98	0.41	21.71	0.58
41	16.54	0.31	17.49	0.16	17.65	0.25	21.5	0.34
46	16.5	0.18	17.31	0.31	17.45	0.29	21.48	0.42
47	16.3	0.54	17.24	0.26	17.23	0.17	21.41	0.29
52	16.28	0.17	17	0.24	17	0.29	21.01	0.25

Table 2: statistical analysis using the student t-test for the %weight loss with time of Nd^{3+} doped and undoped sol-gels (for each time point 8 samples were used)

Time (day)	Ce^{3+} 8.99wt% $\bar{x}$	Error ±	Ce^{3+} 1.28wt% $\bar{x}$	Error ±
0	100	0	100	0
2	98.2	2.37	96	2.01
4	95.35	2.81	94	2.67
8	91.25	1.96	83.32	1.82
10	89	1.52	78.23	1.63
16	74	1.93	59.23	2.24
20	64.58	0.67	48.99	1.05
25	54	1.54	31.27	0.87
30	43	1.32	26	1.09
35	32.69	0.94	24.32	0.73
40	28.25	1.59	22.37	0.46
47	22.3	0.67	21.68	0.82
52	21.5	0.35	21	0.29

Table 3: statistical analysis using the student t-test for the %weight loss with time of Ce^{3+} doped and undoped sol-gels (for each time point 8 samples were used)

Ce^{3+} 0.128 wt% $\bar{x}$	Error ±	Ce^{3+} 0.0128 wt% $\bar{x}$	Error ±	Ce^{3+} 0.00128wt% $\bar{x}$	Error ±
100	0	100	0	100	0
95.61	1.68	89	2.85	90.82	1.98
90.21	2.16	82	2.37	85.91	1.76
81.016	1.75	65	1.91	69	2.31
67.21	1.59	58	1.65	61	1.63
51.32	2.03	31	2.31	35	1.81
35.21	1.67	26	1.64	29	1.74
26.37	1.19	20	1.32	21	1.23
23.99	0.94	19.89	0.98	21	0.85
22.98	0.81	20	0.82	21.04	0.79
21.23	0.62	19.99	0.73	20.23	0.56
21.5	0.53	19.78	0.68	19.78	0.41
21	0.34	19.98	0.51	19.98	0.27

Table 4: Statistical analysis using the student t-test for the %weight loss with time of Ce^{3+} doped sol-gels (for each time point 8 samples were used)

FTIR analysis of doped and undoped sol-gels

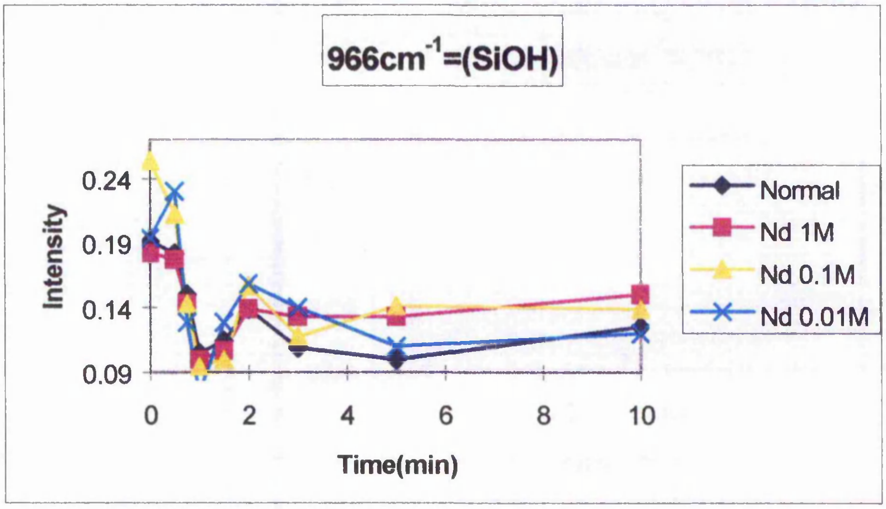

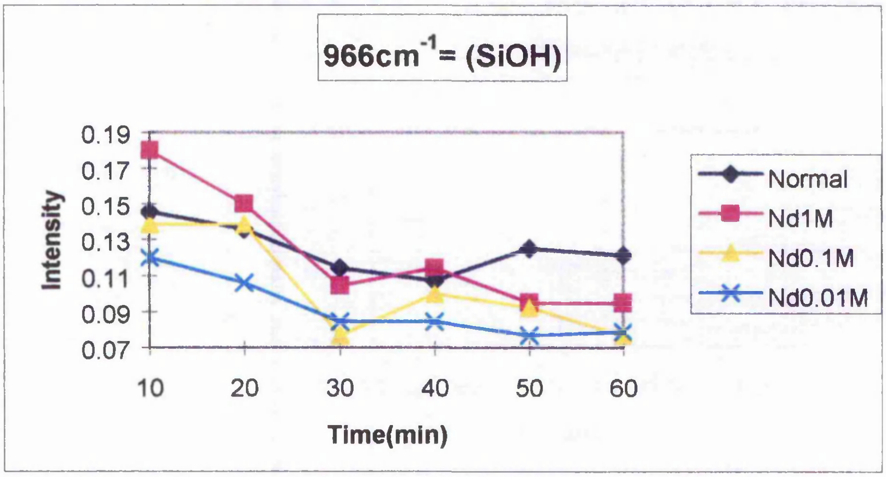

Figure 1: Changes in intensity for the band at 966 cm^{-1} in the presence of various concentrations of Nd^{3+}

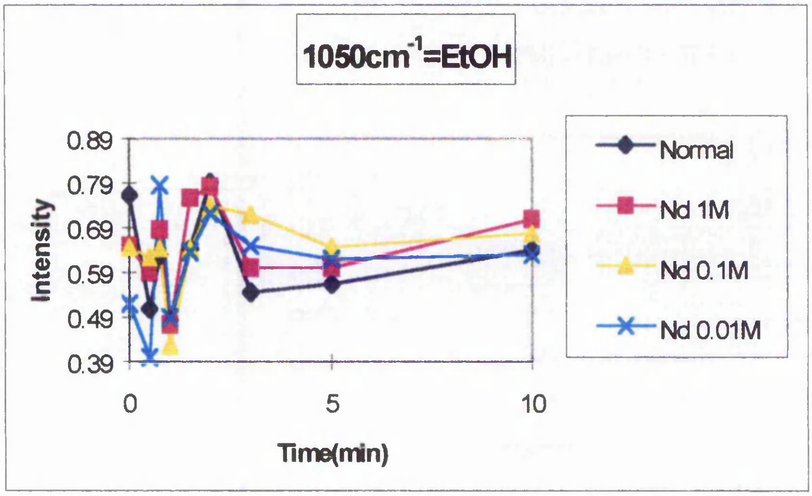

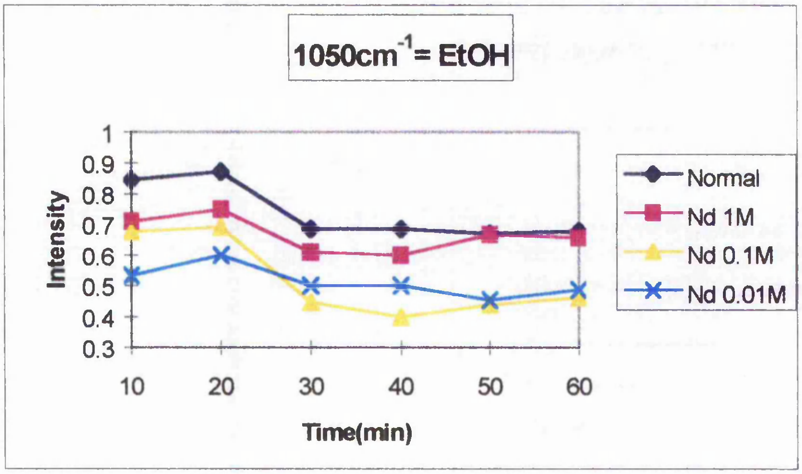

Figure 2: Changes in intensity with time for the band at 1050cm^{-1} in the presence of various concentrations of Nd^{3+}

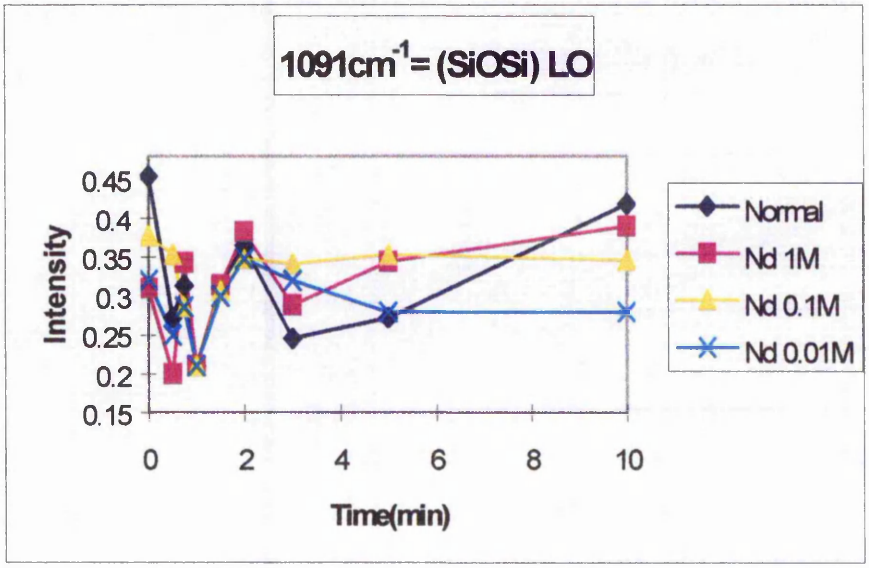

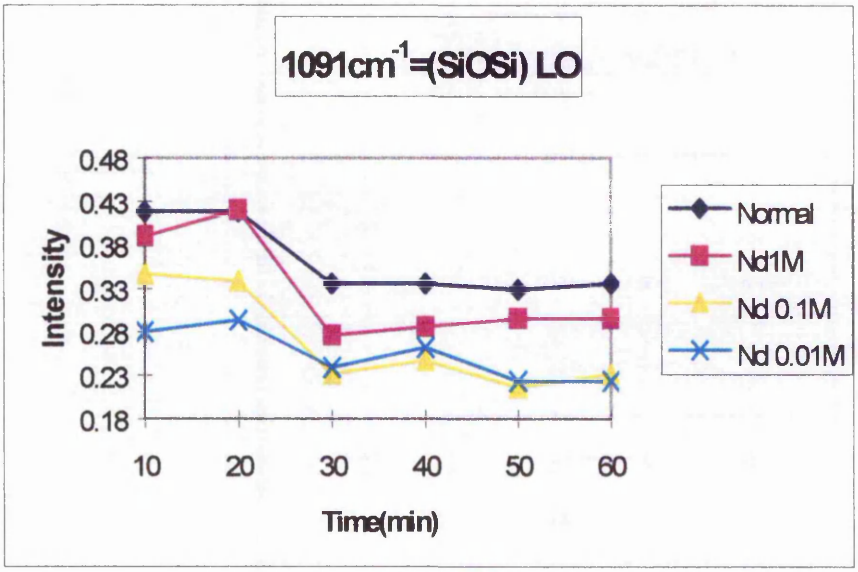

Figure 3: Changes in intensity with time for the band at 1091cm^{-1} in the presence of various concentrations of Nd^{3+}

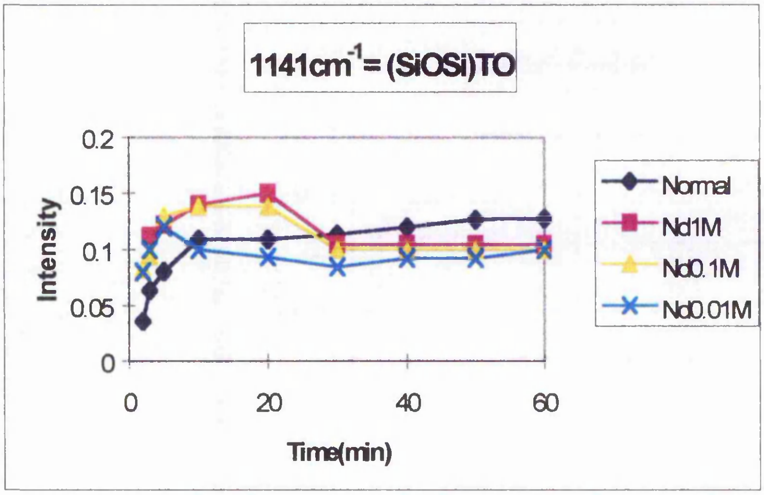

Figure 4: Changes in intensity with time for the band at 1141cm^{-1} in the presence of various concentrations of Nd^{3+}

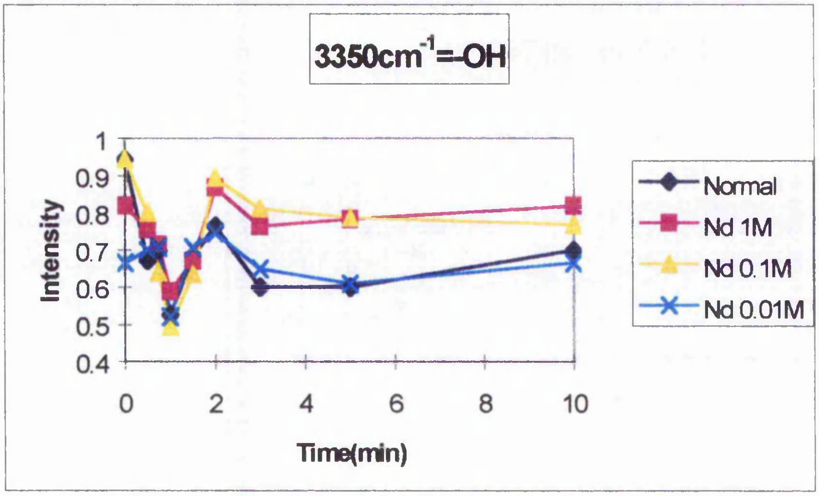

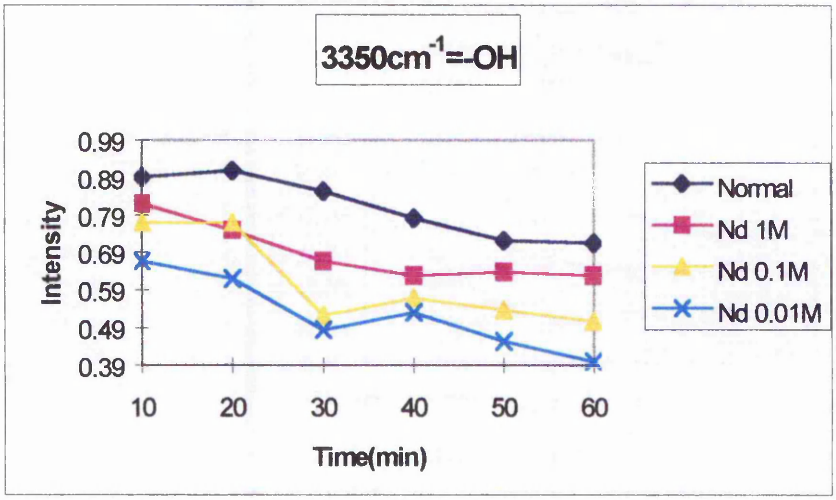

F

igure 5: Changes in intensity with time for the band at 3350cm^{-1} in the presence of various concentrations of Nd^{3+}

Statistical analysis of gelation time versus hydrolysis time for doped (Nd^{3+}, Ce^{3+}) and undoped sol-gels

Time (day)	Normal sol-gel $\bar{X}$ (min)	Error ±	Nd^{3+} 0.128wt% sol-gel $\bar{x}$ (min)	Error ±	Nd^{3+} 0.0128wt% sol-gel $\bar{x}$ (min)	Error ±
0.5	7.57	2.13	107.05	19.8	12.815	2.23
0.75	7.57	2.51	117.012	8.51	6.86	1.09
1	40	8.23	118	13.24	44	9.78
3	39.33	5.27	138	16.24	58.56	16.77
5	62.5	11.4	174	9.83	75	12.33
7	47	14.36	186	17.34	81.96	17.89
9	48	10.01	167	4.21	53	11.41
9.5	55	12.21	169	11.35	54	4.79
10	78	16.78	172	21.56	56	3.27
10.5	62	8.93	184	14.96	89	8.61
11	56.25	11.54	204	18.54	101.93	12.38
11.5	43.23	5.27	187	9.37	89.54	9.71
12	34	12.39	137.65	11.23	79.46	6.93
13	32	4.36	134.2	17.56	84.52	14.62
15	34.25	13.24	133.1	18.57	79.73	9.08
20	44	7.56	151	8.56	74.05	11.57
25	56.5	7.61	185.05	16.37	80	7.69
30	79.5	10.58	190	12.39	111	11.36
35	100	7.98	187	19.11	105	15.67
40	110	8.21	191.7	12.35	100.74	13.86
50	100	8.93	221.6	13.5	106.25	5.33
60	105	7.23	227	6.98	84.5	6.21

Table 1: Statistical analysis using the student t-test of gelation time versus hydrolysis time for Nd^{3+} doped and undoped sol-gels (for each data point 10 samples were used)

$\bar{x}$ corresponds to the average mean of the gelation time.

Time (day)	Nd^{3+} 0.00128wt% sol-gel $\bar{x}$ (min)	Error ±	Nd^{3+} 0.00064wt% sol-gel $\bar{x}$ (min)	Error ±
0.5	5.175	2.21	6.7525	3.08
0.75	6.25	3.42	5.81	2.12
1	20	5.19	7.96	3.19
3	28.2	4.68	9.68	3.57
5	40	6.77	8.65	2.46
7	54	9.32	24.35	5.97
9	27.75	4.21	13.33	4.39
9.5	27.99	5.03	15	4.08
10	28.66	5.27	17.5	4.92
10.5	43	11.08	12	3.29
11	53.5	10.9	10	2.27
11.5	46.5	9.66	18	3.94
12	29.46	4.3	25	4.77
13	26.55	3.75	16.66	4.06
15	29.6	6.39	15	3.51
20	50	11.34	15	3.58
25	38.5	7.98	20	3.71
30	50	12.08	17	4.14
35	56.5	11.67	18	4.21
40	60	7.49	17	4.5
50	52.5	4.82	14.34	2.29
60	60	6.31	14.35	2.81

Table 2: Statistical analysis using the student t-test of gelation time versus hydrolysis time for Nd^{3+} doped sol-gels (for each data point 10 samples were used)

Time (day)	**Nd^{3+} $1.28.10^{-4}$ wt% sol-gel $\bar{x}$ (min)**	**Error ±**	**Nd^{3+} $1.28.10^{-5}$ wt% sol-gel $\bar{x}$ (min)**	**Error ±**	**Nd^{3+} $1.28.10^{-6}$ wt% sol-gel $\bar{x}$ (min)**	**Error ±**
0.5	9.47	2.23	10	3.2	8	1.23
0.75	12.675	5.67	12	2.76	8	2.28
1	10.75	5.09	21	4.68	36.76	7.98
3	22.81	6.86	21.2	7.23	35	7.41
5	17.62	6.57	26	6.69	57	9.54
7	23	8.97	21	4.27	32.25	6.37
9	16.75	7.05	28	7.91	41	7.91
10	32	9.98	62	10.21	71	10.15
11	27.28	9.57	41	11.03	47	8.65
11.5	24.075	8.91	32	9.32	41	8.11
12	23	8.54	28	9.02	31	7.92
13	17.5	8.13	29	9.07	30	6.58
15	17.5	7.95	24	8.71	31	6.92
20	18.66	8.26	30	8.99	44.5	4.63
25	32	9.64	32.57	9.87	51	6.97
30	49.15	10.83	51	11.59	68	7.82
35	47.48	10.57	43	12	87	5.61
40	51	11.26	55	4.32	92	8.09
50	25.43	9.71	24	5.67	88	8.17
60	39.85	11.67	33	2.23	89	9.01

Table 3: Statistical analysis using the student t-test of gelation time versus hydrolysis time for Nd^{3+} doped sol-gels (for each data point 10 samples were used)

Time (day)	Ce^{3+} 0.0897 wt% sol-gel $\bar{x}$ (min)	Error ±	Ce^{3+} 0.0128 wt% sol-gel $\bar{x}$ (min)	Error ±	Ce^{3+} 0.00128 wt% sol-gel $\bar{x}$ (min)	Error ±
0.35	245.76	12.27	69	5.82	26.84	2.28
1	215.76	15.68	64.125	6.08	30.86	2.67
3	195.05	13.94	83.2	8.93	34.6	3.14
5	208.41	14.06	85.544	8.75	62.15	4.58
7	182.33	11.97	49.66	5.09	44.6	3.69
9	191	12.23	58	5.77	39.5	3.15
10	205	14.98	53	5.82	35	3.08
11	187	10.21	49	5.61	31	2.94
12	220	14.92	61.75	6.01	40.2	3.19
13	230	11.25	99	10.02	53.25	3.67
15	265	11.64	76.17	4.75	34.4	3.16
20	185	8.94	81.8	6.25	57	3.83
25	189.4	8.96	68.4	3.29	34.6	2.94
30	199	8.54	45.5	5.21	27	1.97
40	205	9.08	70.17	6.94	47.6	2.52
50	214	8.74	72	6.28	50.2	2.61
60	215	9.68	73	6.12	54.4	3.23

Table 4: Statistical analysis using the student t-test of gelation time versus hydrolysis time for Ce^{3+} doped sol-gels (for each data point 10 samples were used)

^{29}SiNMR spectra of doped sol-gels at various concentration of Nd^{3+} metal ion (0.128M-0.00128M)

10 seconds

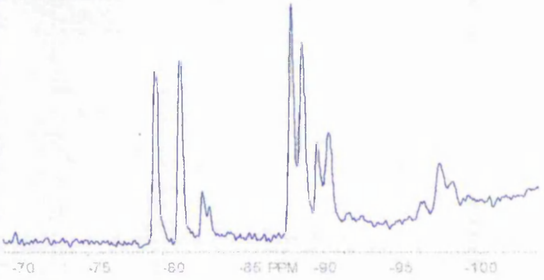

30 seconds

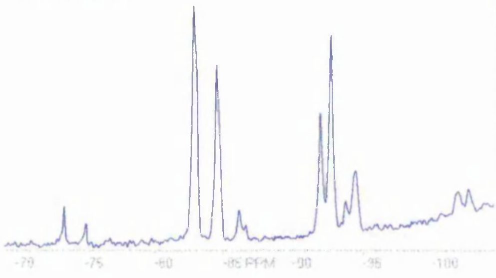

1 minute

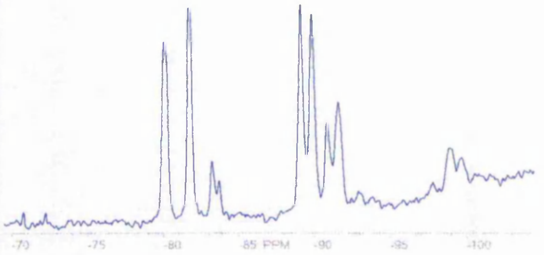

2:30 minutes

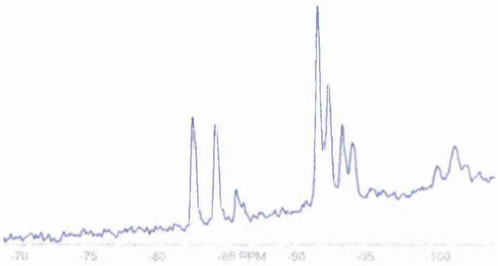

4:30 minutes

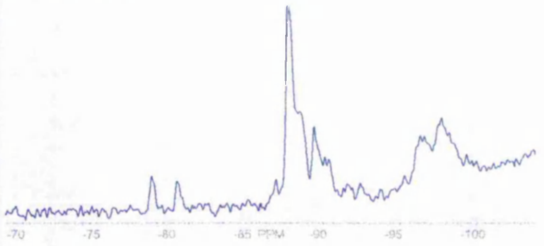

7:30 minutes

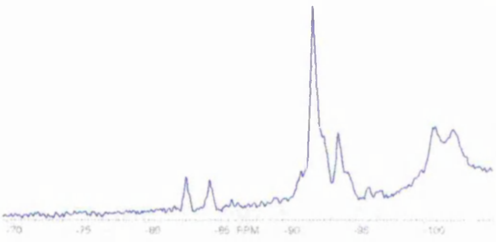

8:30minutes

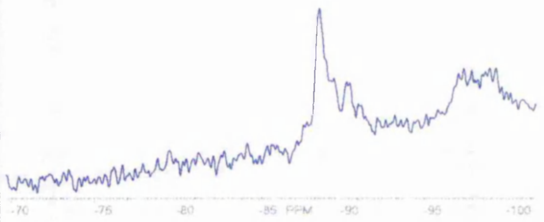

10 minutes

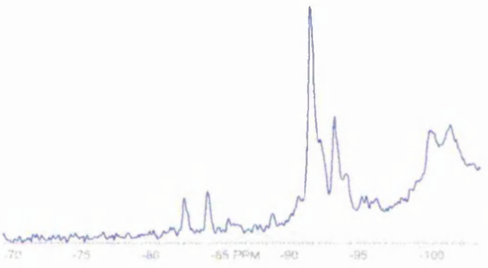

15 minutes

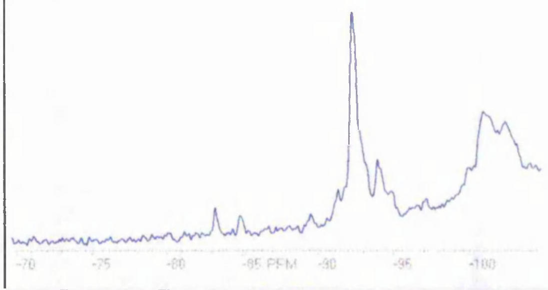

20 minutes

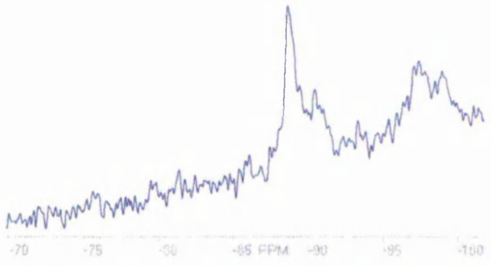

Nd0.128Msol-gel solution (from -70 to -110 ppm)

10 seconds

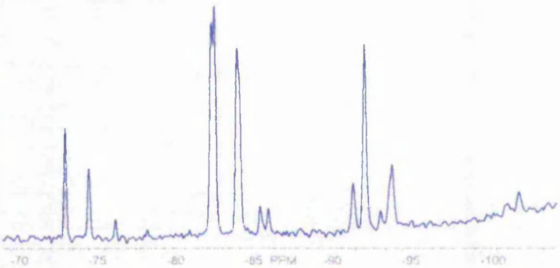

30 seconds

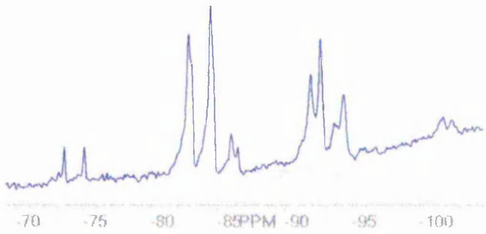

1 minute

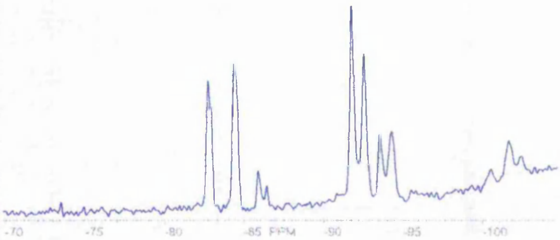

2:30 minutes

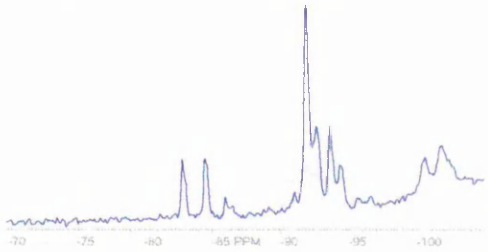

4:30 minutes

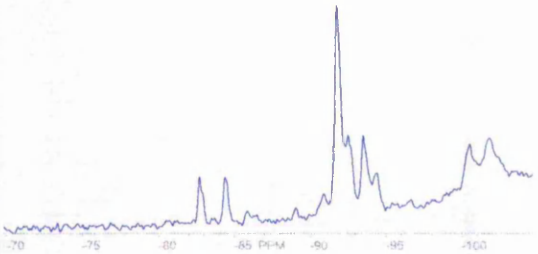

7:30 minutes

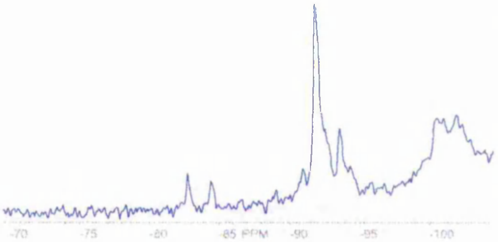

8:30 minutes

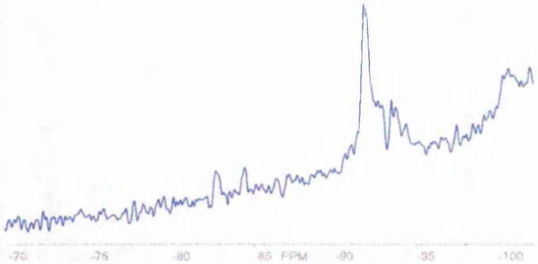

10 minutes

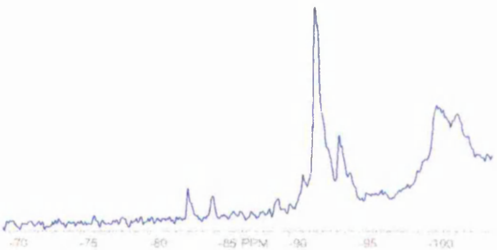

15 minutes

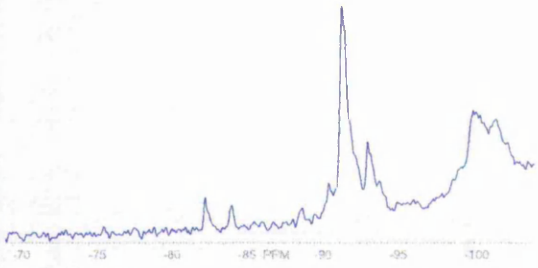

20 minutes

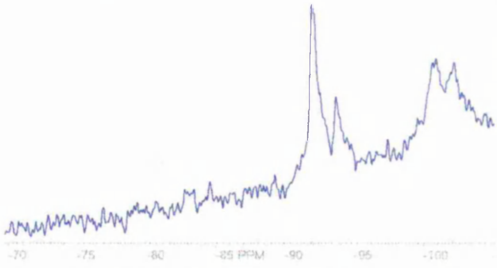

Nd0.0128Msol-gel solution (from -70 to -110 ppm)

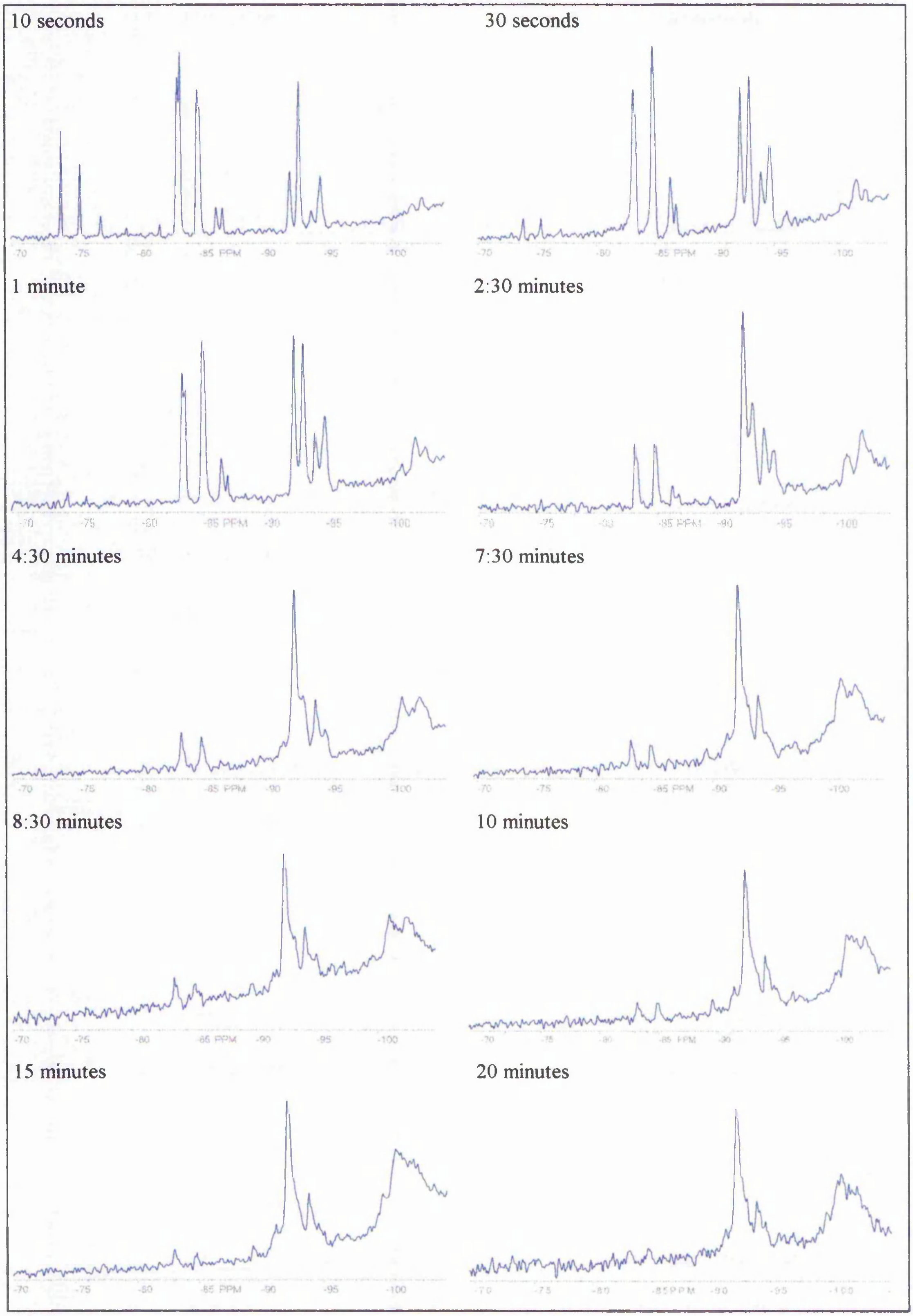

Nd0.00128Msol-gel solution (from -70 to -110 ppm)

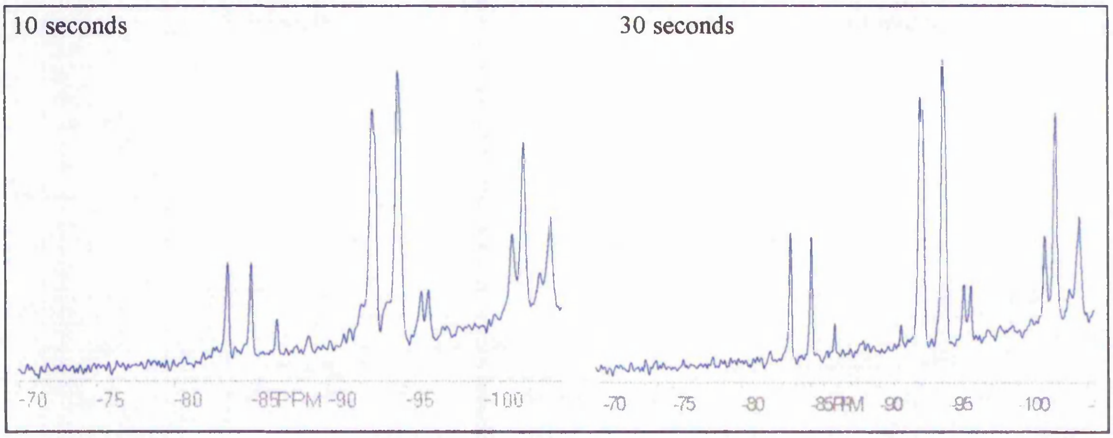

Nd6.4.10^{-4}Msol-gel solution (from -70 to -110 ppm)

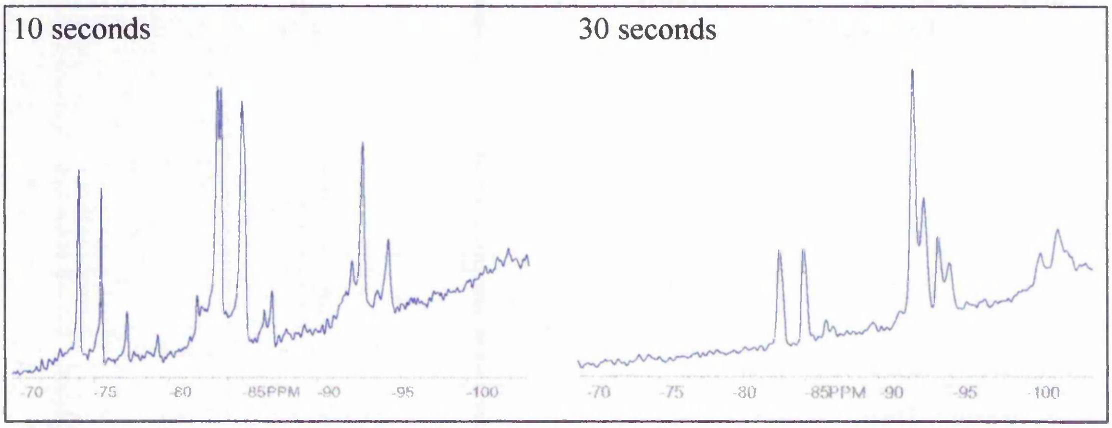

Nd 1.28.10^{-5} M sol-gel solution (from -70 to -110 ppm)

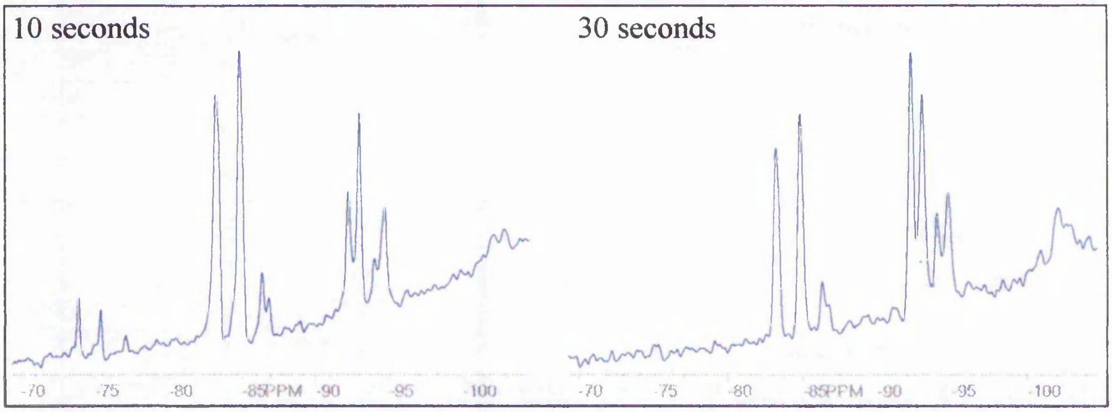

Nd 1.28.10-6 M sol-gel solution (from -70 to -110 ppm)

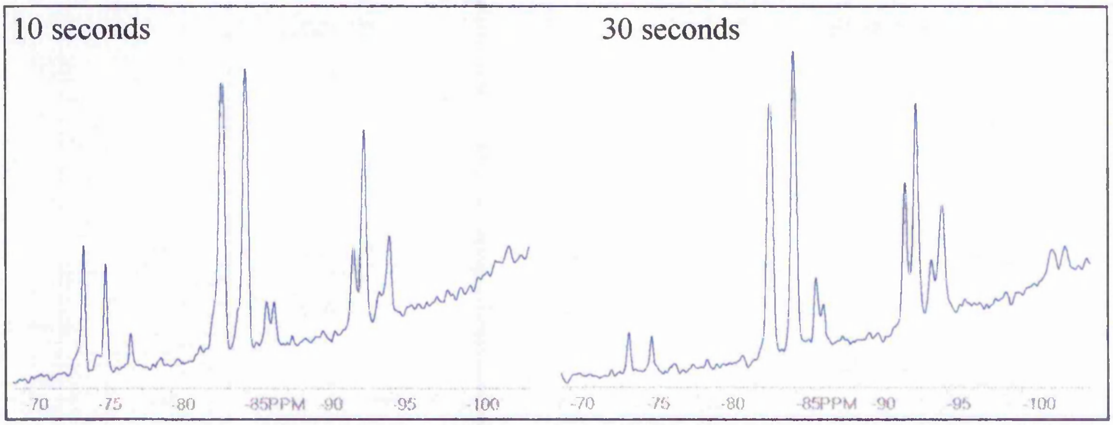

Nd 1.28.10^{-7}M sol-gel solution (from -70 to -110 ppm)

Calculation of the moles of Si present for each type of species

To calculate the number of moles of Si present for each type of species, an external reference standard tetramethylsilane (TMS) was used (see paragraph 3.2.4 on Method for explanation of the technique).

Consequently for every ^{29}SiNMR spectrum a peak corresponding to the silica species from TMS was observed.

The area of all NMR peaks were measured using the software GRAMS/32.

The number of moles of Si present in the observed TMS peak was calculated as follows:

The external reference standard was a solution of 1.5ml of d_6-acetone containing 25% (v/v) TMS which corresponded to 0.375ml of TMS.

The density of TMS is 0.648g/cm^3 and the molecular weight 88.23g/mol.

So $n_{TMS} = 0.375^* (0.648 / 88.23) = 0.002754$ moles.

So for every spectrum, 0.003754 moles of silica correspond to the peak area (x) of the TMS peak.

From this and by measuring the area of all the silica peaks arising from the silica sol-gel solution, it was possible to calculate the number of moles of each silica species present in the sol-gel solution at various times of hydrolysis.

^{29}SiNMR spectra of doped sol-gels with Ce^{3+} metal ion (0.0897M-0.00128M)

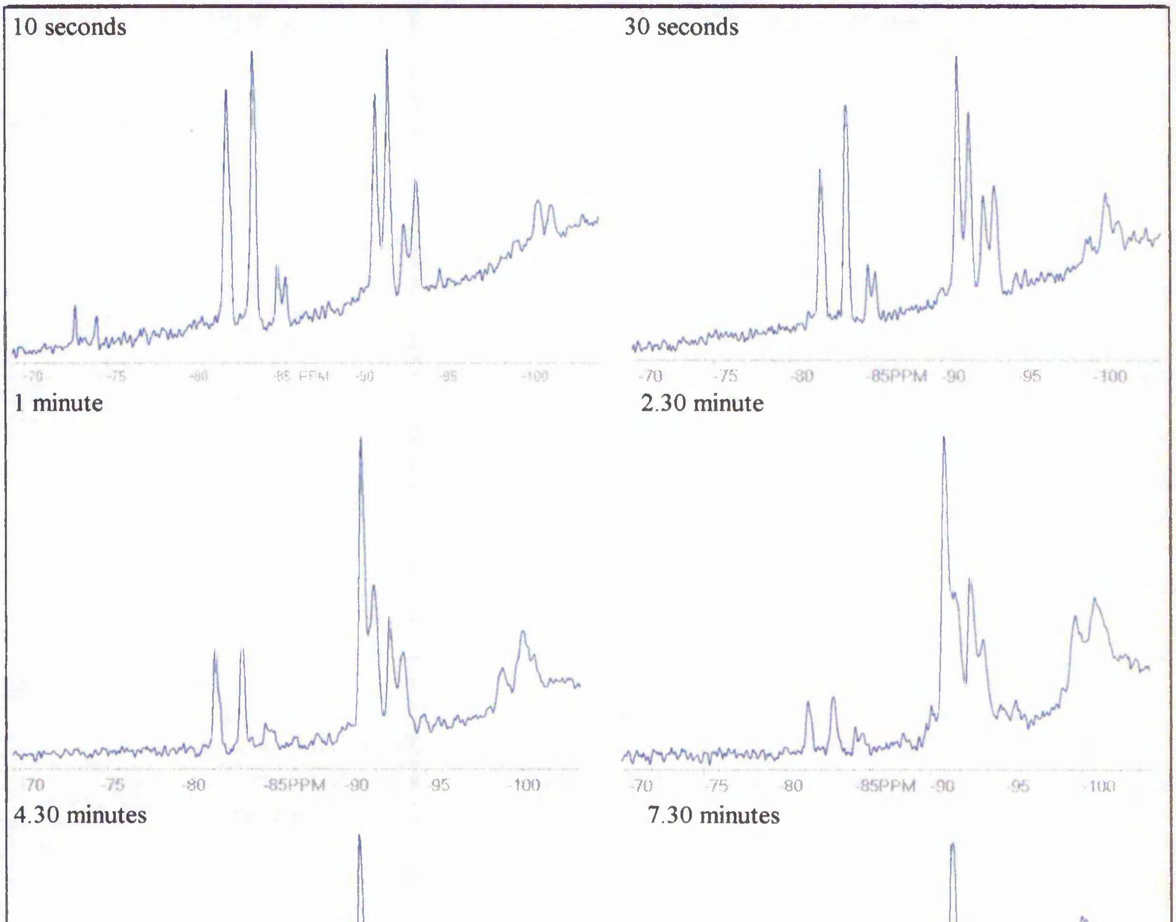

10 seconds

30 seconds

1 minute

2.30 minute

4.30 minutes

7.30 minutes

10 minutes

20 minutes

Ce 0.0897M sol-gel solution (from –70 to –110 ppm)

10 seconds

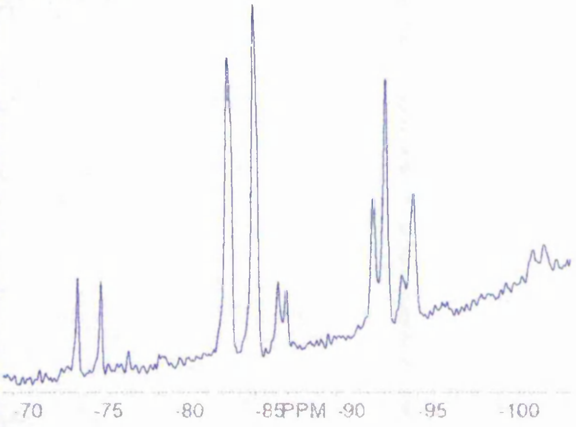

30 seconds

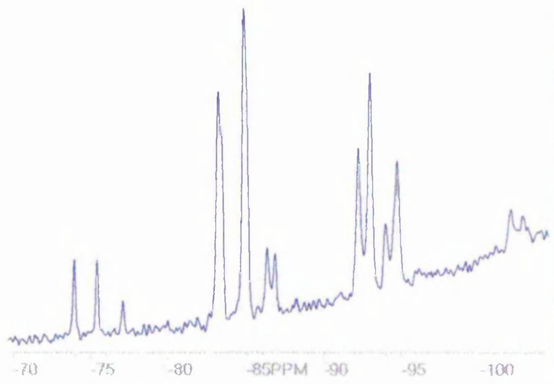

1 minute

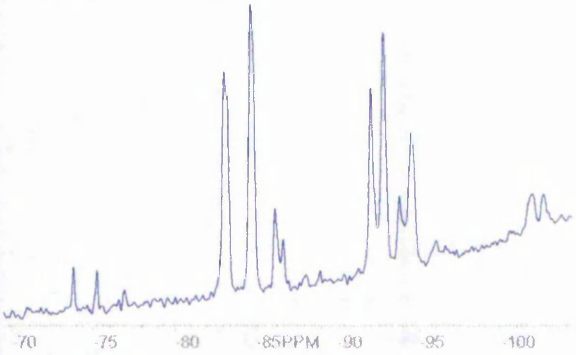

2.30 minutes

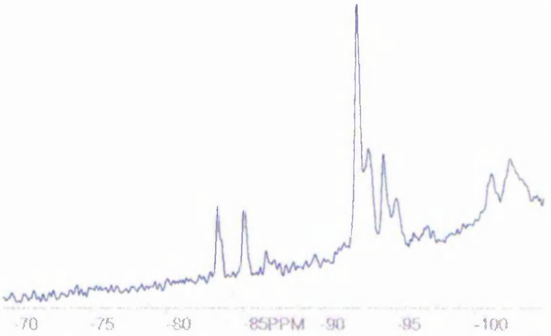

4.30 minutes

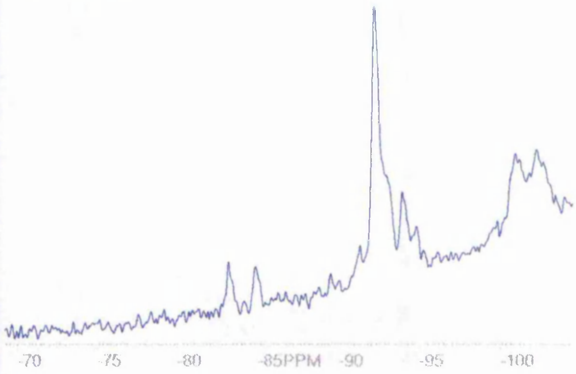

7.30 minutes

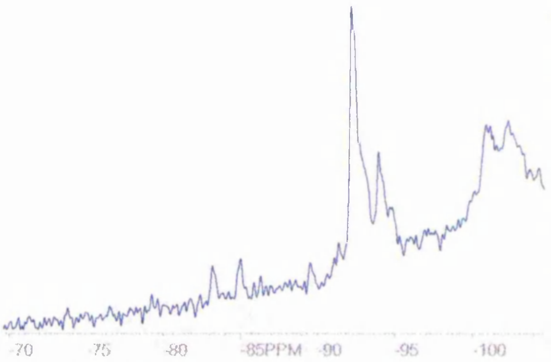

10 minutes

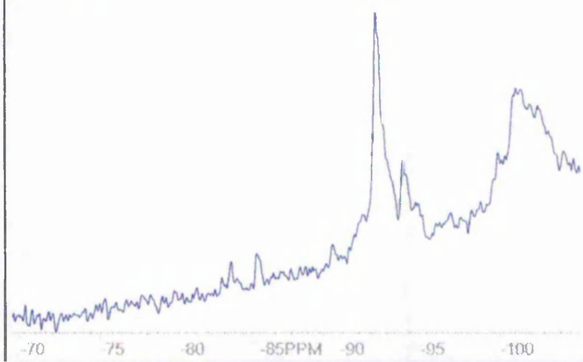

20 minutes

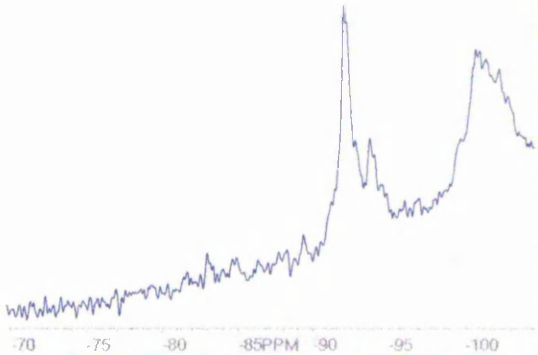

Ce 0.0128M sol-gel solution (from –70 to –110 ppm)

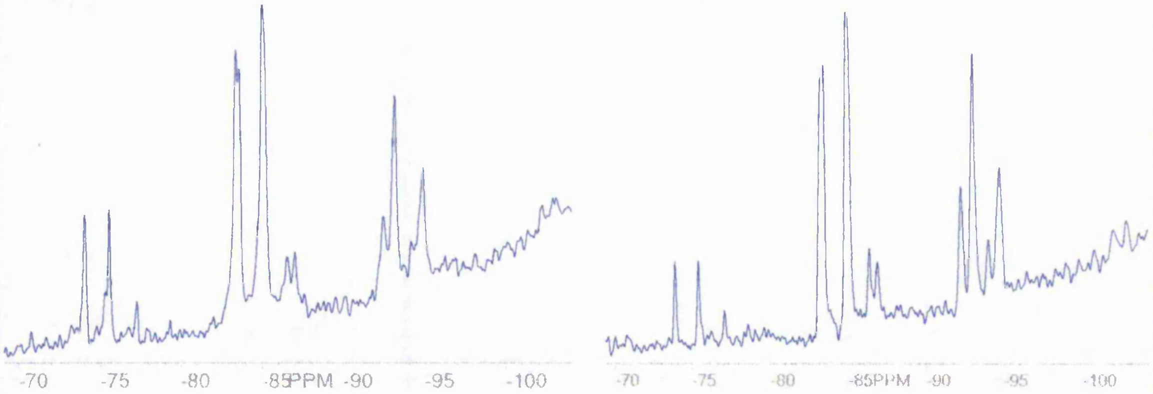

10 seconds

30 seconds

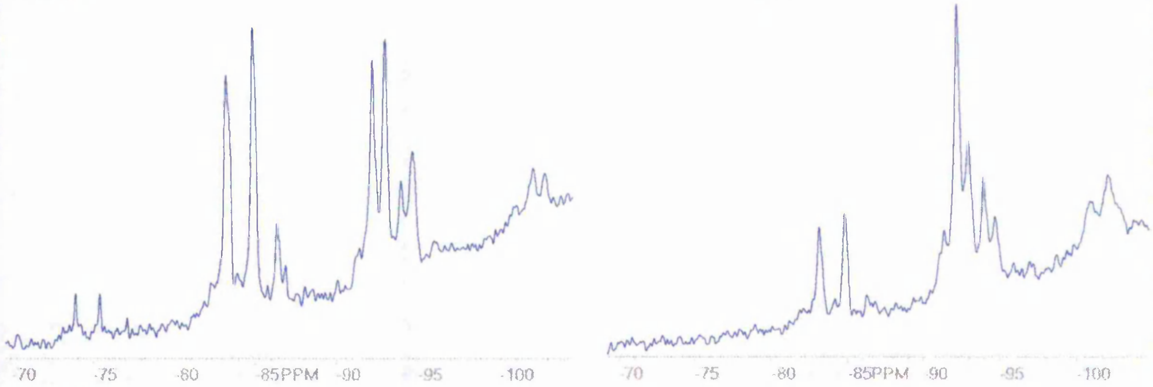

1 minute

2.30 minutes

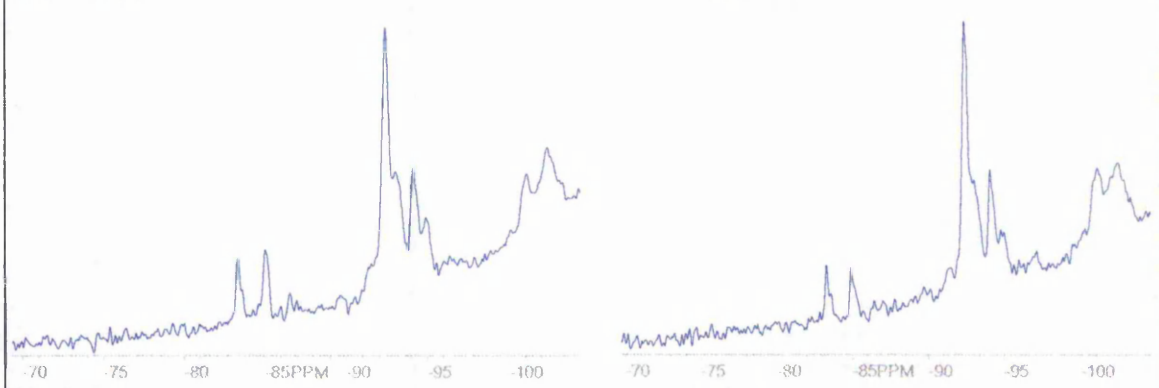

4.30 minutes

7.30 minutes

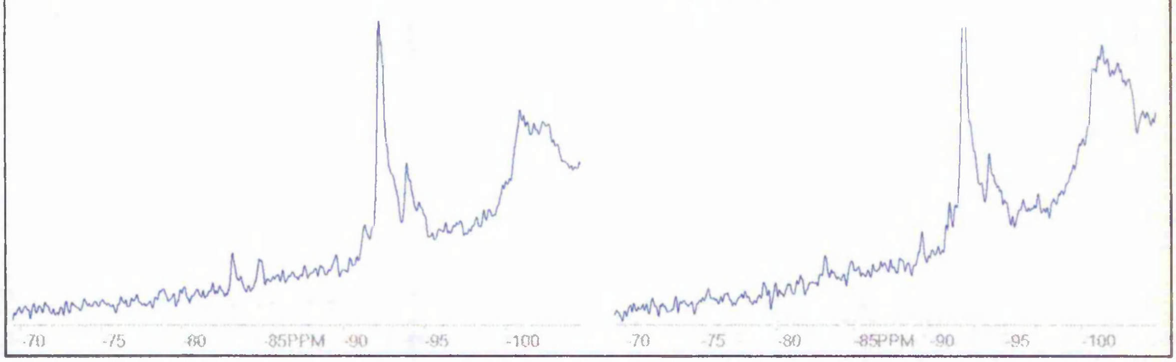

10 minutes

20 minutes

Ce 1.28.10^{-3}M sol-gel solution (from –70 to –110 ppm)

Powder X-ray analysis of ground crystals

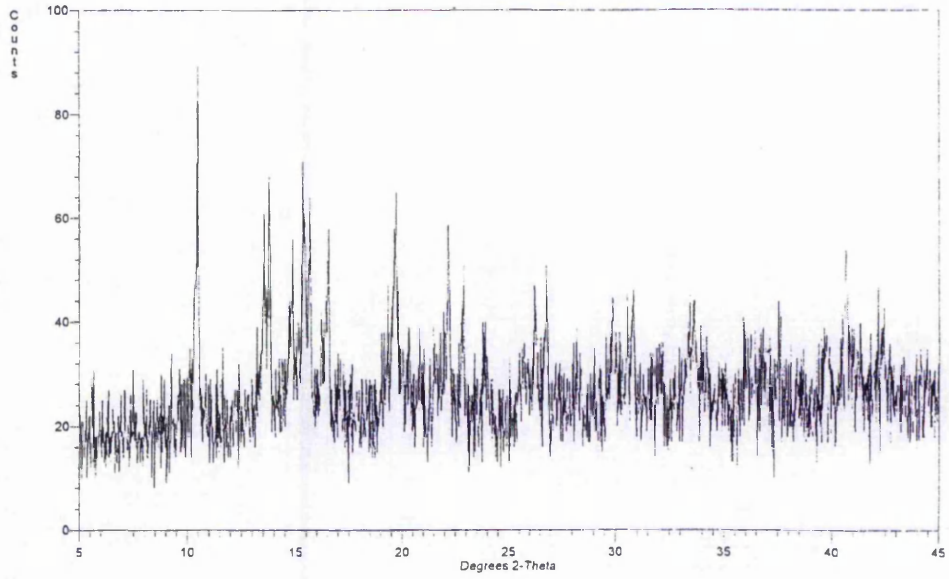

a)

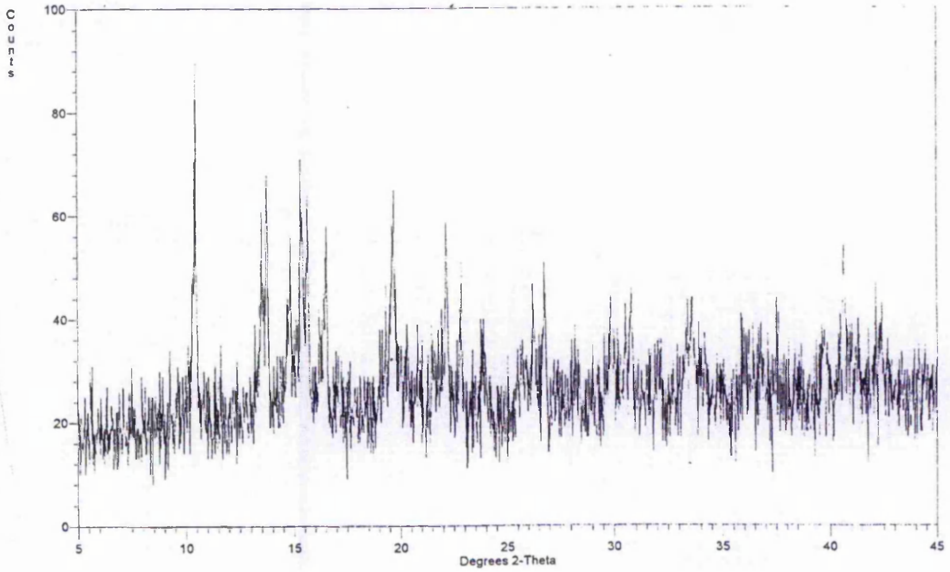

b)

Figure 6.1: Nd^{3+} crystal prepared from $Nd(NO_3)_3.6H_2O$ in water
a) after one day of aging, b) after 3 weeks of aging

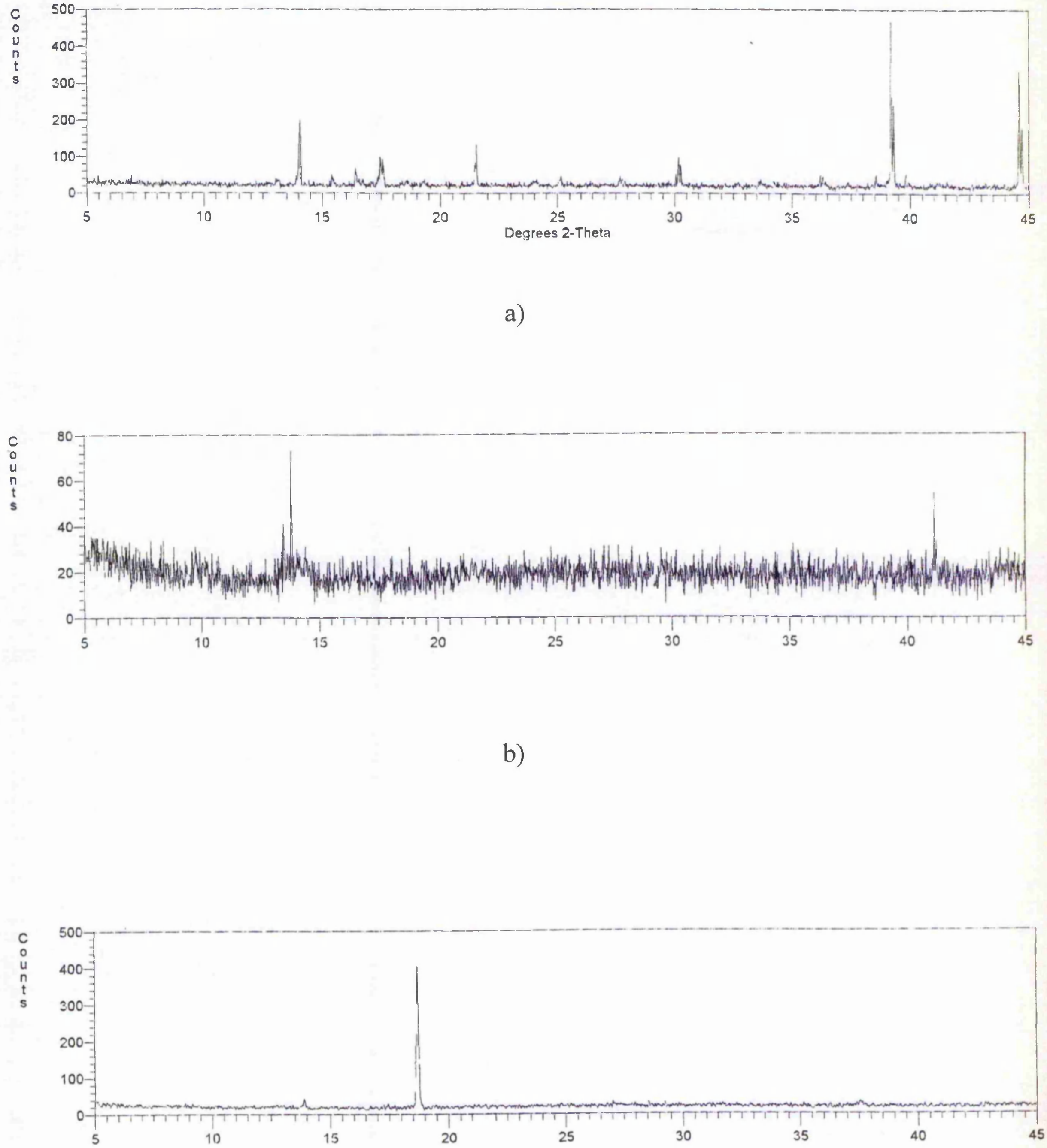

a)

b)

c)

Figure 6.2: Nd^{3+} crystal prepared from $NdCl_3.6H_2O$ in dry ethanol
a) after one day of aging, b) after 5 weeks of aging, c) after 9 weeks of aging